FINAL REPORT

Grant Title: Growth, Characterization and Applications of β-Barium Borate and Related Crystals

Grant Number: N00014-90-J-4107

Period of Performance: August 1, 1990 - October 31, 1993

Dollar Amount: $ 295,000

Scientific Officer: John McMahon
Naval Research Laboratory
Optical Sciences Division
4555 Overlook Avenue
Washington, DC 20375

Principal Investigator: C. L. Tang C. L. Tang

Institution: Cornell University
Ithaca, NY 14853

Final Report to NRL on

Growth, Characterization, and Applications of β-Barium Borate and Related Crystals

(1990 to 1993)

Submitted by

C. L. Tang

Cornell University, Ithaca, NY 14853

Emphasis of our program during the past three years has been on improving the size and quality of β-barium borate (BBO) crystal; developing the growth recipe for lithium triborate crystal (LBO); automation of the growth process of BBO and LBO; characterization of LBO; developing optical parametric oscillators using BBO, LBO, and new nonlinear crystals such as $KTiOPO_4$ (KTP), KTA (arsenate), C(Cs)TA, and R(Rb)TA; and finally helping to establish commercial sources of BBO and LBO crystals and optical parametric oscillators making use of these new crystals. Significant progress has been made in all these areas. The results are summarized below and in the Appendices attached.

I. Crystal Growth

Our initial efforts were on improving the size and quality of high temperature solution grown BBO crystals and developing the growth recipe of LBO. These efforts were highly successful [See Appendices A - C] and the technology developed in our laboratory was licensed and transferred to Cleveland Crystals Inc. This company is now a major supplier of BBO single crystals in this country. The availability of such U. S. grown crystals was instrumental in convincing major laser companies such as Spectra Physics and Coherent to develop laser related equipment that makes use of BBO crystals. Our program has played a leading role in the recent rapid development of OPO technology in both the nanosecond and the femtosecond time domains. [See, for example, attachment in Appendix D].

Since Cleveland Crystals has now become an established American commercial source of BBO based on our licensed technology, we felt that it was a good time for us to try something new. The critical need was to automate the growth process to get away from manual control based upon visual monitoring and the experiences and judgment of the grower. With visual monitoring and human control, there was no hope of significantly

A-1

improving the quality, yield, and growth speed. Real advances in the BBO crystal growth technology cannot happen without automation of the growth process.

For these reasons, we decided to take a chance and devote all our efforts and resources to converting our growth setups to that with computer-controlled and electronic-weighing. This hardware and software development part of the program is now finally completed. We have started our first growth runs. We still have to perfect our growth recipe based on past accumulated experiences and develop it into a computerized recipe. After which, we should get precisely repeatable results with each run and make systematic improvements on quality, yield, and size of the crystals. Without precisely reproducible results, there is no hope for anyone to make systematic improvements effectively.

The initial results from the automated growth setup look very good. We can see minute changes in the growth furnace due to small perturbations in the lab environment. Details of both the computer controlled setups and the initial results were discussed in the progress report we submitted to NRL on March 31, 1993. The latest version of the growth setup which allows the seed to be separately cooled and has new seed mounting scheme is shown schematically in the attatched figure at the end of the text of this report.

II. Characterization of LBO

In addition to the growth of single crystals, it is also important that the crystals are thoroughly characterized. This is especially true for LBO where there is considerable controversy even on such an important parameter as the noncritical phase-matching temperature at 1.06 μm. A detailed LBO characterization program was initiated in our laboratory. The characteristic properties of noncritically phase-matched second-harmonic generation in LBO were investigated. Using an LBO crystal grown in our laboratory, we deomonstrated temperature-tuned noncritical phase-matched second-harmonic generation from 1.025 to 1.253 μm in the temperature range from 190 to -3° C. The noncritical phase-matching temperature for 1.064 μm radiation is found to be 148+/-0.5° C with a temperature acceptance bandwidth of 3.9° C-cm. Spectrum-tuned noncritical phase matching at room temperature has been achieved at 1.215 mm. Angle-tuned critically phase-matched second-harmonic generation of near-infrared radiation has also been achieved. Large angular, temperature, and spectral acceptance bandwidths were obtained. The these results have all been published [Appendices C and E].

III. Applications of BBO and Related Crystals

A substantial part of our efforts has also been devoted to developing the applications of BBO, LBO and other new nonlinear optical crystals, notably the KTP ($KTiOPO_4$)-isomorphs such KTP, KTA, CTA, and RTA. A series of patents covering many aspects of the OPO technology have been generated and licensed to industry. The

BBO nanosecond OPO technology [See review article in Appendix F] licensed and transferred from our laboratory to Spectra Physics[Appendix D] is now a successful commercial venture with over a hundred OPO systems sold within the first year it was introduced. The femtosecond OPO technology pioneered in our program [Appendix G] and transferred to industry is also now being pursued by several major companies including Spectra Physics and Coherent. License agreements with these companies are under discussion.

Other new applications of BBO that we have developed include the first demonstrations of shifting the output of the recently developed Ti:sapphire mode-locked laser to the blue [Appendix H] and the output of the fs KTP OPO [Appednix I] invented in our laboratory to the visible [Appendix J]. We have further demonstrated femtosecond OPO operation in the new crystals such KTiOAsO4 [Appendix K], CsTiOAsO4 [Appendix L], and RbTiOPO4 [Appenix M] for the first time. These OPO's extend the operating range of broadly tunable high repetition rate ultrafast sources into the important spectral range of 3 to 5 μm.

Finally, we have developed a thermal lens spectrometer using a computerized BBO OPO that is capable of continuous tuning from approximately 420 nm to 2 μm for spectroscopic and spectrometric applications. This system allows any selected wavelength within the tuning range to be reached directly and quickly. We demonstrated the versatility of the system by measuring the entire visible (450 to 690 nm) thermal lens spectrum of NO_2 with a computer-controlled automated continuous scan.

In summary, we have very susccessfully developed the growth process of BBO and LBO crystals, characterized these materials, and developed extensive applications of BBO and related crystals. A substantial part of the technologies developed have already been transferred and licensed to industry.

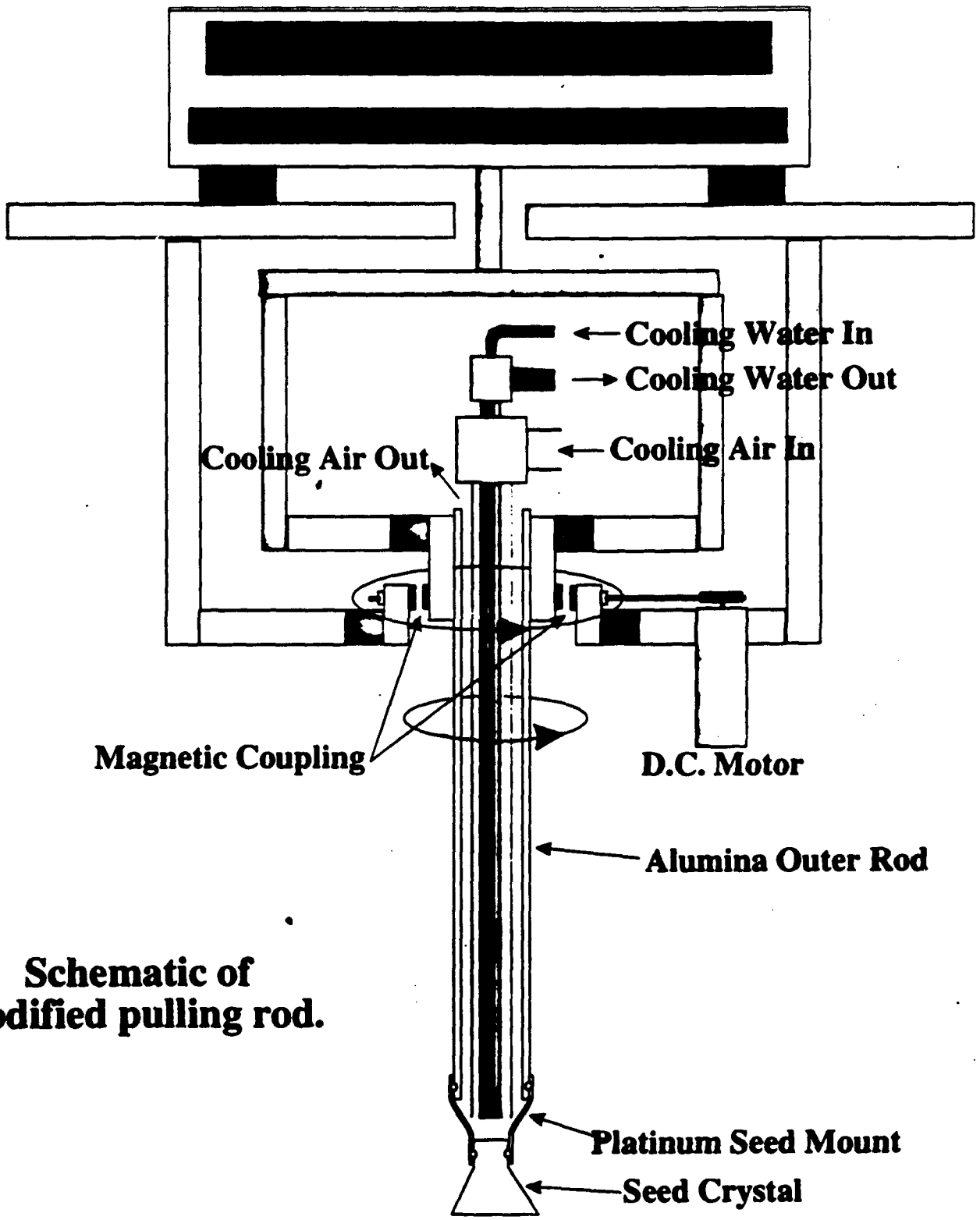

Schematic of modified pulling rod.

Appendix A

Prog. Crystal Growth and Charact. 1990, Vol. 20, pp. 9–67
Printed in Great Britain.

0146-3535/90 $0·00 + ·50

GROWTH AND CHARACTERIZATION OF NONLINEAR OPTICAL CRYSTALS SUITABLE FOR FREQUENCY CONVERSION

L. K. Cheng, W. R. Bosenberg and C. L. Tang

Materials Science Center, Cornell University, Ithaca, New York 14853, U.S.A.

Abstract: During the past decade, important advances have been made in the development of nonlinear optical materials suitable for frequency conversion. Better understanding of the microscopic origins of optical nonlinearities has provided qualitative guidelines for the systematic search and synthesis of many new materials, organic and inorganic, which are particularly promising for the construction of practical devices. Significant progress in the crystal growth technology has allowed the development of many excellent crystals that were once plagued by growth difficulties. We review here some of these advances, placing special emphasis on the high temperature solution growth of nonlinear optical crystals. In particular, we discuss in somewhat more detail the growth and characterization of the newly discovered crystal, barium metaborate (β-BaB_2O_4).

Introduction :-

Since the discovery of second harmonic generation by Franken et. al. in 1961[1], nonlinear optical mixing has been widely recognized as an effective method for the generation of high power coherent radiation in spectral regions where efficient laser sources are unavailable. Devices based on nonlinear optical interactions promise to be efficient, compact, easy to operate, and capable of operating in a wide spectral range. With a single fixed frequency laser, a combination of harmonic generation and optical parametric oscillation can provide fully tunable radiation throughout the UV and the IR[2,3]. The widespread use of these devices has been limited by the lack of materials with suitable characteristics. Substantial progress has been made in the development of nonlinear optical materials recently. Novel materials having attractive properties are being discovered at a rapid pace[4-8], with advances in crystal growth technology making possible the commercial development of promising materials such as urea,

magnesium-oxide doped lithium niobate ($MgO:LiNbO_3$), potassium niobate ($KNbO_3$), potassium titanyl phosphate (KTP), and barium metaborate (β-BaB_2O_4). Preliminary experiments performed on these materials have been very encouraging[9-10] and will undoubtedly lead to an increased use of these crystals in device applications.

In this paper, we shall examine some of these advances. An enormous body of work has been published concerning the development of nonlinear crystals. It is, therefore, necessary to limit the scope of this paper to a few specialized areas. In what follows, we shall be concerned with bulk materials only. The growth and applications of crystal fibers[11], and materials with modulated structures[12-13], though important, will not be discussed. Likewise, we shall not concern ourselves with organic materials. A comprehensive review of organic materials can be found in Chemla and Zyss[14]. In the growth of nonlinear optical cystals, we shall single out the high temperature solution growth technique for discussion. This does not imply that other techniques, such as Czochralski[15], Bridgeman-Stockbarger[16,17] and low temperature solution growth[18], are not important in the development of nonlinear optical crystals.

Characterization of nonlinear optical crystals can be divided into two types: the measurement of optical properties and the investigation of growth defects. The former includes the measurements of intrinsic physical properties which are directly relevant to optical frequency conversion. The latter includes the study of growth defects, such as twinning, phase homogeneity, mechanical stresses, inclusions...etc, that are the result of poor control of crystal growth parameters. Standard techniques such as trace chemical analysis, etching and decoration, x-ray topography, elecron microprobe analysis...etc. can be used for defect characterization. The use of these techniques for crystal characterization has been reviewed by Laudise[19]. We shall be primarily concerned with the characterization of the optical and other relevant physical properties of nonlinear crystals.

This paper is organized in the following way. In section I, we discuss the basic characterization of nonlinear crystals. A set of material parameters is chosen which are useful for the comparison of different materials. The relative importance of these parameters and the relationships among them are discussed. A summary of several promising materials that are suitable for applications in the UV-visible-near-IR range is presented for reference and to aid discussion. In section II, we review several aspects of the high temperature solution growth (HTSG) technique. Particular emphasis will be placed on the top-seeded method. In section III, we discuss, as an example, the growth and characterization of the newly discovered crystal, barium metaborate. In section IV, we conclude this paper by a survey of some of the more important advances in the development of nonlinear optical materials.

CORNELL
UNIVERSITY

Office of Sponsored Programs

120 Day Hall
Ithaca, NY 14853-2801

Telephone 607/255-5014
Facsimile No. 607/255-5058

FIRST CLASS U.S. MAIL

June 6, 1994

Scientific Officer Code: 12621
Guy W. Beaghler
Office of Naval Research
800 North Quincy Street
Arlington, VA 22217-5000

SUBJECT: Final Technical Report for Grant Number N00014-90-J-4107

Dear Mr. Beaghler:

Enclosed are three copies of the subject report. This project, entitled "**Growth, Characterization and Applications of β-Barium Borate and Related Crystals,**" was under the direction of Professor C. L. Tang in the School of Electrical Engineering.

Sincerely,

Eric W. Danly
Assistant Director

DJC/bry
Enclosures

C: C. L. Tang

X: Administrative Grants Officer (1 copies)
Office of Naval Research
Resident Representative N62927
Administrative Contracting Officer
33 Third Avenue - Lower Level
New York, NY 10003-9988

Director (1 Copy)
Naval Research Laboratory
Attn: Code 2627
Washington, DC 20375

Defense Technical Information Center (1 copy)
Building 5, Cameron Station
Alexandria, VA 22314

Please refer to OSP #19988 on all future correspondence.

I. Material Considerations:-

Characterization :-

Hundreds of materials have been identified as possessing optical nonlinearities[1]. To date, only a handful of these materials are routinely used in the generation of coherent radiation. This reflects the many criteria which a nonlinear crystal must satisfy before it can be used in practical applications. The success of the "molecular engineering" approach[2] has led to a better understanding of the relationship between the crystal structure and its optical nonlinearities and made possible systematic search for new nonlinear materials. It is, therefore, appropriate to examine, in an organized way, the desirable characteristics of nonlinear crystals that are suitable for various applications. Qualitative discussion of this topic has been given in a recent review[3]. The following discussion will follow closely the approach taken there.

Traditionally, the usefulness of a nonlinear crystal has been evaluated in terms of the material parameters that are directly related to optical frequency conversion. These included the optical nonlinearities, optical damage threshold, birefringence, dispersion, transparency and optical homogeneity. Little emphasis have been placed on the other characteristics such as crystal growth properties, mechanical strength, thermal stress resistance and crystal fabrication properties such as coating and polishing. Recent experiments in the practical application of nonlinear materials[4,5] have made it clear that more emphasis should be placed on these other properties.

The characterization of a nonlinear optical material includes the quantitative and qualitative specification of these parameters. A general set of parameters is given below. The underlying physical principles for the selections of these parameters are discussed in standard references[6,7]:

d_{eff}^2/n^3 is the nonlinear figure-of-merit [$(pm/V)^2$].The nonlinear coefficient **d** is defined by the expression $P=2\varepsilon_0 dE^2$, where **P** is the nonlinear polarization and **E** is the electric field.

Γ_{max} is the single shot optical damage threshold. It is usually given as an intensity [GW/cm^2] or an energy fluence [J/cm^2]. For certain materials (e.g. urea) which have a cumulative damage property that depends on the duration of irradiation[5], this is not a useful characterization. For CW operation, a corresponding CW damage threshold can be defined.

$n_x(\lambda)$, $n_y(\lambda)$ and $n_z(\lambda)$ are the refractive indices along the principal dielectric axes. For uniaxial crystals, $n_x = n_y$. They defined the material dispersion and the birefringence of a material. In a phase-matched nonlinear optical process in a crystal, the

birefringence is used to compensate for material dispersion[6]. A large birefringence is needed for phase matching near the absorption cutoff.

ρ is the walk off angle. It is the angle between the phase velocity direction and the energy propagation direction of the extraordinary wave in an anisotropic medium. A large birefringence implies a large walk off angle. In certain experimental configurations, it places an upper limit on the length of the crystal that can be used for frequency conversion. In uniaxial crystals, ρ peaks at ~45° from the optics axis.

β_T is the temperature sensitivity, $\partial(\Delta k)/\partial T$ [$cm^{-1}/^oC$]. It is an intrinsic parameter which describes the material's tolerance to temperature variation for a particular frequency conversion process. It is related to the temperature bandwidth (FWHM) by[8] $l\Delta T = 4A / \beta_T$ where $A \approx 1.39$.

β_θ is the angular sensitivity, $\partial(\Delta k)/\partial\theta$ [cm^{-1}/mrad]. It is analogous to the temperature sensitivity above. For critically phase matched processes, a large birefringence implies a small angular bandwidth. Phase-matched frequency conversion processes that have low angular sensitivity can be obtained in a crystal which has a broad transparency and a small birefringence.

β_λ is the spectral sensitivity, $\partial(\Delta k)/\partial\lambda$ [cm^{-1}/A]. It gives the spectral bandwidth that can be efficiently converted. It is useful in designing frequency converters of broad bandwidth radiation such as picosecond or femtosecond pulses.

Δv_g^{-1} is the reciprocal group velocity mismatch [fs/mm], $\partial k_s/\partial\omega_s - \partial k_f/\partial\omega_f$, where s & f stand for the second harmonic and fundamental. It represents approximately the temporal broadening of the second harmonic pulses in a 1 mm thick nonlinear crystal caused by the nonlinear interaction. It is usually significant only in the frequency conversion of subpicosecond pulses.

$\sigma(\lambda)$ is the optical absorption of the material [cm^{-1}] within its transparency range. It is a measure of the intrinsic passive loss of laser light in the material. A large σ at the pump laser frequency generally implies significant heating of the material by the pump laser.

ΔT_F is the fracture temperature as discussed in reference [4]. It is the temperature difference at which an ideal thin plate with 100μm defects fractures. It gives a quantitative measure of the thermal loading capacity of a crystal and is of extreme importance in high average power application.

Other intrinsic and extrinsic parameters should also be specified for the comparison of different nonlinear crystals. The mechanical properties can be specified by the fracture toughness[8] (K_c [KPA $m^{1/2}$]), Mohs hardness and the elastic constants. Chemical characteristics that are worth considering are the presence of ferroelectric phase transitions which may lead to domain formations, compositional inhomogeneity, melting point and susceptibility to attack by moisture and common solvents. Crystal availability can be assessed by considering the crystal growth technique, growth run time, typical crystal yield (i.e. crystal size), predominant growth defects and post-growth processing (such as poling and

detwinning). Crystal that is difficult to grow with high yield will not provide sufficient economic incentive for its commercial development unless it possesses unusually good optical characteristics. A case in point is KTP where despite the enormous expenses, sustained international efforts were devoted to its development. By the same token, favorable growth characteristics can go a long way in bringing a nonlinear optical material with modest characteristics into everyday use. The longevity and popularity of KDP (and its isomorphs) is a classic example.

The full characterization of a nonlinear optical material will involve the proper documentation of these parameters. Techniques for the measurement of these parameters are numerous and can readily be found in the literature. The discussion presented below is necessarily sketchy and is included for completeness.

After confirming that a new material possesses a sufficiently large second order nonlinearity (usually by the powder measurement technique[9]) the optical characterization generally begins with the measurement of the refractive indices. The minimum deviation method[10] is the most commonly used. Careful experiments can readily give values accurate to the fourth decimal place throughout the transparency range of the crystal. The data are then numerically fit to give the appropriate Sellmeier coefficients. For crystals that are useful in the visible and UV, Sellmeier equations having a single UV pole and a quadratic IR correction will usually be sufficient. For infrared materials, such as those used for the doubling of the CO_2 laser, the IR pole must also be included.

The linear refractive index data obtained above must be correlated with the measured second harmonic and sum-frequency tuning curves, which are much more sensitive to material dispersion than the direct measurement of the refractive indices. It should be noted that these nonlinear optical measurements cannot uniquely determine the Sellmeier coefficients, and they should be regarded as a supplement to the linear data. An accurate set of Sellmeier coefficients allows the prediction of many of the parameters outlined above, including tuning curves (second harmonic generation (SHG), sum frequency generation (SFG) & optical parametric oscillation (OPO)), angular sensitivity, spectral sensitivity, group velocity mismatch and the walk off angles. Therefore, the extra effort spent in the accurate determination of the Sellmeier coefficients is well justified.

For materials which have a sufficiently large temperature dependent birefringence, temperature tuning of phase-matched second harmonic generation is possible. In this case the thermo-optic coefficients ($\partial n_{c,o}/\partial T$ [$^oC^{-1}$]) should also be determined. This can be done by placing the prism used in the minimum deviation method (see above) in an oven. The temperature bandwidth is also determined by these coefficients. For materials that support

phase matching by angular and temperature tuning, the temperature dependent Sellmeier equations should be determined[11].

The temperature bandwidth is commonly measured directly by heating the nonlinear crystal in an oven and observing the variation of the SHG intensity as the temperature of the oven is swept past the phase-matching point. An indirect method involving the measurement of the *angular* bandwith at different temperatures had recently been developed[8] and was reported to be more accurate than the direct measurement technique.

Crystal symmetry determines the form of the second order polarization tensor. The second order polarizability tensor is defined by the piezoelectric axes of the crystal. The IRE convention[1,12] should be used to relate the crystallographic axes to the piezoelectric axes. For uniaxial crystals, the principal dielectric axes (i.e. the axes of the index ellipsoid) are the same as the piezoelectric axes. For biaxial crystals, Hobden[13] has proposed the use of the convention of defining the principal dielectric axes with $n_z > n_y > n_x$, where x,y and z are the axes for the optical indicatrix. The second order polarizability tensor can then be transformed from the piezoelectric axes to the axes of the optical indicatrix defined above. The motivation for this assignment scheme is that the phase matching problem (such as the polarizations of the two extraordinary waves in an arbitrary direction) can then be treated analytically[14-16], which in turn allows the evaluation of the d_{eff} coefficient. However, for crystals in the monoclinic and triclinic classes where the *directions* of the principal axes can change with dispersion, a direct computer analysis may prove to be more efficient.

The magnitude of the second order polarizabilities are usually measured relative to another known material by the Maker's Fringe[17] and the wedge[18] techniques. Direct measurement of the SHG intensity can also be used. The quadratic dependence of the SHG process on the pump intensity means that the measurements will be sensitive to fluctuations, such as jitter in the energy and the spatial and temporal intensity profile of the laser. A better tolerance on the laser beam characteristic is provided by the parametric flourescence technique, which depends linearly on the pump intensity. Its use in the measurement of second order polarizability had been reported[19,20]. These and other techniques have been reviewed by Kurtz[21].

Recently, using large aperture, diffraction limited beams of uniform intensity to generate second harmonic in large aperture crystals, researchers at the Lawrence Livermore Laboratory have determined the nonlinear coefficient of KDP to an unprecedented precision[22]. These values are quoted in Table 1 for reference purposes. Advances in crystal growth technology have provided a high degree of control over the material quality of commercial KDP crystals. KDP should therefore be used as the reference material in all relative measurement techniques in the visible and near IR region.

Table 1 : Reliable values of second order coefficients of KDP and their dispersions. The fundamental wave is at 1.06 μm (After reference [22]):-

$$d_{36}(-2\omega,\omega,\omega) = 0.39 \pm 0.01 \text{ pm/V}$$

$$d_{14} / d_{36} = 1.00 \pm 0.05$$

$$d_{36}(-3\omega,2\omega,\omega) / d_{36}(-2\omega,\omega,\omega) = 1.00 \pm 0.05$$

$$d_{36}(-4\omega,2\omega,2\omega) = 0.565 \pm 0.02 \text{ pm/V}$$

Knowledge of the second order coefficients and the angular sensitivity can be used to calculate the threshold power for harmonic generation[4], $P_{th}=(\beta_\theta\lambda_f/C)^2$, where $C=5.456 x d_{eff}/(\lambda_f n_f n_s^{1/2})$. The units are [$GW^{-1/2}$] for C, [pm/V] for d_{eff} and [μm] for λ_f. It gives an estimate of the peak power required for the efficient conversion in *critically* phase matched processes[8]. It combines the influences of the optical nonlinearity and the angular sensitivity, and is particularly relevant in the conversion of high power lasers having poor beam quality. Interested readers should refer to reference [4] for the use of P_{th} in device design.

In the measurement of optical damage and optical absorption, very high quality crystal samples should be used. The optical damage threshold, Γ_{max}, depends on crystal defects, pulse duration, laser wavelength, the refractive indices and the angle of incidence[23]. The generally accepted method for damage threshold measurement is a one-shot-per-site type of measurement. Due to the inherently statistical nature of optical damage phenomena[24], it is arguable that the single shot damage threshold is a good parameter for a material. Depending on the crystal chemistry and growth history, different crystals may have different dominant damage mechanisms, making it difficult to compare various crystals directly. Therefore, unless the detailed damage characteristics are known, Γ_{max} should be treated as a rough indicator only. Good device design practice demands that one stays below Γ_{max} by a safe margin, typically a factor of 3 to 10.

The material constants suitable for the characterization of the thermal and mechanical properties of optical crystals were recently discussed by Eimerl[4]. Experimental techniques

suitable for the measurement of these constants were also reported[8]. For crystals that are ferroelectric, it is necessary to investigate the presence of ferroelectric domains. This can be done by the observation of multiple-peak SHG signal throughout the bulk of the crystal[25]. Type II SHG interaction provides a better resolution for this measurement than type I interaction. In some cases, compositional inhomogeneity can also be investigated with this technique[26,27]. Also, as ferroelectricity implies pyroelectricity, ferroelectric domaining can in principle be investigated with the pyroelectric effect as well[25].

Tables 2 and 3 give some of these parameters for a few useful materials. These materials are grouped into two separate groups based on their damage thresholds alone. Materials listed in table 2 are suitable for conversion of high power pulsed lasers, whereas those listed in table 3 are more suitable for CW and moderate power applications. Properties of organic crystals, including urea, can be found in reference [14] in the previous section. Characteristics of many infrared materials have been given in reference [28].

Criteria for useful nonlinear materials:-

The "ideal" nonlinear crystal does not exist. The applicability of a particular crystal depends on the nonlinear process used, the desired device characteristics and the pump laser. Special material properties that are important in one application may not be significant in another. For instance, efficient doubling of very high power lasers having poor beam quality requires a material with large angular bandwidth[4]. A crystal which has a smaller nonlinearity but allows noncritical phase matching (see below) will perform better than one which is more nonlinear but is critically phasematched. On the other hand, for the doubling of femtosecond optical pulses, the preferred material will be one with a large nonlinearity so that a very thin crystal can be used to avoid dispersive broadening of the second harmonic output pulses.

For a material that has favorable features such as large nonlinearity, high damage threshold, favorable crystal growth habits...etc, an application can invaribly be found that uses the crystal efficiently. From a material point of view, only general criteria can be established to gauge the usefulness of a nonlinear crystal. For specialized applications where device performance requirements are well established, quantitative criteria for the selection of suitable nonlinear crystals can be obtained[4] which are often invaluable in aiding system design. In what follows, we discuss the special features which are particularly important for various device applications. It is implicit in the following discussion that a large nonlinearity and high damage threshold is advantageous in all applications considered below. We shall be interested in radiation source devices. Applications of nonlinear crystals to infrared imaging, optical computing, and time resolved spectroscopy will not concern us here.

Table 2: Properties of several UV, visible and near IR crystals. Unless otherwise stated, all data for 1064 nm. (Data taken from: [22,47]; [4,8,49,56]; & [31,50-52] respectively.)

Crystal	KDP	β-BaB_2O_4	KTP (II)*
Point group	42m	3m	mm2
Birefringence	n_e=1.4599 n_o=1.4938	n_e=1.54254 n_o=1.65510	$n_{x=a}$=1.7367 $n_{y=b}$=1.7395 $n_{z=c}$=1.8305
Nonlinearity [pm/V]	d_{36} = 0.39	d_{22} = 1.6 d_{31} = 0.08	d_{32}=5.0, d_{31}=6.5 d_{24}=7.6, d_{15}=6.1 d_{33}=13.7
Transparency [μm]	0.2 - 1.4	0.19 - 3.3	0.35 - 4.4
Γ_{max} [GW/cm^2]	~ 3.5	~ 13.5	~ 15.0
SHG cutoff [nm]	487	411	~ 990
lΔT [°C-cm]	7	55	22
l$\Delta\theta$ [mrad-cm]	1.2	0.52	15.7
l$\Delta\lambda$ [Å-cm]	208**	6.6	4.5
Δv_g^{-1} @ 630nm [fs/mm]	185	360	Not applicable
OPO tuning range [nm]	~430-700 (λ_p = 266)	~ 410 - 2500 (λ_p= 355)	~ 610 - 4200 (λ_p=532)
ΔT_F [°C]	12	150	Not available
Boule size	40x40x100 cm^3	Ø75 mmx15 mm	~20x20x20 mm^3
Growth Technique	Solution growth from H_2O	TSSG from Na_2O @ ~900°C	TSSG from $2KPO_3$-$K_4P_2O_7$ @ ~ 1000°C
Predominant growth defects	Organic impurities	Flux and bubble inclusions	Flux inclusions
Chemical properties	Hygroscopic (m.p.~ 253°C)	Nonhygroscopic (β -> α ~ 925°C)	Nonhygroscopic (m.p. ~ 1172°C)

* KTP type I interaction gives $d_{eff} \sim d_{36}$(KDP) or less for most processes[56]. The d_{ij} values[31] are for crystals grown by the hydrothermal technique[53-55]. Significantly lower damage thresholds were reported for hydrothermally grown crystals[31]. ** The anomalously large spectral bandwidth is a manifestation of the λ-noncritical phase-matching[57]. This is equivalent to a very good group-velocity matching ($\Delta v_g^{-1} \sim 8$ fs/mm) for this interaction in KDP.

Table 3: Properties of several visible-near IR nonlinear optical crystals. Unless otherwise specified, data are for $\lambda = 1.064\mu m$. (Data taken from: [1,39-43]; [1,27-28]; & [1,30] respectively.)

Characteristics	$KNbO_3$*	$LiNbO_3$**	$Ba_2NaNb_5O_{15}$
Point group	mm2	3m	mm2
Transparency [μm]	0.4-5.5	0.4-5.0	0.37-5.0
Birefringence	negative biaxial $n_{x=c}$=2.2574 $n_{y=a}$=2.2200 $n_{z=b}$=2.1196	negative uniaxial n^o=2.2325 n^e=2.1560	negative biaxial $n_{x=b}$=2.2580 $n_{y=a}$=2.2567 $n_{z=c}$=2.1700
Second order nonlinearity [pm/V]	d_{32}=-12.9, d_{31}=11.3 d_{24}= 11.9, d_{15}=-12.4 d_{33}=-19.6	d_{33}=-29.7 d_{31}= -4.8 d_{22}= 2.3	d_{32}=-12.8, d_{31}=-12.8 d_{24}=-12.8, d_{15}=-12.8 d_{33}=-17.6
$\partial(n^{\omega}-n^{2\omega})/\partial T$ [$^oC^{-1}$]	1.6×10^{-4}	-5.9×10^{-5}	1.05×10^{-4}
T_{pm} [^oC]	181, d_{32}	- 8, d_{31}	89, d_{32} 101, d_{31}
lΔT [^oC-cm]	0.3	0.8	0.5
λ_{SHG}(cutoff) [μm] @ 25^oC	0.860	~1.08	1.01
Γ_{max} [MW/cm^2]	Not available	~120	40
Phase transition temperature [^oC]	225 and 435	~1000	300
Growth technique	TSSG from K_2O @ ~1050^oC	Czochralski @~1200^oC	Czochralski @~1440^oC
Predominant growth problems	Cracks, blue coloration, multidomains.	Temp. induced compositional straitions.	Straitions, microtwinning, multidomains.
Post growth processing	Poling	Poling	Poling & detwinning
Crystal size	20x20x20mm3 (single domain)	Ø100mmx200mm (as grown boule)	Ø20mmx50mm (with straitions)

* There is disagreement on the sign of the nonlinear coefficients of $KNbO_3$ in the literature. Data used here are taken from reference [39] with the appropriate correction for the IRE convention[1]. ** Data are for congruent melting $LiNbO_3$[27]. 5% MgO doped crystals gives photorefractive damage threshold about 10-100 times higher[45,46]. The phase matching properties for these crystals may differ due to the resulting changes in the lattice constants[44].

Nonlinear frequency converters are most commonly used with an efficient, non-tunable laser source. Obviously, the nonlinear crystal should have good transparency at the pump laser wavelength. In the UV to near IR, the typical pump lasers are the ~1.06μm and ~1.32μm lines (and their harmonics) of Nd^{3+}, although there has been much progress in other promising solid-state lasers of paramagnetic ions[29] such as Cr^{3+}, Ti^{3+} and Ho^{3+}. Further into the IR, the most common source is the 10.6μm CO_2 laser. The widespread use of a nonlinear crystal is, to a certain extent, determined by how well its transparency range overlaps with these laser sources. The limited transparency range of most organic crystals (~0.4-2.0μm) has significantly limited their uses in coherent radiation generation. This is in sharp contrast with β-BaB_2O_4 whose broad transparency and large birefringence, has made it one of the versatile crystals in the UV and visible range (see section III).

Specific applications of nonlinear crystals currently of interest can be divided into the following[3]: 1) efficient harmonic generation and up-conversion, 2) optical parametric oscillator, 3) frequency conversion of ultrashort pulses, 4) frequency conversion of high average power sources, 5) frequency conversion of low average power sources, and 6) laser fusion.

1) Efficient Harmonic Generation & Up-conversion: Applications in this area can be divided into two types: conversions of i) a monochromatic source and ii) a broadly tunable laser source. We shall discuss the frequency conversion of a non-tunable source first. Materials that allow noncritical phase matching (NCPM) have a special advantage in this application as it allows the use of very long crystal to improve the efficiency. NCPM denotes the situation of 90° phase-matching, where both the angular sensitivity and the walkoff become negligible. For the SHG process, a uniaxial crystal allows NCPM, at most, of two different wavelengths, namely type I (*o+o ->e* ; *e+e ->o*) and type II (*o+e ->e* ; *e+o ->o*). For a biaxial crystals, six different wavelengths can, in principle, be noncritically phase-matched along the three principal dielectric axes. For a material that has a temperature dependent birefringence, NCPM can be accomplished for a range of wavelength by temperature tuning provided that the thermally induced phase-mismatch due to poor temperature control does not prove to be a problem[30].

Comparison of the $l\Delta T$ values for the materials listed in tables 2 and 3 suggests that the temperature bandwith of a temperature tuned crystal is typically an order of magnitude smaller than that of angle tuned crystals.

For the special case of a biaxial crystal whose refractive indices are given by $n_z(\lambda) > n_y(\lambda) \gtrsim n_x(\lambda)$, we have

$$\delta(\Delta k) = \frac{\partial(\Delta k)}{\partial \theta}\delta\theta + \frac{\partial(\Delta k)}{\partial \varphi}\delta\varphi + \ldots\ldots$$

For phase matching in the XY plane, the first term vanishes, giving a small though nonvanishing first order angular dependence. Such a crystal is attractive as a frequency doubler as it does not impose the stringent requirement discussed above on the exact pump wavelength in NCPM, and hence will be more versatile. It can be seen from table 2 that KTP has this special property. The doubling of 1.06μm light in the XY plane of KTP gives an external angular acceptance[31] of $\delta\varphi \sim 3^{o}$ (NCPM with repect to θ gives $\delta\theta \sim 10^{o}$). For many applications, such a large angular bandwidth is more than adequate. For instance, the threshold power for this process has been estimated[4] to be ~0.05MW, which should be compared to ~67MW with KDP[8].

For the conversion of a tunable laser source, critical phase-matching must be used in order to cover a wide spectral range. Optimal focusing[7] is usually used in these situations. Depending on the phase-matching angle and crystal birefringence, the effect of walkoff may limit the maximum interaction length. The angle between the phase normal and the ray normal, ρ, is given by[21]

$$\tan\rho = n^2 \left\{ \sum_{i=x,y,z} \left(\frac{s_i}{(1/n^2) - (1/n_i^2)} \right) \right\}^{-1/2}$$

where s is $(\sin\theta\cos\varphi, \sin\theta\sin\varphi, \cos\theta)$. This expression is valid for both uniaxial and biaxial crystals.

2) Optical Parametric Oscillator (OPO): The more important characteristics in this application are broad transparency, good birefringence and high damage threshold. Although an OPO can in principle be as efficient as a harmonic generator, it typically has a higher 'inertia' such that a higher pump intensity is needed to initiate the efficient conversion process[8,32]. Unlike harmonic generation, the high intensity pump wavelength is the shortest of the three interacting waves. Since the crystal damage threshold decreases rapidly with wavelength near an absorption edge, a crystal in a parametric oscillator is more susceptible to damage than if it is used in harmonic generation. For materials with large transparency range, one can get around this problem by staying away from the short wavelength cutoff without compromising much on the tunability. A large nonlinearity will, of course, help to lower the parametric oscillator threshold, and thus, the pump power needed for a given conversion efficiency.

3) Short Pulse Generation: The generation of ultrashort pulses in the picosecond and subpicosecond range has seen much progress in the past ten years[33,34]. Many of these laser systems can now be regarded as well established and the amplified output of such lasers can serve as efficient pump sources for frequency converters to generate short pulses in other spectral regions. The doubling of ultrashort pulses is limited by the phase-matching bandwidth of the crystal and the group velocity broadening of the SHG pulse via nonlinear interaction. Both of these limitations can be reduced by the use of thin crystal or by group velocity matching. NCPM consideration is not applicable here. From table 2, it can be seen that for most materials, the allowable crystal length is substantially less than 1mm if pulses of less than 100 femtoseconds are to be generated. A large d_{eff} coefficient is, therefore, very important in the efficient frequency conversion of ultrashort pulses.

In their seminal discussion of the harmonic generation process, Akmanov et. al.[35,36] established a space-time analogy for nonlinear optical processes and applied it to the frequency doubling of ultrashort pulses. They proposed that, like optimal focusing in the spatial domain, there exists an "optimal compression" of the pump pulse duration in the time domain. Also, the SHG spectral bandwith is inversely proportional to the crystal length, that is, $\Delta\lambda = 5.56/\beta_\lambda l$. For a 1 mm long KDP crystal, the calculated spectral bandwidth at 630 nm is 3.4 nm. The spectral width of a transform limited 50 fsec laser pulse at this wavelength is ~8 nm, suggesting possible bandwidth limiting of the SHG process if a 1mm crystal is used to double these pulses. Reduction of the crystal length will allow a larger portion of the pump spectrum to be converted. Akmanov et. al.[35] has analyzed this situation and predicted a linear dependence of the SHG power on crystal length for SHG bandwidth limited processes. This suggested that, together with optimal focusing, a less than linear dependence of the SHG power on crystal length may be possible. Such a slow crystal length dependence will make the optical nonlinearity even more significant, as it allows the process to scale as ~ $(d_{eff}^2 l)$ instead of ~$(d_{eff} l)^2$. Careful SHG experiments with femtosecond pulses should allow direct testing of this conjecture.

Another interesting possibility concerns the damage threshold of optical materials. It is unclear if the optical damage thresholds obtained for different materials with nanosecond pulses can be extrapolated into the femtosecond regime. For instance, photorefractive damage in $LiNbO_3$ involves the ionization, diffusion and subsequent trapping of impurity carriers[37]. It is unclear if such a damage mechanism can respond to femtosecond excitations. It may be worthwhile to re-examine certain nonlinear optical crystals that have large nonlinearity but were rejected for long pump pulse application due to their low photorefractive damage threshold.

4) High Average Power Frequency Conversion: Thermal loading of the nonlinear crystal is an important consideration in this application. Local heating of the crystal due to the absorption of the pump radiation can result in thermally induced phase-mismatch as well as catastrophic crystal damage. Crystals suitable for this application should have good thermal characteristics such as high thermal conductivity, large fracture temperature, small temperature sensitivity and low optical absorption. Higher order effects, such as self-focusing and self-defocusing, should also be considered if very high conversion efficiency is to be obtained.

As many high average power lasers exhibit poor beam quality, materials with a large angular acceptance are especially useful in this application. Eimerl[4] has proposed the possibility of "overdriving" a frequency conversion process under high average power conditions. It was reported that the frequency conversion process becomes particularly sensitive to beam divergence under very high pump intensity. Interested readers should consult reference [4] for details.

5) Low Average Power/CW Devices: These are miniature devices used as a convenient sources of intense coherent radiation and are typically included as a part of another instrument. As such, these devices must be reliable and not require frequent realignment. Most of these devices are based on intracavity frequency conversion (doubling or sum-mixing) of diode lasers. Although the requirements on the nonlinear conversion process are small (~1-5%), the low pump power demands the use of material with large nonlinearity. However, the nonlinear crystal must be of good optical quality (and must retain that quality under normal operating conditions) to avoid interfering with the operation of the pump laser. As in the case of harmonic generation, NCPM is beneficial to the reliable operation of these devices.

6) Laser Fusion: The generation of high energy UV pulse (10 MJ) for inertia confinement fusion represents an extreme in the scaling of nonlinear frequency conversion. The important factors here are low threshold power, good UV transparency, high damage threshold, favorable growth characteristics, cost and reliable material properties which allow modular replacement of system components. The needs for very large aperture (70cm x 70cm) optical quality crystal demands favorable crystal growth characteristics, such as fast growth rate (preferrably normal to the direction of optical interaction for the production of thin plates), crystal chemistry that are not susceptible to small concentration of impurity dopants and scalability of the crystal growth techniques. Reviews on this subjects can be found in reference [4,22].

We have discussed in this section the physical characterization of a nonlinear optical material and outlined the material requirements for several device applications. It is hoped that a better understanding of these requirements will aid in the search and development of novel nonlinear optical materials.

II. HTSG by Top-seeding :-

In the past, high temperature solution growth (HTSG) was primarily used in small scale exploratory research of new materials. However, during the past two decades, it has gained much popularity among crystal growers and is now routinely used in the production of large crystals for optical and electronic applications. The major reason for this increased popularity of the HTSG technique is its versatility. Not only does it allow the growth of materials which cannot be grown directly from melt (e.g. due to incongruent melting or destructive phase transitions), it can also be used to produce higher quality crystals by reducing the crystal growth rate[1].

In this section, we review some of the recent developments in HTSG. In particular, we shall limit ourselves to the specialized technique of top-seeded solution growth (TSSG). Other techniques such as the seeded Bennet-Tolksdorf growth[2,3] and spontaneous flux growth[4] will not be included here. Relevant issues concerning the control of the HTSG process will be very briefly discussed. A survey of recent technological developments in the TSSG technique will be given. There are many excellent reviews of HTSG in the literature[1,4-8]. Particularly indepth discussions of all aspects of HTSG can be found in the classic work by Elwell and Scheel[9].

Basic considerations in HTSG :-

The growth of bulk crystals from high temperature solution is a complex process involving the interactions of many chemical and physical processes. Chemically, we have the solvation and desolvation of solute by solvent, bulk and surface nucleations, crystal growth habits, incorporation of impurities and propagation of defects during growth. Physical processes include the dynamics of mass and heat transport which are governed by complex hydrodynamics. Careful control of many of these processes is needed in order to grow large single crystals from solution. It is, therefore, necessary to have a good understanding of the relative importance of these processes.

In this respect, the theory of crystal growth as developed by Burton, Cabrera and Frank[10] (BCF) has been invaluable in providing useful, admittedly qualitative, guidelines for crystal growth experiments. The currently accepted physical model of crystal growth can be very briefly described as follows. The 'growth unit' in the vicinity of the crystal surface diffuses through a solutal boundary layer and adsorbs onto the crystal surface. It then diffuses along the surface until it reaches a kink where it is incorporated into the crystal. In diffusion limited growth, the rate limiting process is the diffusion of 'growth unit' through the boundary layer. In surface kinetic controlled growth, surface diffusion of the adsorbed 'growth unit' is rate limiting. Typically, growth from solution is diffusion limited. In either case, the BCF theory,

appropriately adapted to solution growth[11,12], predicts similar dependence of the growth rate on supersaturation. At low supersaturation, the growth rate is quadratic, whereas at high supersaturation, a linear growth rate is found. A pedagogic discussion of the BCF theory and related stability analyses of a singular crystal surface can be found in reference [9].

In a seeded growth experiment where the primary objective is the production of a large defect-free single crystal, the relevant factors are: the physio-chemical properties of molten salt solution; the supersaturation; the kinetics of crystal growth; the mechanisms of inclusions and defect formations and the hydrodynamics. It is the proper manipulation of these factors that allows the controlled growth of large defect-free crystals. The optimization of these factors for the growth of bulk crystals from high temperature solutions has been lucidly discussed by *Scheel*[1].

The ideal situation for favorable solution growth can be stated quite simply. i) Chemically, the solvent should have high solubility to give favorable crystal yield. It should also be chemically different from the crystal constituents such that it can be favorably rejected from the growing crystal. ii) The lateral (i.e. parallel to the crystal surface) temperature and solutal concentration gradients should be zero to prevent solvent inclusion by the bunching and overlaying of growth steps[13]. The normal temperature gradient should be large and positive (i.e. the temperature increases as one moves away from the crystal surface) to satisfy the constitutional supercooling condition for high stable growth rate[14]. iii) The bulk solution should be homogeneous (in temperature and supersaturation) throughout to avoid temperature oscillations due to natural convection. Naturally, the supersaturation level should be within the Ostwald-Miers zone such that spontaneous nucleation does not occur.

To create such a situation in a real crystal growth experiment is, however, no easy task. Typically, the only parameters which are at the disposal of the crystal grower are the choice of solvent, the growth temperature and the mechanism for stirring the solution. Due to the coupling of the factors outlined above, it is often impossible to independently effect changes to one of these factors. The need to create favorable growth conditions *local* to the growing crystal and to maintain *global* homogeneity of the bulk solution poses severe challenges to the design of HTSG apparatus. Indeed it is this particular property that is most important in the scaling of a HTSG process for producing larger crystals. In what follows, we shall discuss advances concerning the control of these parameters in the top-seeded method of HTSG.

TSSG is, in many respects, identical to the Czochralski growth. In fact, during its early development, the technique had been called "modified Czochralski growth" [8]. As this earlier name suggests, a high temperature solution is contained in an open crucible and a seed which is attached to a crystal puller type mechanism, is allowed to come into contact with the solution where the growth takes place. The supersaturation can be induced by slow cooling or by

thermal gradient transport. Both resistive heating and inductive heating are in common use. Stirring is usually provided by directly rotating the growing crystal. A schematic of the technique is shown in figure 1.

Despite the similarity, important differences exist between the two techniques. In Czochralski growth, the crystal grows by the solidification of a stoichiometric melt. Crystal growth by solidification is generally (with the exception of certain nonstoichiometric solid solutions[15]) far more forgiving towards temperature fluctuations than in the solution growth

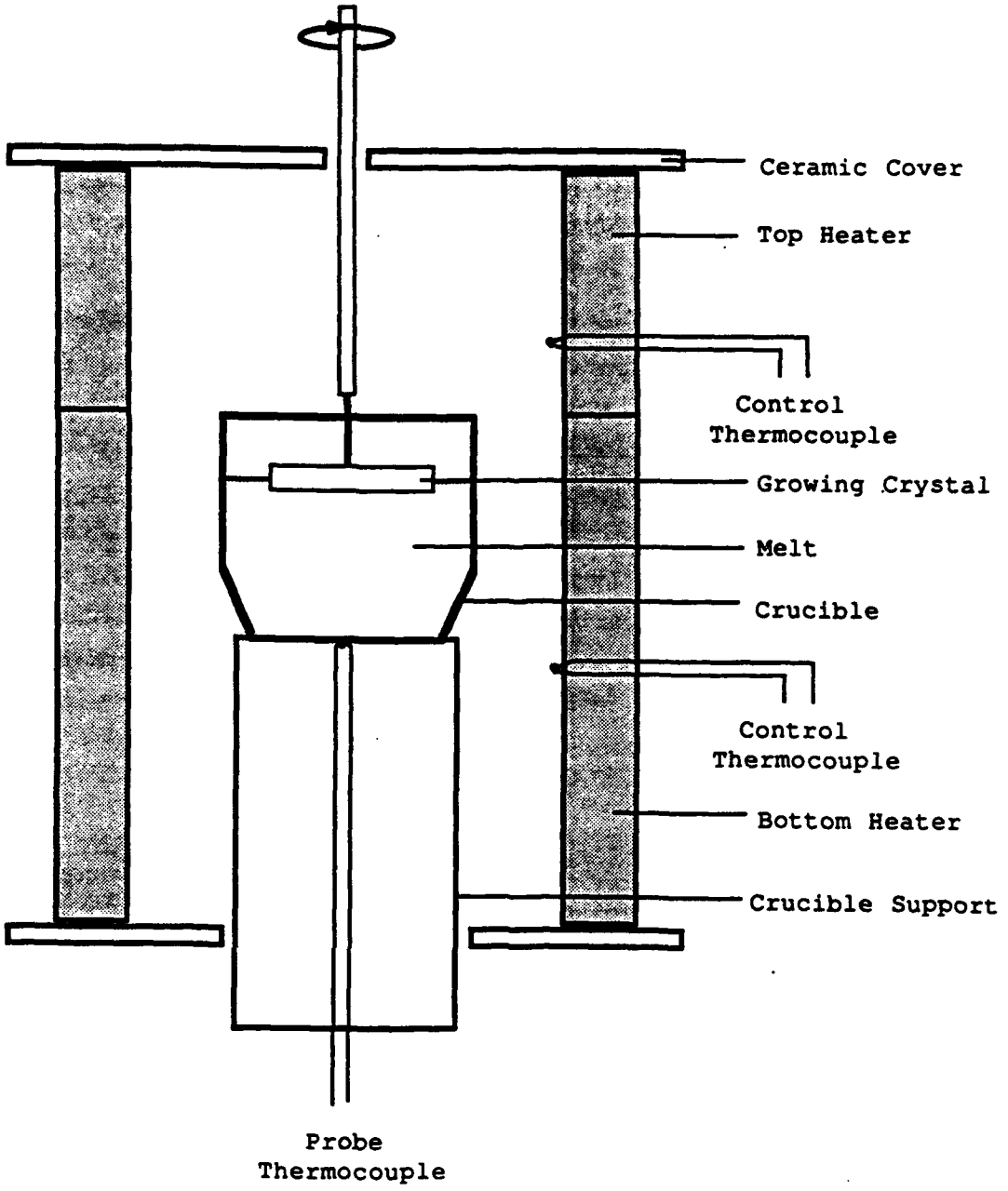

1. Schematic of a typical high temperature top-seeded solution growth set up.

case where one has to work within the limit of the Ostwalds-Miers region. Therefore much attention is needed to avoid large temperature fluctuations both within and above the solution. To ensure growth stability, the growth interface must be in good thermal contact with the solution (either by submerging the crystal entirely or by keeping the growth interface just below the solution surface). Growth via meniscus contact, which is characteristic of the Czochralski method, experimentally has led to poor unstable growth. This is presumably due to the small thermal mass of the meniscus layer and the intrinsic slow growth rate attainable from the solution growth method.

The TSSG technique has many advantages over other HTSG techniques. The most significant of these is that it allows the growth process to be monitored by rather simple means. For systems with growth temperatures below ~800°C, direct visual observation can usually be made. For temperatures well above ~1200°C, indirect methods such as boule weighing[16] may be used. As the typical growth period runs from a week to months, the ability to observe the quality of the growing crystal can lead to substantial savings of system run time since it allows decisions to be made to abort a growth run that has been spoiled by spontaneous nucleation. Correlation of the control parameters to experimental results are also more straightforward.

The importance of real time growth monitoring cannot be overstated. For many crystals, it is empirically found that dissolution of the outer most layer of the seed prior to growth substantially increases the quality of the grown crystal[16-19]. Without real time monitoring, the dissolution can be carried out with repeated success only if very precise solubility data are available. Even then, the finite response time of any thermal system prevents direct scaling of the dissolution recipe which has been developed for a smaller system. During the developmental stage of a new material, reliable solubility data are often unavailable and poor growth initiations can complicate the interpretation of the experimental results, not to mention the risk of losing valuable seed material during the dissolution process. Therefore, it is our opinion that unless absolutely necessary, real time monitoring (such as visual feedback) should not be compromised in the design of a TSSG apparatus.

Another big advantage of the TSSG method is the relative ease of implementation. It allows the simple separation of the crystal from the solution and avoids possible mechanical stress on the grown crystal caused by the differential thermal expansion between the crystal and the solidifying melt. Compared to the Bennet-Tolkdorf spherical crucible technique[20], the top seeding method is relatively inexpensive and does not require re-fabrication of the crucible between runs. The growth process can be initiated with little to no disruption to the temperature of the growth system[21]. One serious drawback of TSSG is that its use is limited to nonvolatile solutions. When volatile solution must be used, the Bennet-Tolkdorf technique is superior.

Recent developments :-

Three areas of developments are particularly relevant to the TSSG techniques: 1) chemistry of molten salt solutions as related to HTSG; 2) investigations of the accelerated crucible rotation technique (ACRT) as an effective method for melt homogenization; and 3) novel designs of TSSG apparatuses.

1) Molten salt chemistry: The highly corrosive nature of high temperature solvents is often blamed for severely limiting the technical implementation of TSSG (see below). Ironically, it is this corrosive property that gives HTSG its versatility. The direct coulombic interactions among the ions of the solvent and solute make the chemistry of HTSG far richer than its low temperature counterpart, where the weak dipolar interaction dominates. For a given material, a high temperature solvent with a sufficiently high solubility can usually be found due to the ion pairing and Debye shielding mechanisms that are present in an ionic liquid. During the growth process, the same coulombic interaction allows the efficient rejection of solvent ions which are of different valences and ionic radii. This is in stark contrast with the low temperature solution growth case where the dipole moment of the solvent must serve the contradicting functions of providing high solubility and high solvent rejection.

Besides some simple and intuitively obvious rules[1,9], there exists no systematic criteria for the selection of an appropriate solvent for a given material. Elwell[22] has emphasized the importance of obtaining better understanding of the physio-chemical nature of fluxed melts. Specifically, Scheel[1] has suggested the need for a better understanding of the roles of certain basic oxides/flourides (e.g. PbO-PbF_2) and other acidic oxide additive (e.g. B_2O_3, V_2O_5) in the growth of oxide compounds. Experiments in the past ten years have provided more insights into the structure of the complex ions in flux solutions[23-25]. Experimental evidence indicates that complex formation in basic oxide solution (e.g. PbO) involves varying numbers of O^{2-} ions. It was speculated[26] that the larger the complexes, i.e. the more O^{2-} ions are around the solute ion, the more unfavorable the growth process. The question concerning the structure of fluxed melts is a very complicated one and it is still too early to say if useful generalizations can be made concerning the selection of various high temperature solvents for a particular purpose.

A very significant development has been reported by Wanklyn[27-28] concerning the modification of growth habits of many refractory oxides, including the rare-earth phosphates (RPO_4) and borates (RBO_3) (where R = rare earth). It was demonstrated that the judicious control of the relative concentrations of the acidic and basic oxides (or flourides), can significantly improve the geometry (i.e. the aspect ratio) of the grown crystal[28]. There are also indications that the acid/base ratio can be employed to reduce spurious nucleations. The exact

mechanism for the habit modification is not well understood, although several explanations had been suggested by the author. Details of these advances have been reviewed by Wanklyn[27] recently.

2) Stirring in TSSG: Stirring of the solution serves two purposes. i) It reduces the natural-convection-induced temperature oscillations by homogenizing the bulk solution. ii) It brings nutrient to the growing crystal efficiently so that a higher stable growth rate can be achieved. The importance of efficient forced convections in crystal growth has gained much recognition during the past decade. This is particularly true in the low temperature solution growth of large KDP crystals used in inertial confinement fusion. The need to eliminate the lateral solutal concentration gradient across a large crystal suface demands very efficient stirring mechanism. Through efficient stirring and rigorous control of spurious nucleations, solution of KDP "can [now] routinely be cooled 12°C below the saturation point"[29]. Discussion of these significant developments will bring us too far from the stated objective of this paper. Interested readers should consult the recent review by Bordui[29].

Due to the small size of the melt volume, the corrosive nature of fluxed melt and the unavailability of cheap machinable high temperature materials, implementation of forced convection in TSSG is technically difficult. The two most widely used stirring mechanisms are the rotation of the seed (or seeds mounted on a stirrer) and/or the rotation of the crucible. Experiments using these techniques can be readily found in the literature[30,31].

A comment is needed concerning the difference between seed rotation and crucible rotation. Based on the model put forward by Carlson[32,33], the maximum stable growth rate was found to be determined by the flow velocity at the growing interface. Therefore direct seed rotation is preferred over crucible rotation as it allows more direct control of the fluid flow at the growth interface. However, during the early stage of a crystal growth experiment, the seed crystal may be too small to provide efficient homogenization of the bulk solution. If crucible rotation is not implemented, natural-convection-induced temperature oscillations may affect the initial growth of the seed crystal. As the growth is most unstable when the crystal is small (i.e. for the same ***bulk*** supersaturation)[33], ways to suppress natural convections at this early stage should be implemented.

Recently, there has been an increasing interest in applying the ACRT to TSSG. Since its invention, ACRT has recieved wide acceptance amoung crystal growers. Its uncanny ablility to homogenize the bulk solution has now been well documented[34,35]. The technique has also been applied to other areas, such as the Bridgeman growth method[36] and greatly improved results were reported. In this technique, the crucible rotation is periodically accelerated and decelerated. The amplitude and period of the acceleration/deceleration cycle are typically ~±10-60 rpm and ~0.5-10 minutes. The mixing effect in ACRT is due to the ensuing spiral

shear flow and Eckman flow as the crucible is being accelerated and decelerated. Details of ACRT can be found in reference [1,9,34-35].

Progress in this area is primarily in the detailed understanding of the ACRT process in the TSSG configuration. Experimental and computer simulations of the hydrodynamics of ACRT in TSSG have been carried out by Rappl et. al.[37] and Mihelcic et. al.[38]. From these investigations, it can be concluded that ACRT can indeed provide effective bulk homogenization in additon to the mixing due to unidirectional seed rotation. It is perhaps safe to conclude also that there exists a region of applicability (i.e. within the ACRT amplitude-period parameter space) beyond which either inefficient mixing or hydrodynamic instability sets in. As these analyses were based on simplified thermal bouncary conditons that were different from those found in typical TSSG experiments, care must be exercised in the use of these results. Simulation experiments using more realistic boundary conditions were reportedly under investigation[38].

Results on the hydrodynamic simulation of TSSG in the *absence* of crucible rotation has been reported by Nikolov and coworkers[39]. The same authors have also investigated the effect of hydrodynamic on the defect structures of TSSG grown YIG crystals[40].

3) Novel designs in TSSG apparatus: The size and complexity of a TSSG apparatus depend very much on the characteristics of the crystal-solvent system as well as on the size and quality of the crystal needed. In general, the more unfavorable the growth characteristics (e.g. spurious nucleation, compositional inhomogeneity, low solubility....etc), the more sophisticated the apparatus must be. Design schematics of several TSSG apparatuses have been reported[16,17,31,41,42].

Two particularly noteworthy technological implementations of TSSG were reported recently. In 1986, Xing and coworkers[16] reported the successful implementation of boule weighing in TSSG for the development of large $KNbO_3$ crystal. By keeping the crystal pulling rate constant and *manually* adjusting the cooling rate, very good diameter control was demonstrated. It was also reported that the boule weighing apparatus facilitated the seeding process by allowing direct monitoring of the growth and dissolution of the seed crystal immediately after its insertion into the melt.

Another significant innovation was reported by Bordui et. al.[17]. In their experiment, a heat pipe furnance with liquid sodium as the heat conducting medium was used to provide a high degree of spatial temperature uniformity in the central region of the furnance cavity. It was reported that the heat pipe furnance successfully reduced the natural buoyancy-driven convection to a negligible level thoughout the entire 230 ml melt volume. Such a high degree of temperature uniformity should prove invaluable for controlling spurious nucleations in

solutions that have a narrow Ostwald-Miers zone. The high efficiency of the heat pipe furnance[43] may also prove to be important in the scaling of the TSSG process. Increased application of the heat pipe furnance to the growth of bulk crystals from TSSG and other methods can be expected.

In summary, we have briefly discussed here issues that are important in the design of TSSG experiments and reviewed some advances in the growth of bulk crystals using the high temperature top-seeded solution growth technique. These advances have recently led to the successful commercial production of large single crystal of several promising nonlinear optical crystals including KTP, β-BaB_2O_4 and $KNbO_3$. In the next section, we shall discuss, as a specific example, the growth and characterization of the recently discovered β-BaB_2O_4 crystal.

III. Crystal Growth and Characterization of β-BaB_2O_4 :-

The existence of a high and a low temperature phase of crystalline barium metaborate was first discovered by Levin and McMurdie[1] in 1949. Wier and Schroeder[2] obtained the far infrared spectra (5-20μm) of the two phases and proposed the planar six-membered boron-oxygen ring $(B_3O_6)^{3-}$ as a viable structural building block for barium metaborate. This was later confirmed by the X-ray measurement of Mighell, Perloff and Block[3], who determined the crystal structure of the high temperature phase barium metaborate.

The possibility of obtaining large second order polarizability in the planar boroxol ring $(B_3O_6)^{3-}$ was first recognized by Chen[4] in 1979. He argued that analoguous to the large nonlinearities obtainable from the benzene ring of organic crystals, there should be a large nonlinearity associated with materials that have the $(B_3O_6)^{3-}$ ring as a structural unit. It was reasoned that due to the large difference in the electronegativity of boron and oxygen, crystals with the planar boroxol ring structural units should be transparent further into the ultraviolet than its organic counterparts, making it particularly attractive for the frequency doubling of visible radiation. Systematic investigations by Chen and coworkers[5-8] subsequently led to the discovery and growth of the new nonlinear optical crystal β-BaB_2O_4.

In this section, we review the growth and characterization of β-BaB_2O_4. Discussion on crystal growth will be based on work reported by Jiang et. al.[8] and on crystal growth experiments carried out in our laboratory. The optical characteristics of β-BaB_2O_4 will be summarized and several applications of the crystal will also be discussed.

Crystal Growth:-

Direct Czochralski growth of barium metaborate yields the high temperature (α) phase crystal belonging to *R* 3c group. Second order nonlinear optical effect is not possible in the α-phase due to the inversion symmetry. The crystal undergoes a structural phase-transition at ~925°C upon cooling, to give the accentric low temperature (β) phase crystal. However, the phase change leads to severe cracking of the crystal, making it necessary to grow large single crystal β-BaB_2O_4 from a high temperature solution.

Numerous fluxes, primarily the alkali oxides and borates (e.g. Na_2O, K_2O, KBO_2, $LiBO_2$, and $NaBO_2$) and the rare earth halides ($BaCl_2$ and BaF_2), had been investigated for the growth of β-BaB_2O_4[5-8]. Jiang et. al. had concluded that the best results were obtained with the BaF_2-BaB_2O_4 and $Na_2O.BaB_2O_4$-BaB_2O_4 systems. Liebertz and Stahr[9] had also reported the growth of small β-BaB_2O_4 crystals from $Na_2B_4O_7$ flux. The details on their growth experiments, however, were not available.

The experimental determination of the liquidus curves and the Ostwald-Miers zone for the BaF_2-BaB_2O_4, $BaCl_2$-BaB_2O_4 and $Na_2O.BaB_2O_4$-BaB_2O_4 systems are given in reference [8]. The applicability of these systems to the growth of large single crystals of β-BaB_2O_4 are also briefly discussed there. Interested readers should consult the original reference for details. In what follows, we shall discuss experiments carried out in our laboratory for the growth of large β-BaB_2O_4 crystals.

Like Jiang and coworkers, we adopted the TSSG technique (see section II) since it is not possible to separate the flux from the β-BaB_2O_4 crystals by chemical etching at room temperature. All crystal growth experiments were carried out in two top-seeded solution growth apparatuses which are similar to the system described by Elwell and coworkers[10]. We have used both the $Na_2B_2O_4$-BaB_2O_4 and the $Na_2O.BaB_2O_4$-BaB_2O_4 systems in our experiments. Although it was possible to obtain small crystals from both of these systems, we found that under similar growth conditions, large transparent crystals were more readily grown from the Na_2O flux. Crystal boules grown from the $Na_2B_2O_4$-BaB_2O_4 system were plagued with small inclusion spots. Microscopic examination revealed a densely pitted growth interface which may be responsible for the observed inclusions. In contrast, the $Na_2O.BaB_2O_4$-BaB_2O_4 system produced crystals with glassy surfaces and very few inclusions. We therefore concluded that Na_2O is the preferred high temperature solvent for the

growth of β-BaB_2O_4. The theoretical yield of the $Na_2O.BaB_2O_4$-BaB_2O_4 system is given in figure 2. The curve was obtained from the phase diagram reported in reference [8]. A melt composition of ~68%:32% = BaB_2O_4:$Na_2O.BaB_2O_4$ was used in our experiments in order to keep the liquidus temperature below the phase transition temperature of the crystal.

Seed crystals were obtained by spontaneous nucleation on a platinum cold finger. A temperature oscillation technique[11] was used to limit the number of nuclei formed. These experiments typically yielded thin crystal boules (~2mm x 40mm in diameter) with fairly large clear regions. Crystal plates of up to ~1cm^2 x 1-2 mm were obtained this way. They were statistically sampled to determine the optimal seeding orientation. It was reasoned that the large crystal plates were formed from nucleii which had a favorable orientation with respect to the melt surface. The preferred seeding direction was found to be with the crystallographic *c* axis

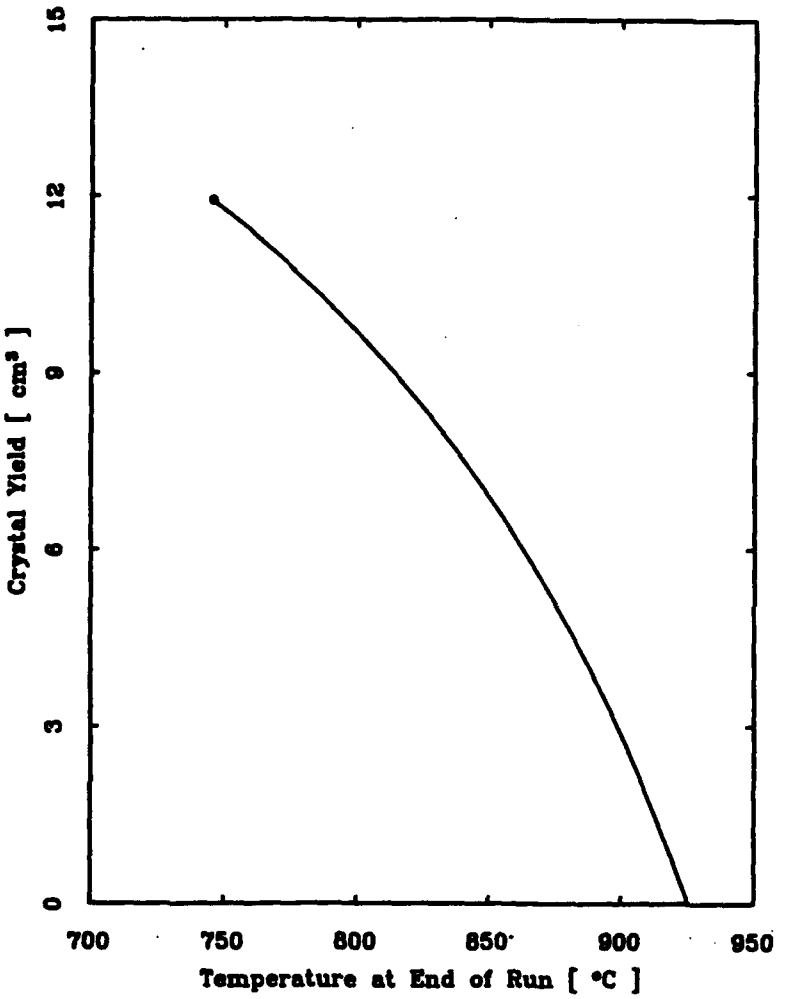

2. Theoretical yield for the $Na_2O.BaB_2O_4$-BaB_2O_4 system. The melt volume is ~ 40 ml. The plot is based on phase diagram published by Jiang et. al. and is found to be in good agreement with our experiments.

normal to the melt surface. This was later confirmed by separate seeded growth experiments (below). It is possible that the method used here to determine the optimal seeding direction may also be applicable to the development of other crystals, especially ones which exhibit a strong anisotropy in growth habits.

The typical growth experiment goes as follows: the starting materials (in powder form) are melted into the crucible in several batches. The melt is homogenized at ~50°C above the

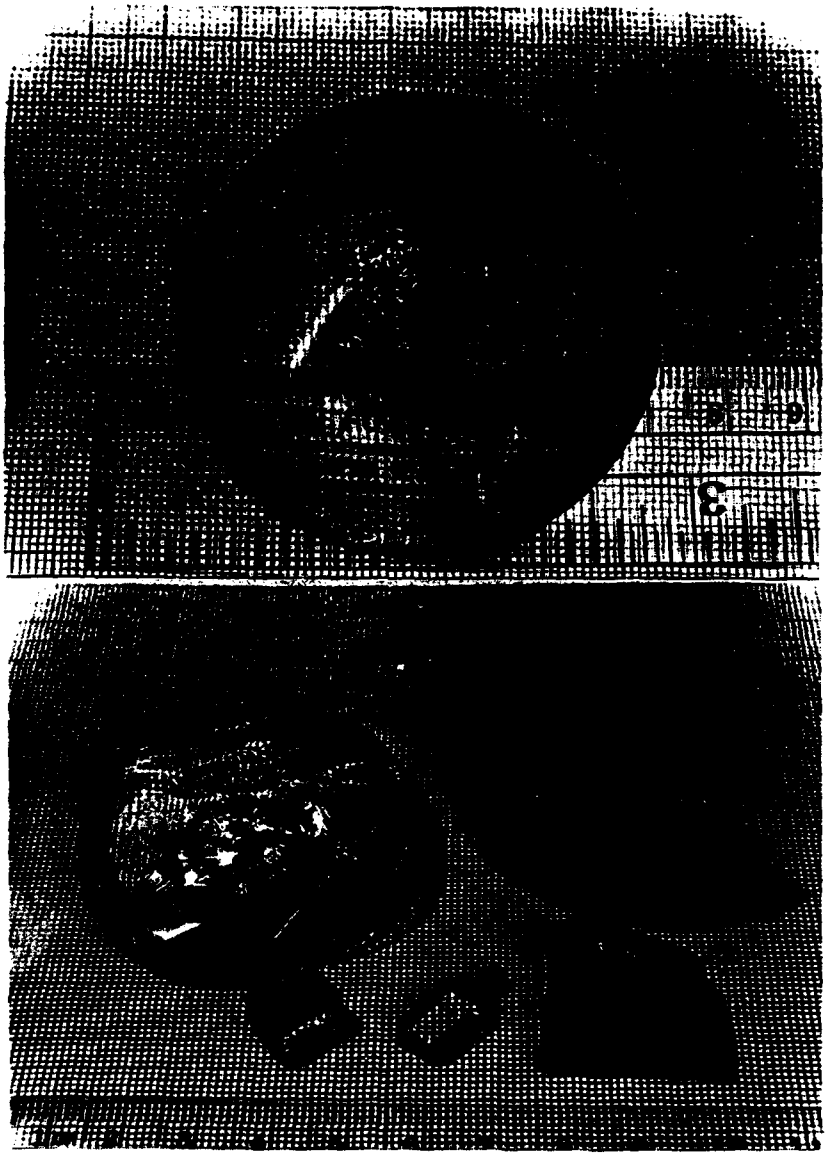

3. β-BaB_2O_4 crystals grown in our laboratory. (Top) The boule shown is 15mm thick with a central inclusion region of ~1-2mm thick. The dark spots are solidified flux attached to the bottom of the boule. (Bottom) -- The translucent appearance of the crystal shown in the upper right hand corner was due to moisture damage of the surface. We observed a long term (~months) surface degradation when the crystal was exposed to a hot and humid environment. The effect is negligible under conditions typical to an optics laboratory.

liquidus temperature for ~ 12-36 hours before seeding. The seed is allowed to come into contact with the melt at a temperature slightly higher than the liquidus temperature to allow the slight dissolution of the seed. The temperature of the system is then reduced in a programmed manner to induce growth. We chose not to submerge the seed entirely so that the growth can be monitored visually throughout the experiment (see section II). At the end of the growth run, the boule is drawn out of the melt by a puller mechanism and slowly cooled to room temperature. Typical crystal boules obtained are shown in figure 3. Crystal boules of up to 15 mm x 60 mm diameter have been produced in our laboratory. Figure 4 is a 10x magnification of the top surface of a typical β-BaB_2O_4 crystal boule. Inspite of the absence of large and well defined crystal facets in β-BaB_2O_4, figure 4 demonstrates that some degree of layered growth clearly exists.

To check the validity of the published phase diagrams, careful measurement of the melt temperature was made in several growth runs such that the experimental crystal yield can be compared to the theoretical crystal yield given above. Table 4 summarizes the results of these experiments. Our results are in better agreement with the phase diagram given by Jiang et. al.[8] than with that given in reference [5]. The small disagreements between our data and the predicted values is likely due to the the uncertainty in the melt temperature measurements and material lost to melt supersaturation at the end of the growth runs.

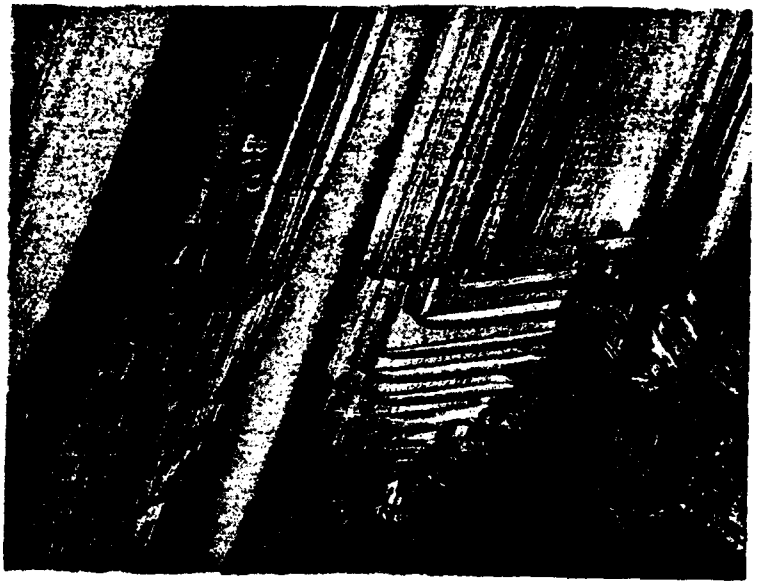

4. Evidence of layered growth observed on the top surface of the as grown β-BaB_2O_4 boule. The bunching of the growth steps at the lower right hand corner is believed to be due to the the depletion of nutrients as the meniscus recedes from the top surface of the boule. Marker represents 200 μm.

Table 4: Crystal yield based on the phase diagram of BaB_2O_4 - $Na_2O.BaB_2O_4$: -

Run #	Growth Range [°C]	Expected yield [cm^3]	Actual yield [cm^3]
011	902 –> 839	5.0	5.2
014	885 –> 825	4.3	4.6
012	893 –> 790	6.7	6.1
015	905 –> 775	8.5	8.7

Growth experiments with the seed oriented at 0°, 40° and 90° (angle between the *c* axis and the melt normal) were carried out to determine the optimal seed orientation and to test the validity of the statistical approach mentioned above. We found unambiguously that the 40° and 90° seeding led to substantially more inclusions and cracks under similar growth conditions. For the 90° seeding run, the cracks were highly parallel and were normal to the *c* axis. This is in agreement with the presence of a cleavage plane normal to the $[00\bar{0}1]$ direction[1,12]. Cleavage planes that are ~45° to the *c* axis have also been observed.

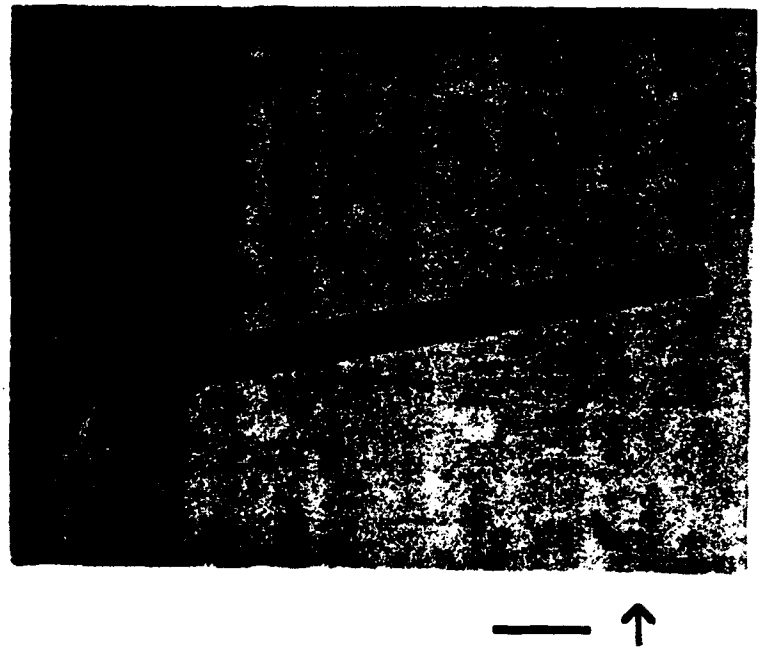

5. A needle-shaped crystal grown under spontaneous growth conditions. The flat ends are due to the $[00\bar{0}1]$ cleavage. The polar axis is in the long direction. Marker represents 200 μm.

Very strong growth anisotropy was observed under spontaneous growth conditions. In this case, β-BaB_2O_4 crystallizes in the form of weakly facetted long needles with the *c* axis in the long direction (see figure 5). Under controlled growth conditions, the crystals do not form any growth facets. This suggests that the interfacial attachment impedance is small compared to the mass transport or thermal transport impedance. Crystal boules shown in figure 3 have the *c* axis normal to the plane of paper. Microscopic examination of the shallow flaw region (~1-2mm thick) at the center of the boule revealed highly regular trigonal pyramids buried under uncontrolled growth. We speculate that these facets are the $\{11\bar{2}1\}$ faces. The presence of the uncontrolled growth made a direct measurement difficult. The cause of the central flaw region is believed to be due to the poor stirring at the center of the boule and the increased melt viscosity at low temperature.

At least two types of inclusions were observed: flux inclusion and bubble inclusion. These are shown in figure 6 and 7 respectively. The flux inclusions are observed near the outer edge (a ~ 2mm thick ring) of the boule. These inclusions were found to be parallel around the entire circumference of the disc-like boule. As one moves along the circumference, the nail-shaped inclusions (5-top) transform into boomerang shapes (5-bottom) and then back to nail shapes which are mirror images of the original ones. This strong trigonal pattern correlates very well with the trigonal pyramid facets observed above. The formation of these inclusions could be attributed to the increased radial temperature gradient and the larger temperature fluctuations near the edge of the crucible.

Figure 7 is a picture of a single layer of small bubbles trapped at the bottom of a crystal boule. The trapping is thought to be due to the interruption of stirring at the end of the growth run. Similar trapping of inclusions has been observed by Scheel and Elwell[13]. The bubbles are believed to be CO_2 formed from trace amounts of unreacted starting material. Regions immediately above these bubbles were found to be virtually bubble free, suggesting that the crystal grows in a way that efficiently rejects the trapping of these flaws[14]. Isolated bubbles have also been seen in the crystal bulk near the center of the boule.

As discussed in section II, the efficiency of solvent rejection by the growing crystal is determined by the chemical difference (e.g. in the ionic radii and the valencies) among the solvent and solute ions. The solvents listed at the beginning of this section all have valencies different from β-BaB_2O_4, that is, they are either alkali oxides/borates or barium halides. The significance of this solvent selection rule was very well demonstrated by the impurity contents in our β-BaB_2O_4 crystals. The metal impurities that are present in the melt and in the crystal are shown in Table 5. Inspite of the high concentration of the Na^+ in the melt (Na^+ is a major constituent in the $Na_2O.BaB_2O_4$-BaB_2O_4 system), only ~100 ppm were detected in the final

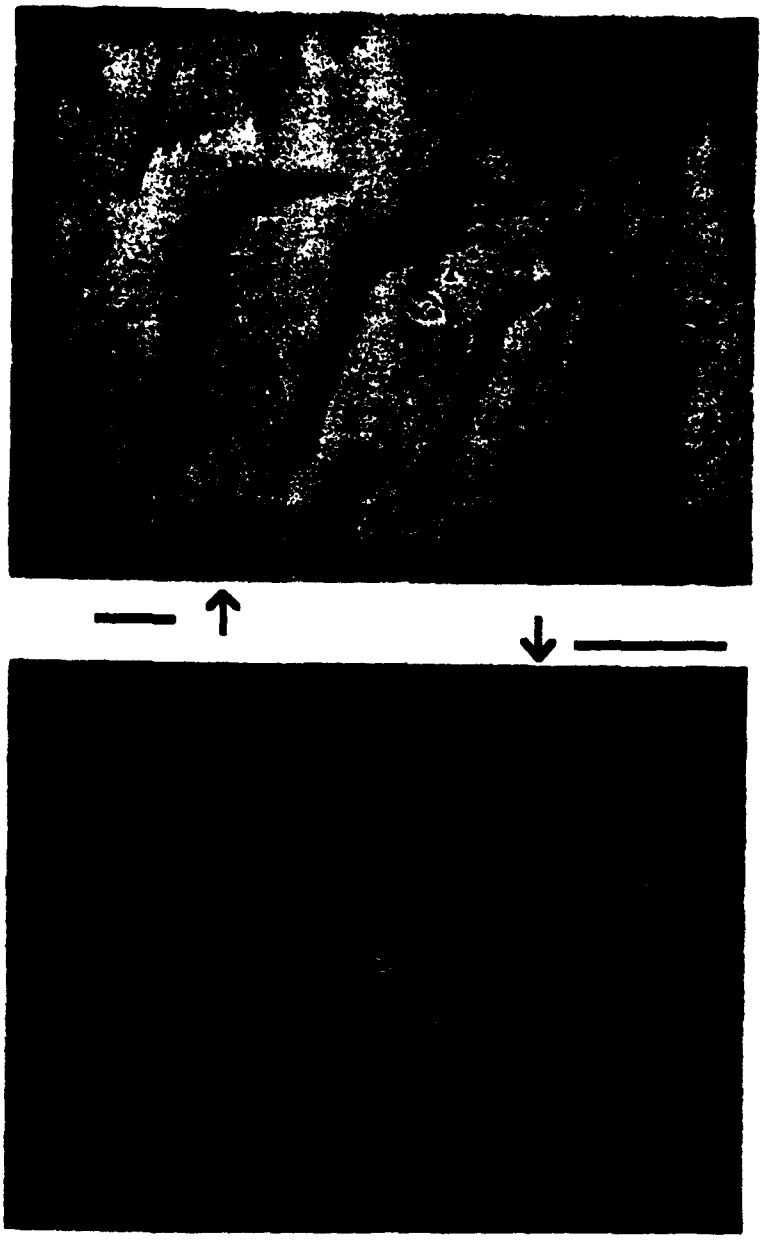

6. Nail-shaped (top) and boomerang-shaped (bottom) flux inclusions observed near the edge of the boule. See text for discussion. Marker represents 200 μm.

crystals. This is in contrast to the divalent cations (Ca^{2+} and Sr^{2+}) which have a partition coefficient of near unity for their incorporation into the crystals. We did not observe any change in the properties of our crystals due to the presence of these impurities.

Our crystal growth experiments indicate that β-BaB_2O_4 possesses many favorable growth characteristics. Large optical quality crystals can be readily grown using the $Na_2O.BaB_2O_4$-BaB_2O_4 system. Crystals obtained from different growth runs show identical physical properties and we found no evidence of any inherent compositional inhomogeneity.

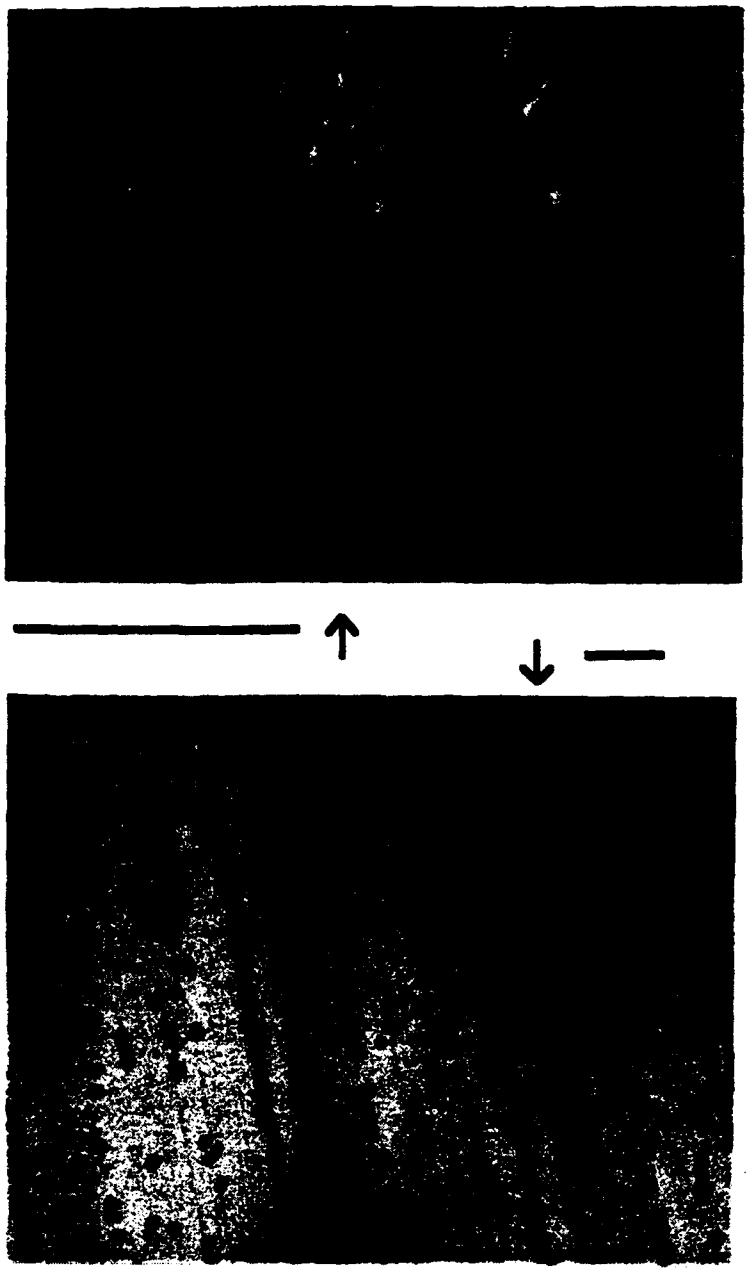

7. Bubble inclusions observed near the bottom surface of the crystal boule. This single layer of bubbles was trapped due to the interruption of stirring at the end of the growth run. Marker represents 200 μm.

Optimization of the growth parameters should allow the elimination of the few microscopic inclusions currently present in our crystals.

The largest crystal that can be cut from our crystal boules is ~ 1 cm^3. This is primarily limited by the thickness of the disc-like boules. To obtain crystals with longer interaction length, it is necessary to produce β-BaB_2O_4 crystal boules with a more favorable aspect ratio. Jiang et. al.[8] had reported that diameter control could not be accomplished by increasing the

Table 5: Incorporation of cationic impurities into β-BaB_2O_4 crystals. With the exception of Na^+ in the melt, all concentrations are in [ppm] :-

Impurities	conc. in melt	conc. in crystal
Na^+	9.05% (solvent)	95
Ca^{++}	118	123
Sr^{++}	917	292

radial temperature gradient as it led to unstable growth. Despite this observation, the problem of increasing the thickness of the β-BaB_2O_4 boule hardly appears insurmountable, especially when it is compared to the problems encountered in the growth of other nonlinear materials (e.g. $KNbO_3$)[15,16]. The technology for the growth of β-BaB_2O_4 is still in its infancy and there is certainly much room for future advances. The challenge for the crystal grower will be to find a timely solution to this problem and give β-BaB_2O_4 a competitive edge over other new nonlinear optical materials that are currently being discovered at a rapid pace.

Properties of β-BaB_2O_4 :-

The physical properties of β-BaB_2O_4 crystals have been studied by several groups using crystals grown by the Jiang et. al.[8] Experiments performed on our crystals gave results which are in excellent agreement with the literature values. We can therefore treat these crystals as identical. In this section, we briefly summarize the important physical properties of β-BaB_2O_4. More detailed information can be found in references [12] and [17].

β-BaB_2O_4 belongs to point group *R* 3c. The crystal structure consists of layers of planar boroxol $(B_3O_6)^{3-}$ rings stacked perpendicular to the *c* -axis, with the barium ions sandwiched between these layers. A depiction of this arrangement is shown in figure 8. The crystal is mechanically hard and the surfaces can be readily polished by standard polishing techniques. It is chemically inert to most common organic solvents and is virtually non-hygroscopic. Dielectric coatings can be applied directly onto the polished crystal surfaces. The crystal is

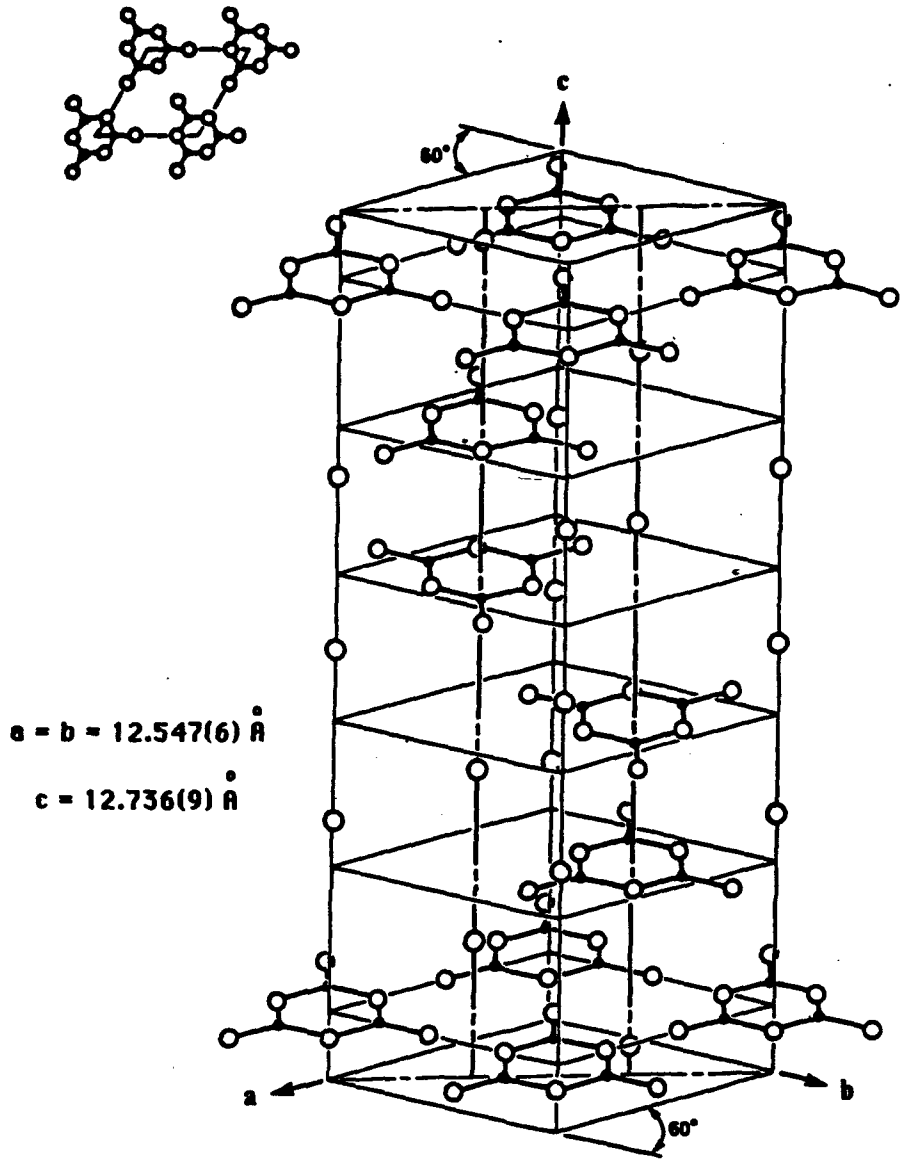

8. Crystal structure of β-BaB_2O_4. (After Eimerl et. al.[12].)

stable up to ~900°C and has a fracture temperature an order of magnitude higher than other nonlinear materials.

β-BaB_2O_4 is optically negative uniaxial and is highly transparent between 0.2-2.2 μm. The absolute UV and IR cutoffs for the ordinary wave are at 190 nm and 3.28 μm respectively. The transmission spectrum for the ordinary wave is shown in figure 9. The currently accepted Sellmeier equations are:

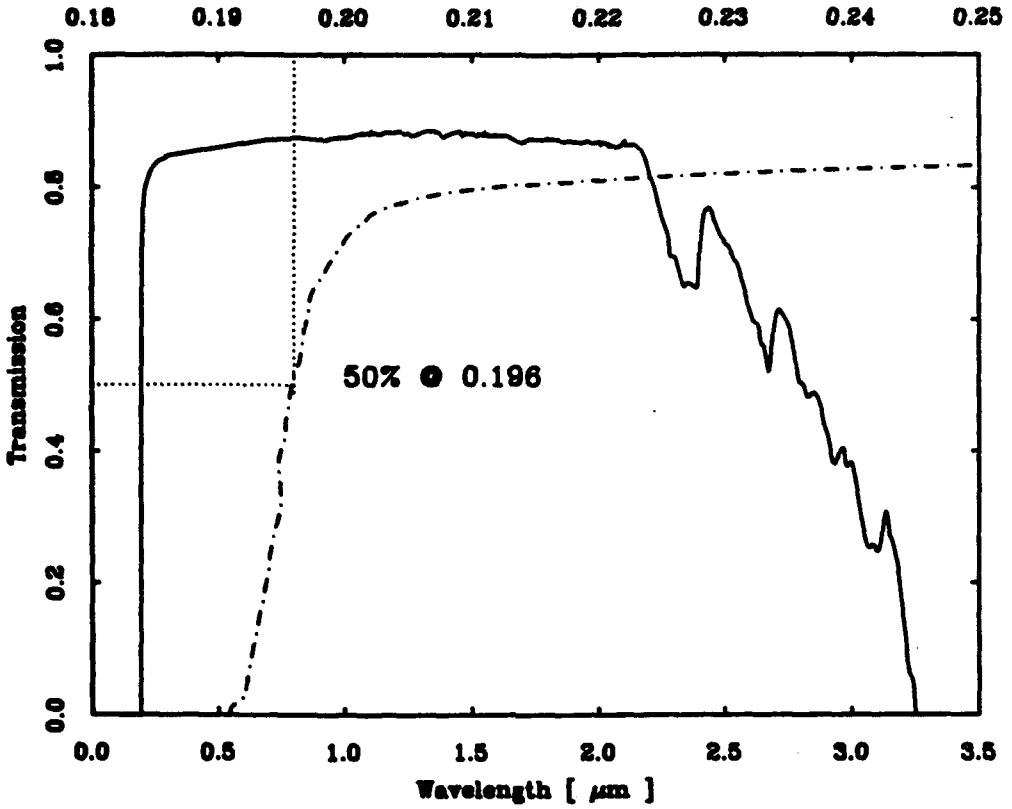

9. Transmission spectrum for the ordinary wave through a ~3 mm thick β-BaB_2O_4 crystal. The dotted lines is a 50 x magnification of the UV cutoff (see upper scale).

$$n_e^2 = 2.3730 + \frac{0.0128}{(\lambda^2 - 0.0156)} - 0.0044\lambda^2$$

and

$$n_o^2 = 2.7405 + \frac{0.0184}{(\lambda^2 - 0.0179)} - 0.0155\lambda^2$$

These equations were obtained by fitting refractive indices between 0.4-1.0 μm. Using these equations, fairly accurate prediction of the SHG and OPO tuning curves can be made in the 0.2-2.0 μm spectral region. It is possible that beyond 2.5 μm, the IR resonant contribution to the refractive indices may become important and a simple quadratic IR correction term in the Sellmeier equations may not be sufficient. Figure 10 shows the type I and type II second harmonic tuning curves for β-BaB_2O_4. The predicted tuning curves for the β-BaB_2O_4 optical parametric oscillator pumped with the 2nd, 3rd and 4th harmonics of Nd^{3+}:YAG laser are given in figure 11. Calcuated tuning curves for other nonlinear optical processes using the Sellmeier equations have been given by Eimerl and coworkers[12] who has also investigated the thermo-optical properties of β-BaB_2O_4.

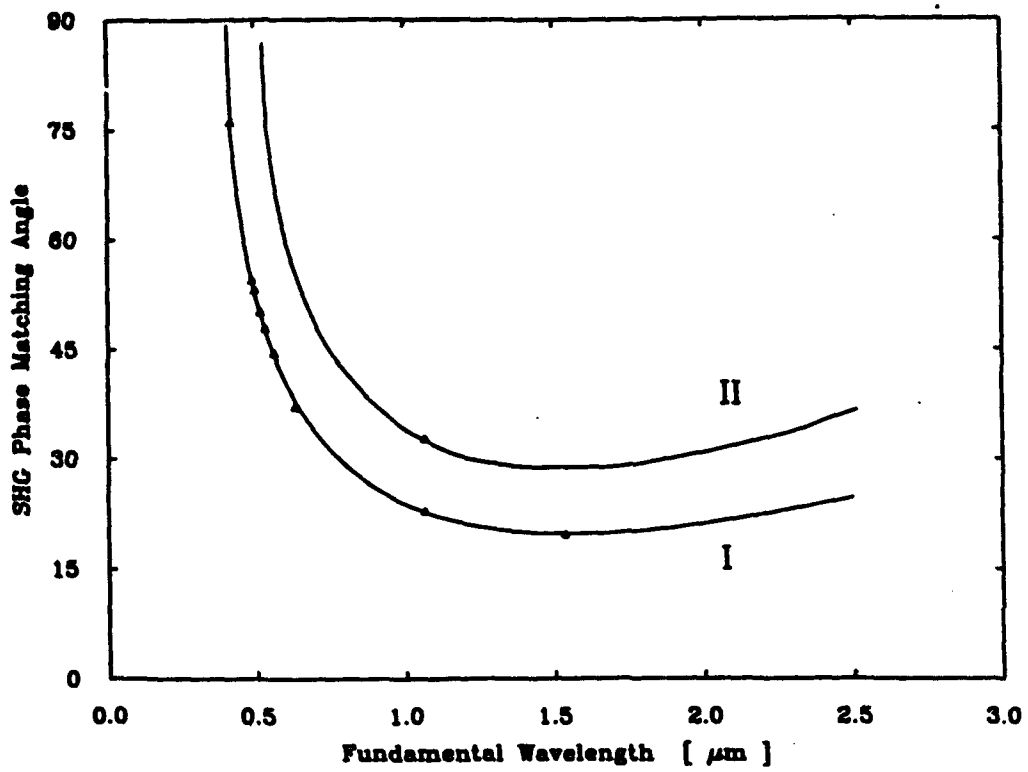

10. SHG tuning curves for β-BaB_2O_4. The data was taken with crystals grown in our laboratory. The solid lines are predictions based on published Sellmeier equations[12]. The agreement is excellent, indicating that our crystals are identical to that grown by Jiang et. al.[8].

In the *R* 3c space group, the effective nonlinear optical coefficient, d_{eff}, is given by[18]:

$$d_{eff} = d_{15}\sin\theta + d_{22}\cos\theta\sin 3\varphi \qquad \text{(Type I, } o + o \rightarrow e\text{)},$$

and

$$d_{eff} = d_{22}\cos^2\theta\cos 3\varphi \qquad \text{(Type II, } o + e \rightarrow e\text{)}$$

Here, θ is the polar angle (i.e. phase matching angle) and φ is the azimuthal angle measured with respect to the piezoelectric x axis. φ is normally chosen to maximize the d_{eff} for the interaction. The standard convention (x perpendicular to mirror plane) is used in defining the piezoelectric axes (see section I). For any three wave mixing process, the phase matching angle with type I interaction is always smaller than with type II. It then follows that in β-BaB_2O_4, type I interaction always has a larger effective nonlinearity than type II. The $\cos\theta$ dependence of d_{eff} in β-BaB_2O_4 represents a major disadvantage when the crystal is used as a UV generator. In principle, a crystal with moderate d_{ij}'s (say ~ $0.5 \times d_{22}(\beta\text{-}BaB_2O_4)$) that do

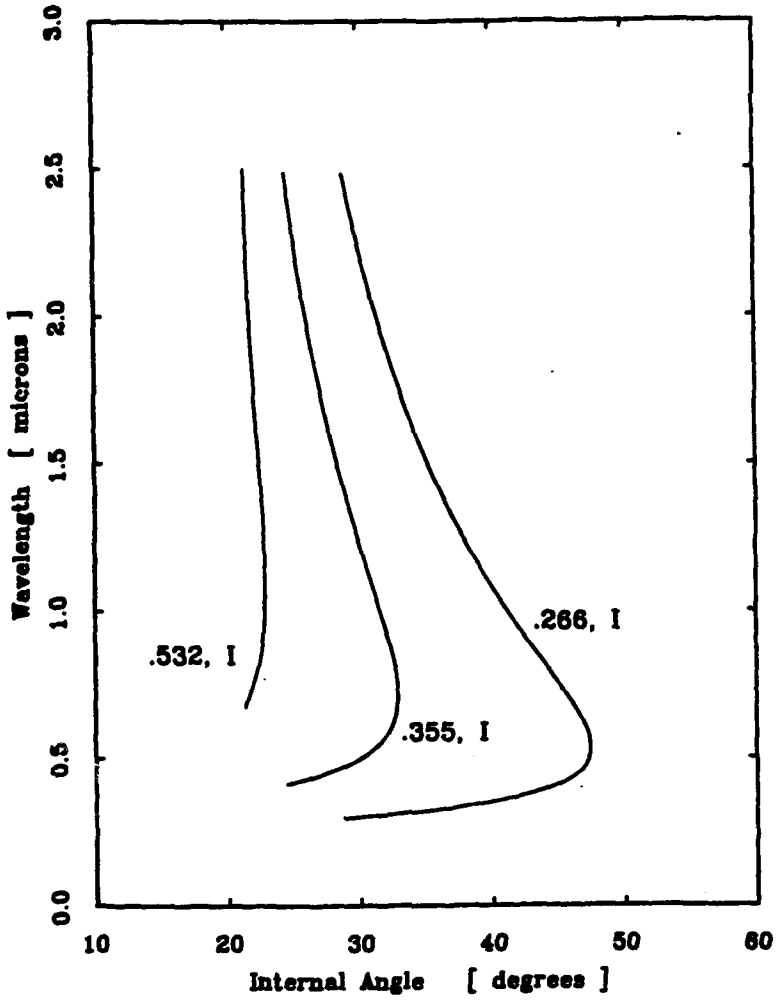

11. Type I OPO tuning curves pumped by the 2nd, 3rd, and 4th harmonics of the Nd^{3+}:YAG. The 2nd and 3rd harmonics (@ ~0.375 and ~0.250 μm respectively) of the alexandrite (Cr^{3+}:$BeAl_2O_4$) laser can also be used to pump the β-BaB_2O_4 OPO instead.

not vanish at 90° (e.g. ~sinθ) can compete favorably with β-BaB_2O_4 provided that it has the UV transparency and is sufficiently birefringent.

A one-shot-per-site damage threshold of 13.5 J/cm^2 was measured using 1 nanosecond pulses at 1.06μm[12]. The damage threshold was found to be dependent on crystal quality (such as inclusions and thermal stress), typically a factor of 2 or 3 times lower for poor quality crystals. The damage threshold at 532 nm had been reported to be ~7 GW/cm^2 with 250 psec pulses. It is unclear if the damage threshold can be further increased by improvement in crystal quality.

β-BaB_2O_4 also holds promise in electro-optic applications[19]. The relevant linear

electro-optic coefficients are listed in Table 6. Although the electro-optic effect in β-BaB_2O_4 is small compared with KD*P, its high fracture temperature makes it the preferred material in high average electric power applications where possible thermally induced crystal damage must be avoided[19,20].

As discussed in section I, a nonlinear crystal must satisfy many criteria in order for it to be practically useful. β-BaB_2O_4 is a good example where its excellent physical properties have proved to be more important than its nonlinearity. Paricularly important are its broad transparency, large birefringence, high damage threshold and resistance to thermally induced crystal fracture. So far, experiments on the β-BaB_2O_4 crystals have primarily exploited its UV transparency. These experiments include frequency doubling of pulse dye-lasers[21], generation of the various harmonics of the Nd^{3+}:YAG laser[17] and the frequency doubling of the Cu vapor laser[22]. The advantage of β-BaB_2O_4 in high average optical power frequency conversion had recently been demonstrated where up to 1 W average output power at 266 nm was obtained[23]. Other applications, such as the optical parametric oscillator and the frequency doubling of ultrashort pulses, should also benefit from the use of β-BaB_2O_4. We are currently investigating these applications.

Table 6: Electro-optic coefficients ($x10^{-12}$m/V) for β-BaB_2O_4 at 632.8nm.

$\|r_{ij}$'s$\|$	Experimental value
r_{22}	2.5
r_{61}	2.5
$r_{13}-(n_e/n_o)^3 r_{33}$	0.055
r_{11}	<0.04

The success of the β-BaB_2O_4 crystal tends to undermine the significance of extending the "molecular engineering" approach to inorganic materials[24]. The possibility of obtaining large optical nonlinearity in inorganic borates opens up a new class of materials which is particularly promising for the development of novel crystal suitable for the generation of deep UV light. The strong coulombic interaction in an ionic solid such as the borates typically provides better mechanical properties over organic molecular crystals. On the other hand, the coulombic interaction also makes the "engineering" of new nonlinear material much more difficult, as it is

impossible to predict if a boron-oxygen structural unit, which is responsible for the large nonlinearity, will be preserved in a specific crystal. Nevertheless, Chen et. al.[25] had examined the various anionic structural units commonly found in inorganic borates and classified them by their microscopic nonlinear susceptibilities. Such a classification serves as a useful qualitative guideline for the otherwise random search for new nonlinear crystals of the borate type. Table 7 presents several anionic structural units which are particularly promising.

Table 7: The calculated microscopic second order susceptibilities (in 10^{-31} esu.) for anionic boron-oxygen groups commonly found in the borates. (After reference [25]) :-

Anionic groups	$(BO_3)^{3-}$	$(B_2O_5)^{4-}$	$(B_3O_6)^{3-}$	$(B_3O_7)^{5-}$	$(B_3O_8)^{7-}$
χ_{ijk}	χ_{111}=0.64 χ_{122}=-0.64 χ_{133}=0	χ_{222}=0.33 χ_{223}=-1.02 χ_{333}=1.04	χ_{111}=1.59 χ_{122}=-1.59 χ_{133}=0	χ_{111}=-2.93 χ_{122}=0.82 χ_{133}=-0.63	χ_{111}=0.29 χ_{122}=1.26 χ_{133}=0.47
e.g.	$LiCd(BO_3)$, $YAl_3(BO_3)_4$		β-BaB_2O_4	LiB_3O_5*	

* The structure of LiB_3O_5 is a three dimensional network of interconnecting $(B_3O_5)_\infty$ chains[26]. The (B_3O_7) 'group' is formed by the sharing of two oxygen atoms among neighboring (B_3O_5) groups. Chen has discussed the difficulty in relating the calculated χ_{ijk}'s to the macroscopic SHG coefficients in this crystal[24].

To date, the second order nonlinear optical effect has been observed in at least six borate crystals, including β-BaB_2O_4, $YAl_3(BO_3)_4$, $Nd_xY_{1-x}Al_3(BO_3)_4$, LiB_3O_5, $LiCd(BO_3)$ and $KB_5O_8.4H_2O$. Although several of these materials have excellent UV transparency, they also possess undesirable properties which reduce their effectiveness as frequency converters into the UV. However, the chemistry of boron-oxygen compounds is rich[26] and the possibility of synthesizing new borate compounds has hardly been explored. It is therefore likely that systematic investigation of the borates will lead to other novel nonlinear crystals with properties that are suitable for general as well as specialized applications.

Outlook and Summary :-

Recent Developments :-

Significant advances in the development of nonlinear optical materials can be divided into three different areas: 1) the discovery of new nonlinear materials; 2) the growth of promising materials; and 3) the modification of material characteristics of existing crystals.

1) New nonlinear materials. Besides β-BaB_2O_4, many promising nonlinear optical crystals were also discovered recently. These included *l* -arginine phosphate (LAP) and its chemical analogs[1,2], lithium triborate[3] (LiB_3O_5), DAN[4], NPP[5], COANP[6], POM[7] and a host of other organic crystals. Particularly attractive are the LAP analogs, which were found to have large nonlinearity, broad transparency, high damage threshold and favorable growth characteristics. As the crystal is grown from low temperature solution, the growth of LAP is in principle scalable and the application of the technology developed in the growth of large KDP crystals and the urea crystals should be possible. Further development of these new nonlinear crystals will undoubtedly lead to a broader application of nonlinear optical devices.

2) Growth of nonlinear optical materials: Many crystals, such as $KNbO_3$, KTP, Tl_3AsSe_3, and $AgGaSe_2$ have long been recognized as attractive nonlinear materials. Their practical applications, however, have been severely hindered by growth related problems. Significant progress has been made in the development of these materials, particularly for the chalcopyrites and KTP.

As seen in table 2 of section I, KTP is phase-matchable from ~0.5-4.5 μm. Due to its high damage threshold and visible-near IR transparency, it represents the only known material which can be used for the generation of high peak power radiation in the near IR. Although commercially available KTP crystals are currently being grown hydrothermally, there is an increased interest in the growth of KTP by the HTSG technique. This is due to the improved optical characteristics of flux grown KTP crystals (e.g. the suppression of the OH- absorption at ~2.8μm, higher damage threshold and lack of domain formations), the faster growth rate and the lower cost of production. Careful investigation of the growth properties of KTP from the $KTiOPO_4$-KPO_3-$K_4P_2O_7$ system by Jacco et. al.[8] and Bordui et. al.[9] has led to the sucessful commercial developments of flux grown KTP. Equally important is the work by Ballman et. al.[10] who have discovered a nonviscous tungstate flux ($3K_2WO_4.P_2O_5$) which holds much promise for the growth of large KTP crystals. An interesting feature of the

KTP-$3K_2WO_4.P_2O_5$ system is its large growth zone, thereby allowing very high theoretical crystal yield if the method of slow cooling is used to induce crystal growth.

As discussed in section I, KTP has a low threshold power P_{th}~0.05MW due to its "quasi-NCPM" property. Using the reported bulk damage threshold[11] of ~300MW/cm^2 for hydrothermally grown KTP crystals, we get: [damage threshold] / [threshold power /cm^2] = $[\Gamma_{max}\text{-cm}^2]/[P_{th}]$ = 6,000. This should be compared with the same ratio for KDP[12] $[\Gamma_{max}\text{-cm}^2] / [P_{th}] \sim 5 / 0.067 \sim 75$, indicating that even hydrothermally grown KTP offers an overwhelming advantage over KDP for the doubling of 1.06μm light. The hydrothermal growth technique is potentially scalable (as it utilizes thermal gradient transport), and large homogeneous crystal can, in principle, be grown from it. This scalability is well demonstrated by the hydrothermal systhesis of large α-quartz crystals. So far, the extreme conditions[13] (~600°C and 30 kpsi) needed for the hydrothermal growth of KTP have made it difficult and expensive to scale the production process to larger volume. Recently, Laudise and coworkers[13] have demonstrated that K_2HPO_4 can be used as an effective mineralizer to reduce the severity of the growth conditions (~400-600°C and 10 kpsi). Jia and coworkers[14] had also reported the successful use of KF as a mineralizer to grow KTP under conditions that are comparable to those used for the production of quartz crystals. These developments should lead to an increased interest in the hydrothermal synthesis of KTP, especially in the production of large single crystals.

For infrared materials, the growth of large single crystals of Tl_3AsSe_3 (Ø25mm x 60mm) has been reported[15]. Coversion efficiency of up to ~28% has been demonstrated using these crystals in the frequency doubling of a Q-switched CO_2 laser[15]. Equally significant is the successful development of post growth processing techniques[16,17] which allows the fabrication of large optical quality chalcopyrite crystals that are suitable for optical device applications. Optical parametric oscillators using the $AgGaSe_2$ crystals have been demonstrated[18], providing fully tunable radiation in the ~3-9 μm range. The device holds much promise as a convenient tunable high power source in the infrared where few high power lasers are available.

3) Improvements of material properties: The concept of improving or modifying the characteristics of a nonlinear optical crystals is not new. For many crystals of the solid-solution type, it is possible to affect changes in certain material properties, such as the birefringence and transparency, by selecting an appropriate composition of the various

elements in the crystals[19]. The most significant recent developments in this area are the improvement of the optical damage resistance in $LiNbO_3$ and KDP. It is now well established that the optical damage resistance of $LiNbO_3$ can be significantly improved by doping the crystal with a small amount of MgO[20]. A two order of magnitude increase in the photorefractive damage threshold has been observed for crystal with > 4.5% MgO concentration[20]. An improved optical damage resistance has also been observed recently in KDP, though the increase in the damage threshold is less dramatic. It was found that by vigorously eliminating trace organic impurities in the growth solution, the damage threshold of KDP can be as high as 20 J/cm^2 (compared to ~ 7-8 J/cm^2 of a typical KDP crystal)[21]. It should be noted that both $LiNbO_3$ and KDP are backed by very well developed crystal growth technology, and the improvement of their physical properties is therefore particularly attractive.

Conclusion :-

In this paper, we have discussed the optical characterization of nonlinear optical materials. We outlined the material properties which are particularly desirable for the construction of six different types of nonlinear optical devices. Based on these considerations, we conclude that the practical application of nonlinear optics in frequency conversion requires the development of a wide range of materials with different characteristics. In our discussion, we have placed particular emphasis on the need to include other non-optical properties, such as the mechanical and thermal properties and especially the crystal growth properties, in the evaluation of a new nonlinear optical material. As three very promising inorganic crystals, namely $KNbO_3$, KTP and β-BaB_2O_4, are currently being grown by the high temperature top-seeded solution growth technique, we reviewed some recent developments directly related to this growth technology. As an example, we discussed the properties, optical and non-optical, of the β-BaB_2O_4 crystals and evaluated its usefulness as a frequency converter for the six different device applications considered. Finally, we surveyed some recent progress in the development of nonlinear optical materials that are suitable for frequency conversion applications. It is obvious from this survey that significant future advances can be anticipated in the development of attractive nonlinear optical devices. The practical realization of these devices will undoubtedly create new opportunities in scientific research and industrial applications.

Acknowledgments :- This work was supported by the Naval Research Laboratory and in part by the National Science Foundation through the Materials Science Center of Cornell University.

References :-

Introduction :-

1. P.A.Franken, A.E.Hill, C.W.Peters and G.Weinrich, Phys. Rev. Lett., 7, 118 (1961).
2. Y.X.Fan, R.C.Eckardt, R.L.Byer, R.K.Route and R.S.Feigelson, Appl. Phys. Lett., 45, 313 (1984).
3. K.Cheng, M.J.Rosker and C.L.Tang, in: Topics in Applied Physics, vol 59, L.F. Mollenauer and J.C.White, eds., pp 209-233, Spriing-Verlag (1986).
4. C.Chen, B.Wu, A.Jiang and G.You, Sci. Sin. Ser. B, 28, 235 (1985).
5. D.Xu, M.Tiang and Z. Tan, Acta Chim. Sinica, 2, 230 (1983).
6. J.Zyss and D.S.Chemla, in: Nonlinear Optical Properties of Organic Molecules and Crystals, vol 1, D.S.Chemla and J.Zyss, eds., pp 146-159, Academic Press (1987).
7. P.Gunter, Ch.Bosshard, K.Sutter, H.Arend, G.Chapuis, R.J.Twieg and D.Dobrowolski, Appl. Phys. Lett., 50, 486 (1987).
8. J.-C.Bumert, R.J.Twieg, G.C.Bjorklund, J.A.Logan and C.W.Dirk, Appl. Phys. Lett., 51, 1484 (1987).
9. C.Chen, Y.X.Fan, R.C.Eckardt and R.L.Byer, Proc. SPIE 684, 12 (1987).
10. J.-C.Bumert,F.M.Schellenberg, W.Lenth, W.P.Risk and G.C. Bjorklund, Appl. Phys. Lett. 51, 2192 (1987).
11. Y.S.Luh, M.M.Feijer, R.L.Byer and R.S.Feigelson, J. Crystal Growth, 85, 264 (1987).
12. W.Wang,Q.Zou,Z.Geng and D.Feng, J. Crystal Growth, 79, 706 (1986).
13. D.Feng, N.Ming, J.Hong, Y.Yang,J. Zhu, Z.Yang and Y. Wang, Appl. Phys. Lett., 37, 607 (1980).
14. D.S.Chemla and J.Zyss, eds., Nonlinear Optical Properties of Organic Molecules and Crystals, vol 1 & 2, Academic Press (1987).
15. B.C.Grabmaier and F.Otto, J. Crystal Growth, 79, 682 (1986).
16. N.B.Singh, T.A.Gould and R.H.Hopkins, J. Crystal Growth, 78, 43 (1986).
17. R.K.Route, R.S.Feigelson and R.J.Raymakers, J. Crystal Growth, 24/25, 390 (1974).
18. P.Bordui, J. Crystal Growth, 85, 199 (1987).
19. R.A.Laudise, in: Crystal Growth and Characterization, R. Ueda and J.B.Mullin, eds., North-Holland Publishing Co., (1975).

Section I :-

1. S.Singh, in: *CRC* Handbook of Laser Science and Technology, vol 4, Optical Materials, Part 1, M.J.Weber, ed., pp.3-228, CRC Press (1986).
2. D.S.Chemla,J.L.Oudar and J.Jerphagnon, Opt.Commun., **18**,54 (1976).
3. A.A.Ballman, R.L.Byer, D.Eimerl, R.S.Feigelson, B.J.Feldman, L.S.Golberg, N.Menyuk and C.L.Tang, Appl. Opt. **26**, 224 (1987).
4. D.Eimerl, J. Quant. Elect. **QE-23**, 575 (1987).
5. See reference [3] in **introduction**.
6. W.Koechner, Solid-State Laser Engineering, Springer-Verlag (1976).
7. A.Yariv, Quantum Electronics, 2nd. ed., John Wiley & Sons (1975).
8. D.Eimerl, L.Davis, S.Velsko, E.K.Graham and A.Zalkin, J.Appl. Phys. **62**, 1968 (1987).
9. S.K.Kurtz and T.T.Perry, J. Appl. Phys., **39**, 3798 (1968).
10. F.A.Jenkins and H.E.White, Fundamental of Optics, 4th. ed., McGraw Hill (1976).
11. M.V.Hobden and J.Warner, Phys. Lett., **22**, 243 (1966).
12. Standards on Piezoelectric Crystals, Prcc. IRE, p. 1378 (1949).
13. M.V.Hobden, J. Appl. Phys., **38**, 4365 (1967).
14. M.Born and E.Wolf, Principles of Optics, 6th ed., Pergamon Press (1983).
15. H.Ito, H.Naito, H.Inaba, J. Appl. Phys. **46**, 3992 (1975).
16. D.Y.Stepanov, V.D.Shigorin and G.P.Shipulo, Sov. J. Quantum. Electron., **14**, 1315 (1975).
17. P.D.Maker, R.W.Terhune, M.Nisenoff and C.M.Savage, Phys. Rev. Lett., **8**, 21 (1962).
18. J.J.Wynne and N.Bloembergen, Phys. Rev., **188**, 1211(1969).
19. R.L.Byer and S.E.Harris, Phys. Rev. **168**, 1064 (1968).
20. A.J.Campillo and C.L.Tang, Appl. Phys. Lett. **16**, 242 (1970).
21. S.K.Kurtz: in Quantum Electronics: A Treatise, H.Rabin and C.L.Tang, eds., Vol 1, Part A, Academic Press (1975).
22. D.Eimerl, Ferroelectrics, **72**, 95 (1987).
23. N. Bloembergen, Appl. Optics, **12**, 661 (1973).
24. N. Bloembergen, IEEE J. Quantum Electron., **QE-10**, 375 (1974).
25. J.D.Bierlein and F.Ahmed, Appl. Phys. Lett., **51**, 1322 (1987).

26. J.E.Midwinter, J. Appl. Phys., 39, 3033 (1968).

27. R.L.Byer, J.F.Young and R.S.Feigelson, J. Appl. Phys., 41, 2320 (1970).

28. R.L.Byer in: Quantum Electronics: A Treatise, H.Rabin and C.L.Tang, eds., Vol 1, Part A, Academic Press (1975).

29. J.C.Walling, in: Topics in Applied Physics, vol 59, L.F. Mollenauer and J.C.White, eds., pp. 331-398, Spriing-Verlag (1986).

30. S.Singh, D.A.Draegert and J.E.Geusic, Phys. Rev. B, 2, 2709 (1970).

31. Y.S.Liu, L.Drafall, D.Dentz and R.Belt, G.E. Technical Information Series Report, 82CRD016, Feb. (1982).

32. M.J.Rosker and C.L.Tang, J. Opt. Soc. B, 2, 691 (1985).

33. R.L.Fork, C.V.Shank, R.Yen and C.A.Hirlmann, IEEE J. Quantum Electron., QE-19, 500 (1983).

34. W.H.Knox, M.C.Downer, R.L.Fork and J.P.Gordon, Opt. Lett., 9, 552 (1985).

35. S.A.Akmanov, A.I.Kovrygin and A.P.Sukhorukov, in: Quantum Electronics: A Treatise, H.Rabin and C.L.Tang, eds., Vol 1, Part B, Academic Press (1975).

36. S.A.Akmanov, A.S.Chirkin, K.N.Drabovich, A.I.Kovrygin, R.V. Khokhlov and A.P.Sukhorukov, IEEE J. Quantum Electron., QE-4, 589 (1968).

37. J.Feinberg, in: Optical Phase Conjugation, R.Fisher ed., Academic Press (1984).

38. See reference [7] and [8] in introduction.

39. Y.Uematsu, Jap. J. Appl. Phys., 13, 1362 (1974).

40. P.Gunter, Appl. Phys. Lett., 34, 650 (1979).

41. W.Xing, H.Looser, H.Wuest and H.Arend, J. Crystal Growth, 78, 431 (1986).

42. D.Shen, Mat. Res. Bull., 21, 1375 (1986).

43. T. Fukuda and Y.Uematsu, Jap. J. Appl. Phys., 11, 163 (1972).

44. See reference [15] in introduction.

45. D.A.Bryan, R.Gerson and H.E.Tomaschke, Appl. Phys. Lett., 44, 847 (1984).

46. G.Zhong, J.Jian and Z.Wu, 11th International Quantum Electronics Conference, IEEE Cat. No. 80 CH 1561-0, June 1980, p.631.

47. Y.Nishida, A.Yokotani, T.Sasaki, K.Yoshida, T.Yamanaka and C.Yamanaka, Appl. Phys. Lett., 52, 420 (1988).

48. See reference [9] in introduction.

49. A. Jiang, F.Cheng, Q.Lin, Z.Cheng and Y.Zheng, J. Crystal Growth 79, 963 (1986).

50. P.Bordui, in: Crystal Growth of $KTiOPO_4$ from High Temperature Solution, Ph.D Thesis, Massachusetts Institute of Technology (1987).

51. Information Sheet on $KTiOPO_4$, Ferroxcube, Division of Amperex Electronic Corp., Saugerties, New York (1987).

52. P.Bordui, J.C.Jacco, G.M. Loiacono, R.A.Stolzenberger and J.J.Zola, J. Crystal Growth, 84, 403 (1987).

53. F.C.Zumsteg,J.D.Bierlein and T.E.Gier, J. Appl. Phys., 47, 4980 (1976).

54. R.A.Laudis, R.J.Cava and A.J.Caporaso, J. Crystal Growth, 74, 275 (1986).

55. S.Jia, P.Jiang, H.Niu, D.Li and X.Fan, J. Crystal Growth, 79, 970 (1986).

56. L.K.Cheng, unpublished.

57. See reference [6] in introduction.

Section II :-

1. H.J.Scheel, Prog. Crystal Growth and Charact., 5, 277 (1982).

2. G.A.Bennett, J. Crystal Growth, 3/4, 458 (1968).

3. W.Tolksdorf, J. Crystal Growth, 3/4, 463 (1968).

4. B.M.Wanklyn, in: Crystal Growth, B.R.Pamplin ed., Ch. 7, Pergamon (1975).

5. D.Elwell, in: Crystal Growth and Characterization, R.Ueda and J.B.Mullin eds., pp. 165-173, North-Holland (1975).

6. D.Elwell, in: Crystal Growth, B.R.Pamplin ed., Ch. 6, Pergamon (1975).

7. H.J.Scheel and E.O.Schulz-DuBois, in: Convective Transport and Instability Phenomena, J.Zierep and H.Oertel Jr. eds., pp.491-513, Braun-Verlag (1982).

8. V.A.Timofeeva, in: Growth of Crystals, E.I.Givargizov ed., vol 13, pp.239-250, Consultant Bureau, New York (1986).

9. D.Elwell and H.J.Scheel, Crystal Growth from High-Temperature Solutions, Academic Press (1975).

10. W.K.Burton, N.Cabrera and F.C.Frank, Phil. Trans. A, 243, 299 (1951).

11. P.Bennema, J. Crystal Growth, 1, 278 & 287 (1967).

12. P.Bennema and G.H.Gilmer, in Crystal Growth: an introduction, P.Hartman ed., Ch. 10, pp. 263 North-Holland, Amsterdam (1973).

13. W.J.P.van Enckevort, Prog. Crystal Growth and Charact., 9, 1 (1984). See figure 36.

14. W.A.Tiller, K.A.Jackson, J.W.Ruter and B.Chalmers, Acta Metall., 1, 428 (1953).

15. H.J.Scheel and P.Gunter, J. Crystal Growth, 65, 541 (1983).

16. See reference [41] in section I.

17. See reference [52] in section I.

18. L.K.Cheng, W.Bosenberg and C.L.Tang, J. Crystal Growth, submitted Jan. 1988.

19. B.Donaldson, The Growth of Urea Crystals for Use in an Optical Parametric Oscillator, Ph.D Thesis, Cornell University (1984).

20. W.Tolksdorf, in: 1976 Crystal Growth and Materials, E.Kaldis and H.J.Scheel eds., pp.639-659, North-Holland (1977).

21. W.Torksdorf, B.Strocka and F.Welz, J. Crystal Growth, 65, 549 (1987).

22. D.Elwell, in: Crystal Growth and Characterization, R.Ueda and J.B.Mullin eds., pp. 155-163, North-Holland (1975).

23. K.Fischer, Kristall Tech., 14, 835 (1979).

24. P.Gornert, J. Crystal Growth, 52, 88 (1981).

25. K.Fischer, D.Linzen and E.Sinn, Phys. Status Solidi (a), 55, K75 (1979).

26. B.M.Wanklyn, J. Crystal Growth, 65, 533 (1983).

27. B.M.Wanklyn, J. Crystal Growth, 37, 334 (1977).

28. B.M.Wanklyn, J. Crystal Growth, 43, 336 (1978).

29. See reference [18] in introduction.

30. R.D.Dawson, D.Elwell and J.C.Brice, J. Crystal Growth, 23, 65 (1974).

31. L.N.Bezmaternykh, V.G.Mashchenko, N.A.Sokolova and V.L. Temerov, J. Crystal Growth, 69, 407 (1984).

32. A.Carlson, in: Growth and Perfection of Crystals, R.Doremus, B.Roberts and D.Turnbull eds., John Wiley & Sons (1958).

33. H.J.Scheel and D.Elwell, J. Crystal Growth, 12, 153 (1972).

34. E.O.Schulz-DuBois, J. Crystal Growth, 12, 81 (1972).

35. H.J.Scheel, J. Crystal Growth, 13/14, 560 (1972).

36. P.Capper, J.J.Gosney and C.L.Jones, J. Crystal Growth, 70, 356 (1984).

37. H.O.Rappl, F.M.Ferraz, H.J.Scheel,R.X.Barros and D.Schiel, J. Crystal Growth, 70, 49 (1984).

38. M.Mihelčić, C.Schroeck-Pauli, K.Wingerath, H.Wenzl, W.Uelhoff and A.van der Hart, J. Crystal Growth, 53, 337 (1981).

39. P.Peshev, V.Nikolov and K.Iliev, J. Crystal Growth, 65, 173 (1983).

40. V.Nikolov, K.Iliev and P.Peshev, J. Crystal Growth, 75, 269 (1986).

41. D.Elwell, P.Capper and M.D'Agostino, J. Crystal Growth, 29, 263 (1975).

42. K.Oka and H.Unoki, Jap. J. Appl. Phys., 23, L770 (1984).

43. C.A.Busse and C.Bassani, in: Temperature, Its Measurement & Control in Science and Industry, J.F.Schooley ed., Vol. 5, part 2, pp.1265-1273, American Institute of Physics, New York (1982).

Section III :-

1. E.M.Levin and H.F.McMurdie, J. of Research NBS, **42**, 131 (1949).
2. C.E.Weir and R.A.Schroeder, J. of Research of National Bureau of Standards, **68A**, 465 (1964).
3. A.D.Mighell, A.Perloff and S.Block, Acta Crystallogr., **20**, 819 (1966).
4. C.Chen, B.Wu, A.Jiang and G.You, Sci. Sin., Ser. B **28**, 235 (1985) and reference therein.
5. Q.Huang and J.Liang, Acta Phys. Sin. **30**, 559 (1981).
6. Q.Huang, G.Wang and J. Liang, Acta Phys. Sin. **33**, 76 (1984).
7. Q.Huang and G.Wang, Acta Phys. Sin. **34**, 562 (1985).
8. See reference [49] in **section I.**
9. J.Liebertz and S.Stahr, Z Kristallogr., **165**, 91 (1983).
10. See reference [41] in **section II.**
11. See reference [6] in **section II.**
12. See reference [8] in **section I.**
13. See reference [9] in **section II**, Ch. 6, p.246.
14. See reference [1] in **section II.**
15. See reference [42] in **section I.**
16. See reference [41] in **section I.**
17. See reference [9] in **introduction.**
18. F.Zernike and J.E.Midwinter, Applied Nonlinear Optics, John Wiley & Sons(1973).
19. H.Nakatani, W.Bosenberg, L.K.Cheng and C.L.Tang, Appl. Phys. Lett., **52**, 1288 (1988).
20. D.Eimerl, IEEE J. Quantum Electron., QE-**23**, 2238 (1987).
21. K.Miyazaki, H.Sakai and T.Sato, Opt. Lett. **11**, 797 (1986).
22. G.Zhang, C.Jin and F.Lin, Acta Optica Sinica, **4**, 513 (1984).
23. K.C.Liu and M.Rhoades, **ThA2**, Conf. on Lasers and Electro-Optics, Technical Digest, Baltimore, Maryland, April 1987.
24. C.Chen and G.Liu, Ann. Rev. Mater. Sci., **16**, pp.204-243 (1986).
25. C.Chen, Y.Wu and R.Li, Chinese Phys. Lett., **2**, 389 (1985).
26. H.Konig and R.Hoppe, Z. anorg. Chem., **439**, 71 (1978).

27. Mellor's Comprehensive Treatise on Inorganic and Theoretical Chemistry, Vol. 5, Part A, Longman (1980).

Outlook and Summary :-

1. See reference [5] in **introduction.**

2. S.B.Monaco, L.E.Davis, S.P.Velsko, F.T.Wang, D.Eimerl and A.Zelkin, J. Crystal Growth, **85**, 252 (1987).

3. See reference [24] in **section III.**

4. See reference [8] in **introduction.**

5. I.Ledoux, J.Zyss, A.Migus, J.Etchepare, G.Grillon and Antonetti, Appl. Phys. Lett., 48, 1564 (1986).

6. See reference [7] in **introduction.**

7. J.Zyss, I.Ledoux, R.B.Hierle, R.K.Raj, and J.-L.Oudar, IEEE J. Quantum Electron., QE-21, 1286 (1985).

8. J.C.Jacco, G.M.Loiacono, M.Jaso, G.Mizell and B.Greenberg, J. Crystal Growth, **70**, 484 (1984).

9. See reference [52] in **section II** .

10. A.A.Ballman, H.Brown, D.H.Olson and C.E.Rice, J. Crystal Growth, **75**, 390 (1986).

11. See reference [31] in **section I.**

12. See reference [8] in **section I.**

13. See reference [54] in **section I.**

14. See reference [55] in **section I.**

15. R.Auyeung, D.Zielke and B.Feldman, **TUH3**, Conf. on Lasers and Electro-Optics, Technical Digest, Baltimore, Maryland, April 1987.

16. H.Matthes, R.Viehmann and N.Marshall, Appl. Phys. Lett., **26**, 237 (1975).

17. R.K.Route, R.S.Feigelson, R.J.Raymakers and M.M.Choy, J. Crystal Growth, **33**, 239 (1976).

18. R.C.Eckardt, Y.X.Fan, R.L.Byer, C.L.Marquardt, M.E.Storm and L.Esterowitz, Appl. Phys. Lett., **49**, 608 (1986).

19. See for example: J.C.Mikkelsen, Jr. and H.Kildal, J. Appl. Phys., **49**, 426 (1978).

20. See reference [45] and [46] in **section I.**

21. See reference [47] in **section I.**

THE AUTHORS

L. K. CHENG

L.K.Cheng was born on June 25, 1960 in Hong Kong. He received the B.S. degree in chemistry from Boston University, Boston, Massachusetts,USA., in 1982, the M.S. degree in applied physics from Cornell University, Ithaca, New York, U.S.A., in 1986 and is currently working towards his Ph. D. degree in applied physics at Cornell University. His current interests include the development of nonlinear optical materials and the use of these materials in practical device applications.

W. R. BOSENBERG

W.R.Bosenberg was born on Aug. 27, 1962 in New Jersey, U.S.A. He received the B.S. degree in physics in 1984 from Rensselaer Polytechnic Institute, Troy, New York, U.S.A.and the M.S. degree in applied physics from Cornell University, Ithaca, New York, U.S.A. He is currently pursuing his Ph. D. degree in the field of applied physics in Cornell University, concentrating on nonlinear-optics.

C. L. TANG

C.L.Tang received the B.S. degree from the University of Washington, Seattle, Washington, U.S.A., in 1955, the M.S. degree from California Institute of Technology, Pasadena, California, U.S.A., in 1956, the Ph.D. degree from Harvard University, Cambridge, Massachusetts, 1960, and as a John Parker Traveling Fellow from Harvard, he also studied at the Technical University, Aachen, Germany, during 1959-1960.

He was a Staff Member and later Principal Research Scientist at the Research Division of Raytheon Company,
Waltham, Massachusetts, U.S.A., from 1960-1964. He has been on the faculty of Cornell University, Ithaca, New York, U.S.A., since 1964 where he is the Spencer T. Olin Professor of Engineering.

Dr. Tang is a Fellow of the Optical Society of America, the American Physical Society and the Institute of Electrical and Electronic Engineers. He is a member of the National Academy of Engineering.

Appendix B

Journal of Crystal Growth 108 (1991) 394–398
North-Holland

Growth of large, high-quality beta-barium metaborate crystals

W.R. Bosenberg, R.J. Lane and C.L. Tang

Materials Science Center, Cornell University, Ithaca, New York 14853, USA

We report recent results of growth experiments that increase the size and quality of beta-barium metaborate crystals suitable for optical applications. Crystals of length 15–23 mm have been produced using large melt volumes and oriented seeds. Decreasing the cooling rate of the solution from 3.7 to 1.5°C/day has dramatically reduced the density of inclusions in the grown material. The results of various growth experiments involving techniques aimed at improving crystal size and quality are discussed.

1. Introduction

Since its discovery, beta-barium metaborate (β-BaB_2O_4, BBO) has established itself as an outstanding nonlinear optical frequency conversion/electro-optical material. Its broad transparency range, large birefringence, large nonlinear coefficient, high optical damage threshold, and excellent mechanical and chemical properties have made it unquestionably the material of choice for ultraviolet frequency conversion (second harmonic generation (SHG) of visible light [1–4] and ultraviolet pumped optical parametric oscillation (OPO) [5–11]) as well as for high average power electro-optic switching (Q-switching of lasers) [12,13]. A number of different solution growth techniques (top-seeded-solution-growth [14–17] and immersion seeding [16]) and fluxes (Na_2O [14–17], B_2O_3 [16], $Na_2B_2O_4$ [14–17], $BaCl_2$ [16], NaCl [18], BaF_2 [16], Li_2O [16,19], $NaCl$–B_2O_3 [18]) have been used to grow BBO. Combining the top-seeded-solution-growth (TSSG) technique with the Na_2O flux has thus far yielded the best results. Despite the success of this growth system, the BBO boules it produces have two undesirable features. First, the boules tend to grow in the form of flat, lens-shaped disks. This characteristic boule shape is undesirable because it severely limits the size of BBO crystals that can be fabricated for optical applications. Secondly, the boules contain flux inclusions. The inclusions tend to be most heavily concentrated in the center of the boule [20] but can also be found at lower densities in other regions. The inclusions scatter transmitted light, decrease the damage threshold of the material [21], and often make the center of the boule, which also happens to be its thickest region, completely unuseable for optical applications.

Our laboratory has been actively developing the growth technology of BBO since 1986. Our early boules [17] and other reported BBO growth experiments [15,16] have suffered from both of the problematic features described above. Over the past two years, we have carried out extensive growth experiments designed to improve crystal size and quality. Here, we report the implementation of growth techniques that have resulted in the largest reported fabricated crystals and have significantly reduced the density of inclusions.

2. Techniques for increasing the size of BBO crystals for optical applications

The goal of the experiments described in this section is to increase the size of crystals for optical applications such as SHG and OPO. The size of these crystals is limited by the characteristic disc shape of the boule and the fact that the preferred boule orientation for growth is with the crystallographic c-axis normal to the solution surface [17]. As shown in fig. 1, the combination of these two

0022-0248/91/$03.50

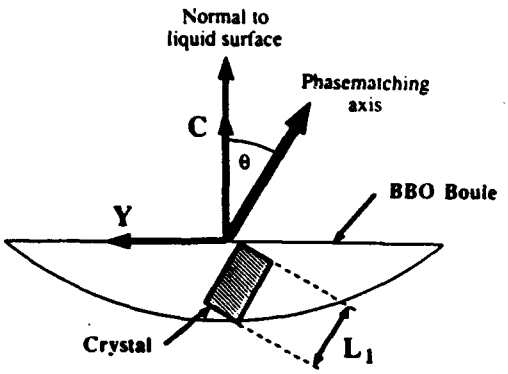

Fig. 1. The combination of the characteristic disc-like boule shape and the preferred growth orientation being with the optic axis (C) normal to the liquid surface limits the available length of BBO crystal, with phasematching angle θ, to a length of ~1 cm (L_1). The figure shows the case for type I phasematching ($o+o \rightarrow e$), where the light must travel in the crystallographic $Y-C$ plane.

factors limits the length of crystals with phasematching angle (θ) less than ~70° (which includes nearly all three-wave-mixing processes for BBO) to less than ~1 cm (L_1 in the figure) for a typical, 1.2 cm thick boule. Two possible approaches to increasing the optical interaction length L_1 include: (1) increasing the thickness of the boule and (2) altering the orientation of the growing boule by forcing growth in another direction with a properly oriented seed. Our laboratory has successfully used both of these approaches to increase fabricated crystal size. A detailed description of the growth apparatus, the starting material preparation recipe, and the basic growth technique that were used in these experiments has been reported in a previous publication [17]; here we will focus on the recently implemented techniques.

The standard TSSG technique for increasing the thickness of a crystal is boule pulling. By raising the crystal out of the solution at a rate commensurate with the growth (cooling) rate, radial growth is retarded in favor of axial growth. We chose to try this method at the outset, because it is the most straightforward and the simplest to implement. For a melt volume of ~150 ml and a cooling rate of 3.7°C/day, we empirically found that steady-state pulling rates of 1.5–2.0 mm/day were required to control the boule diameter. Pulling at these very high rates resulted in poor quality, needle-shaped growth on the bottom surface of the boule. Reduction of the pulling rate to 0.3–0.6 mm/day produced good quality growth, but failed to appreciably alter the aspect ratio of the boule. These results agree with those reported by Jiang et al [16]. Boule pulling cannot, therefore, dramatically increase the boule thickness in the TSSG/Na_2O system.

A second approach to increasing the thickness of the boule is to scale up the melt volume. Most of our growth experiments were carried out in a 150 ml crucible with a diameter of 72 mm. This system produces boules 70 mm in diameter, 12 mm thick, and weighing ~100 g. Thicker boules should be possible by increasing the melt volume and leaving the diameter of the crucible essentially the same. Since the radial growth is limited by the crucible walls, the additional material is forced to grow axially. Although simple in theory, this approach is nontrivial, since the effects of temperature fluctuation, poor melt homogenization, and unstable growth during the seeding procedure are amplified as the solution volume increases.

To test this approach, we built a TSSG system for a 600 ml crucible of 86 mm diameter. The first few boules from this system were of poor quality due to unstable growth conditions at the growth initiation point. However, boules of good quality were obtained by adjusting the standard seeding recipe to have a cooling rate of 0.75°C/day at the growth initiation point, and then increasing the cooling rate to 1.5°C/day once growth on the seed is established. A typical boule grown from the large melt volume system is shown in fig. 2; it has a diameter of 84 mm, a thickness of 18 mm, and a mass of 170 g. This boule was grown over a period of 32 days, corresponding to a temperature range of approximately 904–866°C. The growth recipe for the large melt volume system is still in the process of being fully developed. We expect that by cooling this system over a larger temperature range (915–840°C), boules 20–25 mm thick will be routinely available.

Long crystals suitable for optical applications also can be produced without increasing the boule thickness with the use of oriented seeds. Nonlinear frequency conversion processes are only efficient when phasematching is achieved, that is, when

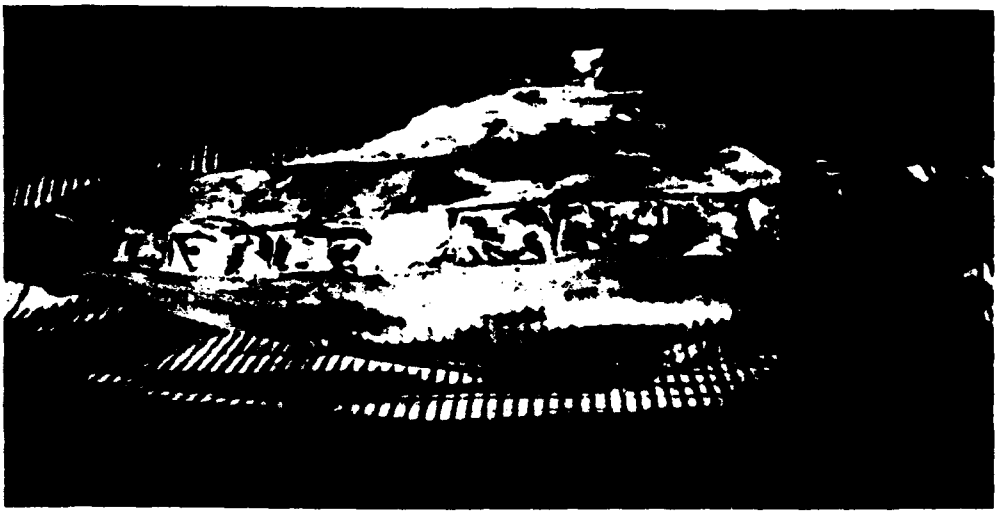

Fig. 2. Side view of a BBO boule grown from a 600 ml solution volume. This boule is 18 mm thick, has a diameter of 84 mm and weighs 170 g. Increasing the melt volume is a viable method of increasing the boule thickness.

photon energy and momentum are conserved [22]. For a given frequency conversion process, phasematching occurs when the light travels at a prerequisite angle with respect to the optic axis (called the phasematching angle, θ in figs. 1 and 3). In order for a piece of crystal to be suitable for frequency conversion, it must be cut so that light can propagate along the phasematching axis. The basic idea behind the oriented seed technique is to force the boule to grow so that the phasematching axis lies in the plane of the disc-shaped boule. This configuration is depicted in fig. 3. Note that L_2 of fig. 3 is much greater than L_1 of fig. 1, corresponding to an approximate five-fold increase in crystal length (from 1 to 5 cm). For BBO, phasematching occurs over the range $20° < \theta < 90°$ depending on the frequency conversion process, requiring that the c-axis make an angle of $0°$ to $70°$ with respect to the liquid surface normal to get the increased crystal length.

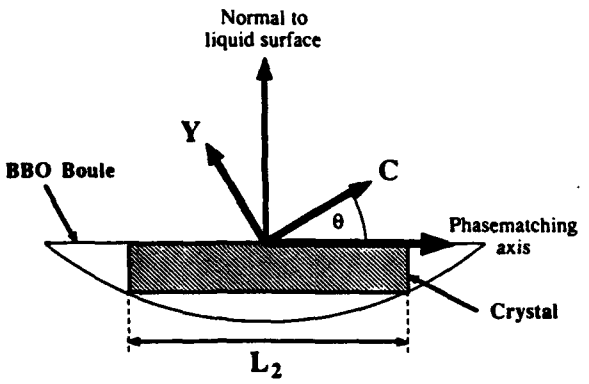

Fig. 3. Long BBO crystals can be produced by using a suitably oriented seed to force the boule to grow so that the desired phasematching axis (at phasematching angle θ with respect to the optic axis (C)) lies along liquid surface. Note that L_2 of this figure is much longer than L_1 of fig. 1, for identical boule size. We have produced fabricated optical crystals as long as 23 mm using this oriented seed technique.

In previous experiments, growth initiated with high angle seeds resulted in large scale cracking of the boules along the weak crystallographic planes [17]. However, improvements in the temperature stability of the furnace ($\pm 0.5°$C), the use higher quality seeds, and reduction of the cooling rate at the growth initiation point (from 3.7 to 0.75°C/day), has reduced the cracking to the point where suitably oriented crystals that exceed 20 mm in length are harvested routinely. Table 1 gives a summary of the characteristics of some of the oriented boules that have been grown for various optical frequency conversion applications. We are currently making adjustments in the growth recipe aimed at eliminating all cracks, so that optical crystals as long as 50 mm will soon be available.

3. Techniques for improving crystal quality

As pointed out in the introduction, BBO boules usually have regions of inclusion-type defects which decrease the optical quality of the material. The boules tend to have the highest inclusion density in the central (and thickest) part of the boule [20]. Inclusions are generally linked to unstable growth conditions, and a standard method of improving the growth stability is by mechanical stirring of the solution [23].

We have tried a variety of different stirring techniques to reduce the density of inclusions. These techniques include no rotation (convective stirring), uniform crucible rotation, accelerated crucible rotation (ACRT) [24], and uniform boule rotation, with rotation rates varying from 0 to 50 rpm. None of these techniques have produced any substantial change in crystal quality. (Though ACRT provides outstanding melt homogenization, and visual observations have indicated increased stirring efficiency [25], this has not been correlated with any noticeable improvement in crystal quality.) We have verified the negligible effect of stirring on boule quality by altering the stirring technique (i.e. switching from ACRT or uniform rotation to no rotation) in the middle of a growth run, and looking for an interface of differing crystal quality that corresponds to the change in stirring in the grown boule. No such interface has ever been observed. Stirring does not appear, therefore, to be a viable way of stabilizing the growth conditions and improving the crystal quality.

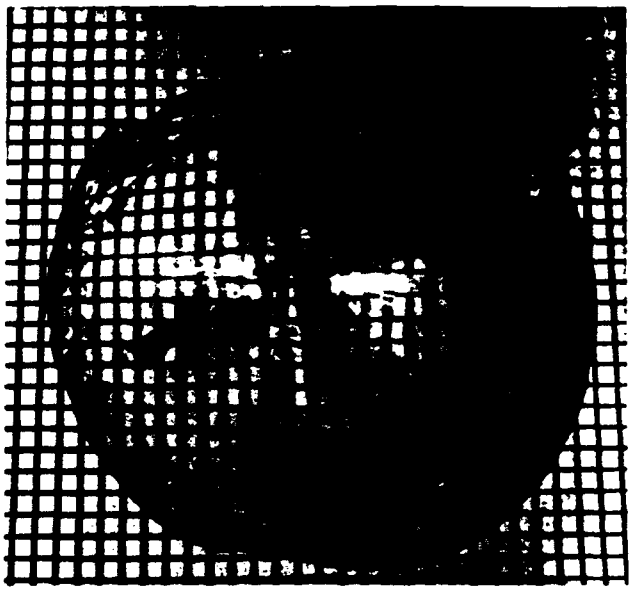

Fig. 4. High optical quality BBO boule grown at the reduced cooling rate of 1.5°C/day (150 ml solution volume). Note the clarity at the center of the boule due to the lack of inclusions. Cooling the solution at this slow rate significantly reduces the density of inclusions. The dark spots seen on the boule are solidified flux that adhered to the surface, and are easily removed during crystal fabrication.

An alternate means of stabilizing the growth is to reduce the supersaturation of the solution by decreasing the cooling rate. In our 150 ml crucible system, we have carried out growth experiments at

Table 1
Parameters of boules grown via the oriented seed technique

Boule number	Phasematching angle [a] (deg)	Boule thickness [b] (mm)	Longest piece cut [c] (mm)	Intended application
1	33.5	15	20	355 nm pumped, type I OPO [d]
2	31.6	12	23	355 nm pumped, type I OPO [d]
3	39	10	20.5	266 nm pumped, type I OPO [d]
4	44	15	15	266 nm pumped, type I OPO [d]
5	48	13	18	532 nm type I, SHG [e]

[a] Measured in type I phasematching plane ($Y-C$ plane) with respect to the optic axis.
[b] Measured near center of the boule.
[c] Measured along phasematching axis.
[d] OPO = optical parametric oscillator.
[e] SHG = second harmonic generation.

a reduced steady-state cooling rate of 1.5°C/day (compared with the previous rate of 3.7°C/day.) A typical boule grown at the reduced rate is shown in fig. 4. As can be seen in the figure, the slower cooling rate completely eliminates the high-density inclusion region in the center of the boule. This region still does contain a few isolated inclusions (~ 100 μm in size), but slower cooling rates produce a marked improvement. One obvious drawback of this approach is the increase in the length of the growth run. The boule in fig. 4 was grown over a period of 62 days compared to the usual ~ 25 days when cooling at 3.7°C/day: Nevertheless, this is the only approach that has resulted in any significant improvement in crystal quality. We are continuing the effort to improve our growth recipe and eliminate the persistent flux inclusions altogether.

4. Conclusions

We have shown that BBO crystals greater than 1 cm in length and of improved optical quality [17] can be grown using the top-seeded-solution-growth technique with the Na_2O flux. Long crystals (15–23 mm) have been obtained by scaling to larger melt volumes and using oriented seeds. Crystals with markedly lower inclusion densities have been produced using slower cooling rates (1.5°C/day for a 150 ml solution). Efforts are currently underway to optimize growth recipes that incorporate all of the described growth techniques. We believe that combining large scale melts, oriented seeds, and slow cooling rates will produce fabricated BBO crystals greater than 5 cm in length that are completely devoid of flux inclusions. The results of these ongoing experiments will be reported as they become available.

Acknowledgements

This work has been supported by the Naval Research Laboratory and the National Science Foundation through the Materials Science Center of Cornell University.

References

[1] K. Miyazaki, H. Sakai and T. Sato, Opt. Letters 11 (1986) 797.
[2] D.W. Chen and J.J. Yeh, Opt. Letters 13 (1988) 808.
[3] C. Zimmermann, R. Kallenbach and T.W. Hansch, Opt. Commun. 71 (1989) 229.
[4] D. Coutts, M.D. Ainsworth and J.A. Piper, IEEE J. Quantum Electron. QE-25 (1989) 1985.
[5] L.K. Cheng, W.R. Bosenberg and C.L. Tang, Appl. Phys. Letters 53 (1988) 175.
[6] W.R. Bosenberg, L.K. Cheng and C.L. Tang, Appl. Phys. Letters 54 (1989) 13.
[7] W.R. Bosenberg, W.S. Pelouch and C.L. Tang, Appl. Phys. Letters 55 (1989) 1952.
[8] H. Komine, Opt. Letters 13 (1988) 643.
[9] Y.X. Fan, R.C. Eckardt, R.L. Byer, J. Nolting and R. Wallenstein, Appl. Phys. Letters 53 (1988) 2014.
[10] M. Ebrahimzadeh, M. Dunn and F. Akerboom, Opt. Letters 14 (1989) 560.
[11] S. Burdulis, R. Grigonis, A. Piskarskas, G. Sinkevicius, V. Sirutkaitus, A. Fix, J. Nolting and R. Wallenstein, Opt. Commun. 74 (1990) 398.
[12] C.A. Ebbers, Proc. SPIE 968 (1988) 66.
[13] C.T. Mueller and N.D. Duong, Q-switched Nd:YAG laser operation with beta-barium borate, in: Conf. on Lasers and Electro-Optics Technical Digest, 1989 (Optical Society of America, Washington, DC, 1989) paper FE4.
[14] Q. Huang and J. Liang, Acta Phys. Sinica 30 (1981) 564.
[15] C. Chen, B. Wu, A. Jiang and G. You, Scientia Sinica B28 (1985) 235.
[16] A. Jiang, F. Cheng, Q. Lin, Z. Cheng and Y. Zheng, J. Crystal Growth 79 (1986) 693.
[17] L.K. Cheng, W. Bosenberg and C.L. Tang, J. Crystal Growth 89 (1988) 553.
[18] B.H.T. Chai, D.M. Gualtieri and M.H. Randles, Proc. SPIE 968 (1988) 69.
[19] K.H. Hubner, Neues Jahrb. Mineral. Monatsh. 335 (1969).
[20] The high density of inclusions in the central region of the boule is clearly visible in fig. 2a of ref. [17].
[21] D. Eimerl, L. Davis, S. Velsko, E.K. Graham and A. Zalkin, J. Appl. Phys. 62 (1987) 1968.
[22] F. Zernike and J.E. Midwinter, Applied Nonlinear Optics (Wiley, New York, 1973) p. 54.
[23] D. Elwell and H.J. Scheel, Crystal Growth from High Temperature Solutions (Academic Press, London, 1975).
[24] E.O. Schulz-Dubois, J. Crystal Growth 12 (1972) 81.
[25] L.K. Cheng, PhD Thesis, Cornell University, Ithaca, NY (1988) p. 54.

Appendix C

Phase-matched second-harmonic generation and growth of a LiB_3O_5 crystal

T. Ukachi,* R. J. Lane, W. R. Bosenberg, and C. L. Tang

Materials Science Center, Cornell University, Ithaca, New York 14853

Received September 23, 1991; revised manuscript received January 29, 1992

The characteristic properties of critically and noncritically phase-matched second-harmonic generation in crystalline lithium triborate (LiB_3O_5, LBO) grown in our laboratory are investigated. Angle-tuned critically phase-matched second-harmonic generation of near-infrared radiation is reported. Temperature-tuned noncritically phase-matched second-harmonic generation from 1.025 to 1.253 μm was achieved in the temperature range 190° to −3°C. Spectrum-tuned noncritical phase matching at room temperature is also achieved at 1.215 μm. Large angular, temperature, and spectral acceptance bandwidths are obtained. The details of the LBO crystal growth process are also discussed.

1. INTRODUCTION

Lithium triborate (LiB_3O_5, LBO) is a newly developed nonlinear-optical crystal that is characterized by a wide transparency range, a small birefringence, a moderate nonlinear-optical coefficient, and a high optical-damage threshold.[1,2] These unique properties, along with its mechanical hardness, chemical stability, and nonhygroscopicity, make LBO an attractive material for certain nonlinear-optical processes.[3–5] Although the relatively small birefringence in LBO tends to limit the phase-matching spectral range, it also leads to the possibility of both noncritical phase matching (NCPM) and a larger angular acceptance for frequency-conversion applications in the visible and near infrared.

For frequency-conversion applications, large angular acceptance and small walk-off are great advantages. However, under critical phase-matching conditions, the direction of energy flow of the second-harmonic (SH) wave walks off that of the fundamental wave because of the birefringence of the nonlinear medium. Also, if a focused beam is employed, because of beam divergence a part of the pump beam may not be phase matched. Walk-off and phase mismatch can sharply reduce the conversion efficiency of the second-harmonic generation (SHG) process. The use of NCPM, in which the Poynting and the wave vectors of the fundamental and the SH beams are collinear, is therefore quite advantageous because of the elimination of walk-off and the minimization of the effect of beam divergence.

Two research groups separately reported the measurements of temperature-tuned noncritically phase-matched SHG in LBO crystals grown at the Fujian Institute of Research on the Structure of Matter.[1,7] Until recently LBO crystals used for optical applications were grown by only two different research groups, the Fujian Institute of Research on the Structure of Matter[1,9] and the Research Institute for Synthetic Crystals.[10] Our laboratory has succeeded in growing LBO crystals and has made measurements of their NCPM properties. Temperature-tuned NCPM was achieved in a LBO crystal from 1.025 to 1.253 μm with radiation produced by a type I, two-crystal, walk-off–compensated β-barium metaborate (BBO) optical parametric oscillator[11] (OPO) pumped by the third harmonic of a Nd:YAG laser. Our measurements[6] of temperature-tuned noncritically phase-matched SHG of 1.064-μm radiation in an LBO crystal grown in our laboratory agree well with the result reported in Ref. 7.

Here we discuss the details of the crystal growth of LBO and the experimental results of the characterization of a LBO crystal for critically and noncritically phase-matched SHG from near-infrared radiation. Details of temperature-, angle-, and spectrum-tuned SHG at NCPM are reported.

2. CRYSTAL GROWTH

The LBO crystal used in this experiment was grown in our laboratory by the top-seeded solution growth (TSSG) technique.[12] The TSSG apparatus used for this growth experiment was similar to the system described by Elwell *et al.*[13] For simplicity we investigated the growth of the LBO crystal using the binary Li_2O–B_2O_3 system. This self-fluxed system was created by adding a stoichiometric excess of B_2O_3. The starting materials were prepared in the following reaction:

$$Li_2CO_3 + 6H_3BO_3 \xrightarrow{900°C \text{ for } 5\text{ h}} 2LiB_3O_5 + CO_2 + 9H_2O.$$

A chemical analysis[14] of the melt determined the exact Li_2O:B_2O_3 ratio of each compound, and the purity of the starting material was at least 97%. The phase diagram of this binary system was reported by Sastry and Hummel,[15] and the relevant portion of their phase diagram is reproduced as the solid curve in Fig. 1. This phase diagram shows that the melting point of LBO (Li_2O:B_2O_3 = 1:3 M ratio) is ~834°C and that LBO melts incongruently above this temperature. In the TSSG technique it is important to know the spontaneous nucleation temperature and the liquidus temperature as well as the phase diagram itself. The crystal growth from the seed will take place just below the liquidus temperature. In order to grow high-quality crystals, one must dissolve the outside layer of a seed crystal and then initiate growth as slowly as possible. Accu-

0740-3224/92/071128-06$05.00

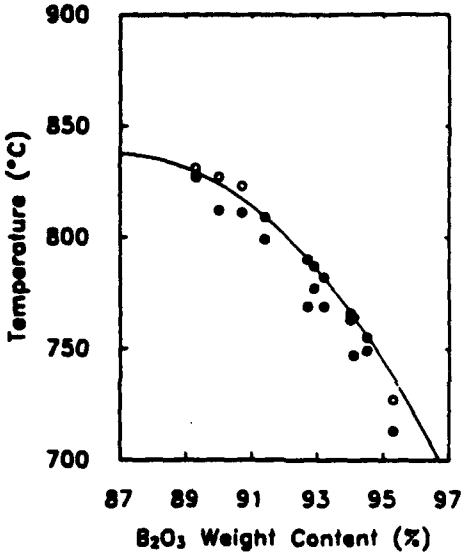

Fig. 1. Phase diagram of Li_2O–B_2O_3 binary system. The closed and the open circles show the spontaneous nucleation temperature and the liquidus temperature, respectively. The solid curve represents the phase diagram reported previously.

rate direct measurements of the spontaneous nucleation temperature were made by using a platinum–platinum: rhodium 13% thermocouple junction as a cold finger. The liquidus temperature was determined by suspending the seed crystal in the solution and observing whether dissolution or growth occurred after the solution was kept at a given temperature for at least 24 h to ensure an equilibrium state. This measurement enabled us to determine the liquidus temperature while imitating the actual crystal growth conditions. These results are plotted as a function of B_2O_3 content in Fig. 1. Overall, we could predict the growth initiation temperature with an accuracy of ±5°C.

A six-sided lathe-shaped crystal, 8 mm × 2 mm × 0.5 mm in size, was obtained by spontaneous nucleation on a platinum cold finger and was used as a seed crystal. After we obtained a large crystal boule, we used *Y*-cut (cut along the dielectric *Y* axis) crystals as seeds to obtain a large-aperture, *X*-cut crystal. Chen *et al.*[1] started the LBO crystal growth from a temperature of 834°C. This implies that the stoichiometric 1:3 mixture of Li_2O:B_2O_3 was used as a melt compound. However, the region in which the B_2O_3 content is lower than approximately 90% is highly temperature sensitive; therefore in this region, compared with the region of high B_2O_3 content, highly accurate temperature control is needed to yield a specific volume of crystal. On the other hand, in the region of high B_2O_3 content (higher than ~94%), it is difficult to keep the melt homogeneous because of the relatively high viscosity of the melt. Although Zao *et al.*[10] reported that a fluoride compound was added to the melt to reduce its viscosity, introducing foreign compounds to the melt may lead to inclusions and hence is not necessarily favorable for high-quality crystal growth. Hence, as a compromise, we preferred to use a melt having a B_2O_3 content between 90% and 94%. A typical crystal-growth procedure is as follows: a melt of Li_2O:B_2O_3 = 9:91 by weight ratio is kept in a platinum crucible (40-mm diameter × 40-mm depth) at a temperature of 814°C, which is 3°C above the liquidus temperature, for at least 24 hs. A *Y*-cut seed crystal is then introduced and kept in contact with the surface of the melt for half an hour, at which time slight dissolution should be observed. The melt is then cooled to a temperature just below the liquidus temperature, 811°C, and maintained at this temperature until no growth takes place on the seed crystal for at least 24 h. The melt is then cooled to 801°C at a rate of 0.5°C/day. After growth the crystal is slowly pulled up from the melt and cooled to room temperature at a rate of 3°C/h. Typically, a 20 mm × 20 mm × 15 mm crystal boule can be produced by this procedure.

LBO is a negative biaxial crystal and belongs to the orthorhombic space group with $mm2$ point symmetry.[10,16] The dielectric axes *X* and *Y* are parallel to the crystallographic axes *a* and *c*, respectively.[2] For the measurements of SHG for various wavelengths at critical phase-matching and NCPM conditions, a crystal was cut from the boule and polished to dimensions of 3.9 mm × 6.0 mm × 4.0 mm along the dielectric axes *X*, *Y*, and *Z*, respectively.

3. CRITICAL PHASE-MATCHING PROPERTIES OF SECOND HARMONIC GENERATION IN A LITHIUM TRIBORATE CRYSTAL

In the following optical experiments a type I, two-crystal, walk-off–compensated BBO OPO pumped by the third harmonic of a commercial Nd:YAG laser was used as a tunable near-infrared laser source. The BBO OPO can provide continuously tunable infrared radiation to 2.5 μm. The linewidth of near-infrared radiation from the BBO OPO was less than 3 nm at the wavelengths between 1.0 and 1.3 μm. The details of the BBO OPO were reported in Ref. 11. The 1.064-μm radiation from the Nd:YAG laser was also used as a near-infrared radiation source.

In order to obtain type I phase-matched SHG in the *X*–*Y* principal plane, the fundamental wave was polarized parallel to the *Z* axis and propagated in the *X*–*Y* plane of the

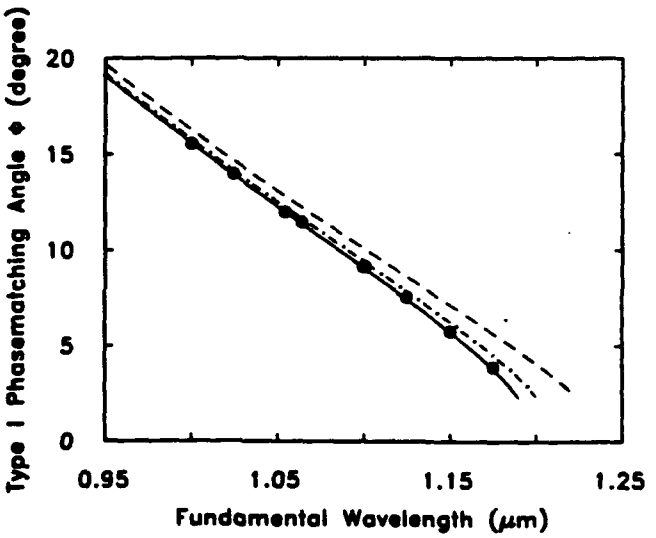

Fig. 2. Tuning curve for Type I SHG in the principal *X*-*Y* plane. The theoretical curves are based on recent Sellmeier equations: solid curve from Ref. 17, dashed curve from Ref. 3, dotted–dashed curve from Ref. 4.

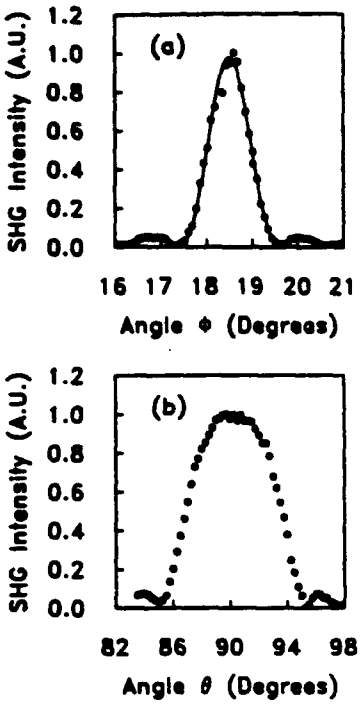

Fig. 3. Angular acceptances for SHG of 1.064-μm radiation at critical phase-matching condition at room temperature for rotation about (a) the Z axis (ϕ direction) and (b) the Y axis (θ direction). The FWHM acceptance angles (external) are 1.0° and 7.4° for rotation in the ϕ and θ directions, respectively.

LBO crystal. The output beams from the BBO OPO and the Nd:YAG laser were collimated and had a diameter of 2 mm and a divergence half-angle of less than 0.3 mrad.

A tuning curve for type I SHG in the X–Y principal plane was measured at the fundamental wavelengths ranging from 1.000 to 1.175 μm and is presented in Fig. 2. The theoretical tuning curves were calculated by using Sellmeier equations.[3,4,17] The discrepancies may be caused by the inaccuracy of the Sellmeier equations in the near-infrared region. New Sellmeier equations from the Fujian Institute of Research,[17] however, seem to make a better fit to our experimental results. In order to minimize measurement errors induced by the crystal fabrication process, we measured second-harmonic intensities on both sides of the X axis and determined the average phase-matching angle by using the following equation[16]:

$$\phi_{PM} = \frac{1}{2}\left\{\sin^{-1}\left[\frac{\sin\phi_l}{n^o(\lambda)}\right] + \sin^{-1}\left[\frac{\sin\phi_r}{n^o(\lambda)}\right]\right\}, \qquad (1)$$

where ϕ_l and ϕ_r are the external phase-matching angles measured from the X axis clockwise and counterclockwise, respectively, and $n^o(\lambda)$ is the ordinary refractive index at wavelength λ. This type I SHG tuning curve in the X–Y plane indicates that noncritically phase-matched SHG for 1.200 μm can be achieved at room temperature.

Angle-tuned SHG of 1.064-μm radiation was measured by rotating the crystal in the ϕ and θ directions, and the results are plotted as a function of the external angle in Figs. 3(a) and 3(b), respectively. As is shown in Fig. 3(a), the phase-matching (external) angle for SHG of 1.064-mm radiation in the X–Y principal plane was determined to be 18.5°, corresponding to an internal angle of 11.4°. The FWHM of the external acceptance angle in the ϕ direction, $\Delta\phi_{ext}$, was found to 1.0°, which corresponds to an angular-acceptance bandwidth $\Delta\phi_{int}l$ of 4.2 mrad cm. This value is in excellent agreement with the theoretical value of 4.1 mrad cm calculated according to the following equation:

$$\Delta\phi_{int}l = \frac{2A\lambda}{\pi(n_{2x}^{-2}\sin^2\phi + n_{2y}^{-2}\cos^2\phi)(n_{2y}^{-2} - n_{2x}^{-2})\sin 2\phi}, \qquad (2)$$

where $A = 1.3916$; l is the crystal length; λ is the fundamental wavelength; n_{2x} and n_{2y} are the refractive indices of the principal X and Y axes, respectively, at the wavelength $\lambda/2$; and ϕ_{PM} is the phase-matching angle.

The angle-tuned SHG intensity curve in the θ direction, shown in Fig. 3(b), can no longer be fitted by a simple sinc^2 function, because the SH intensity is represented by a convolution of the phase-matching function sinc^2 and the function of the phase-matching locus. Figure 4 shows the phase-matching locus for SHG of 1.064-μm radiation calculated by using the Sellmeier equations. As is shown in this figure, in the vicinity of the phase-matching point ($\phi = 11.8°$ and $\theta = 90°$), the locus is broad with respect to changes in the angle θ but sharp with respect to the angle ϕ. This also implies that the θ angle-tuned SH intensity curve is strongly affected by any error in the crystal alignment; that is, if the crystal is placed slightly off $\phi = \phi_{PM}$, a narrower ($\phi < \phi_{PM}$) or broader ($\phi > \phi_{PM}$) angular bandwidth will be observed. Figure 5 demonstrates how the profiles of angle-tuned SH intensity curve in the θ direction are affected by crystal misalignment of the ϕ direction. In Fig. 5 the angle-tuned SH intensity curves were measured as a function of angle near $\phi = \phi_{PM}$. From these careful measurements we obtained an FWHM acceptance angle, $\Delta\theta_{ext}$, of 7.4° at $\phi = \phi_{PM}$. This value corresponds to an angular-acceptance bandwidth ($\Delta\theta_{int}l$) of 31.3 mrad cm. This value is 10% smaller than that reported previously.[1]

Similarly, we evaluated the angular acceptances at various fundamental wavelengths. Figure 6 shows the wave-

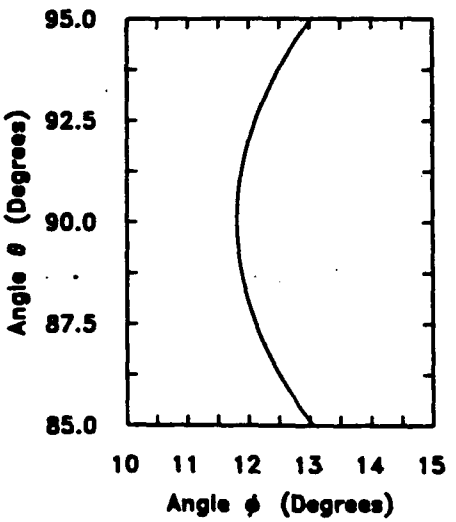

Fig. 4. Phase-matching locus of type I SHG of 1.064 μm. Numerical calculations were made by using published Sellmeier equations.

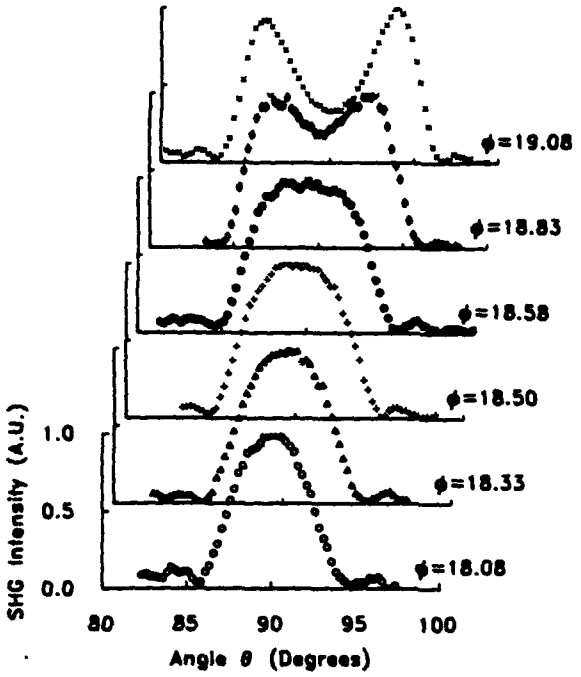

Fig. 5. Angular dependence of critical phase-matched SHG of 1.064 μm. Angle-tuned SH intensity curves in the θ direction are plotted as a function of phase mismatch in the ϕ direction. The phase-matching angle (external) is found to be $\phi = 18.50°$ at $\theta = 90°$.

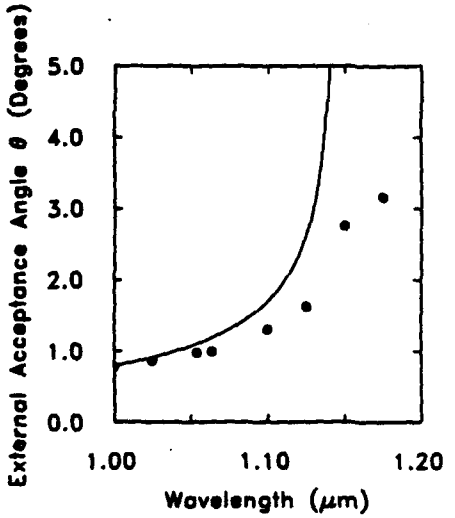

Fig. 6. Wavelength dependence of the external acceptance angle in the ϕ direction. The solid curve shows the theoretical values calculated by using Eq. (2).

length dependence of the angular acceptance at critical phase-matching conditions. The experimental and the theoretical results calculated by using Eq. (2) show good agreement only for wavelengths shorter than 1.15 μm. The first-order approximation for critical phase-matching [Eq. (2)] is no longer valid, because the quasi-NCPM takes place in the longer-wavelength region. However, we have confirmed, as is shown above, that the angular acceptances of the LBO crystal are large enough for practical applications at any of the near-infrared fundamental wavelengths evaluated above.

4. TEMPERATURE-TUNED NONCRITICAL PHASE-MATCHING PROPERTIES OF SECOND-HARMONIC GENERATION FROM 1.025 TO 1.253 μm IN A LITHIUM TRIBORATE CRYSTAL

For the measurements of the temperature-tuned NCPM properties of LBO, the crystal was enclosed within a copper block equipped with resistive heaters and a liquid-nitrogen bath that could maintain the temperature with an accuracy of ± 0.5°C. The temperature of the crystal was monitored and controlled by thermocouples attached to the side surfaces of the crystal. The crystal was heated or cooled at a rate no faster than 1°C/min to avoid any temperature inhomogeneity in the crystal. The incident beam position was 2 mm from the center of the crystal (i.e., 1 mm from the copper wall) to minimize any possible error caused by a temperature gradient between the center of the crystal and the surface of the crystal. Figure 7 shows the temperature-tuning curve for SHG at 1.064-μm radiation. The NCPM temperature (T_{NCPM}) was found to be 148.0 $\pm$ 0.5°C with FWHM of 10.1°C, corresponding to the temperature bandwidth ΔTl of 3.9°C cm. This value [6] of T_{NCPM} for SHG at 1.064 μm agrees with the previously reported[7] value of 148.5°C measured for LBO crystals grown at the Fujian Institute for the Research on the Structure of Matter. We note, however, that our value of ΔTl is ~30% larger than the value reported by Huang *et al.*[7] The origin of this discrepancy is not known. Based on the data presented in Section 3, the crystal alignment and quality in these experiments were excellent. Poor crystal quality would lead to an elevation in the tails of the curves presented in Figs. 3, 5, and 8. This elevation is clearly not seen. In this experimental configuration the measured temperature may be slightly different from the actual temperature of the crystal because of the temperature gradient in the crystal. However, the magnitude of this effect was evaluated and determined to be negligible. When the incident beam was positioned on the center of the crystal (3 mm from the copper wall), where the temperature is believed to be the lowest because of heat radiation from the crystal surface, the difference between T_{NCPM} obtained at this position and that at the original position was less than 1°C and thus was neglected in the following experiments.

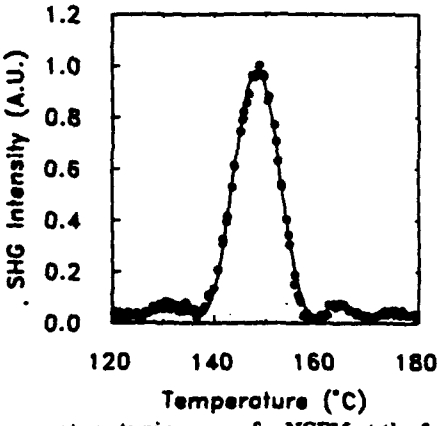

Fig. 7. Temperature-tuning curve for NCPM at the fundamental wavelength of 1.064 μm in LBO crystal. NCPM occurs at 148.0 $\pm$ 0.5°C with a FWHM bandwidth of 10.1°C.

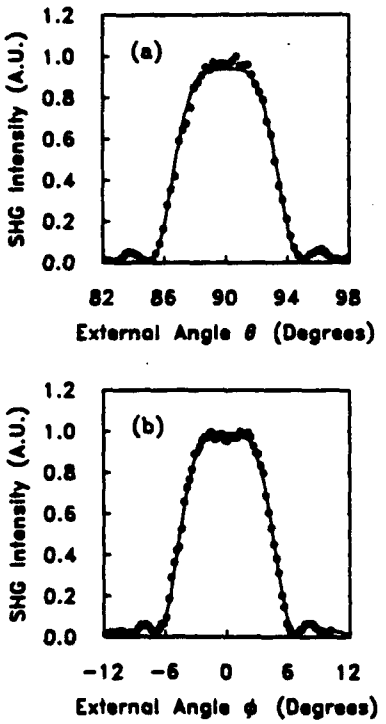

Fig. 8. Angular acceptance for SHG of 1.064-μm radiation at the NCPM temperature of 148.0 ± 0.5°C for rotation about (a) the Z axis (ϕ direction) and (b) the Y axis (θ direction). The FWHM acceptance angles (external) are 9.1° and 6.6° for rotation in the ϕ and θ directions, respectively.

Table 1. Summary of Temperatures for NCPM SHG in LBO at Various Near-Infrared Wavelengths[a]

Wavelength (μm)	Temperature (°C)
1.025	190.3
1.064	148.1
1.110	108.2
1.15	61.1
1.20	24.3
1.25	−2.9

[a]Ref. 6.

While maintaining the crystal temperature at 148.0 ± 0.5°C (NCPM temperature for SHG at 1.064 μm), we measured the acceptance angles $\Delta\phi$ and $\Delta\theta$ by rotating the crystal about the Z axis in the X–Y plane (ϕ direction) and about the Y axis in the X–Z plane (θ direction), respectively. Under NCPM conditions the angular dependence of the SH intensity can be written, with a second-order approximation of a finite phase mismatch, as

$$P\left(\frac{\lambda}{2}\right) \sim \frac{\sin^2[(l\pi/\lambda)(n_2^{\omega})^3(n_{2y}^{-2} - n_{2x}^{-2})(\Delta\phi)^2]}{[(l\pi/\lambda)(n_2^{\omega})^3(n_{2y}^{-2} - n_{2x}^{-2})(\Delta\phi)^2]^2}$$

for the ϕ direction,

$$P\left(\frac{\lambda}{2}\right) \sim \frac{\sin^2[(l\pi/\lambda)(n_1^{\omega})^3(n_{1z}^{-2} - n_{1x}^{-2})(\Delta\theta)^2]}{[(l\pi/\lambda)(n_1^{\omega})^3(n_{1z}^{-2} - n_{1x}^{-2})(\Delta\theta)^2]^2}$$

for the θ direction, (3)

where $P(\lambda/2)$ is the square of the SH intensity at wavelength λ, $\Delta\theta$ and $\Delta\phi$ are the angular bandwidths, and l is the length of the crystal. Figures 8(a) and 8(b) show the angle-tuned SH intensity curves in the ϕ and θ directions, respectively. These curves are fitted well by the function described above. The FWHM acceptance angles (external) were found to be 9.1° and 6.6° for rotations in the ϕ and θ directions, respectively. These values correspond to angular acceptance bandwith of $\Delta\theta l^{1/2} = 71.9$ and $\Delta\phi l^{1/2} = 99.1$ mrad cm$^{1/2}$.

Similarly, temperature-tuned noncritically phase-matched SHG was measured at the fundamental wavelengths of 1.025, 1.064, 1.110, 1.150, 1.200, and 1.253 μm and is summarized in Table 1.[6] Figure 9 shows the temperature dependence for noncritically phase-matched SHG from 512.5 to 626.5 nm as a function of the fundamental wavelength. The theoretically predicted dependence is also plotted. Figure 9 indicates that when a 1.0–1.3-μm source is used for the fundamental most of the visible spectrum can be generated under NCPM conditions in the temperature range from −20°C to 220°C. The blue spectrum should be attainable by going to a higher temperature;

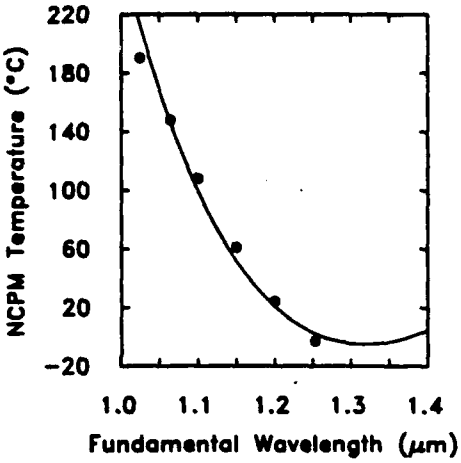

Fig. 9. Plot of the type I NCPM temperature versus the fundamental wavelength producing SH's of 512.5-, 532.0-, 550.0-, 575.0-, 600.0-, and 626.5-nm radiation. The experimental data are based on our previously reported measurements.[6] The theoretical fit is based on newly obtained thermo-optic data[3] and Sellmeier equations.[17] Lin *et al.*[19] have recently reported more extensive results for both type I and type II NCPM (see Note added in proof).

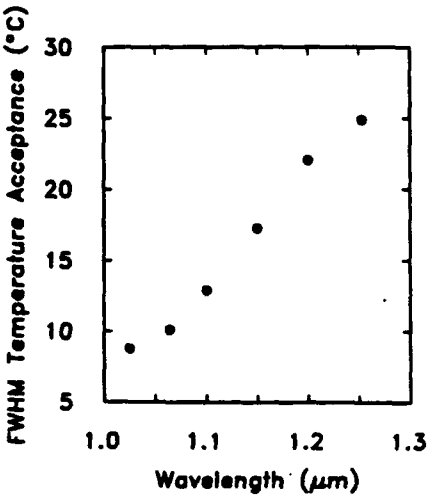

Fig. 10. Plot of the FWHM temperature acceptance as a function of the fundamental wavelength.

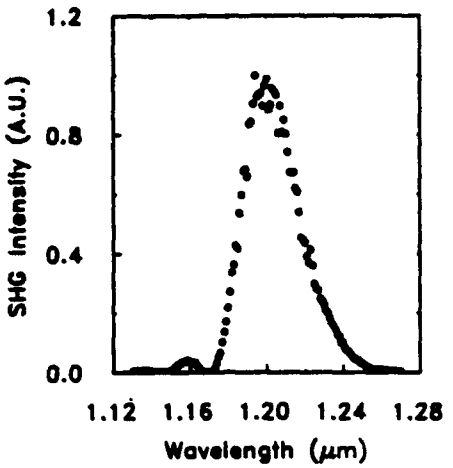

Fig. 11. Spectral tuning curve for SHG in the LBO crystal at room temperature. The NCPM wavelength is found to be 1.215 μm with a FWHM of 33 nm.

that is to say, SHG of 450 nm will be produced by NCPM at approximately 320°C. The FWHM of the temperature acceptance is plotted as a function of the fundamental wavelength in Fig. 10, which shows that the temperature acceptance increases as the wavelength increases.

As mentioned previously, NCPM SHG at room temperature can be achieved at ~1.2 μm. The spectrum-tuned SH intensity was measured and is shown in Fig. 11. The noncritically phase-matched wavelength at 21°C was found to be 1.215 μm with a FWHM spectral width of 33 nm.

5. CONCLUSION

We have reported the growth and the measurements of properties of critically and noncritically phase-matched SHG in a LBO crystal. The optically clear LBO crystal was successfully grown with a self-fluxed TSSG technique in our laboratory. Optimization of growth parameters should be carried out in order to obtain larger LBO crystals with high quality. We have demonstrated angle-tuned type I critically phase-matched SHG in the X–Y principal plane at near-infrared fundamental wavelengths ranging from 1.000 to 1.175 μm. Even for critical phase-matching conditions we confirmed that LBO has a relatively large angular acceptance. Also, we have demonstrated temperature-tuned noncritically phase-matched SHG of the near-infrared fundamental wavelengths ranging from 1.025 to 1.253 μm. For NCPM the problem of walk-off is eliminated, and the efficiency limitation that is due to beam divergence is drastically reduced. These measurements confirm the advantages of using LBO for frequency conversion devices for certain applications, especially in near-infrared and infrared regions. The large angular, thermal, and spectral acceptance bandwidths permit simple coupling between the pump source and the crystal and relax the stability requirements.

Note added in proof: Since the submission of our paper, two papers relevant to the question of temperature-tuned NCPM in LBO have appeared in the literature, Refs. 3 and 19. The thermo-optic data of Velsko *et al.*[3] have now allowed us to calculate a theoretical tuning curve that was not possible in our previously reported results.[6] Our original experiment covered the spectral range from 1.025 to 1.253 μm. The paper by Lin *et al.*[19] presents a more extensive tuning range as well as reporting on both type I and type II NCPM. The results presented in Ref. 19 for temperature-tuned, type I NCPM confirm our original measurements and demonstrate the possibility of phase matching at two wavelengths for the same temperature, which were not previously noted, in the tuning curve.

ACKNOWLEDGMENTS

The authors acknowledge the technical assistance of W. S. Pelouch. This research was supported by the U.S. Naval Research Laboratory, Office of Naval Research, and the National Science Foundation.

*Present address, Japan Synthetic Rubber Company, Ltd., Research Center, 25 Miyukigaoka, Tsukuba, 305 Japan.

REFERENCES AND NOTES

1. C. Chen, Y. Wu, A. Jiang, B. Wu, G. You, R. Li, and S. Lin, J. Opt. Soc. Am. B **6**, 616 (1989).
2. S. Lin, Z. Sun, B. Wu, and C. Chen, J. Appl. Phys. **67**, 634 (1990).
3. S. Velsko, M. Webb, L. Davis, and C. Huang, IEEE J. Quantum Electron. **27**, 2182 (1991).
4. K. Kato, IEEE J. Quantum Electron. **26**, 1173 (1990).
5. W. S. Pelouch, T. Ukachi, E. S. Wachman, and C. L. Tang, Appl. Phys. Lett. **57**, 111 (1990).
6. T. Ukachi, R. J. Lane, W. R. Bosenberg, and C. L. Tang, Appl. Phys. Lett. **57**, 980 (1990).
7. J. Y. Huang, Y. R. Shen, C. Chen, and B. Wu, Appl. Phys. Lett. **58**, 1579 (1991).
8. M. Ebrahimzadeh, G. Robertson, M. H. Dunn, and A. J. Henderson, in *Conference on Lasers and Electro-Optics*, Vol. 7 of 1990 OSA Technical Digest Series (Optical Society of America, Washington, D.C., 1990), postdeadline paper CPDP26-1.
9. C. Chen, Y. Wu, and R. Li, J. Cryst. Growth **99**, 790 (1990).
10. S. Zao, C. Huang, and H. Zhang, J. Cryst. Growth **99**, 805 (1990).
11. W. R. Bosenberg, W. S. Pelouch, and C. L. Tang, Appl. Phys. Lett. **55**, 1952 (1989).
12. D. Elwell and H. J. Scheel, *Crystal Growth from High Temperature Solutions* (Academic, London, 1975).
13. D. Elwell, P. Capper, and M. D'Agostino, J. Cryst. Growth **29**, 263 (1975).
14. L. Shartsis and W. Capps, J. Am. Ceram. Soc. **35**, 169 (1952).
15. B. S. R. Sastry and F. A. Hummel, J. Am. Ceram. Soc. **41**, 7 (1958).
16. V. H. Konig and A. Hoppe, Z. Anorg. Allg. Chem. **439**, 71 (1978).
17. The following Sellmeier equations were obtained in a personal communication from the Fujian Institute of Research on the Structure of Matter (λ in micrometers):

$$n_z^2 = 2.45414 + \frac{0.011249}{\lambda^2 - 0.01135} - 0.014591\lambda^2 - 0.000066\lambda^4,$$

$$n_x^2 = 2.53907 + \frac{0.012711}{\lambda^2 - 0.012523} - 0.01854\lambda^2 - 0.0002\lambda^4,$$

$$n_z^2 = 2.586179 + \frac{0.013099}{\lambda^2 - 0.011893} - 0.017968\lambda^2 - 0.000226\lambda^4.$$

18. L. K. Cheng, W. R. Bosenberg, and C. L. Tang, Appl. Phys. Lett. **53**, 175 (1988).
19. S. Lin, B. Wu, F. Xie, and C. Chen, Appl. Phys. Lett. **59**, 1541 (1991).

Appendix D

Laser Focus World

GLOBAL ELECTRO-OPTIC TECHNOLOGY AND MARKETS

April 1993

- Focus on holography
- Hubble to get corrective optics
- Back to Basics: Visible diode lasers
- Soliton lasers make ultrashort pulses

Technology Guide: Laser materials

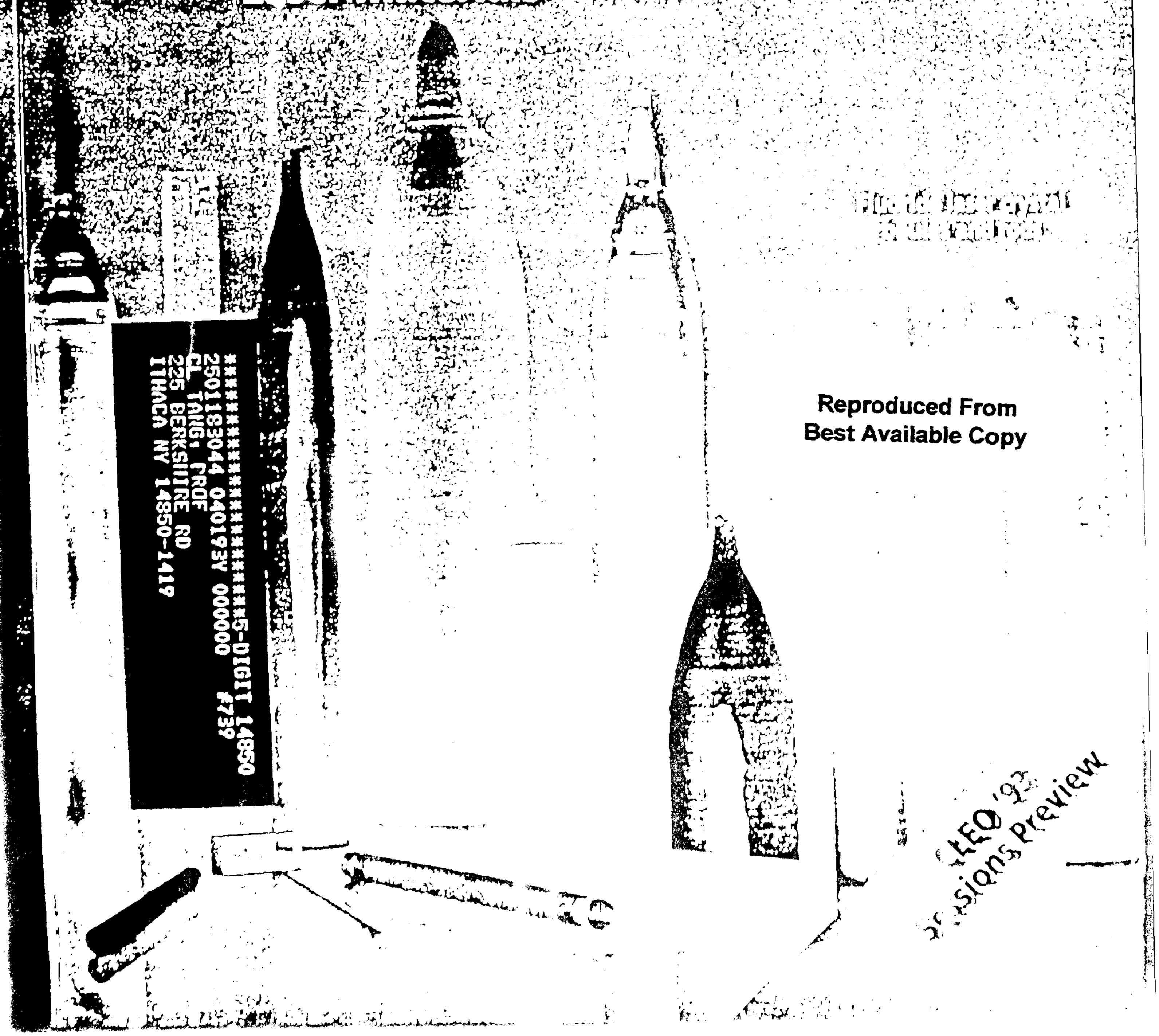

gets—dirt berm, concrete, wood, canvas, and sandblasted aluminum—over the 9.3–10.7-μm range was measured. In addition, data on differential reflectivity of contaminants sprayed on solid targets were obtained. Various chemicals contained in a vapor chamber at a range of 500 m were monitored (with a solid target 1 km behind) to study differential absorption.

Other tests included measurements of aerosol backscatter, transmission through dust, range of distant topographical features, and the system noise level as a function of the number of pulses averaged. These tests produced a great deal of data (at least 200 Mbyte) that will take several months to analyze completely.

Preliminary results are encouraging. The system noise level, determined from the standard deviation of normalized return signals, was 1%–2% for a four-pulse average against a solid target. Cohn says, "This level is significantly lower than with previous devices." Also, calibration of differential absorption by measuring atmospheric water vapor produced results ±5% of the local metrological station, which is within the accuracy of that equipment. Finally, Cohn reports, "The sensor could measure vapor levels of a typical simulant (such as triethylene phosphate) at levels below that of passive systems or previous laser sensors."

The Army has awarded Hughes a follow-on program to improve the laser and sensor. Reducing the size and weight are immediate goals, and additional field tests will be performed. The program extension is expected to continue through mid-1994. Commercial environmental applications include industrial-chemical emission and urban-pollution monitoring.

Heather W. Messenger

PULSED TUNABLE SOURCES

Commercial OPO produces high-energy tunable output

Researchers needing a high-energy tunable source typically resort to Nd:YAG- and excimer-pumped dye lasers, notwithstanding the relative inconvenience and "user-unfriendliness" of dye lasers. Optical parametric oscillators (OPOs) appear to offer an attractive solid-state alternative to high-energy dye lasers.

With this in mind, engineers at Spectra-Physics Lasers (S-PL, Mountain View, CA) have developed a high-energy Nd:YAG-pumped OPO device that is tunable from 400 to 3000 nm and that can be frequency doubled to 200 nm, according to Mark Sobey, general manager of S-PL's Quanta-Ray business unit. The device will eventually become an extension of the recently released MOPO-700 series of OPOs and will further increase the

Continued on p. 20

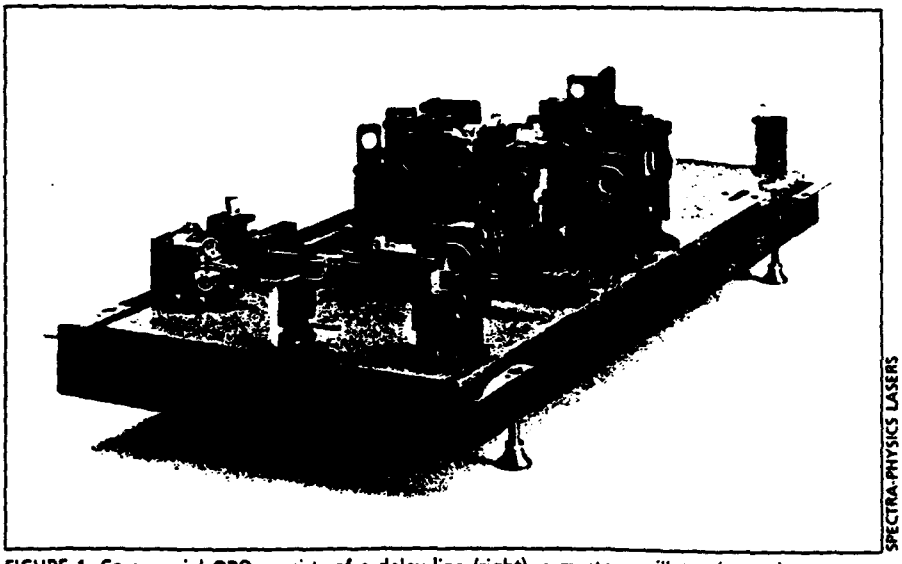

SPECTRA-PHYSICS LASERS

FIGURE 1. Commercial OPO consists of a delay line (right), a master oscillator (center), a power oscillator (left), and a wavelength separator (rear). Not shown is the pump laser, an injection-seeded Nd:YAG model.

Continued from p. 16

tuning range and reduce the linewidth of these products, which currently provide high-energy (>100 mJ) output with narrow linewidth (<0.1 cm^{-1}) at wavelengths from 400 to 2000 nm (see Fig. 1).

Briefly, OPOs are nonlinear optical conversion devices that use a nonlinear crystal to achieve frequency conversion when pumped by a laser. The S-PL development work on OPOs using beta-barium borate (BBO) as the nonlinear crystal has been done in collaboration with C. L. Tang and his group at Cornell University (Ithaca, NY). The Cornell Research Foundation owns a fundamental patent titled "Tunable Optical Parametric Oscillator" (US Pat. #5053641) covering the use of BBO in any type of OPO, to which S-PL has recently been granted an exclusive license. Sobey says S-PL has filed for patents on several aspects of its OPO design, including the master-oscillator/power-oscillator (MOPO) approach to narrow-linewidth, high-energy devices.

System design

The third harmonic from a 1250-mJ Nd:YAG laser pumps the OPO. The Nd:YAG pump beam must be line-narrowed to control the bandwidth of the OPO output beam. This is accomplished using a single-frequency diode-pumped Nd:YVO_4 (vanadate) injection-seeding laser. A by-product of the injection seeding is smoothing of the Nd:YAG laser temporal profile, which results in a substantial (>40%) increase in the 532- and 1064-nm mixing efficiency when generating the 355-nm third harmonic. The addition of a Type I doubler makes it possible to obtain more than 400 mJ at 355 nm from the pump laser. "To the user this means the overall system efficiency, and its cost, are similar to those of Nd:YAG- or excimer-pumped dye lasers," says Sobey.

In the S-PL MOPO design, the master and power oscillators each use a BBO crystal as the parametric conversion medium (see Fig. 2). The master oscillator generates a linewidth-narrowed seed beam of low energy, which controls the linewidth of the high-energy beam generated in the power oscillator. All of the output energy is generated in the power oscillator, so the OPO output energy is constant and independent of the linewidth. Current S-PL products specify energies exceeding 100 mJ with less than 0.1 cm^{-1} linewidths, and S-PL engineers have already observed linewidths less than 0.02 cm^{-1} at similar output energy and wavelengths.

Two variants of the master-oscillator design are intended to address different application requirements. Each uses a short grazing-incidence cavity design, with a servo system to control and couple the rotation of the BBO crystal with the diffraction-grating angle. A small portion of the 355-nm pump energy is split off and used to pump the oscillator above threshold. The grating/mirror pair controls absolute wavelength and linewidth, and the servo system ensures that optimal conversion efficiency is maintained as the wavelength is scanned within the master oscillator.

Use of a similar cavity design, but with an additional precision mechanical stage and more-complex servo

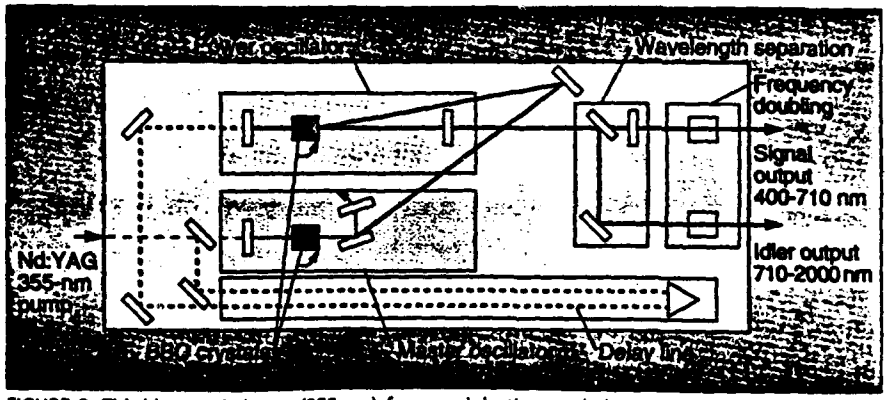

FIGURE 2. Third-harmonic beam (355-nm) from an injection-seeded Nd:YAG pump laser enters master oscillator to create linewidth-narrowed low-power beam that is injected into power oscillator and frequency-converted in BBO. High-energy OPO signal and idler output beams can be tuned over the 400–2000-nm range.

electronics, makes single-mode output possible. In this case, the system continously monitors the cavity length and isolates a single longitudinal mode as the wavelength is scanned. In both cases, the MOPO design apparently achieves an overall conversion efficiency exceeding 20%.

Extending the wavelength range below 400 nm will require frequency doubling of the OPO output. Based on results from existing R&D systems, Sobey says S-PL engineers expect to achieve a frequency-doubling conversion efficiency exceeding 15% when covering the 200–400-nm range. He also says that existing OPO products have been designed with doubling in mind, so they will be able to accommodate a doubling stage when it becomes available. At the longer end of the wavelength range, an additional set of optics will eventually enable the existing products to tune from 2000 to 3000 nm.

Stephen G. Anderson

DETECTOR ELECTRONICS

IR readout electronics capture focal-plane-array signals

Improvements in detector electronic readout systems parallel advances in focal-plane-array detector systems. The SPIE Aerospace and Remote Sensing Symposium, to be held in Orlando, FL, 12–16 April 1993, includes a session devoted to readouts and signal processing: "Infrared detectors and instrumentation." Highlights of four conference papers are described here by Eric R. Fossum, a research technologist in the Imaging Systems Section at the Jet Propulsion Laboratory, Pasadena, CA 91109.

One active area of research in detector electronics centers on implementing cryogenic readout electronics in gallium arsenide (GaAs) materials. GaAs has a lower carrier freeze-out temperature than silicon. The freeze-out of carriers is directly linked to $1/f$ noise in cryogenic circuits. Thus, GaAs-based circuits can potentially operate with lower noise and at lower temperatures than their silicon counterparts.

The development of GaAs field-effect transistors (FETs) for cryogenic readout of discrete, nonmultiplexed detector arrays will be discussed at the aerospace sensing symposium by R. K. Kirschman and J. A. Lipa of Stanford University (Stanford, CA) and M. Omori from Microwave Technology Inc. (Fremont, CA). These small focal-plane arrays (FPAs) would be used on the Gravity Probe B pointing telescope and would operate at 2–3 K. The researchers will report on the evaluation of commercial and foundry GaAs FETs as well as custom GaAs metal semiconductor FETs and circuits operating at cryogenic temperatures.

For larger FPAs, power dissipation is a critical parameter. At higher temperatures, silicon complementary metal-oxide semiconductor (CMOS) circuits can be used in most applications. The development of CMOS-like complementary-heterojunction FETs (CHFETs) fabricated in the GaAs system for very-low-temperature applications will be described by T. J. Cunningham, E. R. Fossum, and S. M. Baier of the Jet Propulsion Laboratory (JPL, Pasadena, CA) and Honeywell (Bloomington, MN). CHFETs contain both p-channel and n-channel transistors, which allow the development of low-power cryogenic focal-plane circuits for space-based astrophysics applications. While the CHFET may resemble the CMOS structure in superficial ways, the lack of a true insulator such as SiO_2 results in a higher gate-leakage current in a CHFET than in CMOS devices. A parametric study of gate-leakage current as a function of both material configuration and geometry will be presented by JPL. A similar study on noise in these circuits will also be described.

For most infrared (IR) detector-readout applications, silicon CMOS is the predominant technology. The use of innovative circuits can improve the performance of the FPA by reducing both temporal and fixed pattern noise. Recent progress in low-power analog circuits for on-focal-plane signal processing will be discussed by B. Pain and others of JPL. Their paper describes work on a background-suppression circuit for long-wavelength IR FPAs that increases effective dynamic range by removing the background pedestal. The circuit also provides offset nonuniformity correction. Other circuits for low-power, high-gain amplifiers and on-chip analog-to-

Measurements of noncritically phase-matched second-harmonic generation in a LiB_3O_5 crystal

T. Ukachi,[a] R. J. Lane, W. R. Bosenberg, and C. L. Tang
Materials Science Center, Cornell University, Ithaca, New York 14853

(Received 21 May 1990; accepted for publication 3 July 1990)

The characteristic properties of noncritically phase-matched second-harmonic generation in lithium triborate (LiB_3O_5, LBO) are investigated. Using an LBO crystal grown in our laboratory, we demonstrate that temperature-tuned noncritical phase-matched second-harmonic generation from 1.025 to 1.253 μm is achieved in a temperature range from 190 to -3 °C. The noncritical phase-matching temperature for 1.064 μm radiation is found to be 148.0±0.5 °C with a temperature acceptance bandwidth of 3.9 °C cm.

Lithium triborate (LiB_3O_5, LBO) is a newly developed nonlinear optical crystal which is characterized by a wide transparency range, small birefringence, a moderate nonlinear optical coefficient, and a high optical damage threshold.[1,2] These unique properties, along with its mechanical hardness, chemical stability, and nonhygroscopicity, make LBO an attractive material for certain nonlinear optical processes.[3,4] For frequency conversion applications, the use of noncritical phase matching (NCPM) is advantageous due to the large angular acceptance and the elimination of walk-off. Measurements of temperature tuned noncritically phase-matched second-harmonic generation (SHG) at 1.064 μm have been made on LBO crystals grown at the Fujian Institute of Research on the Structure of Matter.[1] Until recently, the Fujian Institute has been the only source of LBO and very little has been reported about their growth techniques.

In this letter we report temperature-tuned noncritically phase-matched SHG from 1.025 to 1.253 μm in an LBO crystal grown in our laboratory. Our measurements of temperature-tuned noncritically phase-matched SHG of 1.064 μm radiation show significant discrepancies from that reported previously.[1]

LBO is a negative biaxial crystal and belongs to the orthorhombic space group with mm^2 point symmetry.[5] The dielectric axes X and Y are parallel to the crystallographic axes a and c, respectively.[2] The LBO crystal used in this experiment was grown in our laboratory using the top-seeded solution growth (TSSG) technique.[6] A Y-cut seed was introduced into a slightly unsaturated Li_2O-B_2O_3 solution (91.0% B_2O_3 by weight) at a temperature of 811 °C and grown for 20 days while cooling to a temperature of 801 °C. From the $20\times20\times15$ mm^3 boule a cube of LBO was fabricated and polished to dimensions $3.9\times6.0\times4.0$ mm^3 along the dielectric axes X, Y, and Z, respectively. All measurements by our laboratory reported here were made on this crystal.

For comparison with the theoretical value, we measured the type I phase-matching angle for SHG of 1.064 μm radiation in the X-Y principal plane ($\theta = 90°$, θ is measured from the Z axis and ϕ is measured from the X axis) and determined that $\phi = 11.4°$. This value is in good agreement with the theoretical one, $\phi = 11.8°$, calculated using the Sellmeier equations.[3]

The temperature-tuned noncritically phase-matched SHG and the angular acceptances were evaluated using 1.064 μm radition from a Nd:YAG laser. Temperature-tuned noncritically phase-matched SHG at other fundamental wavelengths in the infrared region was also measured using a type I, two-crystal, walk-off compensated beta-barium metaborate optical parametric oscillator (BBO OPO)[7] pumped by the third harmonic of a commercial Nd:YAG laser. The BBO OPO can provide continuously tunable infrared radiation out to 2.5 μm. The output beams from Nd:YAG laser and the BBO OPO were collimated to a diameter of 2 mm with a divergence half-angle of less than 0.3 mrad. The fundamental beam was linearly polarized parallel to the Z axis and propagated along the X axis.

For the measurements of the temperature-tuned noncritical phase-matching properties of LBO, the crystal was enclosed within a copper block equipped with resistive heaters and a liquid-nitrogen bath that could maintain the temperature within an accuracy of ±0.5 °C. The temperature of the crystal was monitored and controlled by thermocouples attached to the side surfaces of the crystal. The crystal was heated or cooled at a rate no larger than 1 °C/min to avoid temperature inhomogeneity in the crystal. In order to minimize any possible error caused by a temperature gradient between the center and the surface of the crystal, the incident beam position was set at 2 mm from the center of the crystal (i.e., 1 mm from the copper wall).

Figure 1 shows the temperature tuning curve for SHG at 1.064 μm radiation. The noncritical phase-matching temperature (T_{ncpm}) was found to be 148.0±0.5 °C with a full width at half maximum (FWHM) of 10.1 °C, corresponding to a temperature bandwidth (ΔTl) of 3.9 °C cm, for crystal length l. This value of T_{ncpm} for SHG at 1.064 μm differs significantly from the previously reported value of 112 °C measured using LBO crystals grown at the Fujian Institute of Research on the Structure of Matter.[1] The origin of this discrepancy is not fully understood at this

[a]On leave from Japan Synthetic Rubber Co., Ltd., Research Center, 25 Miyukigaoka, Tsukuba 305, Japan.

 0003-6951/90/360980-03$02.00

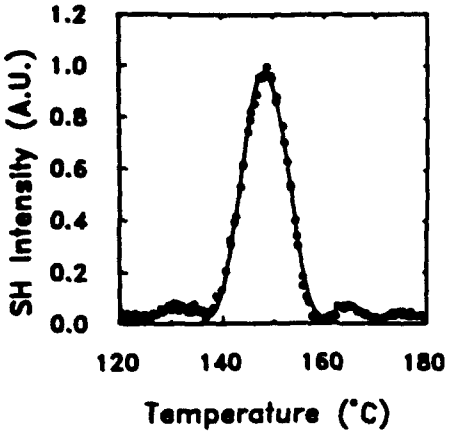

FIG. 1. Temperature tuning curve for noncritical phase matching at the fundamental wavelength of 1.064 μm in LBO. Noncritical phase matching occurs at 148.0±0.5 °C with a FWHM bandwidth of 10.1 °C.

time. However, in this experimental configuration, the measured temperature may be somewhat different from the actual temperature of the crystal due to a temperature gradient in the crystal. The magnitude of this effect was evaluated by changing the lateral position of the incident beam on the entrance surface of the crystal. When the incident beam was positioned on the center of the crystal (3 mm from the copper wall), where the temperature is believed to be the lowest due to heat radiation from the incident crystal surface, the difference between T_{ncpm} obtained at this position and that at the original one was less than 1 °C and thus was neglected in the following experiments.

While maintaining the crystal temperature at 148.0±0.5 °C (NCPM temperature for SHG at 1.064 μm), the acceptance angles $\Delta\theta$ and $\Delta\phi$ were measured by rotating the crystal about the Y axis in the X-Z plane (θ direction) and about the Z axis in the X-Y plane (ϕ direction), respectively. Figures 2 (a) and 2(b) show the angle-tuned SH intensity curves in the direction of θ and ϕ. The FWHM acceptance angles (external) were obtained to be 6.6° and 9.1° for the rotation of the θ and ϕ directions, respectively. These values correspond to angular acceptance bandwidths of $\Delta\theta l^{1/2} = 71.9$ and $\Delta\phi l^{1/2} = 99.1$ mrad $(\text{cm})^{1/2}$.

Similarly, temperature-tuned noncritically phase-matched SHG was measured at the fundamental wavelengths of 1.025, 1.100, 1.150, 1.200, and 1.253 μm which were generated by the BBO OPO. Temperature-tuned SH intensity profiles are shown in Fig. 3. Notice that the FWHM of the temperature bandwidth increases as the temperature decreases. Room-temperature (24 °C) noncritical phase matching occurs at a fundamental wavelength of 1.2 μm corresponding to 600 nm SH radiation. Figure 4 shows the temperature dependence of noncritical phase-matched SH radiation from 512.5 to 626.5 nm as a function of the fundamental wavelength. Figure 4 indicates that by using a 1.0 to 1.3 μm source for the fundamental, most of the visible spectrum can be generated under NCPM conditions in a temperature tuning range of 220 to −20 °C. The blue spectrum should be attainable by going

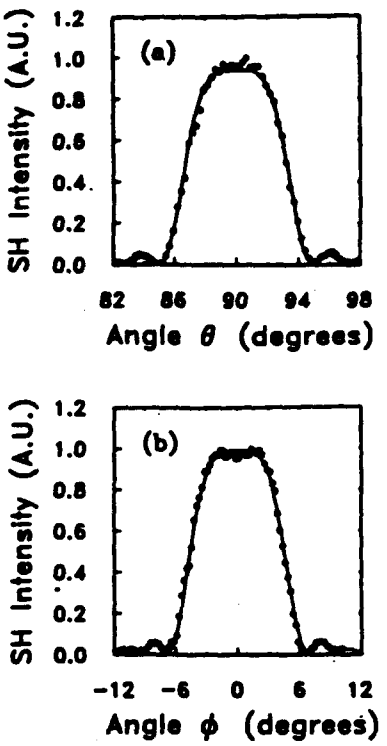

FIG. 2. External angular acceptances for second-harmonic generation of 1.064 μm radiation at the noncritical phase-matching temperature of 148.0±0.5 °C for rotation about (a) the Y axis (θ direction) and (b) the Z axis (ϕ direction). The FWHMs are 6.6° and 9.1° in the θ and ϕ directions, respectively.

to higher temperature, for example, 450 nm SH radiation will be produced by NCPM at ~320 °C.

In conclusion, we have demonstrated temperature-tuned noncritically phase-matched SHG from 1.025 to 1.253 μm in an LBO crystal grown in our laboratory. For noncritical phase matching, the problem of walk-off is eliminated and efficiency limitations due to beam divergence is drastically reduced. These measurements confirm the advantages of using LBO for frequency conversion devices for some applications, especially in the near-infrared

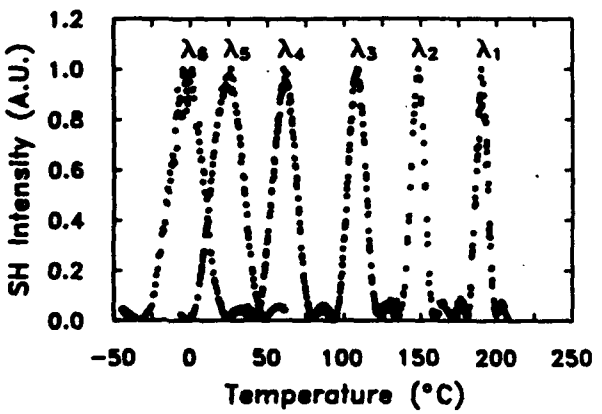

FIG. 3. Temperature tuning curves for noncritically phase-matched second-harmonic generation in LBO at the fundamental wavelengths of $\lambda_1 = 1.025$, $\lambda_2 = 1.064$, $\lambda_3 = 1.100$, $\lambda_4 = 1.150$, $\lambda_5 = 1.200$, and $\lambda_6 = 1.253$ μm generated by a type I, two-crystal, walk-off compensated BBO optical parametric oscillator.

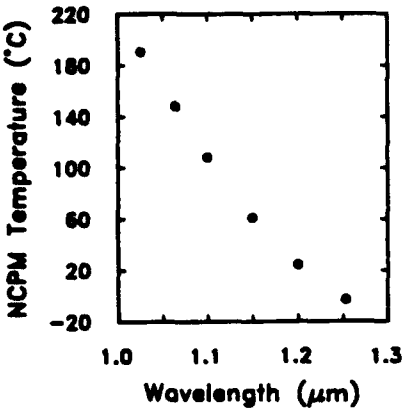

FIG. 4. Plot of the noncritical phase-matching temperature vs fundamental wavelength producing second-harmonic generation at the wavelengths of 512.5, 532.0, 550.0, 575.0, 600.0, and 626.5 nm. Most of the visible spectrum can be generated under noncritical phase-matching conditions in a temperature tuning range of −20 to 220 °C.

and infrared regions. The relatively large temperature and angular bandwidths allow simple coupling between the pump source and crystal, and also relax the stability requirements.

The authors wish to acknowledge the technical assistance of W. S. Pelouch. This work has been supported by the Naval Research Laboratory and the National Science Foundation.

[1] C. Chen, Y. Wu, A. Jiang, B. Wu, G. You, R. Li, and S. Lin, J. Opt. Soc. Am. B 6, 616 (1989).
[2] S. Lin, Z. Sun, B. Wu, and C. Chen, J. Appl. Phys. 67, 634 (1990).
[3] B. Wu, N. Chen, C. Chen, D. Deng, and Z. Xu, Opt. Lett. 14, 1080 (1989).
[4] W. S. Pelouch, T. Ukachi, E. S. Wachman, and C. L. Tang, Appl. Phys. Lett. 57, 111 (1990).
[5] Von H. Konig and R. Hoppe, Z. Anorg. Allg. Chem. 439, 71 (1978).
[6] D. Elwell and H. J. Schneel, *Crystal Growth from High Temperature Solutions* (Academic, London, 1975).
[7] W. S. Bosenberg, W. S. Pelouch, and C. L. Tang, Appl. Phys. Lett. 55, 1952 (1989).

Appendix F

Optical Parametric Oscillators

CHUNG L. TANG, FELLOW, IEEE, WALTER R. BOSENBERG, TAKASHI UKACHI, RANDALL J. LANE, AND L. KEVIN CHENG

Invited Paper

Optical parametric oscillators are powerful solid state sources of broadly tunable coherent radiation covering the entire spectral range from the near UV to the mid IR and can operate down to the femtosecond time domain. As a result of recent advances in nonlinear optical materials research, these oscillators are now practical devices with broad potential applications in research and industry. Recent developments in β-barium borate (BBO), lithium triborate (LBO), and potassium titanyl phosphate (KTP) optical parametric oscillators in particular are reviewed in this article.

I. Introduction

Ever since the invention of the laser, there has always been a great deal of interest in the development of continuously tunable coherent light sources. Such sources would have broad applications in research and industry. The development of tunable oscillators has been difficult because conventional lasers tend to be discrete-wavelength devices involving stimulated emission between quantized energy levels in the laser media. Only when these quantized energy levels are tunable or there are neighboring energy levels that are sufficiently broadened to merge into each other to form a continuous band can a continuously tunable laser be built. Even then, the tuning range tends to be limited.

Optical parametric oscillators are powerful solid-state sources of coherent radiation with potentially very large truly continuous tuning ranges. For example, the recently developed pulsed β-barium borate β-BaB_2O_4 (BBO) optical parametric oscillator (OPO) can be tuned continuously from 415 nm to 2.5 μm with a single set of mirrors when pumped at 355 nm [1]–[5] or from 300 nm to 2.5 μm with multiple sets of mirrors when pumped at 266 nm [3], [4] (Fig. 1). The total conversion efficiency from the pump to useful OPO outputs can be well above 30% at pulsed output energy levels of millijoules to joules depending on the device design and pump source. Although there is still a great deal of room for further improvements, optical parametric oscillators have already been demonstrated to be versatile and practical coherent radiation sources.

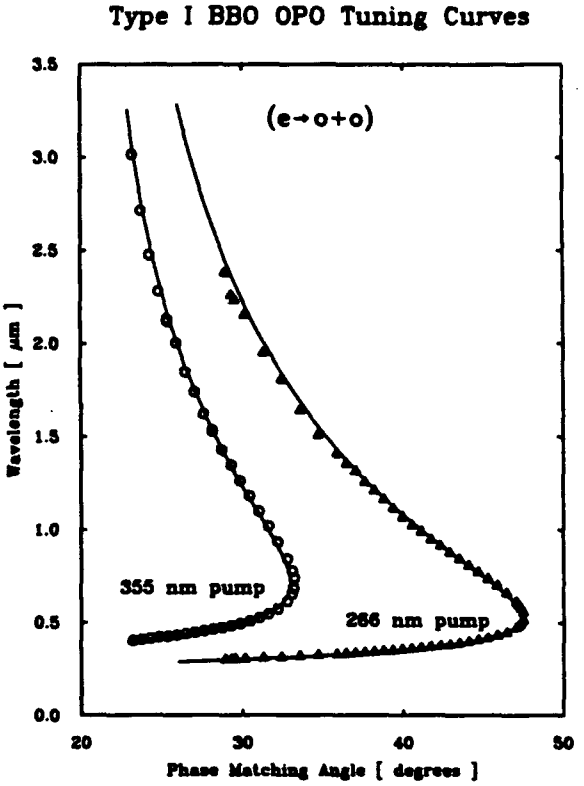

Fig. 1. Type I, 355 nm pumped (Δ) BBO OPO tuning curves determined by parametric luminescence. The solid lines are predictions based on Sellmeier equations reported in [43]. Parametric oscillations have been observed in the range from 415 nm to 2.5 μm using one set of mirrors resonating in the visible when pumped at 355 nm and from 330 nm to 2.5 μm using multiple sets of mirrors when pumped at 266 nm (see, for examples, [1]–[5], [26]–[29]).

The basic idea of the parametric process was known long before the advent of the optical parametric oscillator. There was considerable interest in the microwave parametric amplifier as a low-noise amplitude- and phase-sensitive amplifier in the 1950's [6]. In the optical region, because noise due to the zero-point fluctuations ($h\nu$ per

Manuscript received August 28, 1990; revised June 10, 1991. This work was supported in part by the Naval Research Laboratory, the National Science Foundation, and E. I. DuPont de Nemours & Co.

C. L. Tang, W. R. Bosenberg, T. Ukachi, and R. J. Lane are with Cornell University, Ithaca, NY 14853.

L. Kevin Cheng is with E. I. DuPont de Nemours & Co., Experimental Station, Wilmington, DE 19880-0306.

IEEE Log Number 9107266.

0018–9219/92$03.00 © 1992 IEEE

mode per volume) far exceeds the thermal fluctuations (kT per mode per volume), optical parametric amplifiers are not particularly useful as low-noise amplitude-and phase-sensitive amplifiers even though they are quantum noise limited. Based upon the recently developed concept of "squeezing," through which the quantum noise can be selectively concentrated more in either the amplitude or in the phase-channel, the optical parametric amplifier may conceivably become a useful low-noise device in the optical region by putting the signal in the alternative quieter channel, but the practicality of such an amplifier is far from having been demonstrated. The real interest in the optical domain is in the wavelength tunability of the optical parametric oscillators.

The first proposal and theory of optical parametric oscillator were due to Kroll in 1962 [7]. Shortly after the first demonstration of optical parametric oscillation by Giordmaine and Miller in 1965 [8], there was a period of intense efforts at developing such an oscillator into a practical device. The potential of such a device as a useful source of coherent radiation was clear from the beginning to a hard core group of specialists (including at least one science fiction writer[1]), and a variety of theoretical and experimental studies were carried out [9], [10]. The practical development of such an oscillator was hampered, however, by the lack of suitable nonlinear optical crystals.

Unfortunately, the development of nonlinear optical materials is a very slow and tedious process, with the discovery of useful new nonlinear optical materials often depending on luck. This lack of progress in practical developments coupled with over-optimism on the part of some enthusiasts eventually led to considerable skepticism about the prospects of the optical parametric oscillator as a useful device. In the meantime, progress in the search of new nonlinear optical crystals was slowly being made, leading to many new nonlinear crystals (e.g., β-BaB_2O_4, LiB_3O_5, $KNbO_3$ $KTiOPO_4$, L-Arginine Phosphate, MgO:$LiNbO_3$, $KTiOAsO_4$, $AgGaS_2$, $AgGaSe_2$, and Tl_3AsSe_3, etc.) in the past decade and culminating in the recent rapid progress in optical parametric oscillator technology.

Experimental OPO's in the earlier days [illegible] to be in the infrared, and the widely used crystal [illegible] suffered from severe optical damage problems. Ex[illegible]on to the shorter wavelength part of the spectrum had been more difficult due to the lack of nonlinear optical materials that can be phase-matched in the UV. The first nonlinear material to break this wavelength barrier was crystalline urea. A continuous tuning range from 500 nm to 1.23 μm was achieved with a single set of mirrors resonating in the visible and pumped by the third harmonic ($\sim$ 355 nm) of the output of a Nd:YAG laser [11]. However, although crystalline urea has very high single-shot damage thresholds, it suffers from long-term optical damage problems and was soon superseded by the new nonlinear optical crystal β-barium borate [12], which is comparatively easy to grow and has superior crystal properties.

[1] "Sundiver," by David Brin, p. 243, Bantam Spectra Book, 1980.

The first BBO OPO was reported on at CLEO in 1986 by Fan *et al.* [1], [2] using a 9 mm crystal grown at the Fujian Institute in the Peoples' Republic of China (PRC). It was a doubly-resonant, plano-plano cavity pumped by the second-harmonic of Nd:YAG at 532 nm with a limited tuning range of 0.94–1.22 μm and a conversion efficiency of about 10%. Although this work indicated only modest performance from a BBO OPO, it was the precursor to a whole host of subsequent work.

More recently, the related lithium triborate (LBO) crystal has also appeared on the scene [13]–[15] and is attracting considerable attention as a potentially useful OPO material [16], [17]. For the UV and visible range, these borate crystals are now clearly the materials of choice for OPO applications. From the deep red to about 4.5 μm, the nonlinear crystal potassium titanyl phosphate (KTP) [18]–[20] can meet many of the key requirements for OPO applications, including applications in the femtosecond regime, and shows great promise.

Even though the growth technologies for all of these new crystals still need improvements, OPO's with remarkable performances have already been demonstrated using these three crystals from currently available sources. This article gives a brief review of the operating principle of optical parametric oscillators and the current status of the development of such devices.

II. Basic Concept [9]

The optical parametric process is a nonlinear optical process in which a pump photon, propagating in a nonlinear optical crystal spontaneously or by stimulated emission breaks down into two lower-energy photons of frequencies ω_1 and ω_2 with the total photon energy conserved, i.e., $\omega_p = \omega_1 + \omega_2$. This simple energy conservation condition is the basis of the famous Manley–Rowe relation [6] in the language of microwave parametric amplifier work. The gain mechanism is based upon the stimulation emission process. That is, the rate of emission through the nonlinear optical parametric process is proportional to the photons present; thus the larger the number of photons emitted, the more likely photons will be emitted leading to parametric gain.

It is clear that the frequencies of the two emitted photons cannot be uniquely determined on the basis of this condition alone. For a given w_p there can be a continuous range of choices of ω_1 and ω_2. This is in fact the basic source of tunability of the OPO's. The specific pair of frequencies that will result in any given situation is dictated by the momentum conservation condition, or phase-matching condition: $k_p = k_1 + k_2$, that must also be satisfied.

In a normally dispersive and isotropic medium, the material dispersion is such that the momentum or the magnitude of the k-vector of the pump photon is always too large due to dispersion to satisfy the phase-matching condition. In order to compensate for material dispersion, it must be reduced relative to the sum of those of the emitted photons. The most common approach is to make use of the birefringence in an anisotropic medium to compensate

for material dispersion. In an anisotropic medium, the index of retraction, and hence the magnitude of the k-vector, of an extraordinary wave varies with the direction of propagation. For a negative uniaxial crystal, the magnitude decreases continuously from that equal to the ordinary wave in the propagation direction along the optical axis to a minimum value in the orthogonal direction. The corresponding change in the magnitude of the k-vector is determined by the birefringence of the medium. Thus if the birefringence is sufficiently large to compensate for the dispersion, and if the pump beam is introduced as an extraordinary wave while the signal and idler waves are ordinary waves, a particular pair of frequencies of emitted ordinary photons will satisfy the so-called Type-I phase-matching condition $k_p^{(e)} = k_1^{(0)} + k_2^{(0)}$) for each orientation of the crystal relative to the direction of propagation of the pump photon. These are then the unique frequency outputs of the parametric oscillator for a given pump photon and a particular orientation of the crystal.

As the crystal is rotated, the magnitude of the k-vector or the momentum of the pump photon changes. The frequencies of the resulting pair of emitting photons will then change accordingly. This is the basic tuning scheme of the optical parametric oscillators. The bandwidth of the parametric process is determined by either the pump beam divergence or the spectral width over which the phase-matching condition can be nominally satisfied; that is, the phases of the emitted waves are within, say, $\pi/2$ over the interaction length. In general, the bandwidth varies linearly with the pump beam divergence when the waves do not propagate along a principal-axis direction of the crystal. Such a phase-matching condition is called "critical" and the corresponding allowed interaction length is called "critical phase-matching length." Along a principal-axis, the phase-matching is "noncritical" and the corresponding "noncritical phase-matching length" is not sensitive to the pump-beam divergence; the dependence on the reciprocal of the pump-beam divergence angle in this case is of second-order (see Table 1). The corresponding bandwidth of the parametric process is in practice often determined by the physical length of the nonlinear crystal. The advantages of noncritical phase-matching are possibly narrower linewidths and longer interaction lengths.

With suitable nonlinear optical crystals and pump sources, virtually any wavelength ranging from the UV to the mid IR can now be reached with optical parametric oscillators. The technology is better developed at the present time for the near UV to 4.5 μm range, however, largely due to the availability of large high quality BBO, LBO, $MgO:LiNbO_3$, and KTP crystals. For the 1 to 10 μm range, $AgGaS_2$ and $AgGaSe_2$ [21], [22] show great promise.

III. Recent Developments and Current Status

A. BBO OPO

Compared to other nonlinear optical crystals, BBO has the advantages of being only slightly hygroscopic, mechanically hard, and chemically stable; has a high optical damage threshold; and can be grown to sufficiently large sizes. It is transparent down to 191 nm and has a relatively large birefringence; it can, therefore, be phase-matched over a large spectral range, which means a large tuning range in OPO applications. The effective d-coefficient of BBO is not large, but adequate for OPO applications with reasonable requirements on the length of the crystal and the pump power. Some of the key properties of BBO are summarized in Table 1 along with the known properties of LBO and KTP crystals. It must be emphasized that because these are relatively new materials, some of the numbers listed are still subject to confirmation and possibly revision.

Nearly all of the BBO OPO experiments reported in the literature so far are based on crystals grown using a high-temperature flux growth method, mostly from the PRC (Fujian Institute for Materials Research and Beijing Institute for Synthetic Crystals), with the exceptions of the Cornell University work [23], [24] and some of the experiments carried out at Stanford. Commercial sources in the U.S. have mainly been selling BBO crystals from the PRC. A number of U.S. companies are developing independent sources of such crystals, some with technical support from Cornell and Stanford Universities. Cleveland Crystals is now producing high quality BBO crystals and appears to be the only commercial source of U.S. produced BBO crystals. Researchers in NEC, Japan, have recently reported successfully growing single crystals of BBO from a melt using the Czochralski method [25]. Thus while much remains to be done, it is quite likely that BBO crystals will become more readily available commercially and the cost will come down in the near future.

The BBO OPO's are pumped with either the harmonics of Nd:YAG lasers or XeCl excimer lasers [26]–[28] with injection seeding for narrow linewidth and diffraction limited divergence. The OPO performances and the optical-to-optical efficiencies achievable in the two cases are comparable for comparable pump beams, as might be expected.

In the Nd:YAG pumped case, the most versatile practical OPO is currently the third-harmonic pumped BBO OPO. With the 355 nm pump, the entire near UV to near IR range from 415 nm to 2.5 μm can be covered with a single set of mirrors [3]–[5] resonating from 415 nm to the degenerate point at 710 nm. Well over 30% total efficiency (in terms of useful outputs at the signal and idler wavelengths) has been achieved using two approximately 1-cm long crystals in the walk-off compensated configuration shown in Fig. 2 at a pumping level on the order of 15–20 mJ/pulse. The efficiency is now pump pulse-length limited. That is, within the finite pump pulse duration (typically 7 to 10 ns long), the number of passes the signal pulse can make back and forth between the mirrors of the singly resonant cavity is limited and is less than that needed for the signal pulse to developed to full saturation strength. With sufficiently long pump pulses and eliminating such possible practical problems as the thermal lensing effect, the upper limit of the total efficiency is over 60%. In terms of the output energy, because OPO's are scalable, the output energy depends only

Table 1 Properties of Some Nonlinear Optical Crystals for OPO Applications. Data shown is at 1.064 μm unless otherwise indicated. Γ_{max}-surface damage threshold; $l\Delta T$-temperature-tuning bandwidth; $l\Delta\Theta$, CPM-critical phase-matching acceptance angle; $l^{1/2}\Delta\Theta$-noncritical phase-matching acceptance angle; $l\Delta\lambda$-SHG bandwidth; $\Delta\nu_g^{-1}$-group-velocity dispersion for SHG at 630 nm.

Crystal	LBO	$\beta - BaB_2O_4$ [54]	KTP [54]
Point group	mm2 [44]-[46]	3m	mm2
Birefringence	$n_{z=a} = 1.5656$ [47]-[49] $n_{y=c} = 1.5905$ $n_{z=b} = 1.6055$	$n_e = 1.54254$ $n_o = 1.65510$	$n_{x=a} = 1.7367$ $n_{y=b} = 1.7395$ $n_{z=c} = 1.8305$
Nonlinearity (pm/V)	$d_{32} = 1.16$ [47]-[49]	$d_{22} = 1.6$ $d_{31} = 0.08$	$d_{32} = 5.0, d_{31} = 6.5$ $d_{24} = 7.6, d_{15} = 6.1$ $d_{33} = 13.7$
Transparency (μm)	0.16 – 2.6 [50], [51]	0.19 – 2.5	0.35 – 4.4
$\Gamma_{max(GW/cm^2)}$	~ 25 [47]-[49]	~ 5 [55]	~ 15.0
SHG cutoff (nm)	555 [52]	411	990
$l\Delta T(°C \cdot cm)$	3.9 [53]	55	22
$\Delta\Theta(mrad \cdot cm)$, CPM	31.3 [53]	0.52	15.7
$l^{1/2}\Delta\Theta(mrad)$ $(mrad(cm)^{1/2})$	71.9 [53] NCPM @ 148.0°C	Not available	Not available
$l\Delta\lambda(Å \cdot cm)$	Not available	6.6	4.5
$\Delta\nu_g^{-1}$ @ 630 nm (fs/mm)	240 [52]	360	Not applicable
OPO tuning range (nm)	~ 415 – 2500 [52] ($\lambda_p = 355$)	~ 415 – 2500 ($\lambda_p = 355$)	~ 577 – 4400 nm ($\lambda_p = 532$)
Boule size	20 × 20 × 15 mm^3 [53]	Ø84 mm × 18 mm	~ 20 × 30 × 50 mm^3
Growth	TSSG [53] @ ~ 810°C	TSSG from Na_2O @ ~ 900°C	TSSG from $K_6P_4O_{13}$ Flux @ ~ 950°C
Predominant growth defects	Flux [53] inclusions	Flux and bubble inclusions	Flux inclusions & domains
Chemical properties	Nonhygroscopic [53] (m.p. ~ 834°C)	Slightly hygroscopic ($\beta \rightarrow \alpha$ ~ 925°C)	Nonhygroscopic (m.p.~ 934°C)

on the available pump beam energy and should be readily extendable to the multi-Joule level.

Although it has been demonstrated that, pumping with the 4th harmonic of Nd:YAG at 266 nm, the entire spectral range from 330 nm to 2.5 μm can be covered with multiple sets of mirrors, the mirror coating damage problem at 266 nm is a serious one [3]–[5]. The BBO bulk damage threshold at this wavelength is, however, much higher than that of the mirror coatings that can be achieved with current UV coating technology. With the pump-beam steering scheme shown in Fig. 2 and improved coatings, practical BBO OPO's operating in the 300 to 450 nm range should be possible. Such sources will be of great interest because other sources of tunable radiation in this spectral region tend to be inefficient and cumbersome to use.

Because of the large number of available wavelengths in the UV at relatively high overall efficiencies and average power levels, the gaseous excimer lasers offer great potential as pumps for OPO's. With a carefully designed XeCl laser at 308 nm as the pump, remarkable results on urea OPO's have been achieved at the University of St. Andrews [27], [28]. Continuous tuning range from 537 to 720 nm was achieved with conversion efficiencies approaching 66% over a narrow range near the noncritical phase-matching condition. For BBO OPO's, the entire tuning range extending from 354 nm to 2.37 um with efficiencies on the order of 10% have been achieved. A major problem with the excimer laser pumped BBO OPO's reported so far is that the linewidth of the output is rather large. Without any line narrowing scheme, the reported linewidth in a Type-I OPO can vary from approximately 1 nm at 480 nm to nearly 11 nm at 600 nm [27], [28]. By comparison, the corresponding linewidths of similar Nd:YAG laser third-harmonic pumped oscillators are nearly an order of magnitude narrower [29].

For spectroscopic applications, the linewidth of the BBO OPO is an issue. With a 355 nm Nd:YAG laser pump, the linewidth varies from 0.15 nm far from degeneracy to well over 10 nm at degeneracy. While this may be adequate for some applications in solids as will be shown later, many

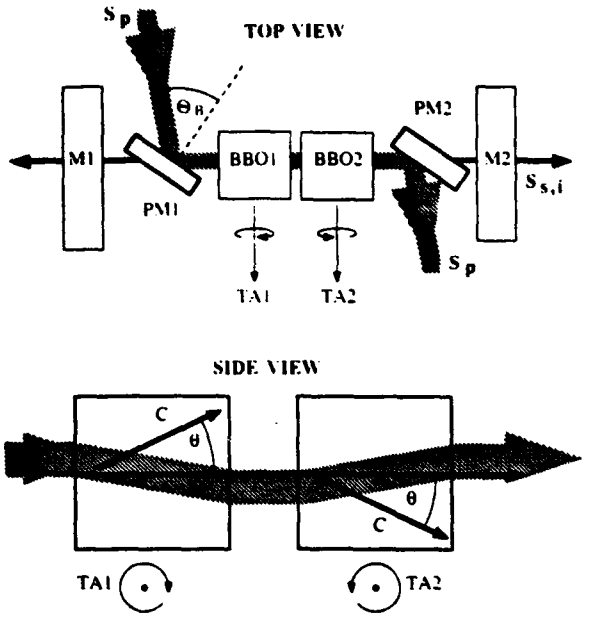

Fig. 2. Walk-off compensated two-crystal configuration of BBO OPO with intracavity UV pump beam-steering mirrors. (For a detailed explanation, see [29].)

applications will require much better spectral resolution. Two different approaches have been used to attack the linewidth problem. The first is to use intracavity dispersive elements [29]. The use of intracavity gratings in much the same way as in pulsed dye lasers has led to dramatically reduced linewidth. Generally speaking, without beam expansion optics, the use of gratings in various configurations can limit the linewidth to on the order of 0.1 nm throughout the tuning range. Because the efficiencies of BBO OPO's are now typically pump pulse-length limited, there is a limit on the OPO cavity length that can be used; this makes it difficult to introduce beam-expansion optics into the cavity without reducing the efficiency of the oscillator drastically. In the case where the cavity-length is not a limiting consideration, much narrower linewidth similar to those achievable in pulsed dye lasers should be possible.

An alternative approach is to use Type-II phase-matching [30] where the signal wave is also an extraordinary wave ($k_p^{(e)} = k_1^{(e)} + k_2^{(0)}$ or $e \rightarrow e + 0$). It is known that this type of phase-matching can lead to narrower linewidth than that using Type I phase-matching ($e \rightarrow 0 + 0$). In BBO, where the effective d-coefficient for Type II interaction is considerably smaller (~ 0.8 p/V), the difficulty has been to obtain a large enough interaction length in a suitably cut BBO crystal. With recent improvements in BBO crystal size and OPO design, Bosenberg *et al.* [30] have shown that Type II phase-matching is a viable means of obtaining narrow linewidth radiation. Using the two-crystal walk-off compensated scheme mentioned earlier (Fig. 2), along with crystals cut for the Type II interaction that are 17 mm and 10 mm in length (Cornell grown), they have demonstrated oscillation over the range of 480 nm to 630 nm and 810 nm to 1.36 μm with conversion efficiencies of 12% and linewidths in the 0.05–0.3 nm range without line-narrowing elements; as expected, they are much narrower than those obtained in the Type I devices

In addition to nanosecond types of OPO's, there has also been considerable interest in using BBO OPO's and optical parametric amplifiers (OPA's) for tunable picosecond pulse generation [31], [32]. Narrow band (< 0.3 nm) and high energy (> 200 μJ) widely tunable (400 nm to 2 μm) picosecond pulses with a better than 30% efficiency have been shown to be possible [31].

It is also of interest to mention briefly some recent examples of the applications of BBO OPO's making use of the tunable radiation in the near IR, where there is a dearth of high power tunable radiation sources to evaluate other nonlinear optical crystals. Figures 3(a) and (b) show the measured tuning curves for second-harmonic generation (SHG) in gadolinium molibdate (GMO) at 70° F. They show that the noncritical phase matching wavelengths for A- and B-cut GMO crystals to be at 1.4029 and 1.410 μm [33], respectively. Such information is of interest in the search for efficient SHG crystals in the minimum-loss and minimum-dispersion regions of optical fibers for long distance communication purposes. Figure 3(c) shows the temperature-tuning curve for noncritical phase-matching SHG in a lithium triborate (LBO) crystal recently measured using the tunable BBO OPO output [34].

Medical and spectroscopic applications and large scale chemical and commercial lidar applications for detecting leaks along gas pipe lines, or for oil exploration, etc., using BBO OPO's are reported to be under development.

B. Lithium Triborate (LBO)

LBO is a newly developed nonlinear optical crystal which is characterized by good UV transparency, moderate birefringence and nonlinear optical coefficient, and a relatively high optical damage threshold [13]–[15]. These unique properties, along with its mechanical hardness, chemical stability, and nonhygroscopicity, make LBO an attractive material for certain nonlinear optical processes. Although the smaller birefringence in LBO as compared to that in BBO tends to limit the phase-matching spectral range, it also leads to the possibility of noncritical phase-matching and larger acceptance angle for frequency conversion applications in the visible and near IR. For OPO applications, the possibilities of achieving noncritical phase matching with standard sources as pumps and temperature tuning are distinct advantages of this material.

The existence of LBO has been known since 1926 [35]. Its usefulness as a nonlinear optical material was first pointed out by Chen in 1987 [36]. All the commercially available LBO crystals have been from the Fujian Institute (up to $\Phi 80 \times 15 mm^3$) grown by a high-temperature self-flux growth method or from Beijing Institute of Synthetic Crystals by a modified flux or flux pulling method. In the U.S., modest sized single crystals have been grown by top-seeded solution growth from a self-flux at Cornell and Stanford Universities and as yet there have been no commercial growers.

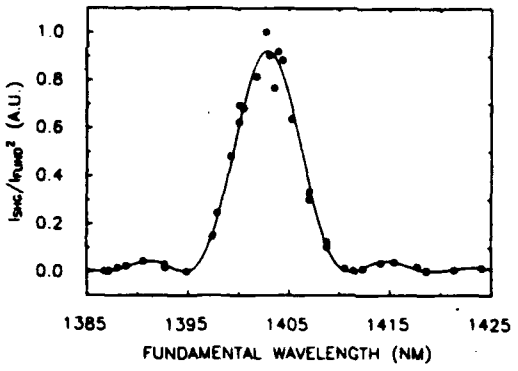

(a)

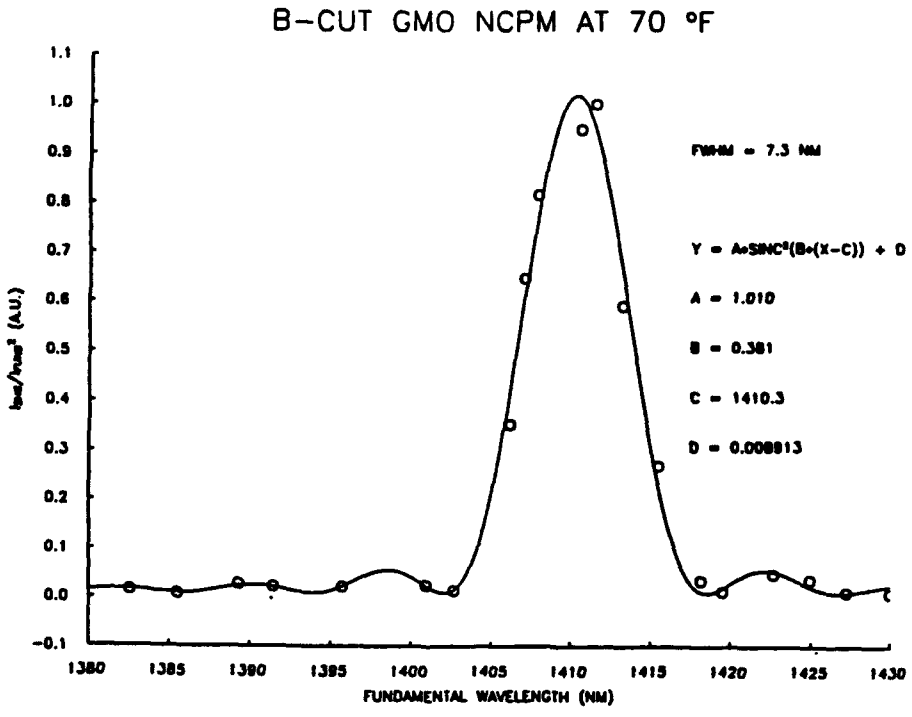

(b)

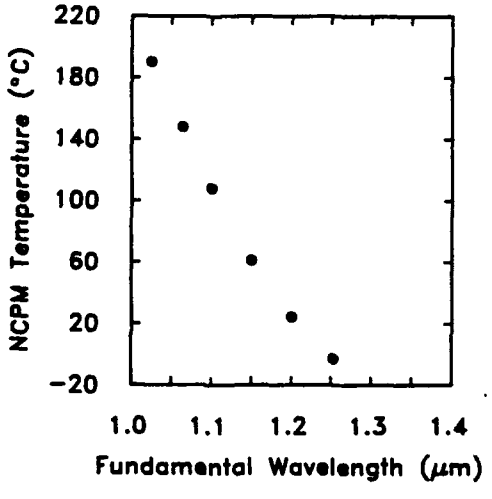

(c)

Fig. 3. Examples of applications of BBO OPO. The tunable infrared output of a two-crystal walk-off compensated BBO OPO was used to determine the wavelengths for noncritical phase-matching (NCPM) second-harmonic generation (SHG) in (a) A-cut and (b) B-cut gadolinium molibdate crystals at 70° F [33], and (c) the temperature tuned NCPM second-harmonic generation curve of lithium triborate crystal [34].

Xu *et al.* [16], have recently reported the successful operation of an LBO OPO with a tuning range of 540 nm to 1.03 μm at an efficiency of 22.1% (at 503.4 nm) pumped by the third-harmonic of Nd:YAG laser output using a $6 \times 6 \times 15.9\text{mm}^3$ crystal grown at the Fujian Institute and cut for Type I phase-matching. The linewidth of the LBO oscillator output is rather large, however: 6 nm at 674 nm, for example. Ebrahimzadeh *et al.* [17], have carried out a series of LBO OPO experiments by pumping with a XeCl laser at 308 nm, also using crystals grown at the Fujian Institute. Tunable radiation throughout the 372 nm to 1.8 um range was obtained. A particular feature of their work is the use made of Type II and noncritical phase-matching, leading to a narrow linewidth, for example, of 0.15 nm in the 375 to 387 nm range and an efficiency of 16.5% with a 16 mm long crystal. With the various UV wavelengths available from other excimer lasers, it is potentially possible to achieve noncritical phase-matching down to 285 nm with narrow linewidths and relatively high efficiencies.

Comparing to BBO, LBO offers interesting possibilities that are yet to be explored. It is unlikely, however, that one will replace the other. The choice will depend on the application and particular engineering design considerations.

C. Potassium Titanyl Phosphate (KTP)

Optical nonlinearity in KTP was first discovered at Dupont in 1976 by Zumsteg *et al.* [18]–[20]. Since then, KTP has been primarily used as the second harmonic crystals in many commercial and laboratory laser systems where premium performance and reliability are needed (e.g., in medical lasers and in field-portable microlasers). Recent advances in the growth of KTP has made available sizable cm long), single domain crystals suitable for the development of the optical parametric device.

Some of the known properties are tabulated in Table 1. It is chemically stable and mechanically robust. Optical dielectric coatings can be readily applied onto polished crystal surface using standard coating techniques. The single-shot damage threshold for high quality hydrothermally grown crystals is sufficiently high ($\sim 30\ \text{GW/cm}^2$ for 30 ps pulse at 526 nm) [18]–[20] to withstand the optical power density in an OPO. Efficient frequency conversion in KTP is restricted to Type II interaction with effective nonlinearity, d_{eff}, ranging from 3 to 7.5 pm/V.

In the nanosecond regime, the efficient operation of a Type II KTP OPO has been reported recently [37]. A diode-pumped Nd:YAG laser is used to pump the OPO at 1.064 μm. With a 15 mm long KTP crystal and a confocal resonator cavity, a 1.06 to 1.61 μm conversion efficiency of 35% was achieved.

Recently, Vanherzeele [19], [20] has reported the generation of broadly tunable (600 nm to 4.5 μm) picosecond pulses at the millijoule level by single-pass OPO/OPA in KTP (Fig. 4(a) and (b)). Using a picosecond ND:YLF (1.053 μm) laser as the pump, a single-pass gain in excess of 10^6 was reported for a seeded KTP amplifier.

KTP and BBO are particularly suited for synchronously pumped OPO for short pulse generation down to the picosecond [38], [39] and femtosecond [40], [41] time domains. In a synchronously pumped picosecond or femtosecond OPO, the pump beam consists of a train of repetitive short pulses each with a spatial extent generally much shorter than the OPO cavity length. Thus the pump pulses are short traveling-wave pulses through the nonlinear crystal. In an OPO cavity of just the right length, the signal pulse will meet and be synchronously pumped by the repetitive pump pulses. For the same average pump pulse power, the peak pump pulse power can be much higher and thus more efficient pumping of the pulsed OPO can be achieved.

Using a mode-locked Nd:YAG pump, Bromley *et al.* [38] have efficiently operated a synchronously pumped singly resonant KTP OPO, producing tunable 70 ps pulses between 1.04 and 1.09 μm with an over-all efficiency of 30%.

The successful use of a nonlinear crystal in OPO depends, to a large extent, on the successful development of its crystal growth technology. KTP is no exception. With

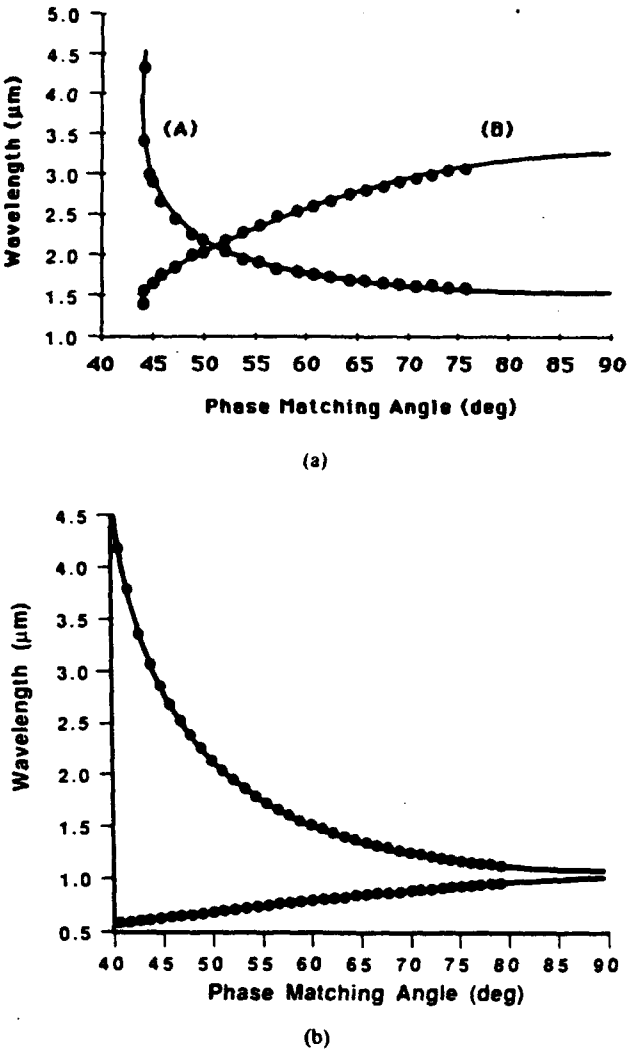

Fig. 4. Single-pass parametric generation tuning curves for KTP in the xz plane: (a) pumped at 1.053 μm and (b) at 526 nm. The tuning gap in (b) is from 1.007 to 1.103 μm and can be removed by going to $\theta \sim 23°$ plane. (Reprinted from [18]).

the recent advances in the flux growth of KTP, routine production of KTP boules of $2 \times 3 \times 5 cm^3$ are now possible. Significant further improvements have also been made in the hydrothermal growth of KTP. Thus the general availability and the usefulness of this crystal should also improve significantly in the future.

D. Tunable Femtosecond OPO's

There is a great need for CW femtosecond laser sources with high pulse repetition rates that are tunable. The only available CW high-repetition rate femtosecond laser operates at approximately 630 nm and is based on the CW mode-locked Rh6G dye laser with DODCI saturable absorber With such a fixed wavelength femtosecond dye laser as a synchronous pump, OPO offers the possibility of converting such pulses in the red to a large spectral range in the deep red to the infrared at effective efficiencies well over 25%. KTP is a prime candidate for such an application because of its relatively large effective nonlinear coefficient. However, because of possible pulse broadening due to group dispersion in the nonlinear medium, the interaction length is severely restricted. For femtosecond pulses, the KTP crystal length must be on the order of a mm or less. Thus to reach OPO oscillation threshold using a CW mode-locked Rh6G dye laser as the pump, the KTP crystal must be synchronously pumped inside the dye laser cavity. Such an intracavity femtosecond KTP OPO has recently been demonstrated by Edelstein *et al.* at Cornell [40], [41]. The OPO produced stable pulses of $\sim$ 100 fs short at 10^8 Hz in the deep red at the mW-level. With one set of mirrors, a tuning range from 820–920 nm and 1.92–2.54 μm has been achieved. With three additional sets of mirrors, the entire range from 700 nm to 4.5 μm can be covered. This KTP OPO is the first broadly tunable CW femtosecond generator of coherent radiation. Other types of femtosecond OPO's [42] using different crystals and pump sources are sure to follow.

Using OPO's to generate broadly tunable femtosecond pulses for studies of ultrafast processes is a promising new direction of OPO research and device development.

IV. Conclusion

Optical parametric oscillators are powerful solid state sources of broadly tunable coherent radiation that can operate down to the femtosecond time domain. As a result of recent advances in nonlinear optical crystal research, OPO's are now practical devices with broad potential applications in research and industry. Recent developments in BBO, LBO, and KTP optical parametric oscillators are reviewed in this article. Although we have emphasized in our discussions these three specific types of OPO's to give an indication of the current status of the OPO technology because of their more recent interests, a variety of other visible and IR OPO's based on older materials such as $LiNbO_3$, $LiIO_3$, $KNbO_3$, $AgGaS_2$, $AgGaSe_2$, etc. have also been improved to the point where they are beginning to find important applications.

Acknowledgment

The authors wish to thank J. Bierlein, C. Chen, M. Dunn, M. Ebrahimzadeh, J. Y. Huang, Y. R. Shen, and H. Vanherzeele for helpful discussions and for providing the background material for this article.

References

[1] Y. X. Fan, R. C. Echkardt, R. L. Byer, C. Chen, and A. Jiang, "Beta-phase barium borate optical parametric oscillator," presented at CLEO '86, post deadline paper ThT4.

[2] Y. X. Fan, R. C. Eckardt, R. L. Byer, J. Nolting, and R Wallenstein, "Visible BaB_2O_4 optical parametric oscillator pumped at 355 nm by a single axial-mode pulsed source," *Appl. Phys. Lett.*, vol. 53, p. 2014, 1988.

[3] L. K. Cheng, W. R. Bosenberg, and C. L. Tang, "Broadly tuneable optical parametric oscillation in β-$BaBO_4$," *Appl. Phys. Lett.*, vol. 53, p. 175, July 1988.

[4] W. R. Bosenberg, L. K. Cheng, and C. L. Tang, *App. Phys. Lett.*, vol. 54, p. 13, Jan. 1989.

[5] W. R. Bosenberg, Ph.D. dissertation, Cornell University, Ithaca, NY, 1990.

[6] W. H. Louisell, *Coupled Mode and Parametric Electronics*. New York: Wiley, 1960.

[7] N. Kroll, "Parametric amplification in spatially extended media and application to the design of tuneable oscillators at optical frequencies," *Phys. Rev.*, vol. 127, p. 1207, 1962.

[8] A. Giordamine and R. C. Miller, "Tuneable coherent parametric oscillation in $LiNbO_3$ at optical frequencies," *Phys. Rev. Lett.*, vol. 4, p. 973, 1969.

[9] See, for example, R. L. Byer, "Optical parametric oscillators," in *Treatise in Quantum Electronics, Vol. 1, Nonlinear Optics*, Pts. A and B, H. Rabin and C. L. Tang, Eds., New York: Academic, 1975.

[10] C. L. Tang, "Spontaneous and stimulated parametric processes," in *Treatise in Quantum Electronics, Vol. 1, Nonlinear Optics*, pts. A and B, H. Rabin and C. L. Tang, H. Rabin and C. L. Tang, Eds. New York: Academic, 1975.

[11] See, for example, L. K. Cheng, M. J. Rosker, and C. L. Tang, in *Tunable Lasers*, L. F. Mollennauer and J. C. White, Eds. Berlin, Germany: Springer-Verlag, 1987.

[12] C. Chen, B. Wu, A. Jiang, and G. You, "A new-type ultraviolet SHG crystal β-BaB_2O_4," *Sci. Sin. Ser. B* vol. 28, p. 235, 1985.

[13] C. Chen, Y. Wu, A. Jiang, B, Wu, G. You, R. Li, and S. Lin, "New nonlinear-optical crystal: LiB_2O_5," *J. Opt. Soc. Amer.*, vol. B6, p. 616, 1989.

[14] S. Lin, Z. Sun, B. Wu, and C. Chen, "The nonlinear optical characteristics of a LiB_3O_5 crystal," *J. App. Phys.* vol. 67, p. 634, 1990.

[15] Z. Zhao, C. Huang, and H. Zhang, "Crystal growth and properties of lithium triborate," *J. Cryst. Growth*, vol. 99, p. 805, 1990.

[16] Z. Xu, D. Deng, Y. Wang, B. Wu, and C. Chen, "Optical parametric oscillation form LiB_3O_5 pumped at 355 nm," presented at CLEO '90, Anaheim, CA, May 1990.

[17] M. Ebrahimzadeh, G. Robertson, M. Dunn, and A. Henderson, "Excimer-pumped LiB_3O_5 optical parametric oscillators," presented at CLEO '90, post deadline paper CPDP 26, Anaheim, CA, May 1990.

[18] F. C. Zumsteg, J. D. Bierlein, and T. E. Gier, "A New Nonlinear optical Material," *J. Appl. Phys.*, vol. 47, p. 4980, 1976.

[19] H. Vanherzeele, "Picosecond laser system continuously tuneable in the 0.6–4 μm range," *Appl. Opt.*, vol. 29, p. 2246, 1990.

[20] C. Van der Poel, S. Colak, J. D. Bierlein, and J. B. Brown, "Efficient type I blue second harmonic generation in periodically segmented $KTiOPO_4$ (KTP) wave guides," presented at CLFO '90, post deadline paper, CPDP 33, Anaheim, CA, May 1990.

[21] Y. X. Fan, R. C. Ekart, R. L. Byer, R. K. Route, R. S. Feigelson, "AgGaSi infrared parametric oscillator," *Appl. Phys. Lett.*, vol. 45, no. 4, pp. 313–315, 1984.

[22] R. C. Ekart, Y. X. Fan, R. L. Byer, C. L. Marquardt, M. E. Storm, and L. Esterowitz, "Broadly tunable infrared parametric oscillator using $AgGaSe_2$," *Appl. Phys. Lett.*, vol. 49, no. 11, p. 608, 1986.

[23] L. K. Chen, W. R. Bosenberg, and C. L. Tang, "Growth and characterization of low temperature phase barium metaborate crystals," *J. Cryst. Growth*, vol. 89, p. 553, 1988.

[24] W. R. Bosenberg, R. J. Lane, and C. L. Tang, "Growth of large, high-quality beta-barium metaborate crystals," *J. Cryst. Growth* vol. 108, pp. 394–398, 1991.
[25] Y. Kuwano and H. Kouta, "Beta-BaB_2O_4 crystal grown by a new method," presented at CLEO '90, Anaheim, CA, May 1990.
[26] H. Komine, "Optical parametric oscillation in a beta-barium borate crystal pumped by a XeCl excimer laser," *Opt. Lett.*, vol. 13, p. 643, 1988.
[27] M. Ebrahimzadeh, M. H. Dunn, and F. Akerboom, "Highly efficient visible urea optical parametric oscillator pumped by a XeCl excimer laser," *Opt. Lett.*, vol. 14, p. 560, 1989.
[28] M. Ebrahimzadeh, A. J. Henderson, and M. H. Dunn, "An excimer-pumped β-BaB_2O_4 optical parametric oscillator tuneable from 354 nm to 2.370 μm," *J. Quant. Elect.*, vol. 26, pp. 1241–1252, July 1990.
[29] W. R. Bosenberg, W. S. Pelouch, and C. L. Tang, "High-efficiency and narrow-linewidth operation of a two-crystal β-BaB_2O_4 optical parametric oscillator," *Appl. Phys. Lett.*, vol. 55, p. 1952, 1989.
[30] W. R. Bosenberg and C. L. Tang, "Type II phase matching in a β-barium borate optical parametric oscillator," *Appl. Phys. Lett.*, vol. 56, p. 1819, 1990.
[31] J. Zhang, Y. Huang, Y. R. Shen, C. Chen, and B. Wu, "Picosecond tuneable optical parametric amplification in barium and lithium borates," presented at CLEO '90, Anaheim, CA, May 1990.
[32] A. Piskarakas, V. Smilgyavichyus, and A. Umbrasas, "Continuous generation of picosecond light pulses," *Sov. J. Quant. Elect.*, vol. 18, p. 155, 1988.
[33] For more detailed information, see K. Kendall, S. K. Kurtz, R. Lane, W. Bosenberg, C. L. Tang, G. Grimouille, L. Oudar, and R. Neurgaonkar, "Non-critical phase matched second harmonic generation by β-Gd2(MoO_4)3 in the near infrared," in *Proc. 7th Int. Symp. on the Applications of Ferroelectrics*, Univ. of Illinois at Urbana-Champaign, June 6–8, 1990.
[34] T. Ukachi, R. J. Lane, W. R. Bosenberg, and C. L. Tang, "Measurements of noncritically phase-matched second harmonic generation in a LiB_3O_5 crystal," *Appl. Phys. Lett.*, vol. 57, p. 980, Sept. 1990.
[35] C. Mazzetti and F. D. Carli, "Borati anidri di litio, cadmio, piombo, manganese," *Gazz. Chim. Ital.*, vol. 56, p. 23, 1926.
[36] C. Chen, in *Proc. Int. Conf. on Lasers*, Xiamen, China, nos. 15–19, Nov. 1987.
[37] L. R. Marshall, A. D. Hay, and R. Burnham, "Highly efficient eye safe laser sources," presented at CLEO '90, post deadline paper, CPDP-35, Anaheim, CA, May 1990.
[38] L. J. Bromley, A. Guy, and D. C. Hanna, "Synchronously pumped optical parametric oscillator in KTP," *Opt. Commun.*, vol. 70, p. 350, 1989.
[39] S. Burdulis, R. Grigonis, A. Piskarskas, G. Sinkevicus, V. Sirutkaistis, A. Fix, J. Nolting, and R. Wallenstein, "Visible optical parametric oscillation in synchronously pumped beta-barium borate," *Opt. Comm.*, vol. 74, p. 398, 1990.
[40] D. C. Edelstein, E. S. Wachman, and C. L. Tang, "Broadly tuneable high repetition rate femtosecond optical parametric oscillator," *Appl. Phys. Lett.*, vol. 54, p. 1728, 1989.
[41] E. S. Wachman, D. C. Edelstein, and C. L. Tang, "Continuous wave mode-locked and dispersion-compensated femtosecond optical parametric oscillator," *Opt. Lett.*, vol. 15, p. 136, 1990.
[42] R. Laenen, H. Graener, and A. Laubereau, "Broadly tunable femtosecond pulses generated by optical parametric oscillation," *Opt. Lett.*, vol. 15, p. 971, 1990.
[43] D. Eimerl, L. Davis, S. Velsko, E. Graham, and A. Zalkin, *J. App. Phys.*, vol. 62, p. 1968, 1987.
[44] V. H. Konig and A. Hoppe, *Z. Anorg. Allg. Chem.*, vol. 439, p. 71, 1978.
[45] M. Ihara, M. Yuge, and J. Krogh-Moe, *Yogyo-Kyokai-Shi*, vol. 88, p. 179, 1980.
[46] Z. Shuquing, H. Chaoen, and Z. Hongwu, *J. Cryst. Growth*, vol. 99, p. 805, 1990.
[47] C. Chen, Y. Wu, A. Jiang, B. Wu, G. You, R. Li, and S. Lin, *J. Opt. Soc. Amer.*, vol. B6, p. 616, 1989.
[48] S. Liu, Z. Sun, B. Wu, and C. Chen, *J. Appl. Phys.*, vol. 67, p. 634, 1989.
[49] On the basis of $d_{12} = 2.69 \times d_{36}$(KDP) and using the value d_{36}(KDP)=0.39 pm/V according to R. C. Ekart et al., *IEEE J. Quantum Electron.* vol. 26, p. 922, May 1990.
[50] C. Chen, Y. Wu, A. Jiang, B. Wu, G. You, R. Li, and S. Lin, (0.16–2.6 μm) *J. Opt. Soc. Amer.*, vol. B6, p. 616, 1989.
[51] S. Zhao, C. Huang, and H. Zhang, (0.165–3.2 μm) *J. Cryst. Growth*, vol. 99, p. 805, 1990.
[52] B. Wu, N. Chen, C. Chen, D. Deng, and Z. Xu, *Optics Lett.*, vol. 14, p. 1080, 1989, calculated by using Sellmeier equations.
[53] T. Ukachi, R. J. Lane, W. R. Bosenberg, and C. L. Tang, *J. Opt. Soc. Amer.*, vol. B9, July 1992.
[54] L. K. Cheng, W. R. Bosenberg, and C. L. Tang, "Growth and characterization of nonlinear optical crystals suitable for frequency conversion," review article in *Progress in Crystal Growth and Characterization*. New York: Pergamon, vol. 20, pp. 9–57, 1990.
[55] H. Nakatani *et al.*, *Appl. Phys. Lett.*, vol. 53, p. 2587, Dec. 26, 1988, estimated surface damage threshold scaled from detailed bulk damage results reported.

Chung L. Tang (Fellow, IEEE) received the B.S. degree from the University of Washington, Seattle, in 1955, the M.S. degree from the California Institute of Technology, Pasadena, in 1956, and the Ph.D. degree from Harvard University, Cambridge, MA, in 1960. As a John Parker Traveling Fellow from Harvard, he also studied at the Technical University of Aachen, Germany from 1959–1960.

From 1960 to 1964 he was a Research Staff Member and later Principal Research Scientist at the Research Division of Raytheon Company. He has been on the faculty of Cornell University since 1964. Currently he is the Spencer T. Olin Professor of engineering at Cornell and Codirector of the Cornell/UCSB/UCSD/RPI Optoelectronics Technology Center.

Dr. Tang is a Fellow of the American Physical Society, the Optical Society of America, and a Member of the National Academy of Engineering.

Walter R. Bosenberg received the B.S. degree in physics from Rensselaer Polytechnic Institute, Troy, NY in 1984 and the M.S. and Ph.D. degrees in applied and engineering physics from Cornell University, Ithaca, NY, in 1987 and 1990, respectively.

Presently he is with Spectra Technology Inc. (STI), Bellevue, WA where he is continuing his work in the areas of solid state laser systems and nonlinear optical frequency conversion.

Takashi Ukachi was born in Hyogo, Japan, on November 3, 1952. He received the B.E. degree in biophysics and bioengineering from Osaka University, Osaka, Japan, in 1976.

He started his professional career at Tokyo Research Laboratory, Japan Synthetic Rubber Co. Ltd., Kawasaki, Japan where he was engaged in research on the development of conducting polymers. In 1981 he spent a year at the Electrotechnical Laboratory, Tsukuba, Japan to study the superconducting organic metals. From 1988 to 1990 he was a Visiting Scientist at the School of Electrical Engineering, Cornell University, Ithaca, NY, where his work involved the growth and the evaluation of nonlinear optical crystals. Since 1990 he has been with Tsukuba Research Laboratory, Japan Synthetic Rubber Co. Ltd., Tsukuba, Japan. His current research interests include the development of organic nonlinear optical materials and their device applications.

Dr. Ukachi is a Member of the Physical Society of Japan and the Japan Society of Applied Physics.

Randall J. Lane was born in Billings, MT on February 7, 1962. He received the B.S. and M. Eng. degrees in applied and engineering physics from Cornell University, Ithaca, NY in 1985 and 1988, respectively.

In 1983, he conducted research on the medical applications of the excimer laser at the IBM T. J. Watson Research Center, Yorktown, NY. This research was continued the following year at New York University Medical Center, NY. In 1985, he spent a year studying the medical applications of the Ho:YLF laser at the Massachusetts Eye and Ear Infirmary, Harvard Medical School, Boston, MA. Since 1989, he has continued to study the growth and applications of nonlinear optical crystals, specifically Beta-Barium Metaborate and Lithium Triborate at the Cornell University Material Science Center laser facility under the direction of Chung L. Tang.

Mr. Lane is a Member of the Optical Society of America.

L. Kevin Cheng received the B.S. degree in chemistry from Boston University, MA in 1982, and the M.S. and Ph.D. degrees in applied physics from Cornell University, Ithaca, NY in 1988.

Currently he is a Research Staff Member in the Advanced Material Science Division in the CR&D Department of the DuPont Company. His current work involves the development of single crystals of the nonlinear optical crystals $KTiOPO_4$, $KTiOAsO_4$, and other related isomorphs, and of waveguide devices based on the epitaxial film growth of these same materials.

Appendix G

Recent advances of the Ti:sapphire-pumped high-repetition-rate femtosecond optical parametric oscillator

P. E. Powers, R. J. Ellingson, and W. S. Pelouch

School of Applied and Engineering Physics, Cornell University, Ithaca, New York 14853

C. L. Tang

School of Electrical Engineering, Cornell University, Ithaca, New York 14853

Received December 17, 1992

The details concerning the resonator configuration, crystal parameters, and operating characteristics of high-repetition-rate and high-average-power broadly tunable femtosecond optical parametric oscillators are reviewed and discussed in some detail. We also report new results on an intracavity-doubled optical parametric oscillator with tunability from 580 to 657 nm in the visible and the first, to our knowledge, high-repetition-rate femtosecond optical parametric oscillator with the new nonlinear-optical crystal In:$KTiOAsO_4$, which can potentially tune to 5.3 μm.

INTRODUCTION

One of the most active new directions of research on optical parametric oscillators[1] (OPO's) is on broadly tunable high-repetition-rate femtosecond OPO's. To generate a peak power large enough to overcome the OPO's threshold, the first high-repetition-rate OPO was coupled intracavity to a colliding-pulse mode-locked dye laser.[2-4] This OPO generated 100-fs pulses at 80 MHz with ~3 mW of average power. After this initial development came a rapid improvement in design simplicity and performance. The first externally pumped high-repetition-rate femtosecond OPO with a high-power hybridly mode-locked dye laser permitted considerable design simplification.[5] This was quickly followed by a demonstration in which the OPO was externally pumped with a high-power high-repetition-rate femtosecond Ti:sapphire laser.[6,7] With the external-cavity Ti:sapphire-pumped OPO the design is simple and the performance robust. The Ti:sapphire-pumped OPO has generated hundreds of milliwatts in both the signal branch (to as much as 680 mW) and the idler branch (to more than 450 mW), adding to more than 1 W of frequency-converted power. The femtosecond Ti:sapphire-pumped OPO has also demonstrated extensive tunability,[8] making it an extremely attractive device for femtosecond applications. In this paper we present a detailed description of the design parameters and the operating characteristics of a Ti:sapphire-pumped femtosecond OPO as well as the most recent results of our use of this device.

FEMTOSECOND OPTICAL PARAMETRIC OSCILLATOR CAVITY DESIGN CONSIDERATIONS

Included in the considerations for designing a femtosecond Ti:sapphire-pumped OPO are the configuration of the resonator and the orientation of the nonlinear crystal. The basic OPO cavity is simple. It can be configured as either a linear or a ring cavity, with or without intracavity dispersion compensation. Since the device is synchronously pumped the cavity length must match that of the Ti:sapphire laser. These geometries are shown in Fig. 1. Both cavities are singly resonant with single-stack mirrors reflecting either the signal or the idler wave. Besides the geometrical differences between these two configurations, the main feature that sets them apart is that as the resonated wave traverses one round trip the pulse passes through the nonlinear crystal twice in the linear cavity and only once in the ring cavity. The advantage of the linear cavity is that it permits double passing of the pump in the nonlinear crystal. This has led to as much as a 20% increase in power in the output of the signal beam.[7] When single-pass pumping fails to bring the OPO comfortably above threshold double passing the pump may permit the OPO to operate well above threshold, resulting in better stability and power. However, the two passes of the signal beam through the crystal lead to more dispersion of the pulse, of which only the linear group-velocity dispersion (GVD) can be compensated for by the prism sequence. The losses from the extra pass through the crystal are more than compensated for by backreflecting the pump. The linear cavity with a backreflected pump does require that the Ti:sapphire pump laser be either feedback insensitive or optically isolated from the backreflection. We used a Ti:sapphire laser that was configured in a ring for double passing the pump because this configuration was not feedback sensitive.[9] The ring-cavity OPO eliminates the second pass through the crystal but does not permit double passing of the pump. When pumped high enough above threshold, the ring-cavity-OPO operation is as robust as the linear cavity with feedback.

0740-3224/93/112162-06$06.00

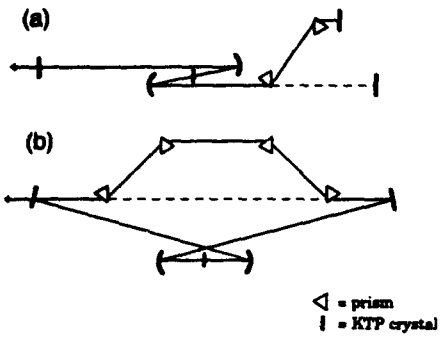

Fig. 1. Schematic of (a) a linear and (b) a ring OPO cavity with (solid lines) or without (dashed lines) intracavity-prism dispersion compensation. The Ti:sapphire pump laser is not shown because its alignment to the crystal depends on whether a type-I or a type-II interaction is chosen and whether the *e* wave or the *o* wave is resonated. Note that for a round trip the pulse passes through the crystal twice for the linear cavity and only once for the ring cavity.

The alignment of the Ti:sapphire pump with the OPO cavity depends on whether the *o* wave (idler) or *e* wave (signal) is resonated. When the idler is resonated the pump and idler should be collinear to maximize the gain. Resonating the signal, however, requires determining how the Poynting vector of the signal walks off the pump. Wachman *et al.*[8] first noticed that the OPO oscillated such that the Poynting vector of the pump and signal were collinear. Hence the pump must be offset from the signal to permit the Poynting vector of the signal to walk onto the pump. This is accomplished by use of a noncollinear phase-matching geometry such that the noncollinear angle between the pump and the signal is equal to the negative of the walk-off angle. The Poynting vector of the signal then walks onto the pump wave and not away from it. The crystal orientation is shown in Fig. 2. Figure 3 plots the value of the Poynting-vector walk-off as a function of the phase-matching angle. In the case of large phase-matching angles this walk-off is small, permitting alignment of the pump through one of the OPO-cavity mirrors. For smaller phase-matching angles the walk-off angle increases, and the pump and OPO-cavity mirrors must be positioned to permit this walk-off. For example, the noncollinear angle for KTP with a type-II interaction is 2.9° at a phase-matching angle of 45°. Using cavity mirrors of $R = 10$ cm curvature would then require that the pump and signal beams be ~4 mm apart at a distance of 5 cm from the KTP crystal.

Suitable focusing parameters for the OPO cavity and the Ti:sapphire pump are determined by considering the respective focused beam sizes inside the crystal and the angular acceptance of the crystal. The theoretical calculations of Cheung and Liu[10] show that, for a configuration in which the Poynting vectors of the pump and resonated wave are collinear, their focused beam sizes in the crystal should be approximately the same. The number of possible focusing combinations that result in equal beam sizes of the pump and signal in the crystal is limited by the fact that not all these focusings will permit oscillation. As the beam waist increases, the peak intensity decreases eventually to a point below the OPO threshold. At the other extreme, when the focused beam size decreases, the angular spread of the focused beam becomes larger than the acceptance angle of the crystal, which then reduces the efficiency of the phase-matched interaction. The angular acceptance can be calculated by plotting the function

$$\left[\frac{\sin(\Delta k l_c/2)}{\Delta k l_c/2}\right],$$

$$\Delta \mathbf{k} = \mathbf{k}_p - \mathbf{k}_e - \mathbf{k}_i \qquad (1)$$

as a function of the phase-matching angle, where Δk is the phase mismatch and l_c is the crystal length. The full width at half-maximum (FWHM) gives the angular acceptance. For a 1-mm-thick crystal the angular-acceptance angle for KTP in the x–z plane is 0.75° for a pump wavelength of 780 nm and a signal wavelength of 1.3 μm. If the OPO's beam diameter is 1 mm, then the focus that matches the crystal's angular acceptance is 7.6 cm (R = 15.2 cm).

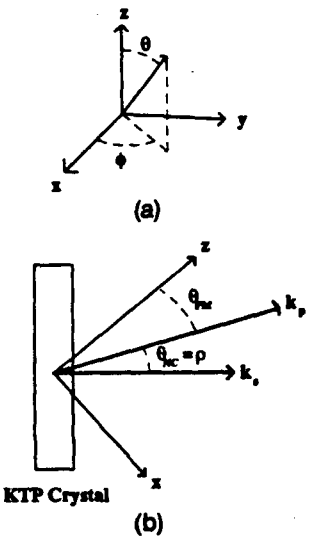

Fig. 2. Crystal orientation. (a) The angles θ and ϕ are defined. (b) The alignment of the KTP crystal for a type-II interaction in which the *e* wave ($\mathbf{k}_e$) is resonated. The pump ($\mathbf{k}_p$) and $\mathbf{k}_e$ lie in the x–z plane at a noncollinear angle that is equal to the negative of the walk-off angle ρ. $\mathbf{k}_e$ is oriented so that its Poynting vector walks onto the pump.

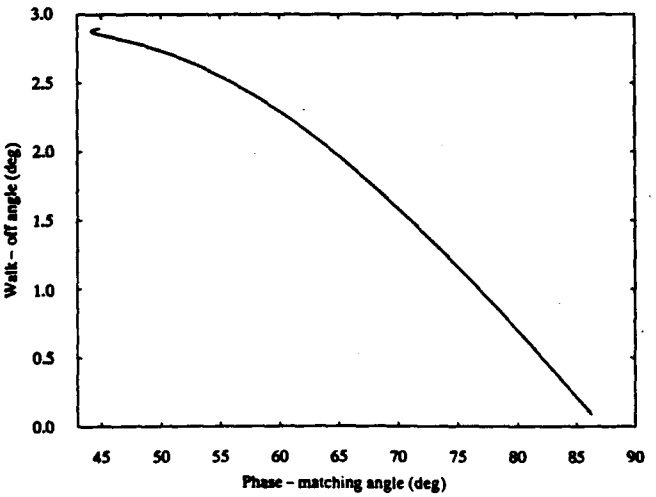

Fig. 3. The Poynting-vector walk-off of the signal from the pump is plotted as a function of the phase-matching angle for a 780-nm pump and a noncollinear angle of 2.8°.

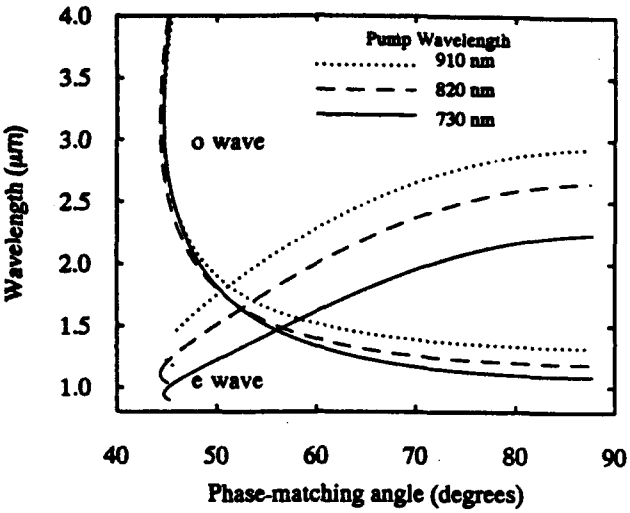

Fig. 4. Tuning curves for a type-II interaction in KTP with a noncollinear angle of 2.8°. The tuning curves for three pump wavelengths covering a large part of the Ti:sapphire's tuning range illustrate the effect of tuning the pump.

In an attempt to optimize the focusing, we varied the cavity focusing mirrors from $R = 7.5$ cm to $R = 20$ cm; corresponding to these changes we varied the pump focus from $R = 10$ cm to $R = 30$ cm so as to keep the signal- to pump-beam-waist ratio approximately constant. We found that with mirrors with a higher radius of curvature the OPO operated nearer to threshold and that at too tight a focus the OPO would not oscillate at all (at $R = 7.5$ cm). Our best performance has been with either $R = 10$ cm or $R = 15$ cm for the OPO-cavity mirrors and either $R = 15$ cm or $R = 25$ cm, respectively, for the pump focusing mirror.

CRYSTAL ORIENTATION

Critical to the successful operation of a femtosecond OPO is the orientation of the nonlinear crystal. In this section we use the properties of the nonlinear crystal KTP as an example to clarify how to determine the alignment that maximizes the gain. The first consideration is to orient the crystal such that the effective second-order nonlinearity, d_{eff}, is maximized. For KTP, d_{eff} is approximated by[11,12]

$$\text{Type I} \quad d_{eff} = 1/2(d_{15} - d_{24})\sin(2\theta)\cos(2\phi), \tag{2}$$

$$\text{Type II} \quad d_{eff} = -[d_{15}\sin^2(\phi) + d_{24}\cos^2(\phi)]\sin(\theta), \tag{3}$$

where θ, the phase-matching angle, and ϕ are defined as in Fig. 2 above. For KTP the values of d_{15} and d_{24} are 2.04 and 3.92, respectively.[13] For these values the type-II interaction always has a larger d_{eff} than does the type-I interaction. For the type-II interaction d_{eff} is maximized for $\phi = 0$ so that the KTP crystal is aligned such that the parametric interactions occur in the x–z plane. It is clear from Eq. (3) that one maximizes d_{eff} for the type-II interaction for a phase-matching angle of 90°; however, it is sometimes advantageous to phase match at smaller angles. Specifically, wavelengths that are not available at larger angles are accessible at smaller phase-matching angles, as shown in Fig. 4.

The tuning curves for KTP with $\phi = 0$ and for various possible Ti:sapphire pump wavelengths are generated as a function of the phase-matching angle θ and are shown in Fig. 4. From this figure it is clear that KTP has a broad tuning range, but to have access to the whole range requires either tuning the pump or changing the crystal phase-matching angle. The Ti:sapphire-pumped OPO offers the advantage that the Ti:sapphire laser itself is tunable, which leads to broad tunability in the OPO. As seen in Fig. 4, tuning the Ti:sapphire laser can lead to a substantial change in wavelength in the OPO. For the region in which θ is <55°, tuning the pump leads to a large change in the e wave's wavelength but only a small change in the o wave. In this region one accomplishes tuning to the longer wavelengths of the o wave by simply changing the phase-matching angle. For angles that are >55°, in which d_{eff} is largest, changing the phase-matching angle leads to a small change in wavelength, so in this region tuning the pump makes more sense.

A consideration that has a direct bearing on the performance of the OPO is the magnitude of the inverse group-velocity mismatch (GVM) between the pump, the signal, and the idler waves. The GVM is approximately −25 fs/mm between the pump and the signal and ~200 fs/mm between the pump and the idler for the majority of the tuning range. This puts a limitation on the crystal's thickness. The crystal should be thick enough to provide high gain but thin enough to limit the effect of GVM.

Additionally, the crystal should be thin enough to phase match the bandwidth of the ultrashort pulse. We generated pulses as short as 57 fs by using a 1.15-mm-thick crystal, with 115 mW in the signal beam. With this 1.15-mm-thick crystal we measured up to 60% pump depletion. Although using a thicker crystal will increase the interaction length and will lead to more power, this has the potential of broadening the OPO pulses. The FWHM of Eq. (1) plotted versus wavelength gives the phase-matching bandwidth. The phase-matching bandwidth for a 1-mm-thick crystal of KTP is 33 nm at a signal wavelength of 1.3 μm; this has a transform-limited pulse width of 53 fs, assuming a sech^2 pulse shape. Increasing the crystal thickness to 1.5 mm decreases the phase-matching bandwidth to 22 nm, and consequently the transform-limited pulse width is 80 fs.

OPERATING CHARACTERISTICS

When the OPO is pumped sufficiently above threshold (1 W at 100 fs or better), the output of the OPO is a stable pulse train. The average-power fluctuations and pulse-to-pulse variations of the OPO are determined almost entirely by the Ti:sapphire pump laser. Even without an active cavity-length stabilizer to length match the OPO and Ti:sapphire cavities continuously, oscillation can be maintained stably for as much as several hours. Operating near threshold decreases the stability of the OPO pulse train, as does operating near 0 GVD.

The OPO pulses are characterized by a chirped and an unchirped regime. The chirped regime is encountered when the cavity is operated with a net positive GVD, and the unchirped regime occurs with net negative GVD. With intracavity dispersion compensation it is possible to vary the GVD from net negative values to net positive values. We observed a flip from chirped pulses to unchirped pulses as we changed from negative to positive net GVD.

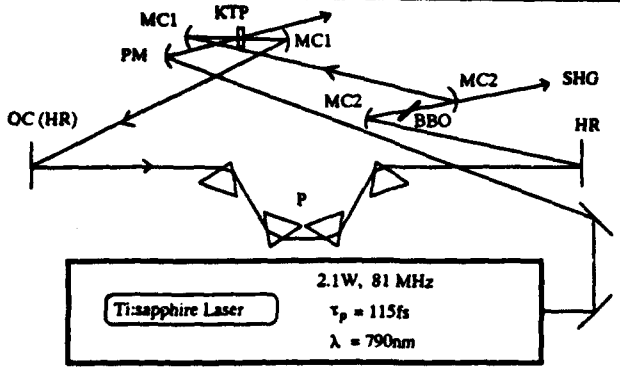

Fig. 5. Ti:sapphire-pumped intracavity-doubled KTP OPO. The Ti:sapphire beam is focused by the $R = 25$ cm pump mirror (PM) onto the 1.5-mm-thick KTP crystal. The KTP gain crystal is cut at $\theta = 45°$, $\phi = 0°$ for type-II phase matching in the positive region of the x–z plane. The OPO curved mirrors (MC1, MC2) at the gain and frequency doubling foci have radii $R = 15$ cm and $R = 10$ cm, respectively. Two pairs of SF-14 prisms (P) spaced 20 cm tip to tip are used for intracavity dispersion compensation. The single SHG output is transmitted through the OPO high reflector (HR) at the doubling focus. OC, output coupler; τ_p, pulse width.

Near the 0 GVD point the pulses spontaneously jump between chirped and unchirped pulses, leading to instability in the pulse train.

Accompanying the signal and idler outputs are several non-phase-matched processes. Non-phase-matched second-harmonic generation (SHG) of the signal wave ($e + e \rightarrow e$), as well as noncollinear non-phase-matched sum-frequency generation between the pump and the signal wave ($o + e \rightarrow o$), have been identified.[6,7,14] We have also identified the noncollinear non-phase-matched sum-frequency generation between the pump and the idler wave. The power in this beam is less than a milliwatt. It is interesting that this wavelength is equal to the non-phase-matched second harmonic (SH) of the signal beam when the signal beam equals 1.5 times the pump beam. We have observed this with a 867-nm pump and 1.3-μm signal. With the signal and idler pulses this gives five synchronous wavelengths.

RECENT ADVANCES

Our most recent efforts have been directed toward generating exceptionally high output powers and broad tunability. For the high-power result we used a Ti:sapphire laser, producing 2.4 W of average power with a 115-fs pulse width. With this pump source we generated 130-fs, 680-mW pulses in the signal branch by using a linear-cavity OPO configuration and a 1.5-mm-thick KTP crystal. This is excellent conversion efficiency and is near the Manley–Rowe limit. The Manley–Rowe relation states that the number of pump photons that are annihilated is equal to the number of signal–idler photon pairs that are created.[15] The limit for a 2.4-W pump at 780 nm and a signal wavelength of 1.3 μm yields 720 mW in the signal beam.

Using intracavity frequency doubling, we have extended into the visible the wavelength range that is accessible to femtosecond OPO pulses. Because the Ti:sapphire-pumped OPO is synchronously pumped, the nonlinear loss of the SHG to the intracavity OPO-signal pulse does not destroy the pulse-shaping process. We generated a total of 240 mW of sub-100-fs pulses at a wavelength of 647 nm and demonstrated tuning of the output from 580 to 657 nm. Because of the optical-power limiting by the nonlinear loss of the SHG,[14] the output of the intracavity-doubled OPO is very stable and quiet. Although no quantitative noise measurements have been made, the output pulse train of the SH is as quiet as the Ti:sapphire laser when viewed on a fast oscilloscope.

The intracavity-doubled OPO, which uses a 1.5-mm-thick KTP crystal that is cut for type-II ($o \rightarrow e + o$) phase matching ($\theta = 45°$, $\phi = 0°$) in the x–z plane, is shown in Fig. 5. We add to the ring cavity an additional intracavity focus of $R = 10$ cm mirrors that are high reflectors centered at 1.3 μm and that transmit ~80% of the SH wavelength. After aligning the OPO with the additional intracavity focus, we use the OPO-signal beam, taken through a 1% output coupler, to align the 47-μm-thick β-BaB_2O_4 (BBO) Brewster-cut crystal for SHG using type-I phase matching. Next we insert the thin BBO crystal at the intracavity focus, regain OPO oscillation, and proceed to replace the OPO's 1% output coupler with a high reflector to maximize the SH output power.

BBO is exceptionally well suited for frequency doubling of ultrashort pulses in the wavelength range of the signal branch of the OPO. The phase-matching curve for SHG in BBO is shown in Fig. 6(a). We refer to the point on the

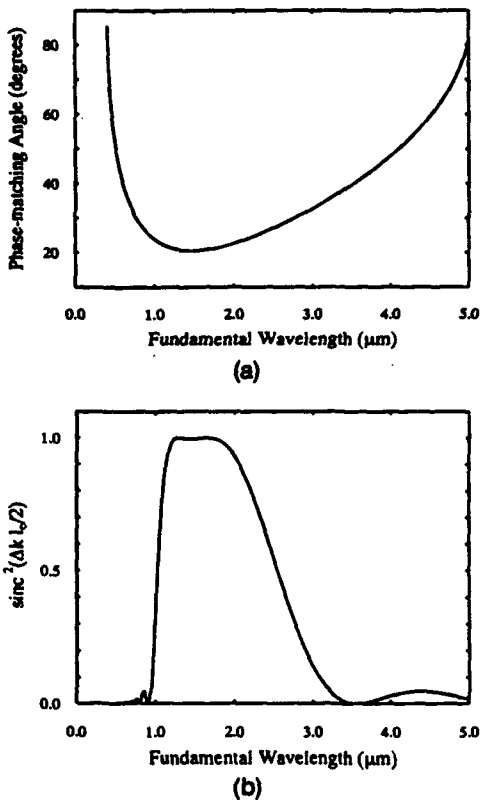

Fig. 6. (a) Phase-matching angle versus fundamental wavelength for type-I SHG in BBO. The degenerate point at which the phase-matching angle is minimized and phase matches a single wavelength occurs at 1.47 μm. The SHG phase-matching bandwidth becomes very large near this degenerate point. (b) The SHG phase-matching spectrum for $l_c = 55$ μm BBO crystal (47-μm-thick crystal at Brewster's angle) that was phase matched for SHG at 1.3 and 1.65 μm.

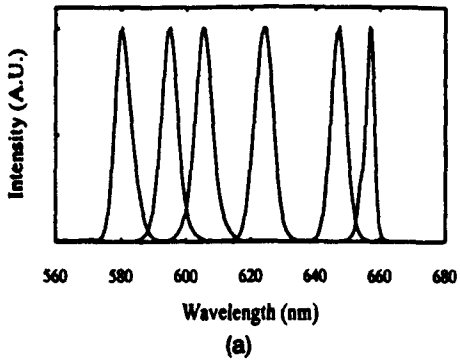

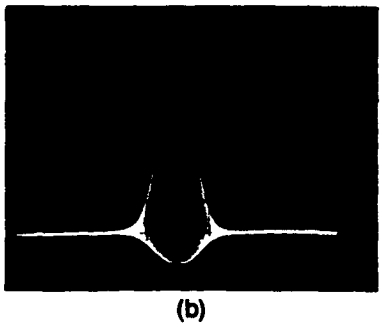

Fig. 7. (a) Intracavity-doubled KTP OPO spectra within the demonstrated tuning range of 580–657 nm. (b) Real-time interferometric autocorrelation for 240-mW total SH produced, at 115-fs pulse width, centered at 647 nm. Although not shown, extracavity two-prism dispersion compensation compressed the pulses to 95 fs with no degradation in pulse shape.

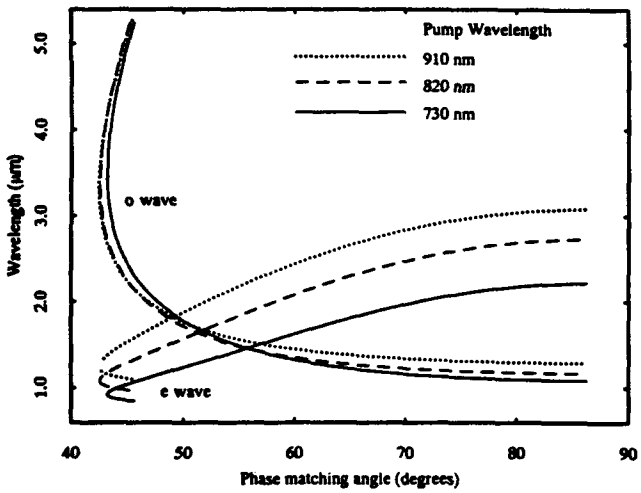

Fig. 8. Tuning curves for a type-II interaction in In:KTA with a noncollinear angle of −2.8°. The tuning curves for three pump wavelengths covering a large part of the Ti:sapphire's tuning range illustrate the effect of tuning the pump.

phase-matching curve at which the slope is zero as the degenerate point. Interestingly, at this degenerate point in the phase-matching curve, which occurs for BBO at ~1.47 μm, the group velocities of the fundamental and SH are matched. As a result, in the regime of 1.47-μm BBO has a small GVM and a large SHG phase-matching bandwidth. It is important to note that this simultaneous matching of the SHG phase and group velocities at the degenerate point also occurs in $LiNbO_3$, another crystal of the $3m$ point group.

In the case of our ultrathin 47-μm-thick BBO crystal the phase-matching bandwidth for 1.3 μm is shown in Fig. 6(b). The two $\mathrm{sinc}^2(\Delta k l_c/2)$ SHG phase-matching curves (at $\lambda = 1.30$ μm and $\lambda = 1.65$ μm) have merged to give a FWHM SHG bandwidth of 1514 nm. Our observations of the intracavity-doubled OPO agree: after tuning the OPO from 1.2 to 1.3 μm, rotating the phase-matching angle of the BBO has no effect on the SHG conversion efficiency. Once the BBO crystal is aligned to double near the center of the OPO-signal tuning curve, tuning the SHG is accomplished by simply tuning the OPO with no adjustment to the BBO phase-matching angle.

As mentioned above, the intracavity-doubled OPO is a stable source of femtosecond pulses in the visible. Figure 7 shows spectra from the demonstrated tuning range and a real-time interferometric autocorrelation of the SHG output. The pulse shape of the OPO fundamental is similarly clean and quiet. The Ti:sapphire-pumped femtosecond OPO and the intracavity-doubled OPO demonstrate very powerful nonlinear-optical-generation techniques that will continue to increase in importance as pump sources are improved and as new pump sources are developed.

To extend the tuning range to longer wavelengths, beyond 4 μm, we have demonstrated optical parametric oscillation with the new nonlinear crystal $In:KTiOAsO_4$ (In:KTA). In:KTA is very similar to KTP but has a larger transparency range, which extends to 5.3 μm. In:KTA's transparency range has no absorption bands as does KTP, for example, at 3.5 μm.[16] Figure 8 shows that phase matching over the transparency region for In:KTA is possible out to 5.3 μm. The In:KTA OPO is aligned in the same way as the KTP OPO.[7] A 1.5-mm-thick In:KTA crystal is oriented for a type-II interaction with a phase-matching angle of ~50°. The e wave is resonated in a linear cavity with prisms with a noncollinear angle that is equal to the negative of the walk-off angle of 2°. We produced pulses at 1.435 μm in the signal branch and 1.662 μm in the idler branch with a 770-nm Ti:sapphire pump. This is the first demonstration, to our knowledge, of a high-repetition-rate OPO with In:KTA, and, as shown in Fig. 8, tuning beyond 4 μm is possible with the appropriate crystal cut and mirror coatings.

CONCLUSION

The high-repetition-rate Ti:sapphire-pumped femtosecond OPO is a robust device that is capable of high average power and short pulse widths, tunable from the visible to the mid-IR. This device produced unchirped pulses with powers as high as 680 mW, pulse widths as short as 57 fs, and tunability from 580 to 657 nm in the visible as well as from 1.16 to 2.2 μm in the IR. In the near future we plan to extend this tuning range to 5 μm with In:KTA, and we are looking at other new materials that would permit us to tune even further into the IR. At the same time, we are also looking into generating OPO pulses that are shorter than 57 fs, to our knowledge the shortest pulses from an OPO yet reported. Finally, as a true test of the OPO's performance, we plan to use the OPO in pump–probe-style experiments to generate high signal-to-noise data.

ACKNOWLEDGMENTS

This research was supported by the Joint Services Electronics Program and the National Science Foundation.

REFERENCES AND NOTES

1. See, e.g., C. L. Tang, W. R. Bosenburg, T. Ukachi, R. J. Lane, and K. L. Cheng, Proc. IEEE **80**, 365 (1992), and the references therein.
2. D. C. Edelstein, E. S. Wachman, and C. L. Tang, Appl. Phys. Lett. **54**, 1728 (1989).
3. E. S. Wachman, D. C. Edelstein, and C. L. Tang, Opt. Lett. **15**, 136 (1990).
4. E. S. Wachman, W. S. Pelouch, and C. L. Tang, J. Appl. Phys. **70**, 1893 (1991).
5. G. Mak, Q. Fu, and H. M. van Driel, Appl. Phys. Lett. **60**, 542 (1992).
6. Q. Fu, G. Mak, and H. M. van Driel, Opt. Lett. **17**, 1006 (1992).
7. W. S. Pelouch, P. E. Powers, and C. L. Tang, Opt. Lett. **17**, 1070 (1992).
8. E. S. Wachman, W. S. Pelouch, and C. L. Tang, J. Appl. Phys. **70**, 1893 (1991).
9. W. S. Pelouch, P. E. Powers, and C. L. Tang, Opt. Lett. **17**, 1581 (1992).
10. E. C. Cheung and J. M. Liu, J. Opt. Soc. Am. B **8**, 1491 (1991).
11. D. A. Roberts, IEEE J. Quantum Electron. **28**, 2057 (1992).
12. Equations (2) and (3) are obtained by approximating $\delta_i^{\delta} \approx 0$ and $M_{\mu} \approx 1$ in Eq. (28) in Ref. 11.
13. H. Vanherzeele and J. D. Bierlein, Opt. Lett. **17**, 982 (1992).
14. D. C. Edelstein, *New Sources and Techniques for Ultrafast Laser Spectroscopy*, Ph.D. dissertation (Cornell University, Ithaca, N.Y., 1990).
15. See, e.g., Y. R. Shen, *The Principles of Nonlinear Optics* (Wiley, New York, 1984), p. 79.
16. F. Ahmed, R. Belt, and G. Gashurov, Appl. Phys. Lett. **60**, 839 (1986).

Appendix H

High-repetition-rate femtosecond pulse generation in the blue

R. J. Ellingson

School of Applied and Engineering Physics, Cornell University, Ithaca, New York 14853

C. L. Tang

School of Electrical Engineering, Cornell University, Ithaca, New York 14853

Received November 20, 1991

We report the generation of high-repetition-rate femtosecond pulses in the blue by intracavity doubling of a mode-locked Ti:sapphire laser using β-BaB_2O_4. To reduce the pulse-broadening effect of group-velocity mismatch, an extremely thin β-BaB_2O_4 crystal is used. By pumping the Ti:sapphire laser with 4.4 W of power from an Ar^+ laser, as much as 230 mW of 430-nm light is produced at a 72-MHz repetition rate and a 89-fs pulse width. This represents an effective conversion efficiency of ~75% from the typical infrared output to the second harmonic. Pulse widths as short as 54 fs are achieved for the blue output.

Extension of the wavelength range accessible to femtosecond pulses has been a topic of much interest. The two techniques used most frequently to generate <100-fs pulses at otherwise unattainable wavelengths are continuum generation and frequency conversion with the use of crystals. Femtosecond pulse generation techniques based on amplification followed by continuum generation permit tunability from the UV into the IR.[1] However, amplification reduces the pulse repetition rate to the order of a kilohertz, and there is often a loss of time resolution in the final pulse. In contrast, frequency conversion in crystals can maintain the high repetition rate of the femtosecond megahertz-rate laser and requires only a single cw pump laser. The higher repetition rate results in much smaller pulse fluctuation and excellent experimental signal-to-noise ratios.

In recent years, much progress has been made in extending the spectral range of high-repetition-rate femtosecond pulses throughout the visible and IR by using frequency conversion in crystals. The 80-MHz femtosecond optical parametric oscillator permits broad tunability throughout the near IR and mid-IR.[2,3] High-repetition-rate femtosecond pulse generation in the UV and blue–green has been somewhat more limited. Colliding-pulse mode-locked (CPM) lasers have directly generated <100-fs pulses in the range of 493 to 554 nm at milliwatt outputs,[4,5] and intracavity doubling of the Rhodamine 6G/diethyloxadiacarbocyanine iodide (Rh6G/DODCI) CPM dye laser has resulted in a 100-MHz source of femtosecond pulses with milliwatt outputs in the 310–315-nm range. The Rh6G/DODCI CPM laser was first intracavity doubled by using KDP.[6] Soon thereafter, β-BaB_2O_4 (BBO) was used to intracavity double the CPM laser with a per-pass conversion efficiency as high as 5.5%, which generated 20 mW of UV output per arm with <100-fs pulse widths, and pulse widths as short as 43 fs.[7] This gives an effective conversion efficiency of nearly 100% from the typical CPM output in the red to the UV.

While the standard Rh6G/DODCI CPM dye laser operates at a wavelength slightly shorter than the tuning range of the Ti:sapphire laser, the broad tunability, the high average output power, and the obvious advantages of a solid-state laser have made the dispersion-compensated mode-locked Ti:sapphire laser[8] an extremely attractive replacement for the CPM dye laser. At present, the mode-locked Ti:sapphire laser can potentially operate with <200-fs pulse widths and >100-mW average power over the range of 700 to 1053 nm.[9] Frequency doubling over this spectral range provides femtosecond pulses from 350 to 525 nm. Doubling of the Ti:sapphire laser outside the cavity has been reported.[10] The best conversion efficiency of 25% was achieved at 750 nm, although no second-harmonic pulse widths were reported and the length of the doubling crystal was not given. The group-velocity mismatch for type I second-harmonic generation (SHG) in BBO at 750 nm is 225 fs/mm, and in order to maintain the narrowest temporal pulse width a thin doubling crystal is required. Use of a thin crystal therefore necessitates a high peak power to achieve high conversion efficiency, and thus intracavity doubling is required to achieve simultaneously the shortest pulses and the highest power in the second harmonic. As discussed further below, extremely high intracavity conversion efficiency is possible, which would result in UV, blue, or green outputs of hundreds of milliwatts average power. Using an extremely thin (55 μm) crystal of BBO, we demonstrate a 72-MHz repetition-rate source of blue pulses of 89-fs duration (FWHM) and 115 mW of power per arm (two arms of BBO; see Fig. 1). Reducing the pulse width for the blue to 54 fs, we measure 45 mW of power per arm.

Figure 1 shows a schematic of the dispersion-compensated intracavity-doubled Ti:sapphire laser. The SF-10 prisms are spaced 50 cm tip to tip. The

0146-3592/92/050343-03$5.00/0

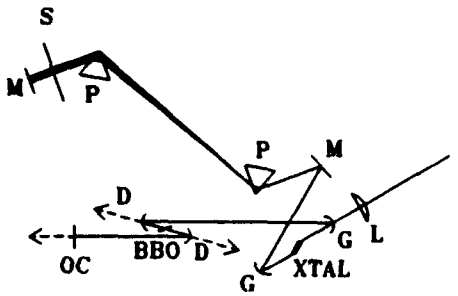

Fig. 1. Schematic of the intracavity doubled Ti:sapphire laser. XTAL, Ti:sapphire crystal; G's, gain mirrors; L, focusing lens; P's, SF-10 prisms; M's, flat mirrors; D, dichroic mirror; BBO, doubling crystal; S, tuning slit; OC, output coupler.

argon pump laser is focused by a 10-cm focal-length lens through one of the $r = 10$ cm gain mirrors onto the 18-mm-long titanium-doped (0.1%) sapphire crystal. The additional intracavity focus at the BBO crystal consists of $r = 5$ cm dichroic mirrors (fused-silica substrates, $R = 100\%$ at 860 nm, $T = 70\%$ at 430 nm). The outcoupler has $T = 1\%$ for the IR and was replaced by a high reflector when the highest power in the blue was generated. Before insertion into the laser cavity, the crystal is aligned for maximum SHG conversion efficiency in the extracavity beam of the mode-locked Ti:sapphire laser operating at the intended doubling wavelength of ~860 nm. The proper alignment of the BBO can be preserved on insertion into the laser cavity.

Pulse-width measurements for both the fundamental (IR) and the second-harmonic light are made by autocorrelation with collinear type I SHG in BBO. The BBO crystal used to measure the IR autocorrelation has a thickness of 0.8 mm and is cut for a phase-matching angle of $\theta = 27.5°$. The BBO crystal used to measure the blue pulse widths has a thickness of 0.67 mm and is cut at $\theta = 69°$. The second harmonic of the blue (215 nm, the fourth harmonic of the Ti:sapphire) is passed through a 0.2-m monochromator and detected by a solar-blind photomultiplier tube. The spectra for the fundamental and second-harmonic outputs from the laser are measured by using a 0.25-m monochromator to disperse the light onto an optical multichannel analyzer.

We point out that the type I SHG cutoff wavelength in the blue for BBO is 409 nm. Below this wavelength, accurate pulse-width measurement requires a more difficult technique such as cross correlating the fundamental beam with the second-harmonic beam by using phase-matched sum-frequency generation. Owing to the significant group-velocity mismatch between the fundamental and second-harmonic pulses for fundamental wavelengths below 820 nm (the group-velocity mismatch is >170 fs/mm for BBO at $\lambda_{IR} = 820$ nm and increases for shorter wavelengths), a thin cross-correlation crystal is required.[7] Thus, for the convenience of using collinear type I SHG autocorrelation to measure the pulse width of the doubled light, we operated the Ti:sapphire laser at $\lambda > 820$ nm.

The intracavity-doubled mode-locked laser is started by a slight mechanical perturbation, usually by a small-amplitude, gentle back-and-forth translation of one prism. Once well aligned, the mode-locked laser operates stably indefinitely (observed for as much as ~6 h), although significant mechanical perturbation can stop mode-locked operation. The mode locking generally is not self-starting. Variation of the intracavity dispersion compensation permits control of the pulse width. On starting, the laser is pushed to shorter pulses simply by adding prism glass and adjusting the focusing slightly to maintain high stability. While the laser stability is excellent even at the longer pulse widths, the oscilloscope trace of the IR mode-locked pulse train indicates somewhat quieter operation as the pulse width is decreased. The spatial mode of the fundamental beam is TEM_{00} with faint, simple higher-order modes superimposed. The blue beam mode is a clean TEM_{00} that shows no sign of higher-order modes, thus verifying that the power of the fundamental lies almost entirely in the TEM_{00} mode.

When the laser is run with a high reflector in place of the outcoupler, 107-fs IR pulses produce 230 mW of second harmonic. Without the intracavity doubling crystal, the maximum output of the mode-locked Ti:sapphire laser operating at 860 nm is ~300 mW for 4.4-W pump power; thus generation of 230 mW of blue power gives an effective conversion efficiency of ~75% from the IR output typical at this pump power. The dichroic mirrors transmit ~72 mW of power per arm of the blue second-

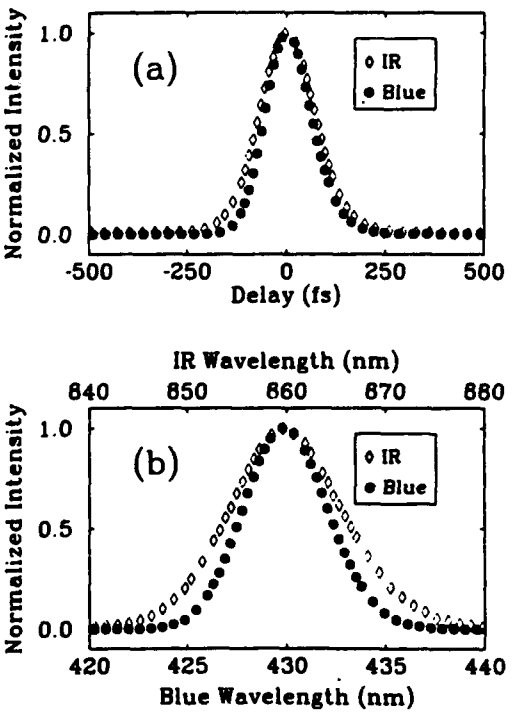

Fig. 2. (a) Autocorrelation data for the fundamental and second-harmonic pulses in the longer-pulse limit. The FWHM for the fundamental is 107 fs, and for the second harmonic it is 89 fs. (b) Spectra for the fundamental and second-harmonic beams. The FWHM for the fundamental is 12.7 nm, which gives $\Delta\nu\Delta t = 0.55$, and for the second harmonic it is 4.9 nm, which gives $\Delta\nu\Delta t = 0.71$.

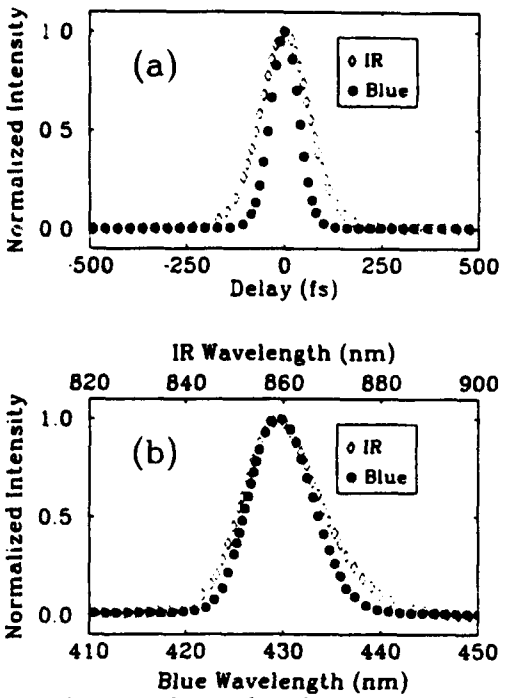

Fig. 3. (a) Autocorrelation data for the fundamental and second-harmonic pulses for the shortest second-harmonic pulses. The FWHM for the fundamental is 93 fs, and for the second harmonic it is 54 fs. (b) Spectra for the fundamental and second-harmonic beams. The FWHM for the fundamental is 18.6 nm, and for the second harmonic it is 7.7 nm. This gives $\Delta\nu\Delta t = 0.70$ for the fundamental and $\Delta\nu\Delta t = 0.67$ for the blue second-harmonic pulses.

harmonic light. On compression of the blue pulses by a dispersion-compensating prism pair, a pulse width of 89 fs is measured (see Fig. 2). The prism pair allows compensation for the dispersion of the dichroic mirror substrate and of other intracavity optics as well as for any upchirp that the pulses may have on generation in the intracavity BBO crystal. The IR pulses are not extracavity dispersion compensated. The spectral FWHM's of the IR and blue are 12.7 and 4.9 nm, respectively, which give $\Delta\nu\Delta t = 0.55$ for the IR and $\Delta\nu\Delta t = 0.71$ for the blue pulses. Pulse widths and time–bandwidth products are determined assuming a $\mathrm{sech}^2(t)$ intensity envelope.

We achieved the shortest blue pulses when running the laser with a 1% outcoupler in place of the high reflector and operating closer to net zero intracavity group-velocity dispersion (see Fig. 3). The power of the IR coupled out is 27 mW, whereas the blue power transmitted by the dichroic mirrors is ~31 mW per arm. The extracavity dispersion-compensated blue pulses have a FWHM of 54 fs and a spectral FWHM of 7.7 nm, which gives $\Delta\nu\Delta t = 0.67$. The IR pulses (which again are not extracavity dispersion compensated) have a pulse width of 93 fs and a spectral FWHM of 18.6 nm, which yields $\Delta\nu\Delta t = 0.70$. It is believed that the IR pulses may be compressed by an extracavity two-prism sequence, and we hope to verify this in the near future. Again, a $\mathrm{sech}^2(t)$ intensity envelope is assumed.

The observed intracavity SHG conversion efficiency of 3.2% per pass for the shortest blue pulses agrees well with the theory (3.5%) for conversion by a nondepleted pump wave.[11] Without the intracavity BBO crystal, we have observed stable mode-locked operation for <100-fs pulses at intracavity powers as high as 8 W. For the same focusing and BBO crystal length presented here, 8 W of intracavity power at a 110-fs pulse width would yield a more than fourfold increase in the output of the second harmonic, or ~500 mW of blue light. For this case, the peak intracavity intensity at the focus would approach the reported single-shot damage threshold for BBO of 50 GW/cm^2.[12] However, this threshold pertains to pulses of 8-ns duration, and we expect the threshold to increase by orders of magnitude for the 100-fs pulse-width regime. The average intensity is orders of magnitude below the long-term damage threshold for BBO.[12]

In conclusion, we have demonstrated highly efficient intracavity doubling of a mode-locked Ti:sapphire laser that yields a source of femtosecond pulses in the blue with the same high repetition rate of 72 MHz, short pulse width, excellent beam quality, and power in the blue representing appreciable recovery of the typical IR output at this 4.4-W pump level. This research represents an extension of intracavity doubling to solid-state mode-locked lasers and results in a source of femtosecond pulses potentially tunable from the near UV into the green, thus broadly expanding the potential spectral range for femtosecond pulses.

The authors thank W. S. Pelouch, P E. Powers, and D. C. Edelstein for helpful conversations. This research was supported by the Joint Services Electronics Program and the National Science Foundation.

References

1. R. L. Fork, C. V. Shank, C. Hirlimann, R. Yen, and W. J. Tomlinson, Opt. Lett. **8**, 1 (1983).
2. D. C. Edelstein, E. S. Wachman, and C. L. Tang, Appl. Phys. Lett. 54, 1728 (1989).
3. E. S. Wachman, W. S. Pelouch, and C. L. Tang, J. Appl. Phys. **70**, 1893 (1991).
4. P. M. W. French and J. R. Taylor, Opt. Lett. **13**, 470 (1988).
5. P. M. W. French, M. M. Opalinska, and J. R. Taylor, Opt. Lett. **14**, 217 (1989).
6. G. Focht and M. C. Downer, IEEE J. Quantum Electron. **24**, 431 (1988).
7. D. C. Edelstein, E. S. Wachman, L. K. Cheng, W. R. Bosenberg, and C. L. Tang, Appl. Phys. Lett. **52**, 2211 (1988).
8. D. E. Spence, P. N. Kean, and W. Sibbett, Opt. Lett. **16**, 42 (1991).
9. For example, the Coherent MIRA laser.
10. Y. Ishida, N. Sarukura, and H. Nakano, in *Digest of Conference on Lasers and Electro-Optics* (Optical Society of America, Washington, D.C., 1991), paper JMB2.
11. A. Yariv, *Quantum Electronics* (Wiley, New York, 1975), p. 431, Eq. 16.7-3, where this equation is divided by 4 for $P^{(\omega)}$ representing the total pump beam rather than by one half of the pump for each mixing wave, and the author has included the factor of ϵ_0 in d_{eff}.
12. H. Nakatani, W. R. Bosenberg, L. K. Cheng, and C. L. Tang, Appl. Phys. Lett. **53**, 2587 (1988).

Appendix I

Ti:sapphire-pumped, high-repetition-rate femtosecond optical parametric oscillator

W. S. Pelouch, P. E. Powers, and C. L. Tang

Department of Applied Physics, Cornell University, Ithaca, New York 14853

Received March 31, 1992

A broadly tunable femtosecond optical parametric oscillator (OPO) based on $KTiOPO_4$ that is externally pumped by a self-mode-locked Ti:sapphire laser is described. Continuous tuning is demonstrated from 1.22 to 1.37 μm in the signal branch and from 1.82 to 2.15 μm in the idler branch by using one set of OPO optics. The potential tuning range of the OPO is from 1.0 to 2.75 μm and requires three sets of mirrors and two crystals. Without prisms in the OPO cavity, 340 mW (475 mW) of chirped-pulse power is generated in the signal (idler) branch for 2.5 W of pump power. The total conversion efficiency as measured by the pump depletion is 55%. With prisms in the cavity, pulses of 135 fs are generated, which can be shortened to 75 fs by increasing the output coupling.

Optical parametric oscillators (OPO's) have recently been exploited in the femtosecond time domain as a source of broadly and continuously tunable radiation. The lack of suitable pump sources has hampered the development of femtosecond OPO's that operate with short pulse widths, a high repetition rate, and high output powers. The high peak power at the intracavity focus of a colliding-pulse mode-locked dye laser was exploited to develop the first femtosecond OPO.[1-3] This resulted in ≥105-fs, 80-MHz pulses at approximately 3 mW of output power. Other researchers resorted to a Q-switched and mode-locked laser (300 pulses at 15 Hz) to pump an OPO producing ≥160-fs pulses (65 fs at one wavelength) at 4.5 mW of average power.[4] More recently a femtosecond OPO was reported that was externally pumped by a hybridly mode-locked dye laser producing 220-fs pulses at 30 mW of average power.[5] In this Letter we describe a Ti:sapphire-pumped OPO capable of producing 75-fs pulses at a high repetition rate (90 MHz) and hundreds of milliwatts of average output power. We believe that these are the shortest tunable pulses ever generated from an OPO.

The Ti:sapphire pump laser is configured in a linear cavity with a 18-mm titanium-doped (0.1%) sapphire crystal and SF-14 prisms (spaced at 40 cm) for dispersion compensation. The crystal is mounted in a copper block and cooled by using a thermoelectric cooler with temperature feedback to maintain a constant 20°C temperature. The laser is self-mode locked as described elsewhere in the literature[6] and produces 2.5 W of 125-fs pulses in a TEM_{00} mode when pumped by a 15-W argon-ion laser. A schematic of the OPO cavity is shown in Fig. 1. The Ti:sapphire laser beam is focused onto a 1.15-mm KTP crystal with polarization along the y axis using a $r = 15$ cm curved high reflector. The pump suffers approximately a 5% transmission loss for each side of the crystal. The KTP crystal is cut at $\theta = 47.5°$ and $\phi = 0°$ for type II phase matching ($o \rightarrow e + o$) and coated with a 250-nm layer of MgF_2 on both sides for high transmission centered at 1.3 μm. The OPO cavity uses two $r = 10$ cm curved mirrors that are aligned for oscillation in the x–z plane of the crystal to provide compensation for walk-off between the Poynting vectors of the pump and the resonated signal branch.[3] The cavity may be aligned with or without the SF-14 prism sequence simply by lowering or raising the prism assembly. The output coupler is 1%, and the other flat mirror is mounted on a piezoelectric transducer for fine length adjustment. A linear cavity design was chosen so that the pump can be retroreflected for double-pass pumping of the KTP crystal.[4] This would result in parametric gain for the signal in both directions through the crystal when the retroreflected pump pulses overlap the signal pulses in the crystal. However, this requires that an optical isolator be inserted between the pump laser and the OPO to reject feedback into the Ti:sapphire cavity.

The OPO is aligned by monitoring the spontaneous parametric scattering using a liquid-nitrogen-cooled germanium photodiode [the peak detectivity is $\sim 10^{13}$ cm $Hz^{1/2}$ W^{-1} at 1.5 μm]. This signal is maximized by adjusting the OPO mirrors and focusing such that the spontaneous parametric scattering makes many round trips in the cavity. Oscillation occurs when the cavity length of the OPO is matched to that of the pump laser cavity; the length mismatch becomes more sensitive near threshold.

With 2.5 W of pump power (125 fs) the OPO produces as much as 340 mW of power in the signal branch through the 1% output coupler. We have measured 60 mW of signal energy reflected from the KTP crystal in one direction (120-mW loss per round trip), which implies a transmission loss of 0.2%. Thus 460 mW of power is generated in the signal branch with an effective output coupler of 1.4%. In the idler branch we have coupled out 475 mW of power, but this may be limited by the physical constraints of collecting and collimating the diverging

0146-9592/92/151070-03$5.00/0

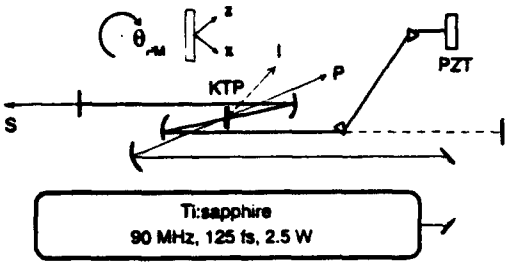

Fig. 1. Schematic of the OPO cavity in the vertical plane. The Ti:sapphire pump (P) is focused onto the 1.15-mm KTP crystal. An enlarged view of the crystal is depicted above and shows the orientation for type II phase matching at the phase-matching angle θ_{PM}. The signal branch (S) is resonated by using a 1% output coupler and a piezoelectric transducer (PZT) for fine length adjustment. The idler (I) exits from the crystal at ~6 deg from the signal. The prism sequence may be raised to allow oscillation without the prisms.

idler radiation that is generated at ~6 deg (external to the crystal) from the signal. The pump is depleted by 55% when the OPO is oscillating and is a measure of the actual conversion efficiency; this value agrees well with the measured power output of the OPO if the crystal reflections and the pump transmission losses are taken into account. Double-pass pumping has not yet been implemented in the OPO since excellent conversion efficiency has already been achieved. If only one pass of the pump were used, then a ring cavity would provide less loss than the linear cavity.

Interestingly, the OPO also produces output at two other non-phase-matched[7] wavelengths that correspond to collinear second-harmonic generation of the signal branch ($e + e \rightarrow e$) and noncollinear sum-frequency generation between the pump and the signal ($o + e \rightarrow o$). For a pump wavelength of 780 nm and a signal wavelength of 1300 nm the second-harmonic wavelength is 650 nm and the sum-frequency wavelength is 485 nm. A total of almost 100 mW of second-harmonic power is generated (50 mW in each direction), but only 10 mW gets transmitted through the infrared optics and output coupler. The collinear second harmonic could be utilized for experimental purposes and is also useful for aligning the signal through extracavity optics, after which it can be easily filtered out. 100 μW of sum-frequency light was measured after the output coupler. In all, the OPO system produces synchronized femtosecond radiation at five different wavelengths.

Without prisms in the OPO cavity the autocorrelation and spectra show signs of significant chirp. The pulse width as measured from the intensity autocorrelation is approximately 500 fs owing to the long decay time of the wings. With prisms in the OPO cavity two regimes are encountered. For net negative group-velocity dispersion (GVD) the pulses are unchirped with a minimum pulse width of 135 fs (fit to a sech^2 shape) and have a smooth spectrum ($\Delta\nu\Delta\tau = 0.45$) [see Figs. 2(a) and 2(b)]. For net positive GVD the pulses are slightly chirped with a broader pulse width and a split spectrum [see Figs. 2(c) and 2(d)]. Near zero GVD the OPO may abruptly flip into either the chirped or unchirped mode. This behavior is in contrast to the observed smooth transition between operation with net negative and positive GVD of the OPO reported in Ref. 2. Therefore a nonlinear chirp must be generated in the KTP, which accounts for the runaway condition in the positive-GVD regime. This would also explain why the time–bandwidth product is 45% greater than the transform limit for the minimum pulse width. This effect is most likely due to self-phase modulation of the signal in the crystal as a result of the high intracavity intensity and large nonlinear index of KTP. Self-phase modulation in KTP was identified as a source of broadening of the pump laser in Ref. 1 and is consistent with the shape of the signal spectrum in Fig. 2(c).[8] It is expected that the pulse widths are approximately constant over the tuning range owing to the relatively constant inverse group-velocity mismatch between the pump and the signal. The larger mismatch for the idler suggests pulse widths approximately 50% greater than the signal.

It was also observed in the unchirped regime that a slight detuning of the length shortened the pulse widths to approximately 75 fs (and reduced the output power by 25%). The pulse width was also decreased to 75 fs by increasing the output coupling at constant zero detuning. This was achieved by inserting a thin glass flat in the OPO cavity and rotating it away from Brewster's angle, effectively reducing the intracavity power by increasing the output coupling to 1.5% (plus 0.4% from the crystal). Therefore this pulse shortening results from a decrease in intracavity power as the OPO is operated closer to threshold, as predicted by theory.[9] The reduction in intracavity power reduces the magnitude of self-phase modulation (both linear and nonlinear chirp) so that less dispersion compensation is required from the prism sequence.

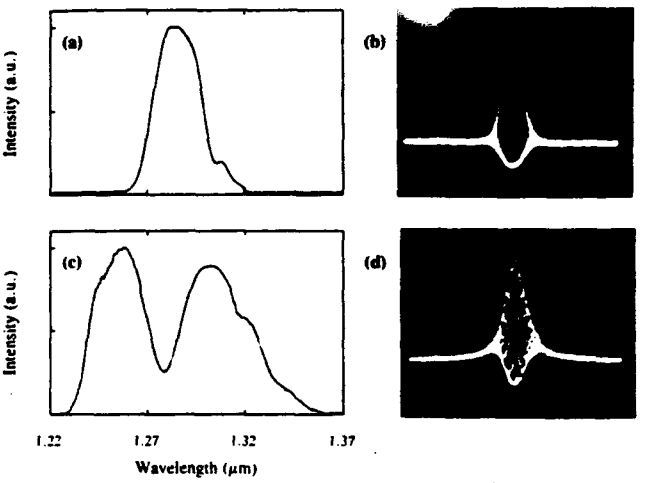

Fig. 2. (a) Spectrum and (b) autocorrelation of the signal pulse for net negative GVD. The time–bandwidth product is 0.45. (c) Spectrum and (d) autocorrelation of the chirped signal pulse for net positive GVD. The abrupt transition between these two regimes suggests a self-phase-modulation process in the crystal.

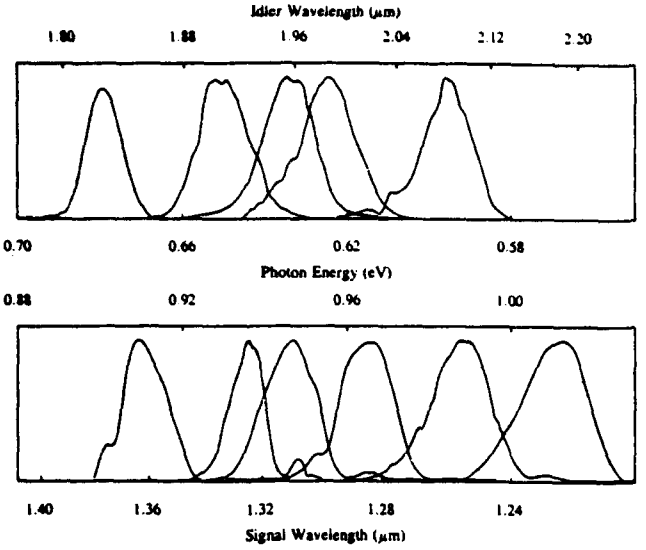

Fig. 3. OPO signal (bottom) and idler (top) spectra obtained by angle tuning the OPO over a range of one set of mirrors. Broad tuning may also be achieved by changing the pump wavelength without rotating the KTP crystal or altering the OPO alignment.

The insertion of the Brewster-cut prism sequence reduces the output power of the signal to 300 mW in the chirped regime, but we believe that with a more careful alignment full recovery of the 340 mW is possible. This loss is primarily due to a small rotation of the signal polarization in the KTP crystal, which is oriented slightly away from $\phi = 0°$. The output power for the unchirped pulses is reduced to approximately 180 mW. This loss of power is not due to simple alignment since the prism is only translated.

Tuning of the OPO is straightforward and may be accomplished by three different means. Adjustment of the length mismatch of the OPO cavity results in a wavelength shift as reported previously[1] and may be used to stabilize the OPO length at a fixed wavelength. The wavelength range over which the OPO will oscillate while the length is adjusted is a measure of how sensitive the OPO is to length variations. The OPO can withstand a 5-μm length variation, which results in a wavelength shift of almost 50 nm. Second, a change in the pump wavelength will tune the OPO without changing the crystal orientation or OPO alignment—only the length of the OPO cavity must be adjusted to match the new pump cavity length. We can tune our Ti:sapphire laser from 765 to 815 nm while maintaining mode locking and cavity alignment. This results in tuning of the signal branch from 1.22 to 1.34 μm and from 2.05 to 2.08 μm in the idler branch. Note that the wavelength of the idler remains relatively fixed, whereas the signal tunes over 120 nm as the pump wavelength is varied over 50 nm. Typically this type of tuning will also result in a change in pump power. Third, the OPO may be tuned in the traditional manner by adjusting the phase-matching angle of the KTP crystal. We can tune over a 100-nm range by freely rotating the KTP crystal and adjusting the cavity length. Beyond this range the OPO alignment needs to be modified. The operation of the OPO is quite robust so that broad tuning is accomplished by iterating between rotating the crystal and adjusting the OPO alignment while maintaining oscillation. Representative spectra are displayed in Fig. 3 for both the signal and the idler. The demonstrated tuning is limited by the optics available in our laboratory, but with appropriate optics the full tuning range will be accessible.

No alignment of the OPO is necessary on a day-to-day basis; length adjustment is all that is required to regain oscillation. Furthermore the OPO is not extremely sensitive to pump steering. Alignment of the pump through two pinholes suffices to recover oscillation if the Ti:sapphire alignment is considerably altered. The output of the OPO is an excellent TEM_{00} mode that is made possible by the tight Z focus shown in Fig. 1. Thus the OPO is a practical laser source for experimental ultrafast research. A feedback circuit to maintain length matching would be useful to maximize stability, although all the data presented in this Letter were obtained without any length stabilization.

In summary, we have reported the development of a high-power, high-repetition-rate femtosecond OPO externally pumped by a self-mode-locked Ti:sapphire laser. More than 1.0 W of the pump laser power is converted to tunable OPO radiation for a conversion efficiency of 55%. Unchirped pulses of 135 fs can be generated across the demonstrated tuning range of the device. Pulse shortening to 75 fs is achieved by increasing the output coupling at the expense of output power.

This research was supported by the Joint Service Electronics Program and the National Science Foundation. We are grateful to L. K. Cheng and J. D. Bierlein of E. I. DuPont de Nemours & Company for providing the KTP material.

Note added in proof: We recently generated nearly transform-limited 57-fs signal pulses at an output power of 115 mW.

References

1. D. C. Edelstein, E. S. Wachman, and C. L. Tang, Appl. Phys. Lett. **54**, 1728 (1989).
2. E. S. Wachman, D. C. Edelstein, and C. L. Tang, Opt. Lett. **15**, 136 (1990).
3. E. S. Wachman, W. S. Pelouch, and C. L. Tang, J. Appl. Phys. **70**, 1893 (1991).
4. R. Laenen, H. Graener, and A. Laubereau, Opt. Lett. **15**, 971 (1990).
5. G. Mak, Q. Fu, and H. M. van Driel, Appl. Phys. Lett. **60**, 542 (1992).
6. See, for example, D. E. Spence, P. N. Kean, and W. Sibbett, Opt. Lett. **16**, 42 (1991).
7. The non-phase-matched process was previously observed by D. C. Edelstein, Ph.D. dissertation (Cornell University, Ithaca, N.Y., 1990).
8. E. M. Wright, J. Opt. Soc. Am. B **7**, 1142 (1990).
9. E. C. Cheung and J. M. Liu, J. Opt. Soc. Am. B **7**, 1385 (1990).

High-power, high-repetition-rate femtosecond pulses tunable in the visible

R. J. Ellingson

School of Applied and Engineering Physics, Cornell University, Ithaca, New York 14853

C. L. Tang

School of Electrical Engineering, Cornell University, Ithaca, New York 14853

Received October 16, 1992

We demonstrate a Ti:sapphire-pumped intracavity-doubled optical parametric oscillator (OPO) that generates a total of up to 240 mW of sub-100-fs pulses tunable in the visible. The OPO consists of a 1.5-mm-thick $KTiPO_4$ (KTP) crystal configured in a ring cavity that is synchronously pumped by a self-mode-locked Ti:sapphire laser operating at an 81-MHz repetition rate and 2.1-W average power, producing 115-fs pulses at $\lambda = 790$ nm. Intracavity doubling of the OPO is accomplished by inserting a 47-μm-thick β-BaB_2O_4 crystal into an additional focus in the OPO cavity. We demonstrate continuous tuning of the second-harmonic output from 580 to 657 nm. The potential tuning range of this intracavity-doubled KTP OPO is approximately 500 to 800 nm.

Since the first demonstration of a high-repetition-rate femtosecond optical parametric oscillator (OPO) that was pumped intracavity of a colliding-pulse mode-locked dye laser,[1] there has been much interest in the development of the femtosecond OPO. The self-mode-locked Ti:sapphire (Ti:S) laser has led to a new level of performance in the high-repetition-rate femtosecond OPO.[2-5] High-repetition-rate femtosecond OPO's have been demonstrated to cover the regions 0.755 to 1.04 μm, 1.20 to 1.40 μm, and 1.45 to 3.20 μm.[1-6] The Ti:S-pumped OPO offers several desirable operating characteristics: high output power, extensive tunability, nearly transform-limited pulses as short as 57 fs,[2] excellent stability, and low amplitude noise. In this Letter we demonstrate a Ti:S-pumped ring-cavity OPO that is intracavity doubled to produce a stable 81-MHz pulse train of ~100-fs pulses tunable from 580 to 657 nm with an average total power generated as high as 240 mW and pulse widths as short as 95 fs.

The Ti:S laser is configured in a standard linear cavity using an 18-mm-long titanium-doped (0.1%) sapphire crystal. The pump beam (11.5W Ar^+, all lines) is focused using an $f = 10$ cm lens through one of the $r = 10$ cm Ti:S cavity mirrors. Dispersion compensation is achieved using SF-10 prisms spaced 45 cm apart; the laser is operated at an 81-MHz repetition rate and produces 115-fs pulses of ~2.1-W average output power at a center wavelength of 790 nm.

The intracavity-doubled ring-cavity OPO is shown schematically in Fig. 1. An $r = 25$ cm dielectric mirror is used to focus the Ti:S laser beam, which is polarized along the KTP's y axis, onto the 1.5-mm-thick KTP crystal. The KTP crystal, which is antireflection coated for $\lambda = 1.3$ μm, is cut at $\theta = 45°$ and $\phi = 0°$ for Type II phase matching ($o \rightarrow e + o$) in the x–z plane. The signal wave is resonated in a ring cavity using $r = 15$ cm mirrors for the KTP focus and $r = 10$ cm mirrors for the doubling crystal focus. The OPO mirrors are coated for a center wavelength of 1.3 μm. The OPO output coupler (OC) is either 1% at 1.3 μm or a high reflecting mirror identical to the other cavity mirrors. The SF-14 prisms are spaced 20 cm tip to tip for dispersion compensation. The 47-μm-thick β-BaB_2O_4 (BBO) crystal, cut and polished in our laboratory, is Brewster-cut for Type I ($o + o \rightarrow e$) phase matching at a wavelength of 850 nm; orientation for phase matching the second-harmonic generation (SHG) at 1.3 μm does not significantly increase the reflective loss suffered by the OPO fundamental. Unlike intracavity frequency doubling of a linear cavity, which results in dual output beams, the unidirectional ring

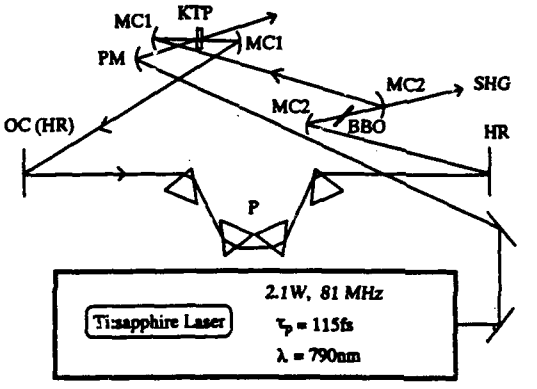

Fig. 1. Schematic of the Ti:sapphire-pumped intracavity-doubled KTP OPO. The Ti:sapphire pump is focused by the $r = 25$ cm pump mirror (PM) onto the 1.5-mm KTP crystal, which is cut for Type II phase matching in the positive region of the x–z plane. The curved OPO high reflectors (MC1, MC2) surrounding the gain (KTP) and frequency-doubling (BBO) crystals have radii $r = 15$ cm and $r = 10$ cm, respectively. The four-prism sequence (P) consists of two pair of 60° SF-14 prisms spaced 20 cm tip to tip. The single SHG output is transmitted through the OPO high reflector (MC2) at the doubling focus.

0146-9592/93/060438-03$5.00/0

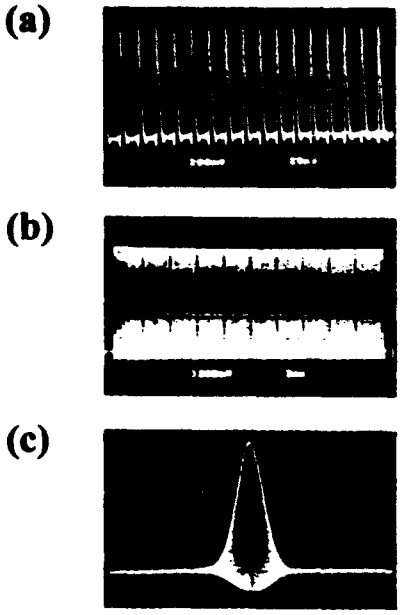

Fig. 2. Fast-photodiode oscilloscope trace showing the SH output of the intracavity-doubled OPO on time scales of (a) 20 ns/division and (b) 2 ms/division. The real-time autocorrelation in (c) shows a pulse width of 115 fs (FWHM, sech^2 fit) at $\lambda = 647$ nm, corresponding to 240 mW of total power generated in the second harmonic.

cavity gives a single output for the second-harmonic (SH) beam.

Alignment of the intracavity-doubled OPO is similar to that of Ref. 5. Initial cavity alignment is performed with the additional frequency-doubling focus inserted but without either the BBO or prism sequence inserted; after the OPO is optimized, the prism sequence is inserted, the cavity length adjusted, and multipass signal maximized to regain oscillation. The OPO is again optimized, and the OPO signal beam output is used to orient the BBO crystal for phase matching at Brewster's angle. Subsequent insertion of the BBO into the additional focus does not destroy the multipass signal through the 1% output coupler, and regaining oscillation is straightforward.

When pumping with 2.1 W, the intracavity-doubled OPO with the 1% OC produces an output of approximately 80 mW in the OPO signal beam at 1.3 μm and 115 mW of total SH light. As discussed further below, the main output of the SH through the OPO mirror is reduced by the Fresnel reflection off the BBO, imperfect transmission through the OPO mirror, and loss from the collimating lens. We replace the 1% OC with a high reflector (HR) to generate the highest SH power. In this configuration, after adjusting the intracavity prisms to yield the shortest SH pulses, we generate up to 240 mW of SH light at $\leq$115-fs pulse width; we measure a 95-fs pulse width using a two-prism sequence (SF-14 glass, spaced 17 cm apart) to remove any chirp on the pulses. Although the OPO cavity is not actively length stabilized (stabilization is straightforward[1]), the SH pulse train exhibits excellent stability as shown in Figs. 2(a) and 2(b). Furthermore, as shown in the real-time interferometric autocorrelation of Fig. 2(c), the pulses are clean and quiet.

Pumping the OPO with 115-fs pulses from the Ti:S laser, typical OPO pulse widths measured from the beam transmitted through the OC range from ~120 to ~170 fs, depending on the intraprism path length. The pulse width of the second-harmonic output measured directly is 115 fs; a pulse width of 95 fs is measured after the two-prism sequence, which reduces the time–bandwidth product from 0.45 to 0.37. The time–bandwidth product of the OPO signal fundamental pulses taken through the OC is 0.45 (sech^2 fit). This suggests that the OPO fundamental pulse may also be slightly chirped. Study of the specific pulse-shaping effects of both the intracavity prisms and the intracavity crystals should be possible by comparing the autocorrelation data for OPO output taken before and after the intracavity prism sequence.

As mentioned previously, the OPO may be tuned by varying the pump wavelength.[2,5] Here we angle tune the OPO by rotating the phase-matching angle of the KTP crystal. Tuning requires slightly adjusting one flat mirror, the KTP crystal, and the cavity length; the OPO continues to oscillate during these adjustments, which take just a few minutes. Tuning of the intracavity-doubled OPO is simplified when using an ultrathin BBO crystal. The Type I SHG tuning curve for BBO is multivalued; i.e., a given phase-matching angle generally matches two distinct wavelengths for SHG. The degenerate point for SHG in BBO occurs at $\lambda = 1.47$ μm, and the SHG group-velocity mismatch also goes to zero at $\lambda = 1.47$ μm. Interestingly, this simultaneous matching of the phase velocity and the group velocity at the degenerate point also occurs in $LiNbO_3$, another crystal of the $3m$ point group. Around this degenerate point in the range of ~1.1 to 1.8 μm, the SHG bandwidth for the 47-μm-thick BBO crystal becomes very large (as large as ~1700 nm, extending asymmetrically from roughly 1.0 to

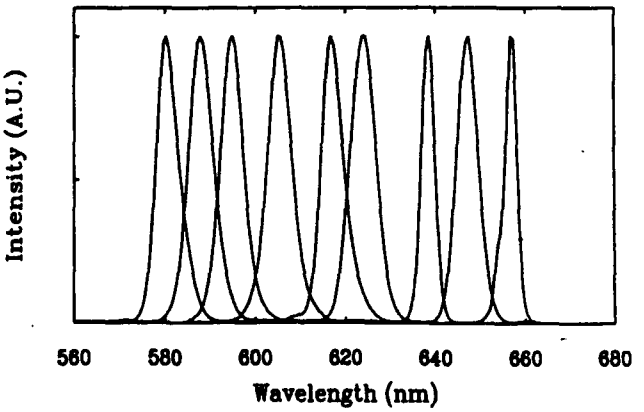

Fig. 3. Spectra showing the demonstrated tuning range of the intracavity frequency-doubled OPO from 580 to 657 nm. Variation in the bandwidth may be explained by a slight length detuning of the cavity from optimal length matching. This effect, as well as adjustment of intraprism path length, has been observed to affect the autocorrelation pulse width.

2.7 μm) as the sinc^2 ($\Delta k l_c/2$) profiles for the two phase-matched wavelengths merge and cross. Our observations agree: e.g., after tuning the OPO from 1.3 to 1.2 μm, rotating the phase-matching angle has no noticeable effect on the conversion efficiency. Thus, when using a thin BBO crystal, tuning of the OPO does not require adjusting the phase-matching angle of the BBO. Representative spectra of the SH output are shown in Fig. 3.

Operating the intracavity-doubled OPO with the 1% 1.3-μm OC, we measure the intracavity circulating power of the OPO fundamental to be 8 W, which yields a SHG conversion efficiency of ~1.4%. Based on this measurement, we estimate that replacing the 1% OC with the high reflector increases both the intracavity circulating power and the SHG conversion efficiency to ~11.5 W and ~2.1%, respectively. Use of a slightly thicker doubling crystal should facilitate the production of good power in the SH when lower Ti:S pump powers are used. The phase-matching bandwidth of even a 300-μm BBO crystal would permit rotation-free phase matching from ~1.2 to 1.6 μm, covering the 600- to 800-nm range in the visible and near infrared.

Although the Brewster-cut BBO crystal minimizes Fresnel loss to the OPO fundamental, this configuration results in the *s*-plane-polarized SH beam's suffering a 21% Fresnel loss at the BBO exit surface. Use of a normal-incidence-cut 1.3-μm antireflection-coated BBO crystal in place of the Brewster-cut piece would reduce the loss of the SH to ≤6%. The only output coupling inefficiency for the SH beam is the transmission through the OPO high reflector. Our OPO mirrors transmit ~80% of the SH, and specially designed single-stack mirrors can increase this transmission to ~90%. Our current configuration, with losses of 21% at the BBO exit surface, 20% at the OPO HR, and 8% at the collimating lens, transmits ~140 mW of the 240 mW total SH produced.

The nonlinear loss (~2% total loss) due to the SHG in the intracavity-doubled OPO is not believed to play a major role in the shaping of the OPO fundamental pulse. The pulse broadening due to linear dispersion of such a thin BBO crystal is insubstantial. Thus it is expected that shorter Ti:S pump pulses obtained by reducing third-order dispersion[7,8] will yield shorter OPO SHG pulses.

When weighting the benefits of doubling external or internal to the OPO cavity, one must consider both the advantages and disadvantages of each scheme. Extracavity doubling of the OPO has the advantage of simpler alignment, but presents the disadvantages of relatively low power (tens of milliwatts should be possible) and poor mode quality for the SH owing primarily to the angular acceptance limitations of using a thicker crystal. Conversely, intracavity doubling achieves approximately an order-of-magnitude greater power in the SH than is possible by extracavity doubling of current OPO output powers. The conversion efficiency is much greater intracavity since the power is ~100 times greater. Furthermore, the transverse mode of the OPO is an exceptionally pure, round TEM_{00} (achievable regardless of the transverse mode of the Ti:S pump laser), and aside from slight irregularity due to BBO surface imperfections, this TEM_{00} mode is imparted to the frequency-doubled beam.

We observe that intracavity-doubling with a thin BBO crystal does not add significantly to the OPO's complexity, nor does it reduce its stability. The linear loss of the additional focus and doubling crystal is estimated to be ≤0.5%, and the OPO's tuning range is not affected by the presence of the BBO; in addition, use of a reasonably thin BBO crystal (≤300 μm) permits hands-off phase matching over the tuning range of the OPO.

In conclusion, we have used an Ar^+-pumped mode-locked Ti:S laser pumping an intracavity-doubled OPO to generate tunable ~100-fs pulses over the range of 580 to 657 nm, with a potential tuning range of ~500 to 800 nm. We have demonstrated what we believe is an important source for high-repetition-rate femtosecond pulses, tunable in the visible, with high average power, short pulse width, excellent spatial mode quality, high peak power, and excellent stability. As extensions of this research, we plan to extend the demonstrated tuning range of the intracavity-doubled OPO to the shortest possible wavelengths by using a shorter-wavelength Ti:S pump beam and OPO mirrors that extend down to ~1.05 μm. We also plan to replace the SF-10 prisms of the Ti:S laser with low-dispersion prisms and optimize the pulse-shaping parameters both of the pump source and within the OPO cavity to investigate short-pulse operation of the OPO.

We thank Randall Lane for cutting the BBO crystal and Mike Watts of Spectra-Physics Lasers, Inc., for his contribution to this Letter. This research was supported by the Joint Services Electronics Program and the National Science Foundation.

References

1. D. C. Edelstein, E. S. Wachman, and C. L. Tang, Appl. Phys. Lett. **54**, 1728 (1989); E. S. Wachman, D. C. Edelstein, and C. L. Tang, Opt. Lett. **15**, 136 (1990); E. S. Wachman, W. S. Pelouch, and C. L. Tang, J. Appl. Phys. **70**, 1893 (1991).
2. W. S. Pelouch, P. E. Powers, and C. L. Tang, in *Digest of Conference on Lasers and Electro-Optics* (Optical Society of America, Washington, D.C., 1992), paper CPD14, p. 27.
3. G. Mak, Q. Fu, and H. M. van Driel, in *Digest of Conference on Lasers and Electro-Optics* (Optical Society of America, Washington, D.C., 1992), paper CWD1, p. 236.
4. Q. Fu, G. Mak, and H. M. van Driel, Opt. Lett. **17**, 1006 (1992); G. Mak, Q. Fu, and H. M. van Driel, in *Digest of Ultrafast Phenomena VIII* (Ecole Nationale Superieure Technique et Avancée, Paris, 1992), p. 394.
5. W. S. Pelouch, P. E. Powers, and C. L. Tang, Opt. Lett. **17**, 1070 (1992); presented at International Quantum Electronics Conference, Vienna, 1992.
6. G. Mak, Q. Fu, and H. M. van Driel, Appl. Phys. Lett. **60**, 542 (1992).
7. C.-P. Huang, Ch. Spielmann, T. Brabec, E. Wintner, and A. J. Schmidt, Opt. Lett. **17**, 204 (1992).
8. B. Proctor and F. Wise, Opt. Lett. **17**, 1295 (1992).

Optical parametric oscillation with $KTiOAsO_4$

P. E. Powers, S. Ramakrishna, and C. L. Tang

212 Clark Hall, Cornell University, Ithaca, New York 14853

L. K. Cheng

Science and Engineering Laboratory, E. I. du Pont de Nemours and Company, Experimental Station P.O. Box 80306, Wilmington, Delaware 19880-0306

Received February 19, 1993

We present what is to our knowledge the first demonstration of a femtosecond optical parametric oscillator using the new nonlinear crystal $KTiOAsO_4$. Powers of as much as 75 mW in the signal branch and as much as 100 mW in the idler branch were coupled out of the cavity. Pulse widths as short as 85 fs in the signal branch and 150 fs in the idler branch were measured. The potential of tuning out to ~5 μm in the idler branch is discussed.

The versatility of the cw femtosecond optical parametric oscillator (OPO) is now being demonstrated with reports of high powers, short pulses, and broad tunability with the use of a $KTiOPO_4$ (KTP) femtosecond OPO.[1-3] This performance can be enhanced further still by the use of new nonlinear crystals with larger nonlinearities and broader transparency ranges. $KTiOAsO_4$ (KTA) is a crystal similar to KTP but has an optical nonlinearity approximately 20% larger and an infrared transparency range nearly 1 μm broader.[4] Recent progress in the crystal growth of single-domain KTA crystals makes possible its use in a femtosecond OPO. We present what are to our knowledge the first results of a femtosecond OPO based on KTA. We achieved powers as high as 75 mW at 93 fs in the signal branch and 90 mW at 170 fs in the idler branch and pulse widths as short as 84 fs in the signal branch and 148 fs in the idler branch. An interferometric autocorrelation of an idler pulse in the infrared is also shown.

The KTA OPO is configured in a linear cavity as depicted in Fig. 1 and is aligned the same as in Ref. 1. KTA is a positive biaxial crystal, with $n_z > n_y > \approx n_x$, where x, y, and z correspond to the piezoelectric axes. The KTA crystal used in this experiment was grown from a $K_6As_2O_{10}$ flux. The crystal is lightly doped (~0.2 wt. %) with indium to promote single-domain crystallization. Initial measurements[4] suggest that indium doping does not affect the optical properties of KTA. As in KTP, d_{eff} in KTA is maximized for a type II interaction ($o \rightarrow e + o$). Phase matching was carried out in the x–z plane such that direct comparison of the performance of our KTA OPO can be made with that of the KTP OPO reported in Ref. 1. In this case, $\mathbf{k}_p$, $\mathbf{k}_s$, and $\mathbf{k}_i$ are in the $\phi = 0$ plane. Since $d_{24} > d_{15}$ and $(n_z - n_y) < (n_z - n_x)$ in KTA, this configuration also maximizes the d_{eff} coefficient, which in the x–z plane is given by

$$d_{eff} = d_{24} \sin \theta . \quad (1)$$

The crystal is 1.47 mm thick, cut at $\theta = 50°$, and antireflection coated on both surfaces from 1.3 to 1.6 μm. The crystal has a reflection loss of 14% per surface at the pump wavelength.

For this OPO, the e wave (signal) is resonated. Resonating the e wave results in a spatial walk-off of the e wave's Poynting vector from its wave vector inside the nonlinear crystal. Previous experimental studies have shown that the OPO operates such that the Poynting vector of the resonated wave and that of the pump wave are collinear.[1,5] To accomplish this when we resonate the e wave, we employ a noncollinear phase-matching geometry. The cavity mirrors are placed such that the angle between the pump and the signal is the negative of this Poynting vector walk-off, so that the Poynting vector of the e wave walks onto that of the pump. The calculated tuning curve for KTA with this geometry is shown in Fig. 2 for a variety of pump wavelengths in the Ti:sapphire laser range. The Sellemeier equations used were similar to those reported in Ref. 4.

A 1.2-W, 90-fs, 780-nm Ti:sapphire pump is focused onto the KTA crystal with an $r = 15$ cm mirror. The corresponding pump power inside the crystal is 1.0 W as a result of the reflection loss at the front

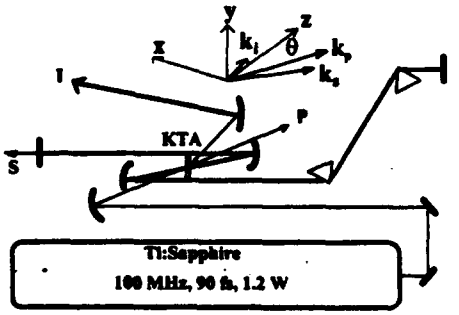

Fig. 1. Schematic of a Ti:sapphire-pumped femtosecond KTA OPO, with the inset showing the directions of $\mathbf{k}_p$, $\mathbf{k}_s$, and $\mathbf{k}_i$ with respect to the crystal axes x, y, and z. The cavity and crystal are aligned such that the Ti:sapphire pump (P) is an o wave, the resonated signal (S) is an e wave, and the nonresonated idler (I) is an o wave. The polarization direction for the o waves is along y, and the polarization direction of the e wave is in the x–z plane.

0146-9592/93/141171-03$6.00/0

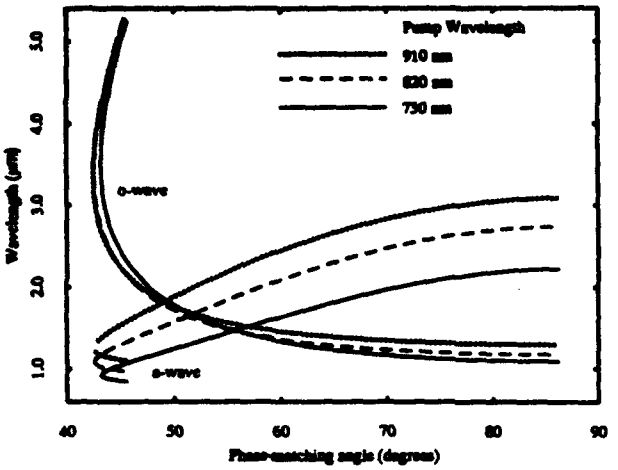

Fig. 2. Tuning curve for a type II interaction in KTA with a noncollinear angle of 2.0°. A tuning curve is generated for three pump wavelengths that cover a large part of the Ti:sapphire laser range.

surface of the crystal. The two curved cavity OPO mirrors have a radius of curvature of $r = 10$ cm and have a high-reflection coating from 1.2 to 1.5 μm. The radii of curvature of the pump focusing and OPO mirrors are chosen such that the spot sizes of the pump and the signal are matched in the crystal. The two flat end mirrors of the cavity consist of a 1% output coupler and a high reflector with the same coating as the curved mirrors. The intracavity dispersion-compensating prism sequence consists of two SF14 prisms spaced at 20 cm arranged such that they can be inserted into or removed from the cavity. The pulse-width measurements of the signal presented herein were made with the prisms in the cavity. A collimating mirror is positioned to collimate and couple out the nonresonated *o* wave (idler). The autocorrelation of the signal and the idler was accomplished with a 0.3-mm-thick BBO crystal. The signal autocorrelation was measured with an RCA Model C31034 photomultiplier tube, while an RCA Model 7102 photomultiplier tube was used for the idler. The quality of the interferometric autocorrelation for the idler is lower than that of the signal, as the sensitivity of the Model 7102 is an order of magnitude less than that of the Model C31034 used for the signal.

The phase-matched outputs of the OPO are the resonated signal and the nonresonated idler. Tunability is achieved by either rotating the crystal about its *y* axis or tuning the pump. Tuning from 1.29 to 1.44 μm in the signal branch and from 1.83 to 1.91 μm in the idler branch was achieved by angle tuning and is shown in Fig. 3. The signal has two operating regimes, chirped and unchirped. The chirped regime is encountered when the OPO is operating with a net positive group-velocity dispersion (GVD). The unchirped regime is achieved by going to net negative GVD, using the prism sequence. The autocorrelation and spectra are typical of chirped pulses and are similar to those reported in Ref. 1. The transition from chirped to unchirped pulses when going from positive to negative GVD is a smooth one. The unchirped regime is characterized by pulse widths approximately 20% or more longer than the pump pulse width, depending on the amount of negative GVD. The shortest pulses are encountered near zero GVD, where signal pulses as short as 84 fs were measured (fitted to a sech^2 shape).

The idler is generated during each pass of the signal through the KTA crystal. Interestingly, the interferometric autocorrelation of the idler wave shows no sign of chirp regardless of whether the signal pulse is chirped or unchirped. Similarly, the spectra of the idler when the signal is chirped or unchirped are nearly identical. Figure 4 shows the intensity and interferometric autocorrelation of the idler pulse with a pulse width of 183 fs at a wavelength of 1.77 μm and a power of 80 mW. The signal pulse for this measurement was unchirped at 94 fs and had a power of 30 mW out of the 1% output coupler. The contrast ratio of the interferometric autocorre-

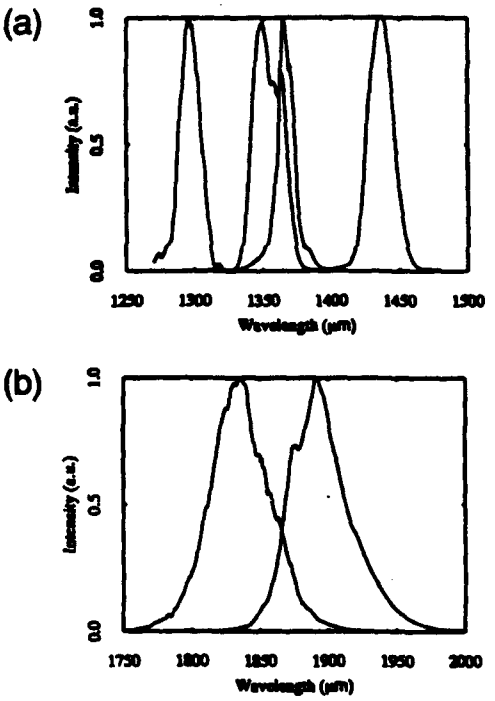

Fig. 3. Spectra of (a) the signal and (b) the idler pulses. This tuning range represents a small portion of the tuning range for the KTA OPO.

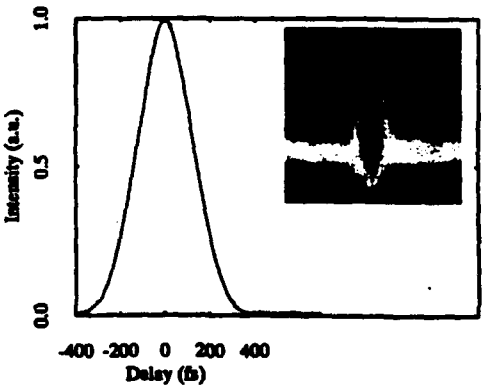

Fig. 4. Intensity autocorrelation of a 183-fs idler pulse at 1.77 μm. The inset shows the interferometric autocorrelation.

lation for the idler pulses is less than 8:1. This is attributed to the fact that the scanning arm of the interferometer requires a small corner cube, which limits the throughput of that arm. The shortest idler pulses, 148 fs at a wavelength of 1.89 μm and a power of 40 mW, were observed for the chirped-pulse signal operation. The total OPO output power (signal plus idler) was greatest for the unchirped signal pulse regime.

Accompanying the phase-matched outputs are several non-phase-matched outputs, as reported with the KTP OPO.[1,2,6] Non-phase-matched second-harmonic generation of the signal pulse, as well as sum-frequency generation between the pump and signal and the pump and idler, are observed.

Although d_{eff} is somewhat larger for KTA than for KTP, the signal and idler powers from the KTA OPO are lower than those from the KTP OPO as reported in Refs. 1 and 2. In fact, for the 1.2-W pump power and 1% output coupling used here, the operation of the KTA OPO is close to threshold, indicating that the oscillation threshold is less than, but close to, 1 W. In comparison, we have operated an OPO using a 1.15-mm KTP crystal and a 1% output coupler with pump powers as low as 500 mW at 100 fs. For the KTA OPO, the conversion efficiency of the pump to signal and idler is 10–15%; the KTP OPO's mentioned above achieved a conversion efficiency as high as 30%.[1] There may be several reasons for the higher threshold and lower conversion efficiency. The KTA OPO was pumped at powers approximately 20% less than the KTP OPO reported in Ref. 1 owing to the reflection loss of the Ti:sapphire pump on the surface of the crystal. More importantly, the KTA crystal used in this experiment shows as much as a 25% fluctuation in output power when we focus on different parts of the crystal, indicating possible defects such as inhomogeneous optical loss and residual ferroelectric domains. The precise nature of the inhomogeneity is not clear, but other KTA crystals have shown index-of-refraction inhomogeneities that are due to the inclusion of the indium dopant in the flux. The possibility of crystal imperfections is relatively high for KTA, as it is a new crystal and its growth technology is still being perfected. Better crystal quality and coating control are expected to yield improved OPO performance.

KTA has the potential for tuning to wavelengths inaccessible with KTP. As Fig. 2 shows, KTA can tune over its whole transparency, range, reaching the important 4–5-μm region, which is inaccessible to KTP. KTA can also tune in the 3.5-μm region, where KTP has an absorption band.[7] Generating pulse widths of the order of 200 fs or less should be possible in this region. The phase-matching bandwidth of the signal that will generate idler pulses in this region is approximately 13 nm, which is capable of supporting a 95-fs pulse. The inverse group-velocity mismatch (GVM) between the signal and pump in this region is less than 100 fs/mm, so the signal pulse width should be of the order of 100 fs. The corresponding idler pulse width should be of the same order, since the GVM between the idler and the pump is even less than that between the signal and pump.

The generation of pulses as short as those generated with the KTP OPO should be possible for signal wavelengths in the 1.2–1.5-μm region. The phase-matching bandwidth in this region is of the order of 40 nm, and the GVM between the pump and signal for KTA is less than 20 fs/mm. KTP has roughly the same phase-matching bandwidth but has a larger GVM. The KTP OPO has demonstrated unchirped pulses as short as 57 fs. The KTA OPO should be capable of producing pulses this short, since KTA has a sufficient phase-matching bandwidth and its GVM is less than that for KTP. The idler pulse width from KTA is probably broader than that for KTP since it has a larger GVM between the pump and idler than does KTP. Even so, the idler pulse width reported in this Letter is to our knowledge the shortest femtosecond idler pulse in the infrared yet reported.

In conclusion, we have demonstrated the successful operation of a high-repetition-rate OPO based on the new nonlinear crystal, KTA, producing unchirped pulses as short as 84 fs at 1.36 μm and 150 fs at 1.89 μm. We have shown tuning from 1.29 to 1.44 μm in the signal branch and from 1.83 to 1.91 μm in the idler branch, and we have discussed the potential of using KTA to reach the important 3–5-μm spectral region. With improved crystal quality, we expect the output power from our KTA OPO to improve. The Ti:sapphire-based OPO is a practical way to generate high-power, broadly tunable pulses and will continue to benefit from the introduction of other nonlinear crystals with larger d coefficients and broader transparency ranges.

The authors thank W. S. Pelouch for useful conversations and J. D. Bierlein for his encouragement. This research was supported by the Joint Services Electronics Program and the National Science Foundation.

References

1. W. S. Pelouch, P. E. Powers, and C. L. Tang, Opt. Lett. **17**, 1070 (1992).
2. Q. Fu, G. Mak, and H. M. van Driel, Opt. Lett. **17**, 1006 (1992).
3. R. J. Ellingson and C. L. Tang, Opt. Lett. **18**, 438 (1993).
4. L. K. Cheng, L.-T. Cheng, J. D. Bierlein, and F. C. Zumsteg, Appl. Phys. Lett. **62**, 346 (1993).
5. E. S. Wachman, W. S. Pelouch, and C. L. Tang, J. Appl. Phys. **70**, 2893 (1992).
6. D. C. Edelstein, "New sources and techniques for ultrafast laser spectroscopy," Ph.D. dissertation (Cornell University, Ithaca, N.Y., 1990).
7. F. Ahmed, R. F. Belt, and G. Gashurov, J. Appl. Phys. **60**, 839 (1986).

Appendix L

High-repetition-rate femtosecond optical parametric oscillator based on $CsTiOAsO_4$

P. E. Powers

School of Applied and Engineering Physics, Cornell University, Ithaca, New York 14853

C. L. Tang

School of Electrical Engineering, Cornell University, Ithaca, New York 14853

L. K. Cheng

Science and Engineering Laboratory, E.I. Dupont de Nemours and Company, Experimental Station P.O. Box 80306, Wilmington, Delaware 19880-0306

Received August 11, 1993

A high-repetition-rate Ti:sapphire-pumped optical parametric oscillator based on the new nonlinear optical crystal $CsTiOAsO_4$ is described. The operation of this optical parametric oscillator is characterized for a 90°-cut crystal by use of a type II interaction. Tuning from 1.46 to 1.74 μm is demonstrated, and there is the potential for tuning from 0.9 to 5 μm with angle tuning. Powers of 100 mW in the signal and the idler branches are obtained. Pulse widths as short as 64 fs are generated with and without prisms in the cavity.

The successful demonstration of high-repetition-rate optical parametric oscillation by use of the nonlinear crystals KTP (Refs. 1 and 2) and $KTiOAsO_4$ (KTA; Ref. 3) shows great promise in generating tunable femtosecond pulses from 1 to 3 μm for KTP and from 1 to 5 μm for KTA. The cesium analog of KTA, $CsTiOAsO_4$ (CTA), is another candidate for use as a nonlinear crystal for an optical parametric oscillator (OPO). CTA has roughly the same transparency range as KTA, extending out to 5 μm in the infrared and a nonlinearity of the order of that of KTP.[4] The tuning characteristics of CTA are, however, quite different from those of both KTP and KTA. In particular, for the Ti:sapphire pump wavelengths, the CTA OPO oscillates at and near the important 1.55-μm spectral region for a noncritically phase-matched crystal. We demonstrate for the first time to our knowledge the successful operation of an OPO based on the new nonlinear crystal CTA. This Letter describes the experimental setup and the results obtained with this OPO.

The CTA crystal is 1 mm thick, is cut at $\theta = 90°$, and is antireflection coated on both surfaces centered at 1.5 μm. For this crystal cut, the Poynting vector and the **k** vector of a beam propagating through the crystal are collinear, which permits a collinear-pumped OPO. The CTA crystal is aligned for a type II interaction ($o \rightarrow e + o$), which, for this crystal cut, means that the pump and the OPO o wave are polarized along the y axis and the e wave is polarized along the z axis of the CTA crystal. The **k** vectors of the pump and both the e wave and the o wave from the OPO are along the x axis. For a 90° crystal cut, the phase matching is noncritical, so there is little variation in the wavelength of the OPO output beams for a change in crystal angle. For this noncritical phase-matching regime, we tune the OPO by changing the pump wavelength. The theoretical tuning curve for $\theta = 90°$ based on the Sellmeier equations given in Ref. 4 is shown in Fig. 1.

A schematic of the experimental setup is shown in Fig. 2. The CTA OPO is pumped with a 1.1-W 67-fs Ti:sapphire laser, tunable from 760 to 820 nm. To achieve a collinear pump geometry, we focus the pump with an $R = 15$ cm curved mirror through one of the OPO curved mirrors onto the CTA crystal. The transmission of the pump through this mirror varies from 27% to 80% over the Ti:sapphire laser's tuning range; the pump experiences another 5% reflective loss at the surface of the CTA crystal. The OPO resonator mirrors consist of two $R = 10$ cm curved mirrors and a flat mirror, all coated with a single-stack high-reflecting coating centered at 1.5 μm. The other mirror in the cavity, the output coupler, reflects 98% at 1.5 μm. Because the CTA OPO is a synch-pumped system, it is length matched to the Ti:sapphire cavity. The CTA OPO cavity has a removable intracavity-dispersion-compensating prism pair. The prisms are SF14 prisms and are spaced at 14 cm.

For the collinear cavity configuration, we can easily resonate either the e wave or the o wave by choosing the appropriate mirror coating. Resonating the o wave is advantageous because, over a large pump wavelength range, the o-wave wavelength changes only slightly; for example, tuning the pump from 700 to 850 nm tunes the o wave from 1.56 to 1.60 μm, as seen in Fig. 1. This permits us to generate the o wave near 1.58 μm and to tune the e wave from 1.27 to 1.82 μm. The advantage of resonating the e wave is that the group-velocity mismatch between

0146-9592/94/010037-03$6.00/0

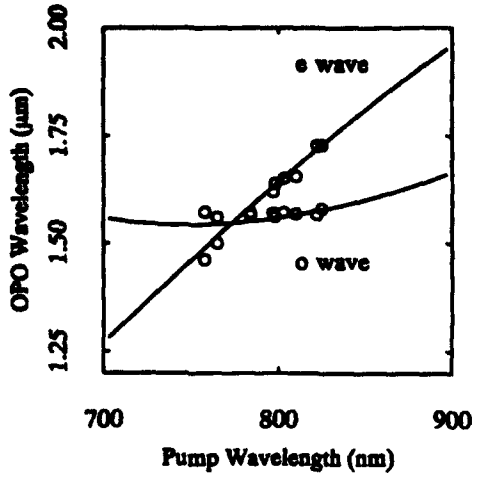

Fig. 1. Theoretical tuning curves based on the Sellmeier equations in Ref. 4. Also shown are the measured values (circles) from the CTA OPO.

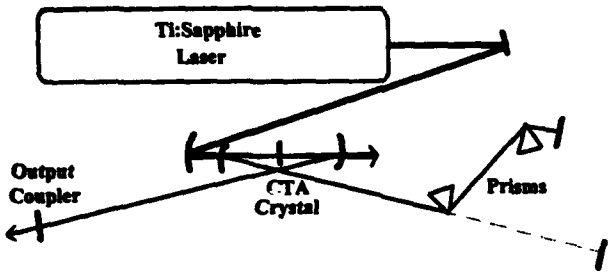

Fig. 2. Schematic of the experimental setup showing collinear pump geometry. The Ti:sapphire pump is focused onto the CTA crystal. The resonated OPO wave is coupled out of the 2% output coupler; the other wave is coupled out of the cavity through reflection losses from the prisms and transmissive losses from the cavity mirrors. The prisms may be removed from the cavity to permit oscillation without prisms.

the pump and the *e* wave is small, near 30 fs/mm, compared with ~200 fs/mm between the *o* wave and the pump. This should permit us to use longer crystals without lengthening the pulse width substantially.

As Fig. 1 shows, for a 90°-cut CTA crystal the wavelengths of the OPO *e* wave and *o* wave are close for pump wavelengths near 770 nm. In this range the OPO mirrors can resonate either the *o* wave or the *e* wave. Without prisms in the cavity, a simple change in output coupler position determines which wave is resonated since the two waves travel at different group velocities in the CTA crystal. For example, the difference in output coupler position between resonation at 1.56 μm and at 1.61 μm (for a 792-nm pump) is approximately 50 μm.

Resonating the *o* wave without prisms in the cavity yields powers of as much as 100 mW in each wave for a 670-mW pump (inside the crystal), giving a conversion efficiency of approximately 30%. Typically the pulses generated are chirped; however, length detuning the cavity can result in chirp-free pulses at the expense of output power. Near degeneracy, where the OPO cavity mirrors reflect the *e* wave and the *o* wave, the nonresonated *e* wave is a set of pulses spaced by approximately 400 fs. This is a result of the different cavity round-trip times for the nonresonated *e* wave and the resonated *o* wave. After one round trip the *o* wave is coincident with the next pump pulse, whereas the nonresonated *e* wave is not. The interaction of the pump with the *o* wave amplifies the *o* wave and generates a new *e* wave; hence two *e*-wave pulses are present after one round trip. Each successive round trip adds a new pulse to the *e*-wave train. Ultimately the losses from the cavity limit the number of *e*-wave pulses in each set.

The operation of the CTA OPO when the *e* wave is resonating without prisms gives powers similar to those obtained when the *o* wave is resonating. The power is ~70 mW per branch for a 400-mW pump (inside the crystal). The output of the *e* wave is chirp free, and we observed pulses as short as 62 fs (assuming a sech^2 pulse shape) at an average power of 70 mW for the CTA OPO for pumping with a 65-fs Ti:sapphire pump. The output of the nonresonated *o* wave is a set of pulses similar to that seen on the output of the *e* wave when the *o* wave is resonated.

The behavior of the CTA OPO with prisms is similar to that reported for the KTP OPO (Ref. 1) and the KTA OPO.[3] There is a transition from chirped to chirp-free as the net cavity group-velocity dispersion (GVD) changes from net positive to net negative GVD. The shortest pulses are encountered near zero GVD. In both cases of resonating the *e* wave or the *o* wave near this zero-GVD point, the pulse width of the resonated wave is approximately equal to the pump pulse width. The shortest pulses measured were 64 fs for resonating the *e* wave with a 67-fs Ti:sapphire pump pulse width. The time–bandwidth product for the operation of the OPO near zero GVD was measured to be $\Delta\nu\Delta\tau \approx 0.34$, assuming a sech^2 pulse shape. A typical interferometric autocorrelation is shown in Fig. 3. The power coupled out of the cavity with prisms is reduced by approximately a factor of 2. For example, when the

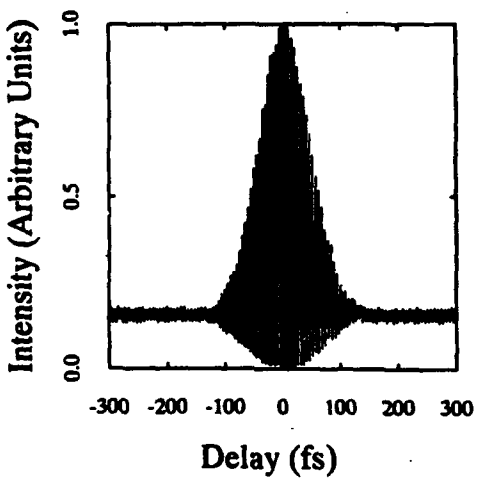

Fig. 3. Autocorrelation of the resonated *e* wave from the CTA OPO. This autocorrelation is a typical output pulse from the CTA OPO; it is 72 fs, assuming a sech^2 pulse shape. Note that the contrast ratio of the peak to background is 7.7:1, which is close to the ideal 8:1 contrast ratio.

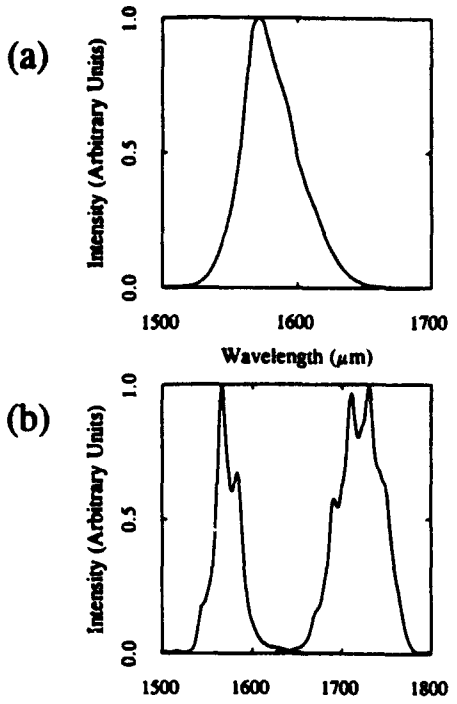

Fig. 4. (a) Typical spectrum of a resonated wave with prisms in the cavity, (b) typical spectra of a nonresonated wave with prisms in the cavity.

o wave is resonating with prisms at 1.58 μm, 55 mW of the *o* wave is coupled out of the 2% output coupler, whereas 100 mW is coupled out without the prisms. This is similar to the power drop reported in Ref. 1.

With the prisms in the cavity the nonresonated wave is coupled out of the cavity through the output coupler and the prism sequence. The prisms are Brewster cut and are oriented in the cavity such that the resonated wave experiences low reflective losses; the nonresonated wave is orthogonally polarized to the resonated wave so that it experiences ~20% loss per prism surface. The transmission for the nonresonated wave through the entire prism sequence is approximately 17%. The output of the nonresonated wave out of the output coupler shows two pulses. The amplitude of the second pulse is largest when the wavelength of the nonresonated wave is close to that of the resonated wave so there is little transmissive loss from the OPO cavity mirrors.

For the 90° crystal cut, we accomplished tuning by changing the Ti:sapphire pump wavelength. Figure 1 shows the measured values for the CTA OPO. Tuning the Ti:sapphire pump from 758 to 820 nm generates the outputs from the OPO from 1.46 to 1.73 μm. A difference between the resonated wave and the nonresonated wave was observed. A typical spectrum obtained from the resonated wave is shown in Fig. 4(a), and two typical spectra from the nonresonated wave are shown in Fig. 4(b). These spectra were all obtained with prisms in the cavity. The difference that we noted was the modulation on the spectra from the nonresonated wave. This modulation is even stronger when the prisms are not in the cavity, and we suspect that it is due to the presence of multiple pulses. The spectrum of the resonated wave does not show this modulation with or without prisms in the cavity.

A much broader tuning range can be accessed with different crystal cuts and optic sets. The potential tuning range for a Ti:sapphire-pumped CTA OPO is from 0.9 to 5 μm.

In summary, we have demonstrated the successful operation of a high-repetition-rate femtosecond OPO based on the new nonlinear crystal CTA. Chirp-free pulses as short as 62 fs at an average power of 70 mW are generated. Tuning from 1.46 to 1.73 μm demonstrated in this Letter realizes the possibility of the use of this device in the 1.55-μm region. We believe that, with appropriate OPO cavity optics that will permit high transmission of the Ti:sapphire pump, the increased pump power will give conversion efficiencies as high as that observed with the KTP OPO.

This research was supported by the Joint Services Electronics Program and the National Science Foundation.

References

1. W. S. Pelouch, P. E. Powers, and C. L. Tang, Opt. Lett. **17**, 1070 (1992).
2. Q. Fu, G. Mak, and H. M. van Driel, Opt. Lett. **17**, 1006 (1992).
3. P. E. Powers, S. Ramakrishna, C. L. Tang, and L. K. Cheng, Opt. Lett. **18**, 1171 (1993).
4. L. K. Cheng, L. T. Cheng, F. C. Zumsteg, J. D. Bierlein, and J. Galperin, J. Cryst. Growth **132**, 280 (1993).

High-repetition-rate femtosecond optical parametric oscillator using $RbTiOAsO_4$

P. E. Powers

School of Applied and Engineering Physics, Cornell University, Ithaca, New York 14853

C. L. Tang

School of Electrical Engineering, Cornell University, Ithaca, New York 14853

L. K. Cheng

Science and Engineering Laboratory
E.I. Dupont de Nemours and Company
Experimental Station P.O. Box 80306
Wilmington, DE 19880-0306

Abstract

A high-repetition-rate Ti:sapphire-pumped optical parametric oscillator (OPO) based on the new nonlinear optical crystal $RbTiOAsO_4$ (RTA) is described. Tuning from 1.03 μm to 1.3 μm in the signal branch and from 2.15 μm to 3.65 μm in the idler branch with powers as high as 250 mW in the signal and 200 mW in the idler is presented. The possibility of extending the tuning range beyond 3.65 μm is discussed.

The demonstration of a Ti:sapphire-pumped high-repetition rate optical parametric oscillator (OPO) with intracavity dispersion compensation based on $KTiOPO_4$ (KTP)[1] has been quickly followed by demonstrations of OPO's based on $KTiOAsO_4$ (KTA)[2] and $CsTiOAsO_4$ (CTA)[3]. These OPO crystals have nonlinearities on the same order as KTP and transparency ranges extending out to 5 μm. Another crystal in this class, $RbTiOAsO_4$ (RTA), also has these favorable characteristics.[4] Furthermore, the tuning characteristics of RTA are sufficiently different from these other crystals that it may be better suited to reach particular wavelengths. This letter reports on what we believe is the first demonstration of optical parametric oscillation in this newly available crystal, RTA. The results of the RTA OPO are presented and they are compared to those of the previously demonstrated high-repetition-rate KTP based OPO. Operation of the RTA OPO is shown to extend the achievable wavelength to 3.65 μm, and the possibility of tuning farther into the infrared is discussed.

The experimental setup and cavity alignment are similar to those of the KTP OPO reported in Ref. 1 . The schematic of the experimental setup is shown in Figure 1. The RTA OPO is pumped with a 1.8 W, 80 fsec Ti:sapphire laser which is tunable from 760 nm to 820 nm and runs at 80 MHz. The Ti:sapphire laser is focused onto the RTA crystal with an R=15 cm mirror. The generated signal (*e*-wave) is resonated in a linear cavity which consists of two R=10 cm curved mirrors, a flat high reflector, an output coupler, and a removable intracavity dispersion compensating prism pair. The OPO cavity mirrors are coated with a single-stack high reflector coating centered at 1.1 μm. Several output couplers were used, with the highest efficiency obtained using a 5% output coupler. The prisms are SF14 and are spaced at 17 cm. The pump and resonated signal are arranged in a noncollinear geometry that compensates for Poynting vector walkoff of the resonated *e*-wave. The angle between the pump and signal is approximately 2.5° inside the crystal.

The angle between the pump and idler k-vectors changes depending on the idler wavelength. An R=10 cm aluminum mirror is positioned to collect and collimate the idler. As the RTA OPO is a synchronously-pumped system, it is length matched to the Ti:sapphire cavity.

The RTA crystal is a positive biaxial crystal with a transparency range extending out to 5 μm. Two RTA crystals cut at $\theta=53^{\circ}$ with thicknesses of 1.8 mm and 3.0 mm are used. The 1.8 mm crystal was used for all measurements in this letter, except for idler wavelengths greater than 3 μm where the 3 mm crystal was used. Both surfaces of the crystals are antireflection coated centered at 1.0 μm. The crystals are aligned in the cavity for a type II interaction ($o \rightarrow e + o$) which maximizes d_{eff}; Figure 2 shows the crystal orientation. For the type II interaction the pump and the OPO *o*-wave (idler) are polarized along the y-axis and the *e*-wave (signal) is polarized in the x-z plane. The crystal is placed in the cavity so that the Poynting vector of the resonated *e*-wave walks onto the Poynting vector of the pump *o*-wave. The tuning curves for a type II interaction using various pump wavelengths in the Ti:sapphire tuning range are shown in Figure 3.

Similar to the KTP OPO reported in Reference 1, the RTA OPO operated in one of two regimes where the pulses were either chirped or chirp-free. As reported with the KTP OPO, the chirped pulses were seen when the net group velocity dispersion (GVD) was positive. The chirp-free pulses were encountered when the prisms in the cavity were adjusted for net negative GVD. Two differences in operation between the RTA OPO and the KTP OPO were noticed. As reported in Ref. 1, the highest power coupled out of the KTP OPO occurred when operating without prisms in its cavity. With the RTA OPO the power was the same with or without prisms in the cavity. The second difference is that we did not observe a change in power in going from net positive to net negative GVD when changing the amount of prism glass in the cavity. In fact, the highest signal power coupled out of the cavity in the signal branch was for chirp-free pulses (net negative

GVD) with a pulsewidth of 76 fsec. Otherwise the signal output of the RTA OPO was similar to the KTP OPO, giving output pulses as short as the pump and powers as high as 250 mW. The shortest pulses in the signal branch were measured to be 58 fsec, pumping with a 68 fsec Ti:sapphire pulses, assuming a sech^2 pulse shape. A chirp-free interferometric autocorrelation of the signal is shown in Figure 4. The time-bandwidth product for the chirp-free signal pulses was $\Delta\nu\Delta\tau \approx .35$. The signal was tuned from 1.3 to 1.03 so as to tune the idler farther into the infrared. Tuning to longer wavelengths than 1.3 μm in the signal would require a longer wavelength optics coating than the one used here.

The output of the idler was most likely chirped as indicated by a large time-bandwidth product of 1.6. An intensity autocorrelation using a Ge photodiode was made at 2.25 μm measuring 250 fsec. The near transform limit of the signal pulses and the large time-bandwidth product of the idler pulses indicate that with compression, much shorter idler pulses should be possible. Spectra from 2.1 to 3.65 μm in the idler were measured and are shown in Figure 5 a). There is a break in the tuning at 2.8 μm due to a water absorption. Tuning was achieved by rotating the RTA crystal and then peaking up the cavity. The power in the idler was typically as high as the power in the signal branch, with the highest output power measuring 200 mW which, along with signal power, gives a maximum conversion efficiency of 25%. As shown in Figure 5 b), the power in the idler drops off for long wavelengths. The operation of the OPO for long idler wavelengths was more sensitive to length matching and cavity misalignment, indicating that the OPO was close to threshold. To get as high above threshold as possible in the long idler wavelength range, the output coupler was replaced with a high reflector so as to reduce cavity loss. The Ti:sapphire pump power was increased to 2.5 W and the 3 mm RTA crystal was used. These changes allowed for tuning out to 3.65 μm in the idler.

The near-threshold operation for the longer wavelengths is attributed to the noncollinearity of the idler with the pump and signal. As seen in Figure 2, the noncollinear geometry which compensates for the Poynting vector walkoff of the resonated signal from the pump also forces the nonresonated idler to steer off both the signal and the pump. The angle between the idler and the pump increases as the idler wavelength increases, and the larger this angle, the smaller the effective interaction length and the higher the threshold. When the OPO is operating near its maximum output power, the angle between the pump and idler inside the crystal is approximately 4°; when the idler tunes out to 3.65 μm, this angle increases to 9°. To tune out beyond 3.65 μm when resonating the *e*-wave would further increase this angle and would require a further increase in the pump power to remain above threshold.

Alternatively, to extend the tuning range farther into the infrared, the *o*-wave could be resonated in a collinear geometry. In this case since both the pump and the resonated waves would be *o*-waves, the Poynting vectors of these two waves would automatically overlap. The nonresonated *e*-wave would walk off at an angle of approximately 2.5°. The OPO should be able to handle this walkoff angle considering that when resonating the *e*-wave, the OPO operates with an angle between the idler and the pump of 4° or more. The most important consideration, however, is that beyond 3.7 μm, there is a broad absorption feature. [5] This same feature is present in KTA and CTA as well. The absorption coefficient at 4 μm is approximately .04 mm^{-1} which for a 1.5 mm crystal would give 6 % absorption. For the OPO to handle this large an absorption loss in the crystal, the pump power has to be correspondingly higher. However, oscillating the *o*-wave should allow for tuning to at least 3.65 μm without the power loss seen when resonating the *e*-wave.

In conclusion, we have demonstrated the successful operation of a high-repetition-rate OPO based on the new nonlinear crystal, RTA, producing chirp-free pulses as short as 58 fsec with powers as high as 250 mW in the signal branch and 200 mW in the idler branch.

We have shown tuning from 1.03 to 1.3 μm in the signal branch, and from 2.15 to 3.65 μm in the idler branch. With different crystal cuts and optics coatings the RTA OPO can additionally access wavelengths from 1.3 to 2.15 μm, and we believe the OPO may be tuned to longer wavelengths than 3.65 μm by resonating the longer wavelength *o*-wave. And finally, with further optimization we believe shorter pulses and higher power may be obtained from the RTA OPO.

This research was supported by the Joint Services Electronics Program and the National Science Foundation.

References

1 W. S. Pelouch, P. E . Powers, and C. L. Tang, Opt. Lett. **17**, 1070 (1992).

2 P. E. Powers, S. Ramakrishna, C. L. Tang, and L. K. Cheng, Opt. Lett. **18**, 1171 (1993).

3 P. E. Powers, C. L. Tang, and L. K. Cheng, Opt. Lett. **19**, 37 (1994).

4 L. K. Cheng, L. T. Cheng, J. Galperin, P. A. Morris, and J. D. Bierlein, Journal of Crystal Growth , (1993).

5 R. A. Stolzenberger, personal communication (Crystal Associates, Waldwick NJ).

Figure Captions

Figure 1 Schematic of Ti:sapphire-pumped RTA OPO with a noncollinear geometry. The *e*-wave (signal) is resonated in the cavity and is coupled out with a 5% output coupler. The nonresonated o-wave (idler) is collected with an R=10 cm aluminum mirror. The intracavity prisms can be removed from the cavity if dispersion compensation is not required.

Figure 2 Crystal orientation in the OPO cavity showing the directions of the **k**-vectors ($\mathbf{k}_p$, $\mathbf{k}_s$, $\mathbf{k}_i$) and Poynting vectors ($\mathbf{S}_p$, $\mathbf{S}_s$, $\mathbf{S}_i$). ρ is the walkoff angle, θ is the phasematching angle.

Figure 3 Theoretical tuning curves for a type II interaction in RTA with a noncollinear angle of 2.5°. A separate tuning curve is calculated for three pump wavelengths in the Ti:sapphire laser range.

Figure 4 Interferometric autocorrelation of a 76 fsec signal pulse at 1.2 μm.

Figure 5 (a) Spectra of the idler pulses.

(b) Idler power as a function of wavelength for a 2.5 W Ti:sapphire pump and the 3 mm RTA crystal. The output coupler is replaced with a high reflector.

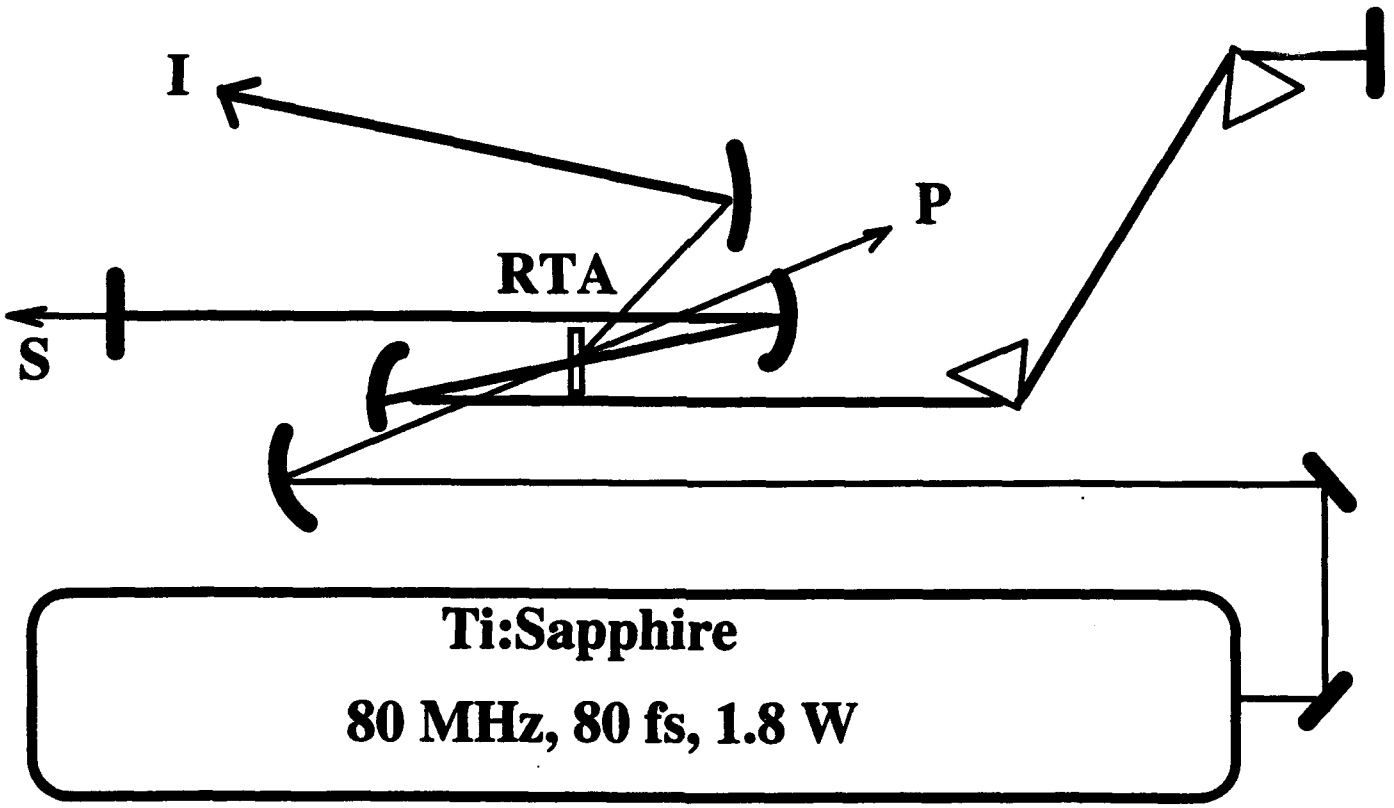
I
P
RTA
S
Ti:Sapphire
80 MHz, 80 fs, 1.8 W

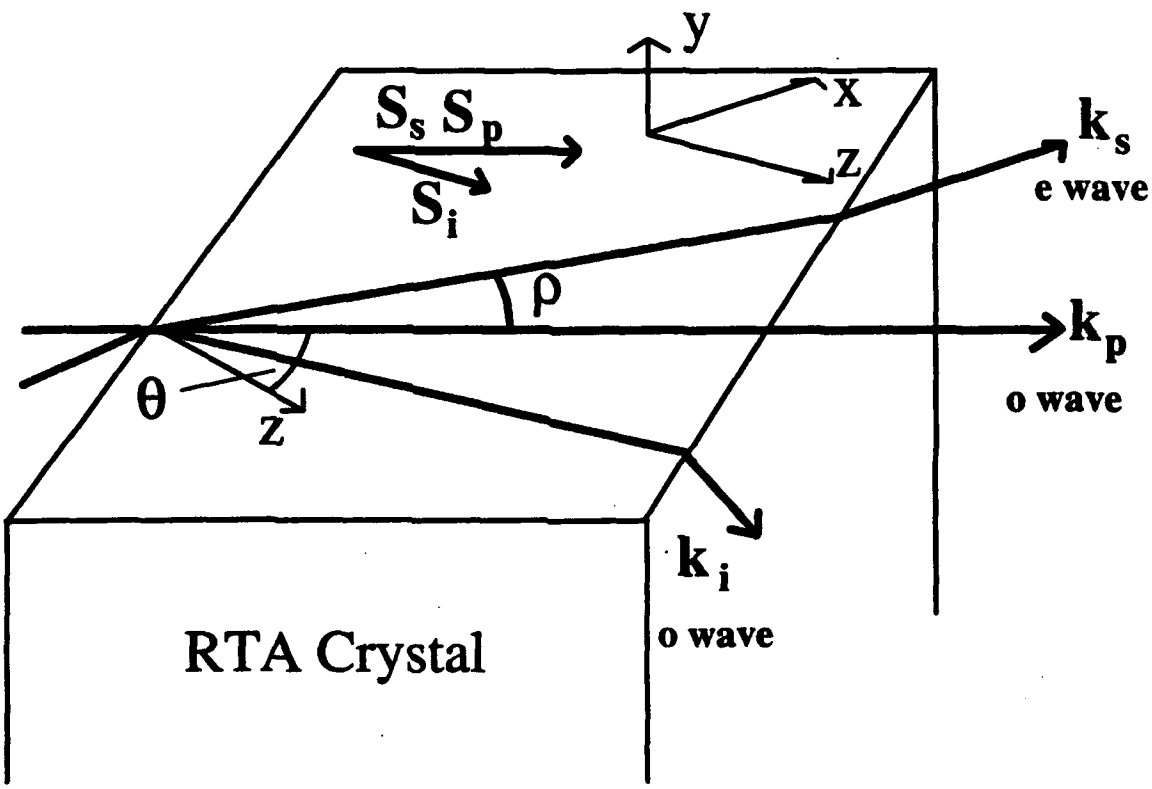
y
x
z
S_s S_p
S_i
k_s
e wave
ρ
k_p
o wave
θ
z
k_i
o wave
RTA Crystal

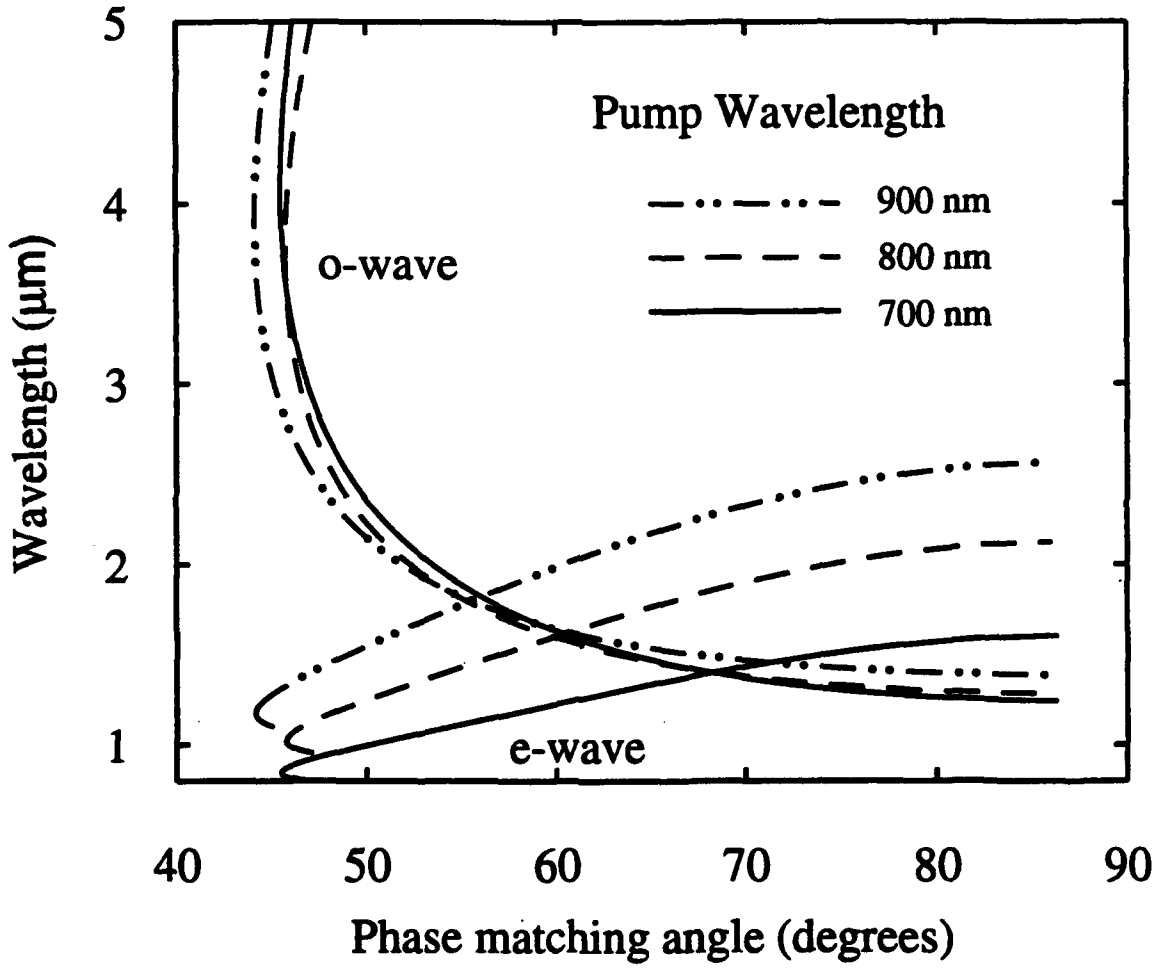
Pump Wavelength
900 nm
800 nm
700 nm
o-wave
e-wave
Wavelength (μm)
5
4
3
2
1
40
50
60
70
80
90
Phase matching angle (degrees)

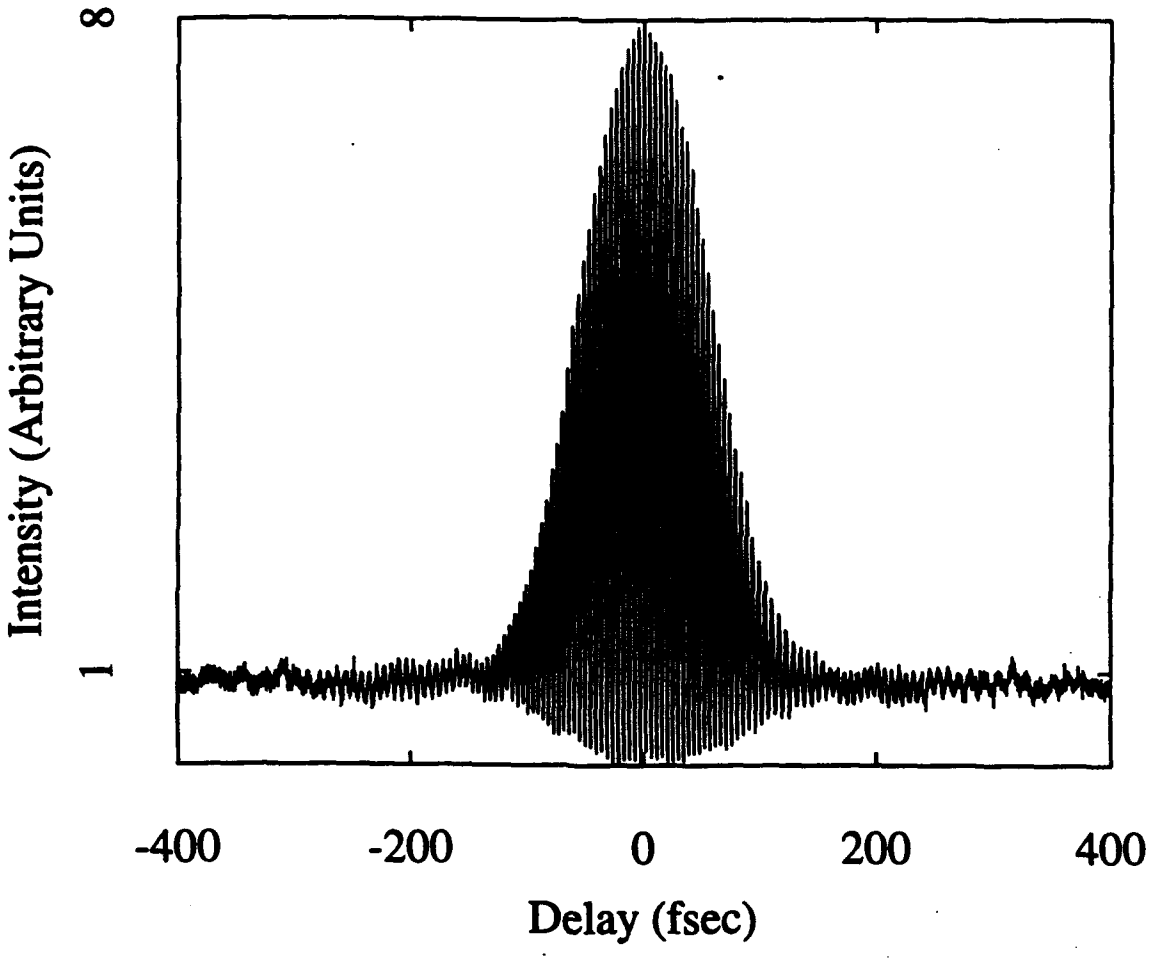
8
1
Intensity (Arbitrary Units)
-400
-200
0
200
400
Delay (fsec)

a)

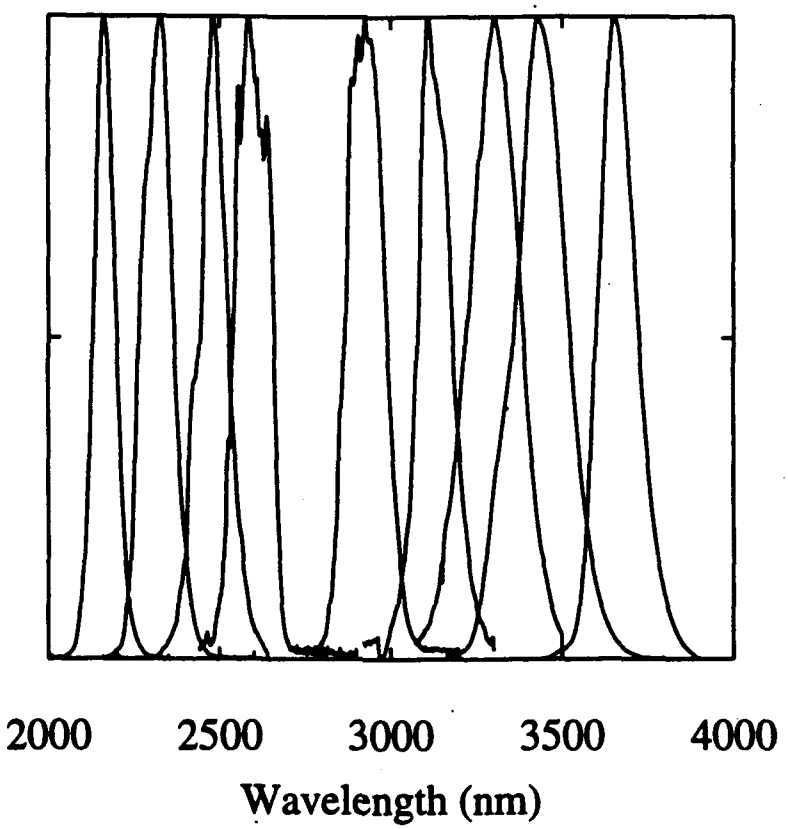
2000
2500
3000
3500
4000
Wavelength (nm)

b)

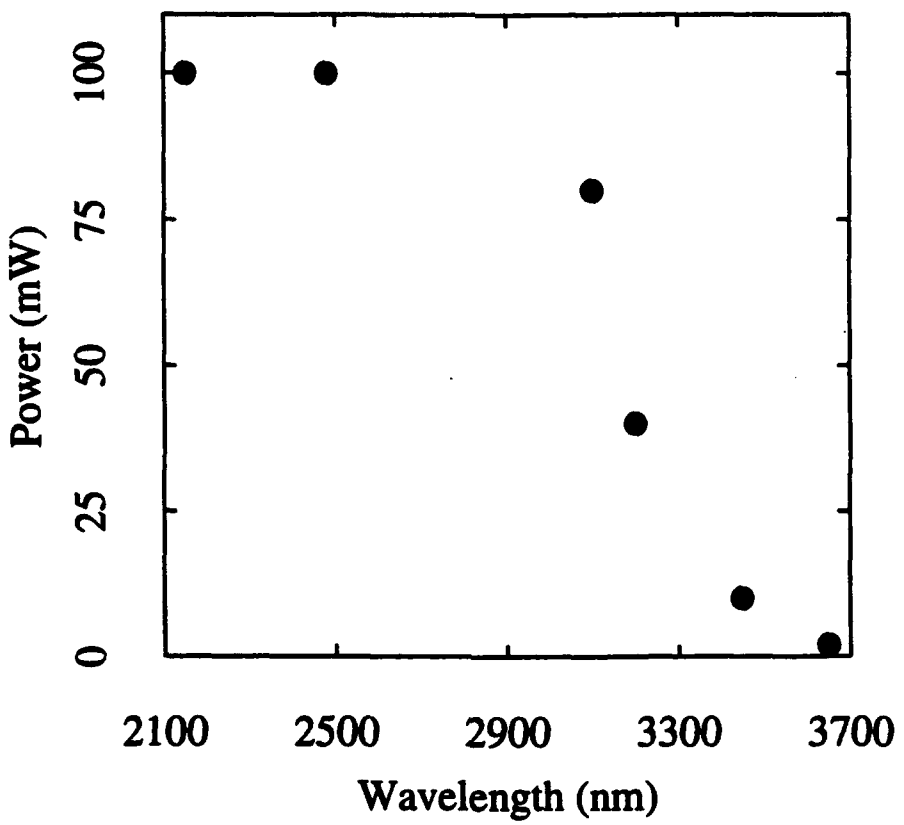
Power (mW)
0
25
50
75
100
2100
2500
2900
3300
3700
Wavelength (nm)

Appendix N

a reprint from Applied Optics

Thermal lens spectrometry using a broadly tunable optical parametric oscillator

Shuichi Kawasaki, Randall J. Lane, and Chung L. Tang

We present a computerized optical parametric oscillator that is capable of continuous tuning from approximately 420 nm to 2 μm for spectroscopic and spectrometric applications. This system allows any selected wavelength within the tuning range to be reached directly and quickly. We demonstrate the versatility of the system by measuring the entire visible (450–690-nm) thermal lens spectrum of NO_2 with a continuous scan.

Key words: Thermal lens spectrometry, optical parametric oscillator, β-barium borate.

1. Introduction

For many spectroscopic and spectrometric applications, such as nonlinear, photothermal, and fluorescence spectrometry, widely and continuously tunable laser sources are required. Until recently, dye lasers have been generally used for tunable laser spectroscopy. However, the tuning range of dye lasers tends to be severely limited. Each dye can cover only a few hundred angstroms, and the total range that can be covered by laser dyes is limited from approximately 400 nm to 1 μm. To extend beyond the primary dye laser tuning range, complicated nonlinear optical techniques are required. From the beginning since the laser was invented, there has always been a great deal of interest in truly continuously tunable laser sources that can cover a wide spectral range. The recently developed optical parametric oscillators (OPO's) are such sources.

The basic idea of an OPO[1–3] is not new and there had been some early applications[4,5] of the $LiNbO_3$ OPO to IR gas spectroscopy. However, because of the limitations of the nonlinear optical crystals available for use in the early OPO's, the applications had been limited and the field laid dormant for many years. As a result of recent advances in nonlinear optical crystal technology and the rapid progress in OPO research and development,[6] such oscillators have finally reached the stage at which they can now be used readily for a wide variety of spectroscopic and spectrometric applications. In this paper we report the first application of the recently developed broadly tunable β-barium borate (BBO) OPO[7–9] to thermal lens spectrometry (TLS). As an example, one obtains the visible thermal lens spectrum of NO_2 by use of a computer-controlled automatic scanning system. The detailed features of the spectrum reproduce exactly the known spectrum of NO_2. The details of the BBO OPO developed, the experimental results, and the unique features of OPO TLS are discussed in this paper.

2. Experimental Setup

A. β-Barium Borate Optical Parametric Oscillator

Figure 1(a) shows the cavity configuration of the OPO.[10] The basic principle of the OPO is simple. UV photons (355 nm) from the pump beam (third harmonic of a Nd:YAG laser) that propagate through the nonlinear BBO crystals break down by spontaneous and stimulated emission into lower-frequency photons called the signal (visible) and the idler (IR) photons. The Fabry–Perot cavity formed by mirror 3 and the grating provides the optical feedback that leads to oscillation of the OPO. Mirrors 1 and 2 transmit the signal and idler but reflect the UV pump photons.[8] The grating is oriented in the Littrow configuration so as to reduce the oscillator linewidth to 0.2–0.6 nm throughout the tuning range.[10] We used two BBO crystals to compensate[10] for the walk-off effect because the Poynting vector and the k-vector of the pump wave are not in the same direction. We grew the crystals in our laboratory by using the top-seeded high-temperature solution growth technique.[11–13] The lengths of the crystals are 9 and 8.5 mm and are cut for type-I phase matching at 28.6°.

The authors are with the School of Electrical Engineering, 326 Phillips Hall, Cornell University, New York 14853.

Received 14 July 1992; revision received 22 December 1992.
0003-6935/94/060992-05$06.00/0.

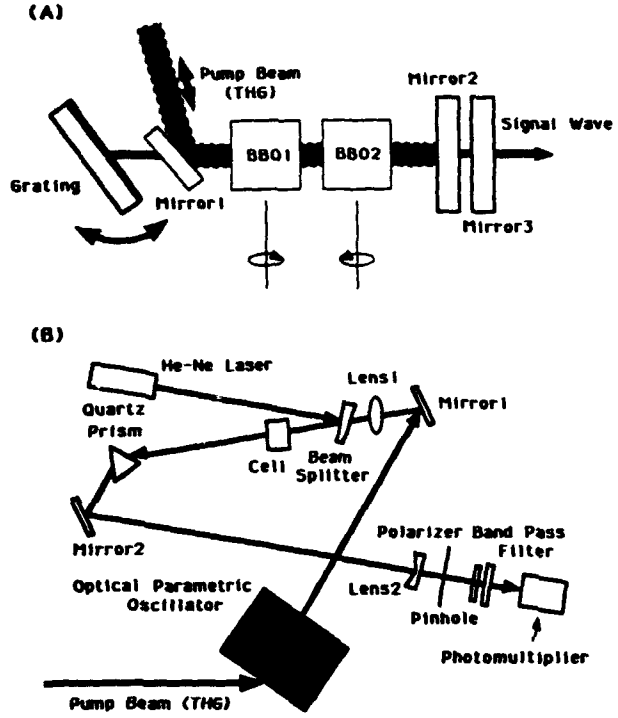

Fig. 1. Experimental setup: (A) cavity configuration of the OPO; (B) block diagram of the thermal lens spectrometer using the BBO OPO; TGH, third harmonic generation.

The two crystals are mounted on separate rotational stages that are connected to a motor controller, which is in turn controlled by a standard personal computer. This system allows the two crystals to be set to phase-matching angle corresponding to the desired output wavelength simultaneously. The grating (Milton Roy) that was used has 1800 grooves/mm with a blaze angle of 26.5°. The grating was also placed on the same kind of rotational stage and controlled by the computer to set the desired angle. The grooves are positioned normal to the polarization of the OPO signal beam to improve the broadband diffraction efficiency and the line-narrowing effect.

The pump source was a Q-switched neodymium-doped yttrium aluminum garnet (Nd:YAG) laser system followed by third-harmonic generation (THG). We reduced the pump beam diameter to 2 mm by use of a telescope; the typical pulse property used for the experiment was 12 mJ with a 5–6-ns pulse duration at 355 nm. The pump beam was steered through the cavity by use of mirror 1 and was reflected back along the same optical axis by use of mirror 2. Both mirrors are 355-nm high reflectors. The incident angles are 55° and 0°, respectively, for mirrors 1 and 2. The output coupler of the OPO is a standard multilayer dielectric-coated mirror with 50% reflectivity at 550 nm. The resonated OPO signal beam is diffracted by the grating, and the first-order diffracted beam is reflected back along the cavity axis. This Littrow configuration minimizes loss from the grating.[10,14] The cavity length is 75 mm from the center of the grating to the surface of mirror 3.

B. Measurement of the Spectrum

We measured the linewidth of the OPO beam by using a 0.5-m monochromator equipped with a photodiode. Wavelength resolution was set to 0.2 nm during the experiment, which also corresponded to the monochromator's wavelength accuracy. The signal from the photodiode was sent to a boxcar averager (EG&G Model 162) and then read into the computer. The spectrum was displayed in real time on the computer screen. The intensity fluctuation of the OPO output was also measured. We used a hot mirror to isolate the signal wave from the idler.

Figure 1(B) is a block diagram of the thermal lens spectrometer based on a direct incidence system.[15,16] We focused the signal beam from the OPO into a 1-cm flow cell (Hellma Cells, Inc.) by using lens 1 (100-mm focal length). We aligned a He–Ne laser beam (Spectra-Physics, Inc. Model 105-1), which was used as the probe beam, coaxially with the signal beam by use of a quartz wedge. The beam passed through the sample cell without focusing. The probe beam is isolated through the quartz prism and expanded to 10 mm by lens 2. After the beam passes through a polarizer, one can measure the intensity of the beam center by use of a photomultiplier (Thorn EMI Electron Tubes, Ltd., 9658R) with a bandpass filter (632.8 nm) and a pinhole with an aperture of 1.2 mm. The thermal lens spectrum was also displayed on the screen in real time.

The sample of nitrogen dioxide was diluted to 0.5% in dry air as supplied from Matheson. The flow rate of the sample was kept at 40–50 cc/min during the experiment. The gas was bubbled through an NaOH solution and was discharged.

3. Results and Discussion

A. Performance of the System

To maintain narrow linewidth oscillation over this wide range, it is important to have synchronized operation and precise alignment between the two crystals and the grating. We measured the generated wavelength that depends on the crystal angle for two crystals over the entire tuning range and we derived an equation for the tuning curve with a fifth-order polynomial fit to these data. The error in selecting a given wavelength was confirmed to be within the accuracy of the rotational stage. Figure 2 shows the typical OPO output at 620 nm. One can obtain the spectrum by using the first-order diffracted beam from the Littrow configured grating, which was blazed for optimum efficiency around this range. The full width at half-maximum (FWHM) linewidth is estimated to be 0.45 nm from the spectrum. The observed value without a grating is close to 1.5-nm FWHM.[10] Thus, one can successfully use the grating to reduce the linewidth by a factor of 3 at this wavelength. The spectral shape, which is almost symmetric, also indicates that the angles of two crystals are well synchronized with that of the grating.

Above 620 nm the linewidth increased slightly to

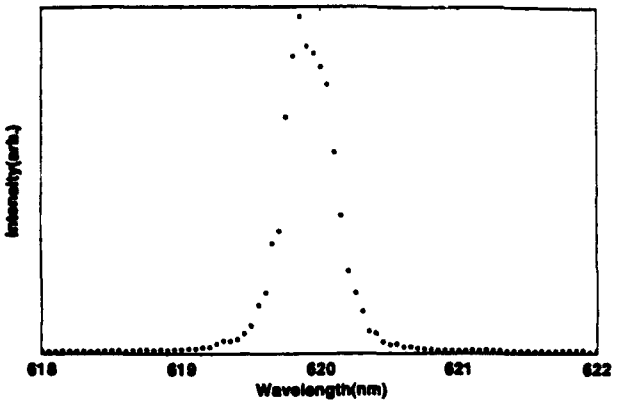

Fig. 2. OPO spectrum that was obtained by using a grating in Littrow for narrow linewidth oscillation. We measured the signal in 0.05-nm steps and averaged 30 points/step.

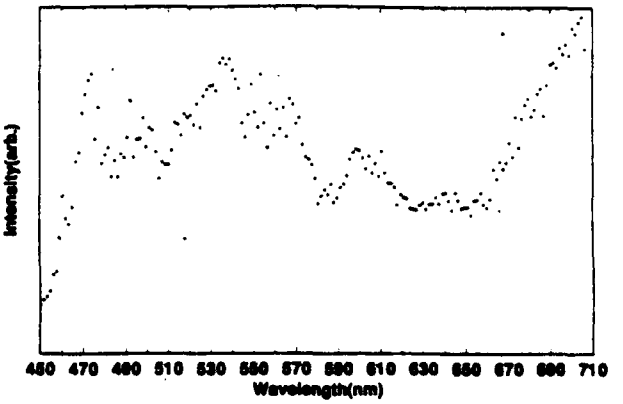

Fig. 3. Tuning curve of the signal wave. We measured the signal in 1.5-nm steps and averaged 50 points/step. The sensitivity of the photodiode was taken into account.

0.5–0.6 nm, which is caused by broadening of the phase-matching bandwidth of the crystal near the degenerate point. Careful alignment of the crystal angle and grating should produce narrower oscillation. Precise alignment of the cavity cannot be maintained during automatic scanning since the accuracy of the rotational stage is limited to 0.005°. This, however, can be improved with a higher resolution grating. A 2400-grooves/mm grating gives a linewidth of 0.15 nm at 650 nm without sacrificing efficiency significantly as mentioned in the next paragraph. One can achieve a narrower linewidth by inserting an étalon ($F = 10$) into the cavity. The étalon decreases the linewidth to almost that of the pump beam, but the threshold increases drastically, which results in low efficiency. Besides, it is difficult to synchronize the crystals, grating, and étalon over the wide spectral range. The Littman configuration can also decrease the linewidth to that of the étalon configuration, but its low efficiency still remains a problem. The linewidth of the OPO is also affected by the linewidth and divergence of the pump beam. However, one can easily solve these problems by using an injection-seeded Nd:YAG laser.[17] A single longitudinal mode can be obtained with that pump laser, but the difficulty in stabilizing the cavity leads to a limited tuning range. Finally, a proper configuration should be chosen depending on the application, trading off the advantages of simplicity, wide tunability, high efficiency, and narrow linewidth. With a properly designed and engineered device, one can combine wide tunability with narrow linewidth. It is, however, not the purpose of this paper to report such a device.

Figure 3 shows the output intensity of the signal wave of the OPO as a function of wavelength from 450 to 706.5 nm. The OPO was scanned at 1.5 nm/step and 50 points were averaged at each step. The intensity was corrected for the spectral response of the photodiode that was used for the measurements. The scanning time was approximately 14 min. This spectrum shows the intensity of the signal wave (over 680 nm the hot mirror used cannot isolate the signal wave from its corresponding idler, the intensity above this region includes that of the idler wave). A jump in the output intensity around 475 nm is seen from étalon effects that are due to internal reflections that are no longer lost from the cavity when the surfaces of each crystal rotate into a position that is normal to the cavity axis. The conversion efficiency was greater than 10% for most of the tuning range and 13% at 650 nm. It was 12% when we used a 2400-groove/mm grating and 3% with an additional étalon at 650 nm. This spectrum was measured to show that there are no spectral gaps over the entire tuning range. Therefore, the spectral transmission variation of the hot mirror was not considered, which is the main cause of irregular intensity fluctuation. The wavelength dependence of the intensity also depends on the transmittance of the output coupler.

The tunable range of this system is actually 450–1675 nm, limited by the cavity mirrors that were used. The wavelength accuracy of this system was measured for several wavelengths over the tuning range and was confirmed to be within half of the linewidth of the oscillation beam at each point. The response of the system depends mostly on the rotational rate and the minimum step of the rotational stage. In our system the crystals and grating are directly mounted on the rotational stages. Therefore, any wavelength can be selected within a few seconds, although the scanning time is limited by the repetition of our Nd:YAG laser (10 Hz) and the desired amount of averaging at each point.

This compact, solid-state BBO OPO system has several desirable performance characteristics for spectroscopic applications. High output power and efficiency relative to conventional sources without an amplifier stage make sensitive measurements possible especially for spectrometry such as TLS. TLS is known as a highly sensitive analytical method. For example, it has been reported that TLS is almost 1000 times more sensitive than conventional absorption spectrometry for probing NO_2 diluted in air.[15] Because of this sensitivity, only a small sample volume is needed and excellent spatial resolution can be attained, that is, the actual sample volume needed

for the thermal lens signal is defined only by the beam cross section and the confocal distance of the focusing lens. In our demonstration the OPO beam was tightly focused, which led to a short confocal distance (<1 mm). This is not claimed to be optimum but was good enough to allow the use of a 1-cm flow cell. The thermal lens signal was strong enough for a demonstration that allowed us to obtain a spectrum comparable with that measured with a 1.2–1.3% sample with a 7.5-cm cell.[18] Furthermore, the BBO OPO TLS system makes a fingerprinting assignment (which has been of interest but unachievable with conventional dye lasers) feasible because of its broad tunability. These characteristics are quite suitable for a remote-sensing device. In Subsection 3.B we discuss more about the measurement of the NO_2 thermal lens spectrum.

B. Thermal Lens Spectrum of NO_2

Figure 4 shows the thermal lens spectrum of NO_2 from 450 to 690 nm. Each peak corresponds well with previously reported spectra.[18] In this experiment the idler was not isolated. However, absorption of the idler wavelength by the sample was small and so could be neglected.[19] Since the intensity of the thermal lens signal is proportional to the laser power, intensity variations over the tuning range will affect the amplitude of the spectral peaks. This is the reason the peaks under 470 nm are relatively small. During a scan over such a wide spectral range, dispersion of the focusing lens and the beam splitter might have influenced the signal intensity. In this experiment, however, we estimated the confocal distance to be less than 1 mm. Over the spectral range, the focal point and the focal length changed by less than 0.1 mm and a few millimeters, respectively. Since we employed the direct incidence method, these factors should have had no significant effect on the spectrum.

Figure 5 shows the spectrum of the same sample between 600 and 680 nm, reproducing exactly the known spectrum of this molecule.[18] Because NO_2 shows a complicated spectrum,[19] finer details of the spectrum cannot be resolved at this resolution. As the excitation beam is tuned toward the wavelength of the He–Ne laser, it can spuriously give a positive signal at the photomultiplier tube. However, since the OPO beam is polarized linearly and has a fast rise time, it can easily be separated by using a polarizer and by changing the gate position of the boxcar.

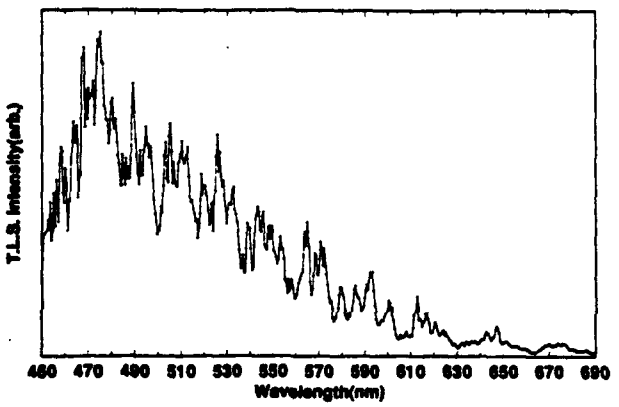

Fig. 4. Thermal lens spectrum (T.L.S.) of NO_2 from 450 to 690 nm. We measured the signal in 0.5-nm steps and averaged 50 points/step. The sample was diluted in dry air to 0.5%.

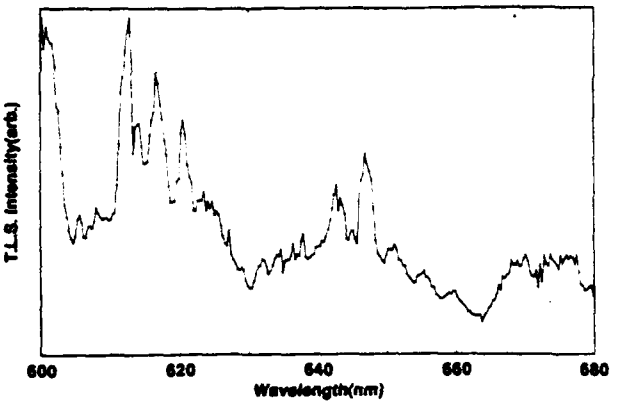

Fig. 5. Thermal lens spectrum (T.L.S.) of NO_2 from 600 to 680 nm. We measured the signal in 0.3-nm steps and averaged 100 points/step.

4. Conclusions

In this study we have reported on a computerized BBO OPO system with a narrow linewidth oscillation of 0.2–0.6 nm over its visible tuning range. We demonstrated its performance by measuring the thermal lens spectrum of NO_2. The tunability of our system, 450–1675 nm, is much broader than that of commercially available dye laser systems that require dye changes to achieve a wide spectral region. Our system also tunes more quickly and easily over its whole tuning range. The OPO system is completely solid state (exccept for the YAG laser pumped by a water-cooled flash lamp) and consists of commercially available components. This makes it a very practical tunable laser system. The system succeeded in measuring the entire visible thermal lens spectrum of NO_2 in a single scan with adequate resolution to resolve the important peaks, thus demonstrating excellent pointing stability and wide tunability. It can be optimized with the appropriate optics to produce tunable ultraviolet, visible, and infrared radiation. Therefore, the BBO OPO has significant practical advantages as a laser source in many spectroscopic and spectrometric applications.

This work has been supported by the U.S. Naval Research Laboratory, the National Science Foundation, and the Japan Society for the Promotion of Science. S. Kawasaki acknowledges the Japan Society for the Promotion of Science Fellow for Research Abroad.

References

1. N. M. Kroll, "Parametric amplification in spatially extended media and application to the design of tunable oscillators at optical frequencies," Phys. Rev. **127**, 1207–1211 (1962); S. A.

Akhamanov and R. V. Khoklov, "Concerning one possibility of amplification of light waves," Sov. Phys. JETP **16**, 252–258 (1963).
2. See, for example, C. L. Tang, "Spontaneous and stimulated parametric processes," in *Nonlinear Optics*, H. Rabin and C. L. Tang, eds., in Vol. 1 of Treatise in Quantum Electronics (Academic, New York, 1975), parts A and B.
3. See, for example, R. L. Byer, "Optical parametric oscillators," in *Nonlinear Optics*, H. Rabin and C. L. Tang, eds. Vol. 1 of Treatise in Quantum E·ctronics (Academic, New York, 1975), parts A & B.
4. T. Henningsen, M. Garbuny, and R. L. Byer, "Remote detection of CO by parametric tunable laser," Appl. Phys. Lett. **24**, 242–244 (1974).
5. R. A. Baumgartner and R. L. Byer, "Remote SO_2 measurements at 4 μm with a continuously tunable source," Opt. Lett. **2**, 163–165 (1978).
6. See, for example, C. L. Tang, W. R. Bosenberg, T. Ukachi, R. J. Lane, and L. K. Cheng, "Optical parametric oscillators," Proc. IEEE **80**, 365–374 (1992).
7. L. K. Cheng, W. R. Bosenberg, and C. L. Tang, "Broadly tunable optical parametric oscillation in β-BaB_2O_4," Appl. Phys. Lett. **53**, 175–177 (1988).
8. W. R. Bosenberg, L. K. Cheng, and C. L. Tang, "Ultraviolet optical parametric oscillation in β-BaB_2O_4," Appl. Phys. Lett. **54**, 13–15 (1989).
9. W. R. Bosenberg, "'Development of beta-barium metaborate optical parametric oscillator," Ph.D. dissertation (Cornell University, Ithaca, N.Y., 1990).
10. W. R. Bosenberg, W. S. Pelouch, and C. L. Tang, "High-efficiency and narrow-linewidth operation of a two-crystal β-BaB_2O_4 optical parametric oscillator," Appl. Phys. Lett. **55**, 1952–1954 (1989).
11. C. Chen, B. Wu, A. Jiang, and G. You, "A new-type ultraviolet SHG crystal—β-BaB_2O_4," Sci. Sin. Ser. B **28**, 235–243 (1985).
12. L. K. Cheng, W. R. Bosenberg, and C. L. Tang, "Growth and characterization of low temperature phase barium metaborate crystals," J. Cryst. Growth **89**, 553–559 (1988).
13. W. R. Bosenberg, R. J. Lane, and C. L. Tang, "Growth of large, high-quality beta-barium metaborate crystals," J. Cryst. Growth **108**, 394–398 (1991).
14. S. Burdulis, R. Grigonis, A. Piskarskas, G. Sinkevicius, V. Sirutkaitis, A. Fix, J. Nolting, and R. Wallenstein, "Visible optical parametric oscillation in synchronously pumped beta-barium borate," Opt. Commun. **74**, 398–402 (1990).
15. K. Mori, T. Imasaka, and N. Ishibashi, "Determination of nitrogen dioxode by pulsed thermal lens spectrophotometry," Anal. Chem. **55**, 1075–1079 (1983).
16. S. Kawasaki, T. Imasaka, and N. Ishibashi, "Thermal lens spectrophotometry using a tunable infrared laser generated by a stimulated Raman effect," Anal. Chem. **59**, 523–525 (1987).
17. Y. X. Fan, R. C. Eckardt, R. L. Byer, J. Nolting, and R. Wallenstein, "Visible BaB_2O_4 optical parametric oscillator pumped at 355 nm by a single-axial-mode pulsed source," Appl. Phys. Lett. **53**, 2014–2016 (1988).
18. D. K. Hsu, D. L. Monts, and R. N. Zare, *Spectral Atlas of Nitrogen Dioxide* (Academic, New York 1978).
19. A. E. Douglas and K. P. Huber, "The absorption spectrum of NO_2 in the 3700–4600 Å region," Can. J. Phys. **43**, 74–81 (1965).